

**An investigation of the effects of reward and metabolic cost
on movement vigor**

by

Garrick W. Bruening

B.S., University of Arizona, 2015

M.S., University of Colorado, Boulder, 2017

A thesis submitted to the
Faculty of the Graduate School of the
University of Colorado in partial fulfillment
of the requirements for the degree of
Doctor of Philosophy
Department of Integrative Physiology
2021

Committee Members:

Alaa A. Ahmed, Chair

Rodger Kram

Alena M. Grabowski

Roger M. Enoka

Anne K. Silverman

Garrick W. Bruening, (Ph.D., Integrative Physiology)

An investigation of the effects of reward and metabolic cost on movement vigor

Thesis directed by Prof. Alaa A. Ahmed

Nearly every movement we make reflects a decision. This decision likely involves a trade-off between maximizing reward and minimizing effort. How fast we move, vigor, can reveal how we value reward and effort when making movement decisions. The goal of this dissertation is to gain further insight into how reward and effort affect movement vigor, and how we can use computational models of effort to improve predictions of movement effort.

First, I evaluated how subjects responded to reward when given in a probabilistic manner. Subjects made reaching movements to multiple targets, while we altered the probability of receiving a fixed reward amount from completing the movement. Vigor was influenced by the probability of reward. Interestingly, the vigor of the following movement was faster following a reward compared to the absence of reward, and faster still the more surprising the reward was. This suggests that vigor is also modulated by the history of reward and reward prediction error.

Next, I focused on the effect of effort on vigor. I measured both the metabolic cost and vigor of reaching with increasing mass and found that metabolic cost increased and movements slowed with added mass. I found that movement slowing was best explained by the maximization of a utility that considered the rate at which both reward was to be acquired, effort was to be expended, and where effort, critically, was represented as metabolic cost.

Lastly, I focused on determining the ability of oft-used models of metabolic cost to explain the metabolic cost of reaching. I developed a neuromechanical model of the arm to estimate the metabolic rate of experimental reach data. I found that while many metabolic cost models can reasonably predict the experimental data, effort representations used in motor control research fail to adequately capture the metabolic cost of reaching.

Together, these studies provide a better understanding of the effects of reward and effort on

movement vigor and how we can use computational models of effort in research, potentially informing future work aimed at understanding the neural, psychological and biomechanical determinants of why we move the way we do.

Dedication

To all the people who have helped me become a scientist and excite me to do new, interesting, and fun things every day. I cannot express how much everyone who has helped me mean to me. Thank you.

Acknowledgements

I want to thank a lot of people, there are too many to individually thank. If you think you helped me, you did and I appreciate it immensely.

Specifically, I want to thank:

My family, who have pushed me every step of the way to go further and do better. The constant push got me here. Additionally Winky, Dobbie, Albie, and Grindie who we're the best fluffy boys I could hope for.

All my friends, whether I know you through frisbee, skiing, bluegrass, or have known you forever, you have kept me sane through all of this. I can't imagine a better group of people to be around.

The greater lab group, talking science has always been a great pleasure with everyone in the labs. Specifically the neuromechanics, applied biomechanics, locomotion, and neurophysiology labs. You have all taught me so much about science.

Prof. Alena Grabowski, who taught me you should believe in your science and fight for it.

Prof. Rodger Kram, who showed me it is possible to always be excited for science.

Prof. Roger Enoka, who made me excited to hear his criticism as it always led to improving my research.

And last, specifically the neuromechanics lab, ran by Alaa Ahmed. I would not be here without Alaa and all the lab members who have come and gone. They've always pushed me to be a better scientist and researcher, this work was supported by this team, and I can't imagine another team to have done this with.

Contents

Chapter

1	Thesis Objectives	1
1.1	Introduction	1
1.2	Specific Aims	2
1.3	Chapter 2 - A decision-making approach to understanding movement vigor	2
1.4	Chapter 3 (AIM 1) - The effects of reward expectation and reward prediction error on movement vigor	3
1.5	Chapter 4 (AIMS 2 - 4) - The role of effort in determining preferred movement speed	4
1.6	Chapter 5 - An overview of musculoskeletal modeling of movement	4
1.7	Chapter 6 (AIM 5) - A validation of metabolic energy models in arm reaching	5
1.8	Significance	5
2	A decision-making approach to understanding movement vigor	6
2.1	Utility	6
2.2	Reward	7
2.3	Effort	10
2.4	Effects of Reward and Effort on Movement	16
2.5	Summary	23
3	The effects of probability of reward and reward prediction error on movement vigor	25
3.1	Abstract	25

3.2	Introduction	26
3.3	Methods	28
3.4	Results	33
3.5	Discussion	41
3.6	Conclusion	44
4	The role of effort in determining preferred movement speed	45
4.1	Abstract	45
4.2	Introduction	46
4.3	Results	48
4.4	Discussion	65
4.5	Conclusion	69
4.6	Methods	69
5	An overview of musculoskeletal modeling of movement	85
5.1	Introduction	85
5.2	Estimating Muscle Forces	87
5.3	Dynamics (Step 1-3)	90
5.4	Muscle Properties (Step 4, 6)	90
5.5	Activation Dynamics (Step 7)	97
5.6	Energetics Models (Step 8)	103
5.7	Evaluation Studies	104
5.8	Summary	108
6	A validation of metabolic energy models in arm reaching	109
6.1	Abstract	109
6.2	Introduction	110
6.3	Methods	112

6.4 Results	121
6.5 Discussion	130
7 Conclusions	136
Bibliography	139
Appendix	
A Mass Results Supplemental	154
A.1 Movement Metrics	154
A.2 Alternative models predicting movement duration	155
B Metabolic Rate Modeling Supplemental	165
B.1 Supplemental Methods	165
B.2 Biomechanical Model	167
B.3 Data Processing and Statistics	199
B.4 Limitations	201

List of Tables

Table

4.1	Normalized movement durations for experiment 2a, 2b, 2c, gross metabolic cost and net metabolic cost.	67
6.1	Properties of the forearm and upper arm rigid segments for example subject of 56.81 kg and 1.62 m. The values for Forearm $Cent_L$ and I_{COM} are for 0 added mass at the hand.	118
6.2	Muscle Properties. For L_{OPT} , the letter corresponds to which author the value was taken from or if it was estimated. C(28), L(110), M(141), E (estimated).	119
6.3	Linear estimates for each metabolic representation. The linear estimate is shown as mean \pm standard error.	124
6.4	Parameterization values for each representation. Each value shown mean \pm standard error with the 95% confidence interval in parenthesis. The a parameter represents some offset at infinite movement duration, for this analysis a value greater than 0 is indicated with a *. A scaling parameter, b , is not important to this analysis. How each representation scales with mass, c , and how they are affected by time, d , are tested to determine if they are different than the parameters found in the metabolic rate with equation B.52. This non-difference from metabolic rate effect of time is indicated with a †.	128

A.1 Movement duration (s) from experiment 2a, 2b, and 2c. Data is shown as mean ± standard deviation.	154
A.2 Peak velocity (m/s) from experiment 2a, 2b, and 2c. Data is shown as mean ± standard deviation.	154
A.3 Reaction time (s) from experiment 2a, 2b, and 2c. Data is shown as mean ± standard deviation.	155
A.4 Movement duration and predictions for experiment 2a. Ut represents Utility, RWD represents reward. These values are found fitting one α value to experiment 2a/2b, then applying it to 2c.	155
A.5 Movement duration and predictions for experiment 2b. Ut represents Utility, RWD represents reward. These values are found fitting one α value to experiment 2a/2b, then applying it to 2c.	156
A.6 Movement duration and predictions for experiment 2c. Ut represents Utility, RWD represents reward. These values are found fitting one α value to experiment 2a/2b, then applying it to 2c.	156
B.1 Properties of the forearm and upper arm rigid segments for example subject of 56.81 kg and 1.62 m. The values for Forearm $Cent_L$ and I_{COM} are for 0 added mass at the hand.	176
B.2 Properties of the forearm and upper arm rigid segments for example subject of 56.81 kg and 1.62 m. The values for Forearm $Cent_L$ and I_{COM} are for 0 added mass at the hand.	176
B.3 Muscle Properties. For L_{OPT} , the letter corresponds to which author the value was taken from or if it was estimated. C(28), L(110), M(141), E (estimated).	182
B.4 Coefficients for polynomial fits to moment arm lengths.	184
B.5 Coefficients for polynomial fits to moment arm lengths.	185
B.6 Activation and deactivation times using the Umberger Model	189

List of Figures

Figure

3.2 Effects of expected value on peak velocity and reaction time. (A) Average velocity traces split by reward probability and aligned to peak velocity. Data is averaged across all trials and not within subjects. Shown with mean plus standard error. (B) Average velocity traces difference from 0 p(R) reward condition. 0 p(R) traces are averaged for each subject, then subtracted from every trial for the other probabilities for that subject. We then calculate the average traces off this difference to have a subject specific difference. At the peak velocity we see the increase in velocity for p(R) equal to 1 and 2/3, but a decrease in probability for 1/3. (C, E) Shows the difference of each subject average from the specific subject average of p(R) = 0. The effect of probability on the difference in vigor metric from 0 p(R) rewarded condition for peak velocity (C) and reaction time (E). Red dashed line indicates no change from the 0 p(R) condition. This change is calculated by subtracting the mean of the 0 p(R) reward condition from every movement. (D, F) Subject specific difference averages from p(R) = 0 for peak velocity (D) and reaction time (F).	35
3.3 Effect of prior reward on peak velocity (A) and reaction time (B). Metrics are shown as subject average differences from the average of p(R) = 0. (A) Peak velocity increases with probability of reward only when rewarded on the previous trial. (B) Reaction time did not increase or decrease with probability of reward when split by reward on the previous trial.	36
3.4 Reward modulates vigor on the following trial. We calculate the trial-to-trial differences for each metric and split this by previous reward. We then average each subject and prior reward condition and calculate a paired t-test. (A) Peak velocity was higher on trials following rewarded trials compared to those following unrewarded trials ($p = 0.0234$). (B) Reaction time was higher following rewarded trials compared to unrewarded trials ($p = 0.0016$). Grey lines indicate specific subject average changes. A * indicates a difference between prior reward and no prior reward. A + sign indicates a difference from 0.	38

3.5 Reward prediction error results. Horizontal dashed line indicates the mean of 0 RPE. Reward prediction error is calculated as the reward obtained minus the expected value of the target. Positive RPE indicates a low expected value, with a reward. Low RPE indicates a high expected value with no reward. (A) Peak velocity affected by reward prediction error. As rewarded prediction error becomes more positive, the change in trial-to-trial peak velocity increases. (B) Reaction time trial-to-trial changes increase as reward prediction error becomes more positive, though this may be driven primarily by prior reward. (C) On the same movement, the outward minus inward reach difference in peak velocity becomes lower the more positive the RPE. This indicates that subjects slow down less when there is a good outcome vs a bad outcome.	40
4.1 Experiment 1 setup. (A) Subjects made horizontal planar reaching movements while breathing into a mouthpiece. Mass was added at the hand. (B) Subjects made out-then-back reaching movements across a range of added masses and speeds to four targets 10 cm from the home circle. There were seven distinct speeds, and subjects completed six speeds with each mass. The two heaviest masses corresponded with the six slowest speeds; the two lighter masses corresponded with the six faster speeds. The number of trials within each speed was set to allow for approximately five minutes of reaching.	49
4.2 Experiment one results. (A) Gross metabolic power increases with added mass and movement speed (shorter durations). (B) Gross metabolic cost of a movement. Gross metabolic cost shows a distinct minimum, and this minimum duration increases with added mass. (C) Increased mass and speed (shorter duration) increased subjects' endpoint error. (D, E) Mass did not affect subjects' movement consistency. Faster movement speed did lead to less consistency (increased variance). (F) Reaction time increased with added mass and longer movement durations.	51

5.5 Results from tracking error simulation from Miller (131). The solid bars represent the energy model from the tracking simulation, and the white bars represent an adjustment to eccentric work. MA97 is the Minetti and Alexander model (136), B04 is the Bhargava model (18), H06 is the Houdijk model (90), LW07 is the Lichtwark model (114), U10 is the 2010 Umberger Model (180). The solid bars represent the original metabolic model, white bars represent adjusted estimates for eccentric contractions.	106
5.6 Results from optimal simulation from Miller (131). a is the Minetti and Alexander model, b is the Bhargava model, c is the Houdijk model, d is the Licthwark model, e is the 2010 Umberger Model. f is an estimate from blood flow in walking guinea fowl.	106
5.7 Relationship between collected metabolic cost and simulated metabolic cost from Koelewijn (107). The seven models were BHAR04 (18), HOUD06 (90), UMBE03 (181), LICH05 (114), MINE97 (136), MARG68 (127), and KIMR15 (102).	107
6.1 Description of experimental protocol and arm model. A. Subjects were in a seated position while collecting metabolic data. Mass was placed on a robotic manipulandum that subjects would hold onto. Subjects would make reaching movements to four different targets at six different speeds with four different masses added to their hands. B. Neuromechanical model of the arm with two joints and eight muscles. C. A flow chart describing calculation of metabolic and neuromechanical effort representation.	114
6.2 Correlation coefficients of representation predicting metabolic rate. In both plots the x axis is representation, with metabolic representations on the left and neuromechanical effort representations on the right. A. Computed R^2 values for the best fit minimizing Active State squared. B. R^2 value as a function of the minimization parameter and the predictor variable for a linear fit. Each bar is a different minimization function, and each grouping is a different neuromechanical effort representation.	123

6.3 Linear model fits between the metabolic representations and the collected metabolic rate data. In each panel the solid line represents the linear model, and the shaded region shows the standard error bounds of the linear model, and the dashed line represents the line of unity. Each data point is colored by mass added at the hand. One data point (movement duration = .54, net metabolic rate = 295) is removed from this figure to improve visualization, but it is not removed for any linear models or analyses. A. The Bhargava 2004 model (18). B. The Umberger 2010 model (180). C. The Uchida 2016 model (179). D. The Lichtwark 2005 model (114). E. The Margaria 1968 model (127).	125
6.4 The linear model fits for the four neuromechanical variables and their squared counterparts when minimizing active state squared. In each panel the solid line represents the linear model and the shaded region shows the standard error bounds of the linear model. The data points are colored by mass added at the hand. Panel A, B shows torque and torque squared, C, D muscle force and muscle force squared, E, F muscle active state and muscle active state squared, G, H neural drive and neural drive squared.	126
6.5 Parameterization values for each representation. Each Value shown mean \pm standard error. In this plot we show the scaling of mass, c , and time, d for each representation. If the parameterized value is not different than the parameter from metabolic rate as determined by equation B.52, it is indicated with a *.	129

6.6 Parametric curves for metabolic rate, metabolic representation, and select neuromechanical representations. Data points indicate the metabolic rate or calculated representation, and lines indicate parametric fits. As the scale for the representations may not be very good, the linear model is applied to each parametric fit to get each representation on the same relative magnitude to metabolic rate. This allows us to see how each representation scales with mass and time when compared to the metabolic data and metabolic rate parametric fit. A. Metabolic Rate. B. Bhargava Model. C. Umberger model. D. Uchida Model. E. Lichtwark Model. F. Margaria model. G. Torque ² . H. Active State ² . I. Neural Drive ² .	133
A.1 Alternative model SSE comparisons to preferred reaching speed. Exact SSE's can be found in the text. Each color represents a single model. Here we compare six models to preferred duration. Four are utility maximizing models, and two are effort minimization models. We test the utility from earlier shown in equation 4.5. Utility net is the same formulation as the previous utility, except the effort term is net metabolic cost instead of gross and is shown in equation A.1. We also fit a model with sum of squared torque as the effort term in the utility model (Eq. A.3). The speed accuracy with cost model is similar to our utility model, just lacking the temporal discounting of reward and effort. This formulation is shown in equation 4.7. The efficiency model is the reward gained divided by total effort (Eq. A.5). Reward here is represented by the probability of success function. Each utility model is fit with a single α value to experiment 2a and 2b, then used to predict experiment 2c. Gross cost and net cost are models that minimize the effort associated with a movement, with gross metabolic cost (Eq. A.6) and net metabolic cost (Eq. A.7). These two models have no α value fitted, as these models are derived from the metabolic data.	163

A.1 (A) Sum of squared errors for each individual experiment and model. We find that our utility model (Eq. 4.5) does a good job across all three experiments, but maybe not the best. Utility net also provides a comparable SSE across all three. Utility with torque² has a poor representation of the movement durations. The speed-accuracy with cost model does a comparable job to the utility model with gross and net cost, however this model may be poor because for experiment 2c this model is only affected by cost and not by the speed-accuracy trade-off. Gross cost and net cost only provide good predictions for one experiment. Gross cost predicts experiment 2c well, and net cost predicts 2b fairly well, but not the others.

(B) By summing the error across three experiments, we can see that the utility models (baring torque2) provide the highest explanatory power of preferred duration.

Utility with gross metabolic cost and net metabolic cost both provide low SSEs. The model for speed-accuracy with cost provides the lowest SSE, but it is driven by experiment 2a and 2b and may not be a valid model for experiment 2c. Minimizing gross cost and net cost provide poor explanation of all three experiments.

(C) The same plot as panel A, except with normalized to 0 kg added durations. We see this is where gross and net metabolic cost have good predictions and have comparable predictions with utility.

B.1 A. Subjects were in a seated position while collecting metabolic data. Mass was placed on a robotic manipulandum that subjects would hold onto. Subjects would make reaching movements to four different targets at six different speeds with four different masses added to their hands. Metabolics was collected over the whole trial, but we used only the last three minutes in data analysis. B. Diagram of the simulated arm and the eight different muscles. C. A flow chart showing where the neuromechanical proxies are calculated.	169
B.2 Example traces for muscle force (A), Active state (B), Neural Drive (C), and the Energy model (D). All example plots are for a reach towards target 2 at the fastest speed when minimizing Active State Squared. Muscles are colored to match the arm diagram in Figure B.1.	170
B.3 Modeling flow chart for simulating reaching movements.	171
B.4 Target Orientation from start position (home).	173
B.5 Movement trajectories compared to model simulation using minimum jerk trajectories. Dashed lines represent the simulated movement, solid lines represent the average of the metabolic data, and shaded bars are one standard deviation from the mean. Each column from left to right is increasing in added mass to the hand (0 kg, 2.27 kg, 4.55 kg, 9.90 kg). The top row shows the distance from initial positions as a function of time. Bottom row is velocity as a function of time. The lines are color coded by the intended movement duration with darker (purple) representing shorter durations and lighter (yellow) lines longer movement durations.	174
B.6 Diagram for variables in the inverse dynamics of a two-link arm using Euler angles and the Lagrangian Method (165).	178
B.7 Diagram of the 8 simulated muscles and which muscles they represent.	183
B.8 Muscle moment arms and lengths.	186
B.9 Length dependence of maintenance heat rate used in equation B.35. This graph is from Bhargava (18).	195

Chapter 1

Thesis Objectives

1.1 Introduction

Every day we make hundreds of goal-directed movements under a range of circumstances. For each task, we must choose which movement to make to achieve our goal. For example, if a person wanted to summit a mountain, how would they complete the task? Would they run up the mountain as fast as they could or take a slow and steady approach all the way up? When reaching for an apple on the table, would a person reach slowly or more vigorously? When making these movements humans can control a number of things, such as their movement vigor (defined as the movement duration, reaction time, and peak velocity), final endpoint, what path they take, the muscles they activate, and much more. When humans make arm reaching movements, the kinematics of these movements look very similar across a population (55). This similarity has led to the proposition that there is some common metric that humans share that is optimized for when making movement decisions. This common metric can be thought of as the utility, or goodness, associated with the movement (166). Current theories propose that we choose our movements such that we attempt to maximize their utility, and that this utility is composed of the reward one expects to acquire minus the effort associated with acquiring the reward. This thesis explores how reward and effort can affect movement vigor, and how we can use modeling techniques to estimate effort.

1.2 Specific Aims

In this dissertation, I focus on the effects of reward and effort on movement vigor and on whether a decision-making framework can explain those effects. I also investigate how well neuromechanical effort representations and metabolic representations can represent the metabolic rate of arm reaching.

- AIM 1 (chapter 3): Examine the role of reward expectation in selection of the vigor of reaching movements.
- AIM 2 (chapter 4): Measure the effects of added mass on the metabolic cost of reaching.
- AIM 3 (chapter 4): Quantify the effect of increased effort on the vigor of reaching movements.
- AIM 4 (chapter 4): Explain movement preference using metabolic cost and a utility framework.
- AIM 5 (chapter 6): Determine the accuracy of multiple effort and metabolic models in predicting the metabolic cost of reaching.

1.3 Chapter 2 - A decision-making approach to understanding movement vigor

According to this utility framework, humans and other animals attempt to maximize the expected utility which is represented by the sum of the reward in the movement minus the sum of the effort. Chapter 2 explores and develops this utility framework and the effects of reward and effort. As reward increases, one would expect movement vigor to increase as well. Reward has been consistently shown to affect movement kinematics and vigor. Increasing or adding reward tends to reduce reaction time and increase velocity when making saccades or reaches (135; 173; 175; 199). However, less is known about when this reward is less deterministic, and more probabilistic. In saccades we do see that as the expected value of a movement increases, saccadic reaction times

decrease (135). However, recent evidence indicates that subjects are not affected by reward but primarily affected by reward prediction error (162). We generally expect that as reward increases movement vigor will increase as well.

The complementary effect to reward, effort is generally labeled as the cost of making the movement, though it is hard to quantitatively represent. Movement choices, including reaching speed and preferred direction, have been shown to be affected by effort in arm reaching where subjects tend to reach in low effort directions and reach faster in those directions as well (35; 63). While the effect of reward on decision making has been extensively studied, the role of effort and its neural representation is decidedly less understood. Thus, a long-standing question is how humans represent effort when making these movements. Metabolic cost has become a common representation of effort (152; 166), and the minimum metabolic speed has been shown to match preferred walking speed (152). Metabolic cost has recently been used in arm reaching to show that over time humans can learn to optimize this cost and that speed and distance reached can affect reaching metabolic rate (92; 166). In reaching movements, the relationship between preferred reach duration and metabolic cost has not been investigated, unlike walking.

1.4 Chapter 3 (AIM 1) - The effects of reward expectation and reward prediction error on movement vigor

To address AIM 1, we apply a probabilistic reward paradigm to arm reaching movements in chapter 3. Subjects make a series of arm reaching movement to targets that were rewarded 0%, 33%, 66% and 100% of the time. We evaluate how expected value, reward history, and reward prediction error affect movement vigor. Interestingly, we find that expected value does not affect reaction time but does increase peak velocity. More specifically, reward history and reward prediction error may play a large effect in determining movement characteristics in arm reaching.

1.5 Chapter 4 (AIMS 2 - 4) - The role of effort in determining preferred movement speed

To determine if metabolic cost can predict optimal reach duration, we completed two experiments and developed a computation model presented in chapter 4. The first experiment determined how mass and speed affect the metabolic cost of reaching movements and whether there is an optimal speed that minimizes the cost. In the second experiment, subjects make reaching movements unconstrained by time across a range of masses to find if increasing effort affects movement speed and duration. By comparing the results of these two experiments, we find minimizing metabolic cost alone cannot predict the preferred reaching speed. However, a utility framework that maximizes the trade-off of reward and effort can predict movement duration across multiple experiments.

1.6 Chapter 5 - An overview of musculoskeletal modeling of movement

Because metabolic cost is often difficult to measure in single movements, frequently a proxy is simulated from a biomechanical model of the task to estimate effort or metabolic cost (15). These models simulate the dynamics of movement by estimating muscle forces needed to reproduce the movement. The background for the use and development of musculoskeletal modeling is shown in chapter 5. There are many steps to accurately simulating movement including calculating joint torques using inverse dynamics, modeling muscle properties, estimating neural drive from activation dynamics, and simulating metabolic rate. These models solve the under-determined system by minimizing one of many possible objective functions. Models estimate the effort (or metabolic cost) of a movement through many representations ranging from joint torque (183) to energy use in activated muscles (179; 180). The use of simulated metabolic cost has become very common in biomechanics research, but the validation of these metabolic representations has only recently been attempted (107; 131). This validation has shown promising results in walking, where these metabolic representations show a decent approximation of metabolic rate though this validation has yet to be completed for arm reaching.

1.7 Chapter 6 (AIM 5) - A validation of metabolic energy models in arm reaching

Using metabolic rate in arm reaching is a relatively new paradigm, and thus the validation has yet to be completed. In chapter 6, I address AIM 5 by developing a biomechanical arm model and simulate the metabolic rate of arm reaches. We use kinematic and metabolic rate data across and range of masses and speed along with a biomechanical model to determine the accuracy metabolic representations. We find similar results to walking but highlight some important short comings of the metabolic representations. Specifically, we found that these metabolic representations vastly under-predict the effect of very fast movements in arm reaching.

1.8 Significance

This research adds to the body of knowledge of how reward and effort affect movement choices. These data sets show how humans respond to reward and effort, while also providing a possible simpler method to estimating effort in arm reaching studies. Specifically, we show new examples of where minimizing cost of a movement does not predict movement speed while a utility framework can. We expand this utility framework by adding information about how expected value affects our choice to move and how reward prediction error may be a large driving force of movement vigor. These results can help us understand what drives and motivates movements, and how we can better treat pathological gaits and other movement disorders. Last, we validate multiple representations of effort and metabolic rate using a neuromechanical arm model and show some possible weak points of these representations. This will allow researchers to make more rapid and accurate predictions of cost in movement studies, primarily in arm reaching.

Chapter 2

A decision-making approach to understanding movement vigor

2.1 Utility

To help explain our movement choices, it has been proposed that, similar to an economic decision, movements are chosen such that the utility, or goodness, of the movement is maximized (167). The challenge lies in finding what aspects of a movement determine its utility. In economic decision making, utility is often determined by the sum of the expected monetary gains and losses. Similar to an economic decision, every movement leads to some gain (task completion and reward) and a loss is incurred via the effort associated with completing that movement. Thus, the framework of movement utility assumes that movement choices are considered based on the total reward to be obtained minus the amount of effort it would take to obtain that reward. There are many factors influencing how we evaluate the reward and effort of a given movement. To describe these factors, we start with the following equation:

$$J = \frac{R - E}{1 + \gamma T} \quad (2.1)$$

where R represents the reward for completing a movement, E the effort of the movement, γ is a discounting factor, and T the time to complete the movement. In the following sections I explain each of these terms, how they can be represented, and how they affect movement decisions.

2.2 Reward

2.2.1 Reward Decision Making

Bernoulli was one of the first people to propose the concept of utility in human behavior through changes in utility due to the current state of an individual (14). He proposed a simple example to explain how utility may not reflect explicit reward in decision making. Take two people, one with \$1000, and the other with \$10. If both were given another \$100, who would have the largest change in utility due to the increase in money? This leads to the main theory that "the utility resulting from any small increase in wealth will be inversely proportionate to the quantity of good previously possessed." Using that, it would follow that for the person starting with \$10, the increase in utility would be much greater. The next step in defining utility comes from how people evaluate utility under risky choices.

Kahneman and Tversky used the framework from Bernoulli and conducted an experiment where the reward for choices were also probabilistic (100). Subjects would make choices on multiple risky choices, and then this was compared to what the expected value theorem would predict (5). For example, one choice was as follows:

Choice A	Choice B
• 4,000, p=0.80	• 3,000, p=1.00

They tested 95 subjects, and 80 of them chose choice B. However, the expected value theorem would predict otherwise as the expected value of option A is 3,200 while the expected value from option B is 3,000. There is clearly something about the weighting of the choices that is not optimal for subjects' decisions in terms of pure gain in value. This is deemed the certainty principle, that subjects tend to prefer higher probability choices compared to lower probability choices even though the lower probability choice may have a higher value. Another effect, called loss aversion or the reflection effect, where subjects value losses more than gains in economic decisions is also demonstrated. In the end Kahneman brings up value and how this relates to gains and losses. The

main theory proposed by Bernoulli and Kahneman is that as gains and losses increase, the value of those choices change slower. A gain of 1 vs 2 has a greater difference in value than a gain of 2 to 3. This known as the law of diminishing returns (129). This leads to the idea that every choice may have a subjective value associated with them, that is not the mathematically optimal solution.

For a movement task we can view the reward as the implicit value gained from completing the movement and the losses as the effort associated with completing the movement.

2.2.2 Quantifying reward

We can see that reward has some impact when making financial decision, but how are movements and other choices affected? To include reward into a utility model we first need to know how to quantify reward. Many studies have shown that animals and humans can respond to a multitude of rewards. Walton et al. trained rats on different amounts of food pellets, Smith et al. used sugar water to train rats, and Summerside et al. showed effects of an auditory reward having an effect on movement (170; 173; 185). Reward can take many forms such as food (185), information (198), or an auditory stimulus (173) and that reward can be used to incentivize movements or decision making.

Altering reward can be done in multiple manners, but can these currencies be traded? Green (67) trained rats to press a lever to choose between pellets and water with a certain number of lever presses for each. In this paradigm water and pellets were the reward, and lever presses the effort. When the number of key presses the rats had to do to acquire water or pellets, the relative spending was reflected by change in effort. This experiment demonstrated that both of the rewards could be represented by some common currency, the number of pellets. Getting the exact value of these rewards however is difficult, so often some quantifiable measure is used. For humans, a monetary reward is often used. Levy and Glimcher (112) ran an experiment to test how money correlates with water and food rewards. They found that the value of the monetary rewards was correlated to that of the food and water rewards. In rats and humans, we see that the value of a reward can be evaluated and then traded for other rewards. While these rewards are generally

given with a short time delay of the task, the utility framework has a component of time that may affect how reward is evaluated. In the next section we will see how time affects reward evaluation.

2.2.3 Temporal Discounting of Reward

What happens however when rewards are not instantly granted? Samuelson (159) proposed that rewards later may not be as valuable because of uncertainty in gaining that reward. If we wait for a reward, were not 100% sure that the reward will come. Mazur (128) evaluated how this risk affects decisions in pigeons. The birds would make choices between feeding for set amounts of time with set amounts of delay before they could begin eating. He showed that as delay increased for a decision, the preference for that decision would also decrease. This tendency is termed temporal discounting, that a preference for reward later decreases as time passes.

This phenomenon of temporal discounting has also been demonstrated in humans (19; 57; 71; 109; 142). But there may be many external motivators for how humans discount reward with time such as family background, early cognitive ability, and the home environment (31; 187). However, we still want to integrate temporal discounting into the utility framework. Myerson (142) proposed two forms of modeling the temporal discounting rate, exponential (159) and hyperbolic (3; 128). Exponential discounting is more associated with risk involved with not attaining the reward and takes the form in eq. 2.2. Hyperbolic discounting takes the form in eq. 2.3. In both equations V is the value of the reward at the current time, A is the amount, D is the delay, and k is the hazard rate. Myerson shows that hyperbolic discounting generally predicts subjects' choice preference more accurately than exponential discounting. In these equations, V is the value of the reward after time T, A is the initial value of the reward, and k is the discounting rate.

$$V = Ae^{-kT} \quad (2.2)$$

$$V = \frac{A}{1 + kT} \quad (2.3)$$

Every movement made requires some amount of time to execute. From sending the signal from the CNS to the muscles to generating torques to completing the movement takes time. As this time increases, the value of that reward decreases due to temporal discounting described early (142; 168). Studies have shown that movement vigor and temporal discounting rate are linked (19; 31; 168). These find that subjects who are more impulsive, also have a relatively high vigor in similar movements (saccades). To reduce the loss from completing a movement, subjects increase their vigor to attain the reward quicker. People who are impulsive have very steep discounting rates, thus they tend to complete their movement quicker as to not lose as much of the value. However, this leads to a trade-off of reward and vigor. Where the more reward one can get from completing the movement, the more effort a subject needs to invest to increase vigor.

These results show that decision making and movement can be altered by reward in multiple manners across different populations. Increasing reward generally leads to an increase in vigor and an increase in accuracy, but there is some cost of time with temporal discounting and some effect of risk assessment.

2.3 Effort

2.3.1 Representing Effort

To gain any amount of reward through movement, some effort needs to be expended. The utility framework proposes that subjects consider both the amount of reward to be attained and the expected effort to gain that reward (166). There is some interaction between reward and effort that is currently being explored in decision making and movement (37). However, it is relatively unclear how the brain evaluates and represents effort in movement as there are many possible ways effort may be represented. To begin to quantify effort, we first need to define what effort is.

Effort can take either cognitive or physical forms depending on the task presented (166; 189). Cognitive effort can be better defined as the level of engagement with demanding tasks (189). There are many factors that can influence cognitive effort such as difficulty, motivation, attention,

or control. Cognitive effort however is not any single one. Physical effort results from the process of creating mechanical force in muscles which requires some change in chemical states (47). How effort is represented is very important to determining the effects on the task. For example, playing a game of chess may be very cognitively demanding and not physically difficult, while running is very physically difficult and not necessarily cognitively difficult. Here we focus on representing and quantifying physical effort.

As we describe the factors that influence movement utility, our primary concern is the representation of physical effort. Physical effort costs are generally easier to quantify than cognitive effort but can still take many forms. The effort in a movement can be estimated by many things such as the number of key presses, grip force, resistive forces while moving, metabolic cost, and many others (15; 67; 73; 139; 166). Green et al. found that the number of required key presses can influence economic trade-off decisions in rats (67). Grip force has also been shown to be a reliable effort cost, influencing how much effort an individual is willing to invest to gain a monetary reward (73).

An important question in these studies is how the subjective value of effort varies with the objective value of any given effort metric. For example, does a grip force of 100N feel double the effort of a grip force of 50N? Or does it feel more or less than that? Hartman et al. showed that when using grip force as an effort metric to earn reward, a parabolic subjective valuation model best predicted outcomes (73). Similar results were found by Morel et al. using resistive forces in movement to quantify subjective effort and suggests that the 100N would be more than 2x more difficult than 50N. (139). These metrics all measure an external variable from movement; however indirect measures of effort can be estimated from internal models of the joints and muscles simulated from the movement dynamics.

There are many internal models that can be used to estimate effort in movement. A common indirect measure of effort in the field of computational motor control is the integral of torque about each joint. The integral of torque about each joint has been a long-standing estimate for cost, and multiple variations on this torque-based measure of effort exist. Sum of torque squared is a common

representation and the sum of rate of torque change has also been used (15; 183). Kistemaker et al. showed that the integral of endpoint force squared poorly represents how subjects choose to make reaching movements (106). These estimates are calculated from joint and endpoint forces, but simulations of individual muscles are also used.

Estimates of effort can also be calculated by integrating some variable of individual muscles. Collins et al. tested multiple approximations for effort including total muscle force, total squared muscle force, and total muscle stress (33). Berret used mechanical work of the muscles to estimate effort (16). Instead of using muscle force or joint torque, Li et al. estimate effort from the signal sent from the central nervous system to the muscle groups (113). These metrics are generally calculated using a musculoskeletal modelling approach which is discussed in chapter 2.

Across a range of fields, including behavioral ecology and locomotion energetics, the energy the body expends to complete a movement has been widely used as a representation of effort (92; 138; 152; 166; 167). In the next section I will describe what metabolic (energetic) rate and cost are and how it varies with movement demands.

2.3.2 Metabolic Rate

A common metric used to determine the effort of a movement is the amount of metabolic energy expended to complete a specific task (166). To complete a movement, animals and humans both need to convert chemical energy to mechanical energy through either aerobic respiration or anaerobic respiration. In both cellular respiration methods, energy is converted by changing the chemical states of fat, carbohydrates, protein, and oxygen (O_2) to energy (ATP), carbon dioxide (CO_2) and other waste products. The different cellular respiration methods produce different amounts of energy per energy source. The exchange between O_2 to CO_2 is relatively constant in aerobic respiration; using indirect calorimetry we can attain an estimate of metabolic rate.

Indirect calorimetry is the method to determine energy usage by measuring the changes of chemical concentrations in expired gas. Here we deal with only aerobic respiration as indirect calorimetry cannot account for parts of the anaerobic respiration process (24; 103; 117). The

equation to estimate metabolic rate assumes a constant exchange between O_2 and CO_2 , which does not apply to anaerobic respiration. The general form of the equation is shown in equation 2.4. In this equation \dot{E} (joules/sec) represents the metabolic rate, \dot{O}_2 is the rate of oxygen consumption, \dot{CO}_2 is the rate of carbon dioxide production, and N is the amount of excreted nitrogen. The constants c_1-c_3 are determined on a per species basis (103).

$$\dot{E} = c_1\dot{O}_2 + c_2\dot{CO}_2 - c_3N \quad (2.4)$$

Subjects need to be at a metabolically steady state when computing metabolic rate. Metabolic rate data needs to be collected over a period of time greater than 2 minutes and averaged over that time to attain a good estimate of metabolic rate. Movements are generally completed at a steady work rate for more than 2 minutes, and only the last two minutes of data is used to compute metabolic rate. This is due to the lag of metabolic rate to external work. The metabolic rate of movement changes about 30-60s after the external work begins. This leads to the difficulty in estimating metabolic rate for single movements, as the single movements generally take much less time than 2 minutes.

There are several common reported metrics for metabolic rate or cost. The metabolic rate, the metabolic cost, and the metabolic cost per distance (COT) are three of the most common metrics. Metabolic rate is calculated as shown in the previous paragraphs (eq. 2.4). Total metabolic cost is the metabolic rate of the movement integrated over time. Metabolic cost per distance is calculated by integrating the rate over time, then dividing by distance traveled. In most studies, metabolic cost or rate is normalized to subjects' body mass. We want to determine the effect of speed, mass, and movement pattern (e.g., sloped walking and reaching) on metabolic rate to lead us to better understand what affects effort and movement decisions.

2.3.2.1 Altering Metabolic Rate

Speed has long been studied as a way to alter metabolic rate (152). Ralston et al. found that the metabolic rate of walking increased linearly with velocity squared. In running, there is a similar trend that increasing speed will increase metabolic rate. This has historically thought to be a linear increase with average velocity, but recent work has shown that it may be a curvilinear increase with speed instead of a linear increase (11; 152). Changing the speed of a movement can change the metabolic rate of the movement.

Changing the mass of an organism or how much mass a subject needs to move may also change metabolic rate. West et al. theorized that mass would scale metabolic rate; and shows that metabolic rate scales with body mass to the $3/4$ power (188). Bastien et al. tested the effect of adding mass on metabolic rate in human walking by adding a percent of body mass to subjects walking with a backpack (10). They report that metabolic rate increased for a given speed depending on the amount of mass added. Adding mass at different locations of the body also increases metabolic rate, and the more distal a mass is placed, the larger the increase metabolic rate (27). Reducing body weight or mass in walking reduces the metabolic rate of walking, while increasing the amount of weight the body supports or the amount of mass the body redirects can increase the metabolic rate (66).

Walking and running on different slopes has also been shown to alter metabolic rate. For a given speed, increasing the slope at which subjects walked increased the metabolic rate; and walking downhill tended to decrease the metabolic rate (137; 138). These studies mainly deal with walking or running, though other types of movements can also be used for altering metabolic rate or cost.

Recently, metabolic rate has been measured in arm reaching (92; 166). Work from our lab has shown that for a given movement duration, metabolic rate increases with movement distance and speed (166). It is unclear, however, how the metabolic rate of reaching scales with direction and mass. Some studies show that metabolic rate increases in a sublinear fashion with increasing body

mass (166; 188). We expect to see sublinear increases in mass lead to increases in the metabolic rate of arm reaching.

Running, walking, and cycling are commonly used as paradigms to research metabolic rate; but all three have much larger changes over resting metabolic rate compared to reaching. In arm reaching, metabolic rate is difficult to collect due to the changes in metabolic rate from resting as arm reaching is not a highly physically demanding task. Measuring metabolic rate of single movements is also difficult or impossible using aerobic respiration, so often an alternative representation of effort to metabolic rate is used.

2.3.3 Alternative Representations of Metabolic Rate

When experimenting in decision-making paradigms, subjects are presented with different movement choices and are instructed to choose one and then make that movement. These choices have varying rewards and effort costs associated with them. To use metabolic rate as a measure of effort though, subjects would need to make the decision, then complete that task repeatedly for 2-3 minutes to reach a steady metabolic rate (117). This is impractical and thus measuring the metabolic rate of single movements is difficult, leading to the use of simulated biomechanical models to estimate effort for a single trial (15). These models range from the sum of torque around each joint to energy liberation in human muscles (15; 179; 183).

The most common metabolic rate representations attempt to estimate metabolic rate in the muscles from shortening/lengthening heat (energy) rates and activation/maintenance heat (energy) rates (18; 41; 179; 180). These metabolic rate models consider many muscle properties and scale them depending on heat rates of shortening and lengthening contractions. The most basic model assumes that muscles are 25% efficient at converting chemical energy sources into mechanical energy sources for shortening (concentric) contractions. This model also assumes that muscles are 120% efficient during lengthening (eccentric) contractions (4x more than shortening) (56; 181). More complicated models also take into account how much energy it takes to keep muscles activated, as an estimation of cost from the central nervous system. There is also some amount of mechanical

work to move the joints and muscles that is taken into account. These energy models take the general form shown in eq. 2.5, with \dot{E} representing the metabolic rate, \dot{h}_{SL} being the shortening and lengthening heat rate, \dot{h}_{AM} the activation and maintenance heat rate, and \dot{w} the amount of mechanical work. These will be discussed more in a later chapter in this dissertation (5.6).

$$\dot{E} = \dot{h}_{SL} + \dot{h}_{AM} + \dot{w} \quad (2.5)$$

In this section I have described the various ways in which effort is represented in movement and decision-making research: from key presses to grip force to sum of joint torques to metabolic rate or cost. A wealth of evidence in both humans and other animals suggests that metabolic cost is a reasonable representation of effort, albeit difficult to measure. Thus, we will substitute the effort term in the movement utility equation with an expression for the metabolic cost of movement. Now that we have an expression for utility describing the interactions of effort and reward, we want to determine the effects of reward and effort on movement characteristics.

2.4 Effects of Reward and Effort on Movement

2.4.1 Utility - Combining Reward and Effort

Once we have representations of reward and effort, how do they interact to determine the utility, or goodness, of our movement choices? First, we take all the rewards and all the effort associated with a movement into account. The rewards and efforts of a movement are both integrated or summed and then both discounted by time. This is represented by equation 2.6. In this equation J (joules/sec) is utility, R (joules) is reward, E (joules) is effort, γ is a temporal discounting factor, and T (seconds) is time or movement duration. The reward (R) is represented in many ways as discussed in section 2.2.2, and effort (E) represented as discussed in section 2.3.1.

$$J = \frac{R - E}{1 + \gamma T} \quad (2.6)$$

In this framework, subjects do not maximize the reward or minimize the effort, subjects try to maximize the total utility gained from the movement (167). Reward is discounted by time, as future reward is devalued by how much time will elapse to receive the reward due to the unpredictability of receiving it (142). This movement utility framework assumes that effort is discounted in the same way, that expending the same amount of energy later has a smaller negative utility. As task success is required to attain the reward, reward can also be scaled by the probability of task success similar to the expected value of the outcome or the speed accuracy trade-off (40; 135). The speed accuracy trade-off shows that as a subject moves faster, the probability of task success decreases.

Effort can be represented by a function of metabolic cost, parameterized by mass (m), distance (d), and time (T) (166). The metabolic cost of the movement, E , is the total cost of the movement (joules). Mass is represented as the effective mass of the arm (kg), distance as how far the subject moved (m), and time to complete the movement (sec). This is calculated by multiplying metabolic rate by movement duration (eq. 2.7).

$$E = a_1 T + \frac{a_2 d^{a_3} m^{a_4}}{T^{(a_5 - 1)}} \quad (2.7)$$

The final form of the utility model for arm reaching is shown in equation 4.5. The probability of reward, $P(R|T, m, d)$, may be affected by movement duration, mass, and distance. The probability of reward can be calculated using inverse logistic regression from the kinematic data. The mass of the movement is represented by m , distance by d , and a_1-a_5 are fitted parameters from metabolic data.

$$\begin{aligned} \text{Utility (J)} &= \frac{R - E}{1 + \gamma T} \\ &= \frac{R * P(R|T, m, d) - \left(a_1 T + \frac{a_2 d^{a_3} m^{a_4}}{T^{(a_5 - 1)}}\right)}{1 + \gamma T} \end{aligned} \quad (2.8)$$

2.4.2 Utility Framework Predictions

The next question regards what happens to the utility of a movement when you alter reward or effort, and also how does reward and effort affect the optimal movement durations. What predictions can we make about altering reward and effort regarding movement duration? Shadmehr et al. provide a computational model for how utility is affected by reward and effort, and what utility can tell us about self-selected movement durations (166). Figure 2.1 shows how altering reward and effort can affect the total utility of a movement and thus the optimal movement duration.

In the utility framework, if we increase the initial reward the utility will also increase and shift the optimal duration lower (faster movement, fig. 2.1B). The inverse is also true; decreasing reward predicts slower movement durations by shifting the optimal duration higher (slower movement, fig. 2.1B). The utility framework's predictions for effort are similar but opposite to reward. Utility predicts that increases in effort will increase the optimal movement duration (slower movement, fig. 2.1C), and decreasing effort will decrease the optimal movement duration (faster movement, fig. 2.1C).

2.4.3 Effect of Reward on Movement Vigor

Now we know that our decision-making process can be altered by the amount of reward and time involved with a decision, the next question is how are movements affected? If we consider movements to be a decision, one should expect to see similar relationships as previously discussed. A metric used to determine how movements are affected is termed vigor, it is represented by the time to acquire a reward including the reaction time and movement duration (31; 155; 166; 173). Vigor can be reaction time, movement duration, velocity, or other movement related metrics. We are interested in the effect of reward on movement vigor.

Eye movements (saccades) are good movements to study the effects of reward, as under normal conditions the velocity of saccade is easily predictable by the main sequence (9). Takikawa

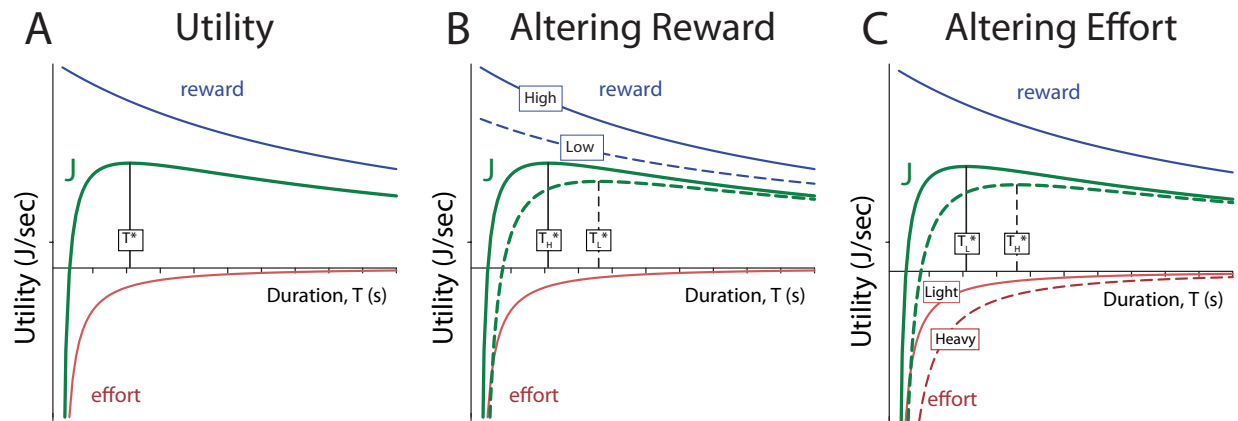


Figure 2.1: How utility is affected by reward and effort and the effects on optimal movement duration. Adapted from Shadmehr et. al (166). J is the total utility of the movement given a movement duration. T^* represents the optimal movement duration. A. The base utility framework predicts when combining reward and effort. B. How the movement duration predicts change when altering reward. Higher reward leads to lower predicted movement durations. T_H^* represents the optimal movement duration for high reward, and T_L^* for low reward. C. How movement duration changes with effort, where higher effort leads to higher predicted movement durations. T_H^* represents the optimal movement duration for a heavy mass, and T_L^* for a light mass.

showed that non-human primates will saccade faster towards more rewarding targets (more juice) and will also initiate the movement earlier (175). This type of behavior has also been shown in humans as well. Xu-Wilson had subjects saccade to different types of pictures such as a face, a bench, and a noisy image (198). He found that subjects tended to have higher saccade vigor when moving to a face rather than a noisy image, indicating that information has some intrinsic value, and this modulates vigor. The effect of reward is not only specific to movement speed and initiation though in saccades. Manohar also showed that saccades were also more accurate when reward was paired with the saccade in the presence of some distractor (125). Other types of movements may also show this response to rewarding stimuli. Altering the reward with an auditory-visual stimulus in arm reaching tasks can also increase the vigor at which people move (173). Summerside et al. find that humans are faster and are more accurate reaching towards targets when they expect an auditory and visual reward for completing the movement. Completing these tasks and movements also take some amount of time and effort to be invested to attain the reward. We next want to know how effort can affect movement behavior.

2.4.3.1 Reward History and Reward Prediction Error

We have seen that reward can affect movement vigor on a single movement, but an interesting question is how history of reward can alter multiple movements. To explain how reward history may affect movement vigor and choices we look towards foraging theory (29; 199). Foraging theory posits that as the average reward rate within an environment increases, we should also see an increase in movement vigor within that environment. Applying this to reaching studies, we would expect that following a rewarding outcome or as reward increases/decreases through the experiment that movement vigor will follow suit. Summerside et al. examined this but found that while reward affected the current movement, generally there were no lasting effects on subsequent trials following that reward.

One possible reason is that subjects tend to only care about whether their expectation of the outcome aligned with that outcome (162). We define this as reward prediction error (RPE), the

difference between the reward acquired and the expected value of that reward. Reward prediction error has been not only shown to modulate dopamine signaling but also saccade vigor (13; 161; 162). Following a positive reward prediction error (a good outcome), Sedaghat-Nejad et al. found that the vigor was highest and on negative reward prediction errors (bad outcome) had the lowest vigor saccades. Within our utility framework we are interested in exploring how the expected value and history of reward can impact movement choices.

2.4.4 Effects of Effort on Behavior

Once we have a measure for effort, we want to determine how effort affects movement decisions. The utility framework can make predictions on the effect of effort on behavior. When presented with the option of two movements for the same reward, one will choose the movement that has the lowest effort cost. We would expect that increasing the effort of a movement would increase preferred movement durations and also affect gait patterns in walking and running.

The idea of minimizing metabolic (energetic) cost has been widely studied using walking speed or gait pattern as the optimization variable. While walking, humans tend to prefer to walk at speeds that minimize the gross metabolic cost of transport (152). Ralston et al. show that the metabolic cost of transport as a function of walking speed is parabolic; there is a speed at which metabolic cost of transport is minimized and that people tend to select a walking speed around this minimum. Adding mass to horses increased the metabolic cost of transport of trotting and decreased the preferred trotting speed for horses (191). This trend is also seen in humans, where adding mass reduced the preferred walking speed (93). Sloped walking studies have shown that increases in slope increase the metabolic cost of transport while walking (138), and changes to slope angle affect the speed at which subjects choose to walk (137). Together these studies highlight the important role metabolic cost plays in determining movement speed. These were tested using a single gait pattern (i.e., walking or trotting) for the person or animal, but subjects may alter their choice of gait depending on effort costs.

Selection of gait may reflect the tendency to reduce effort in movement. Hoyt et al. show

that horses tend to choose their gait patterns that minimize the total metabolic cost of transport (91). This tendency has also been shown in humans, where subjects choose to transition from running to walking at speeds where the two were energetically similar (43). In split-belt treadmill walking, subjects tended to adapt gait patterns that aligned with a metabolic minimum by altering asymmetry and leg work (160). Thus, in walking, these studies show that animals and humans implicitly choose gait patterns that align with a desire to reduce metabolic cost.

Walking may be viewed as an unconscious choice when moving. How is the desire to reduce effort shown when subjects make choices? The tendency to move in manners that reduce effort can also be seen in arm reaching studies (63). Goble et al. tested subjects making directionally free arm reaching movements. They found that subjects tended to reach in directions that minimized the intervention of muscle torque for regulation of the interaction torques. This meant that subjects tended to reach in directions where the effective mass (166) of the arm is lowest (45° and 225° off right horizontal). In arm reaching this is generally termed the inertial ellipse of the arm. The inertial ellipse of the arm describes the arms resistance to force given a direction. A force applied to the hand at 45° and 225° direction off right horizontal will move the hand faster than if the force was applied in the 135° and 315° off right horizontal. Goble showed that subjects tend to reach where this size of this ellipse is smallest. When adding more mass to the arm, it only increased the bias along this ellipse (186). This has also been demonstrated in a more constrained two target arm reaching task (35). Similar to Goble et al., Cos et al. showed that target location influenced preference of reaching direction because of the biomechanical properties of the arm. This reach direction preference was shown to also affect movement vigor (velocity, accuracy, etc.) (64). Subjects reached further, reached faster, and accelerated faster in the direction of the inertial ellipse that was smallest. Altering inertial properties of the arm may not be the only method of increasing effort in reaching or movement tasks.

Another method to alter effort could be to increase accuracy costs, which reduce the speed of cognitive and motor tasks (40). The more accurate subjects need to be the more effort subjects would need to expend to complete the task with similar movement speed. Dean et al. show that as

the accuracy costs increase, the speed at which subjects make reaching movements also decreases. In saccades, reward has been shown to 'pay the cost' of the increased effort due to accuracy (125). This study showed that when reward is increased, subjects can overcome both the costs of speed and accuracy to complete tasks both faster and more accurately. Effort clearly has some effect on movement behavior, but it may not be the only biomechanical variable optimized during movement.

The utility framework presented suggests that humans do not choose the optimal movement trajectory or speed to minimize only metabolic cost but also take additional factors into account such as time and reward (106; 172). Summerside et al. examine how subjects evaluate the costs of time and speed when choosing between walking or running certain distances to find indifference points between these two gait patterns (172). They found that subjects choose to move in a manner that does not just minimize energetic cost but optimize a more complicated model of utility. Kistemaker et al. show that when horizontal forces are added at the hand during reaching movements to make the simulated energetic minimum not a straight line, subjects still tended to reach in a straight line. However, other simulations show that movement trajectories do minimize the simulated cost in certain conditions (176).

We have seen that altering effort can have effects on movement kinematics across multiple paradigms. When walking, subjects tend to choose speeds and gait patterns to reduce the metabolic cost of movement. In reaching, subjects choose to reach in directions where the effective mass of the arm is lowest and reach slower with added mass.

2.5 Summary

In summary, by maximizing the utility function we may be able to attain reasonable predictions of the speed at which subjects make reaching movements given the reward and effort associated with their movement. We aim to investigate how reward and effort can both affect the decisions that people make and the movement that follows as well. By altering the expected reward at the end of a movement and also how much effort it takes to make such a movement we can determine how humans respond to changing reward and effort landscapes. The next two chapters

explore these changing reward and effort landscapes and how they affect human movement vigor with the goal of integration into a utility framework.

Chapter 3

The effects of probability of reward and reward prediction error on movement vigor

3.1 Abstract

Recent findings have demonstrated in both saccades and reaches that reaction time and peak velocity speed up for greater expectation of reward (172; 175; 199). Thus far, reward is often delivered deterministically; it is certain whether a movement will be rewarded or whether it will not. However, expectation of reward can also be modulated by its probability; and increasing probability of a reward in theory should also lead to increased vigor or movements (defined by a movement's reaction time and peak velocity). It is less clear what happens when the same reward amount is probabilistically given. Further, in addition to the expectation of future reward, it has been suggested that the history of reward and the degree to which it was a surprising outcome, may have an influence on movement vigor. This degree of surprise is reflected in the magnitude of the reward prediction error, the difference between the expected outcome and the actual outcome. In this study we investigate how expected value of reward and reward history impact movement vigor. Subjects ($n=24$) made 10 cm out-and-back reaching movements to one of four cued targets, that were probabilistically rewarded. The targets with probabilistic reward allowed us to broadly categorize reaches in terms of expected value, whether they followed a rewarded reach or not, and reward prediction error on the previous reach. We found that peak velocity increased with increasing probability of reward. Interestingly, we found a strong effect of reward history as well. If a reach was rewarded, the following movement was faster, while if a reach was unrewarded, the following

movement was slower. Furthermore, we observed that even if the target was rewarded, the degree to which that reward was surprising, the reward prediction error, influenced the vigor of the following movement. Reaches following a large positive prediction error were faster than reaches following a small, yet still positive prediction error. Conversely, reaches following a surprising negative outcome (high negative reward prediction error) were slower than those following less surprising, but still negative outcomes (low negative prediction error). Taken together, these results demonstrate that reward plays multiple fascinating roles in determining the vigor of our movements.

3.2 Introduction

Many decisions in our lives are influenced by the expected reward at stake. Whether this choice is deciding between risky gambles or how long to harvest food within a berry patch, it has been shown that the choice is strongly modulated by the reward at stake (29; 100; 199). Individuals tend to choose the gamble with the higher expected reward and harvest longer in patches of higher quality (greater reward). Intriguingly, recent evidence shows that the movement to acquire reward is also affected by how much reward is at stake (125). This suggests that when deciding to move, the expected value of the reward gained at the end of a movement may be reflected in movement vigor.

When humans make movements, one of the primary goals is to acquire some reward at the end of the movement. This reward can take many forms including juice, food, money, or information. As this reward value increases, the vigor of movements tends to increase (30; 135; 147; 167; 198). When rewarded with juice, monkeys will saccade faster towards targets that are rewarded vs non-rewarded (175); humans making saccades to images that have a range of rewarding stimuli saccade faster towards high reward targets (199); in reaching humans also reach faster towards targets that flash and beep compared to targets that do not (173). This indicates that an important factor in movement is to acquire reward and reach a more rewarding state and that vigor is affected by the magnitude of reward (167).

Foraging theory may provide some insight into how reward and expected value can affect

movement vigor (166; 199). Foraging theory proposes that animals' decisions about how long to harvest rely on maximizing a global capture rate, which is quantified as the total expected reward to be gained minus the total effort to be expended, all divided by the total duration (29). Recent work has proposed an extension of this theory to explain not only decisions about how long to stay, but also decisions about how fast to go, that is, movement vigor (145; 157; 199). This decision-making framework proposes that with every movement we maximize the total utility gained from the movement, determined by the net rate of reward. Theory predicts that movements are faster towards targets when they are rewarded compared to when they are not, aligning well with previous findings (173).

While past studies have shown that the expected value of reward influenced vigor, the expected value of the reward has always been deterministic in that some targets were consistently rewarded while others were not. However, in theory, the expected value of the reward is not only influenced by the magnitude of the reward at stake but the probability of acquiring that reward. Indeed, one study has shown that when saccades to targets are rewarded in a probabilistic manner, monkeys react more quickly with increasing probability of reward, and accordingly with increased expected value (135). Notably, an effect of the probability of reward on movement speed or in reach vigor has yet to be determined.

In addition to reward expectation, there are at least two other factors that may influence movement vigor. First, reward history, as well as current reward, may also influence movement vigor (148; 173; 199). Following a good outcome, where subjects gain reward, one would expect a movement with increased vigor. As the average rate of reward (receiving more reward) in the environment increases, the vigor of movements within that environment should also increase. The opposite has also been observed, when receiving a bad outcome movement vigor also decreases. Second, when these rewarding outcomes are not pre-determined before the movement, a reward prediction error (RPE) will result as there is a difference between the outcome and the expected reward. Reward prediction error has been shown to affect the firing rates of dopamine neurons, and recent work has remarkably shown an influence of RPE on saccade reaction time (13; 161; 162).

In this study, we sought to investigate how reward expectation, reward history, and reward prediction error affect movement vigor. Participants made reaching movements to a set of targets that were probabilistically rewarded with a pleasant beep and flash. By altering the probability of reward of each target, we found that the expectation of reward did increase peak velocity towards the target. Reward history also played a major role in determining vigor, where a good outcome on the previous trial increased peak velocity on the current trial. The effect of reward history was further modulated by reward prediction error. When the reward obtained was less likely (high reward prediction error), the subsequent movement was invigorated to a greater extent than when the same reward was more likely (low reward prediction error). Together these results indicate a combined effect of expectation of reward, reward prediction error and reward history on reach vigor.

3.3 Methods

This study was completed by 24 young adults (age 24 ± 3.75 , height 173 ± 7.6 cm, weight 74 ± 11.34 kg, 9F/15M). All subjects were right-handed and gave written informed consent as approved by the University of Colorado Institutional Review Board.

Subjects made reaching movements towards four targets that were probabilistic rewarded with a flash and a beep (fig. B.1). Reaching movements were made using Kinarm End-Point Lab with their right hand while seated with their arm unsupported. Subjects gripped a robot handle that controlled a yellow cursor display in the plane of movement using an inverted screen that reflected the location of the cursor and hand onto a mirror. A visual blocker was placed in between the hand and the mirror to obscure vision of the hand.

A trial involved a subject moving a cursor from the home circle towards one of four cued targets located on the perimeter of 10 cm circle, centered on the home circle. Targets were arranged equidistantly around the circle's perimeter. Throughout the reach, a grey ring (radius 10 cm, centered on home) indicated how far subjects would need to move once a target appeared. A trial began with a subject holding the cursor in a home circle in a central location (size) for 400 ms.

One of four targets (size, red) would then appear at 45° , 135° , 225° , 315° from the right horizontal. As subjects initiated the movement towards the target, the home circle would disappear. Subjects would need to reach past the 10 cm in the general direction of the target ($\pm 45^\circ$ from the target). Once a subject reached far enough (past the grey ring), the target circle would either flash yellow and be accompanied by a pleasing tone for a reward or turn grey to signal no reward. If the target was rewarded, the subject would receive 10 points indicated by a display at the top of the screen. After indication of a completed trial with either a rewarded or non-rewarded target, the home circle would re-appear, and the next trial would be ready to begin.

Subjects completed 16 familiarization trials, followed by 720 total main experiment trials. In the familiarization trials, subjects were cued to reach to the targets, but none of the targets were rewarded. The following 720 trials were broken up into four blocks, during each block the probability of reward for a specific target was held constant. The probabilities of being rewarded, $p(R)$, for the four targets were 1, $2/3$, $1/3$, and 0. A block was also broken up into 5 sets of 36 trials, where subjects would reach to each target 9 times within the 36, randomly selected without replacement. To remove the effect of learning as much as possible, at the beginning of each block, subjects were informed of the specific target probabilities.

3.3.1 Data Acquisition/Processing

Experimental trials were ran on a Kinarm End-Point lab (BKIN Technologies), and kinematic data was collected using the Dexterit-E software provided with the End-Point lab (version) at 1000 Hz. Data was exported to C3D files and analyzed using MATLAB 2020b and Python 3.6. Position, velocity, and acceleration in the x-y directions were acquired through the analysis scripts provided by Kinarm. Statistical Parametric Mapping (SPM) was computed using Python 3.6 (cite). Statistical analysis and data visualization was completed in R (version).

3.3.2 Kinematic Metrics Calculations

We sought to examine how movement characteristics were modulated by the expected reward of the immediate movement, as well the reward outcomes the most recent movement.

The primary movement metrics that are calculated in this study are reaction time, movement duration, peak velocity, maximum excursion, angular error, and peak return velocity. Reaction time is calculated as the time from target presentation to movement onset. Movement onset is determined by first calculating the velocity towards the target by differentiating the distance from the center of the target. Next, we found the first point that in the previous 50 ms the standard deviation of the velocity towards the target was below 2e-3, which identified the time of movement onset. Movement duration is calculated as the time from movement onset to the first time the subjects' hand was 10 cm away (euclidean distance) from the home circle. Peak velocity is the peak velocity between movement onset and when the subject reaches further than 10 cm. Maximum excursion is the furthest the subject reached during the entire trial. Angular error is the angle difference between the vectors from the home circle to the center of the target and the vector from the home circle to where the subject crosses 10 cm. Peak return velocity is the peak velocity on the return movement. We also calculated the difference in outward and return peak velocity.

To investigate the effects of prior reward and reward prediction error on movement characteristics, we also calculated the trial-to-trial within-subject difference in all metrics by finding the difference between the metric on the current trial and the metric on the previous trial.

Each trial was classified by reward expectation, history of reward, and reward prediction error. Reward expectation was simply the probability of reward on that trial. History of reward was a binary classification based on the most recent trial; a trial either followed a trial that was rewarded or one that was unrewarded. Lastly, trials were classified by the reward prediction error (RPE) experienced at the end of the previous trial. Reward prediction error is the reward gained minus the expected value. The experimental setup allowed for five different RPE classifications. When a movement towards a 1/3 p(R) target was rewarded, this was a highly unlikely positive

event and thus constituted a high, positive RPE (+RPE). In contrast, a high negative RPE (-RPE) occurred when a movement to a 2/3 p(R) target was not rewarded. Similarly, a low +RPE followed a rewarded 2/3 p(R) target, and a low -RPE followed an unrewarded 1/3 p(R) target. Movements to the 0 p(R) and 1 p(R) targets resulted in no (0) RPE, since the subject knew they would be consistently unrewarded, or rewarded, respectively.

3.3.3 Statistical analysis

We tested the effect of reward expectation on the measured movement kinematics using a linear-mixed effects regression model (LMER) with a main effect of probability of reward and trial with a random effect of subject and target. To determine the effect of prior reward on movement kinematics, we computed an LMER with main effects of probability on the current trial and reward on the previous trial, an interaction of the two, and a random effect of subject. To investigate the effects of reward prediction error, we computed an LMER with main effect of RPE and random effect of subject. To compare specific conditions, we compute paired t-tests on data aggregated by subject and condition. These t-tests are corrected for six tests using the Holm-Bonferroni method.

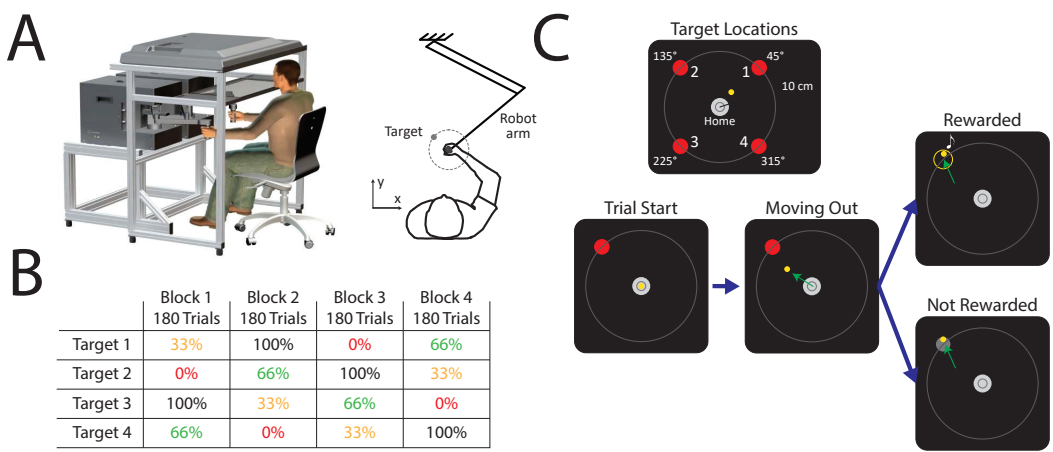


Figure 3.1: Experimental Setup. A. Subjects completed reaching movements on a Kinarm End-Point lab while in a seated position. B. Subjects completed 4 blocks, consisting of 180 trials each. Within each block, reward probability of a target was held constant. When a new block began, reward probabilities would change, and then be held consistent throughout the block. C. The top panel shows the target and home circle locations for the trial. The trial began when subjects held a yellow cursor in the home circle. A target would then appear in 1 of 4 locations, and subjects would then make a rapid out-and-back reach towards the target. Upon reaching the target distance, the target would either flash and beep, constituting a rewarded trial, or remain the same color, constituting an unrewarded trial.

3.4 Results

The goal of this study was to determine if the expected value of reward and reward history affect movement vigor in arm reaching. Movement vigor is reflected in the total time to reward acquisition. Therefore, our analysis will focus on peak velocity and reaction time, where increases in peak velocity and/or reductions in reaction time reflect increased movement vigor. Subjects completed a series of arm reaching movements to targets that were probabilistically rewarded with an audiovisual stimulus. Subjects completed 4 blocks of reaching. In each block, each target was assigned one of the following reward probabilities: $p(R) = 0, 1/3, 2/3, \text{ and } 1$.

3.4.1 Effect of expected value on movement vigor

We begin our analysis with the effect of expected value on movement vigor. Our main hypothesis is that as reward expected value (equivalent to probability of reward) increases, movement vigor will increase as well. When using a linear mixed effect model with main effect of probability and random effect of subject, we found that peak velocity does increase with expected value (Fig. 3.2A, B, C; LMER, $\beta = 3.82\text{e-}3, p = 4.4\text{e-}3$). However, the effect of probability on peak velocity is not necessarily linear. For example, for movements towards the $p(R)=1/3$ target, our data suggests that peak velocity actually decreased compared to no reward at all. Furthermore, a paired t-test between $p(R)=0$ and $p(R)=1$ targets did not reveal an effect of probability ($p = 0.529$). This is despite the fact that previous studies have consistently observed greater peak movement velocity to consistently rewarded targets compared to the same targets when not rewarded (173; 175). Taken together, while a main effect of probability was observed, certain aspects of vigor modulation remain unexplained.

Interestingly, reaction time was not affected by reward probability (Fig. 3.2D, E, F; LMER, $\beta = -2.22\text{e-}3, p = 0.07$). Further analysis using a paired t-test between the $p(R)=0$ and $p(R)=1$ targets confirmed that reaction time was not affected by reward probability ($p = 1$). While visually, the general trend of the data suggests that reaction time decreases with expected value, the variability

in reaction time for our data was very high leading to a null finding (Fig. 3.2F). Approximately one third (9) of subjects actually increased their reaction time as probability of reward increased.

3.4.2 Prior Reward influences movement vigor

Evidence suggests that recent reward may be a primary modulator of movement vigor (13; 148; 162; 199). We thought that perhaps recent reward history may be modulating vigor in addition to the effects of probability reported above.

Indeed, our results indicate that the effect of probability may be determined by whether the previous trial was rewarded or not (Fig. 3.3A, B). A linear mixed-effects model on peak velocity that considers both probability and prior reward, shows that while there is no main effect of probability of reward ($\beta = 4.21\text{e-}5$, $p = 0.98$) and no main effect of prior reward ($\beta = 3.47\text{e-}3$, $p = 0.065$), there is an interaction between the two ($\beta = 7.85\text{e-}3$, $p = 0.0094$). To investigate the interaction, we split the data set into two subsets based on whether the previous trial was rewarded or unrewarded and tested the main effect of probability again. Doing this we found that only when the previous trial was rewarded, is there a main effect of probability of reward ($\beta = 7.91\text{e-}3$, $p = 2.46\text{e-}4$). There was no effect of probability when the previous trial was not rewarded ($\beta = 6.40\text{e-}5$, $p = 0.976$). Thus, the effect of probability of reward on peak velocity was primarily present in the trials following a rewarded trial.

In contrast to peak velocity, reaction time did not seem to be affected as strongly by probability of reward or prior reward. We found no main effects of probability, prior reward or an interaction (Probability: $\beta = -3.36\text{e-}3$, $p = 0.055$; Prior Reward: $\beta = 2.02\text{e-}3$, $p = 0.19$; Interaction: $\beta = 2.9\text{e-}3$, $p = 0.24$). Moreover, when analyzing previously rewarded and unrewarded trials separately, we still did not see a significant effect of probability (Prior Reward: $\beta = -4.516$, $p = 0.79$; No Prior Reward: $\beta = -3.35\text{e-}3$, $p = 0.052$). Interestingly, in the subset of trials that were not rewarded on the previous trial there is a small effect of probability of reward on reaction time, although not significant ($p = 0.05175$). This indicates that reaction time may decrease with increasing probability of reward but only when the previous trial was not rewarded.

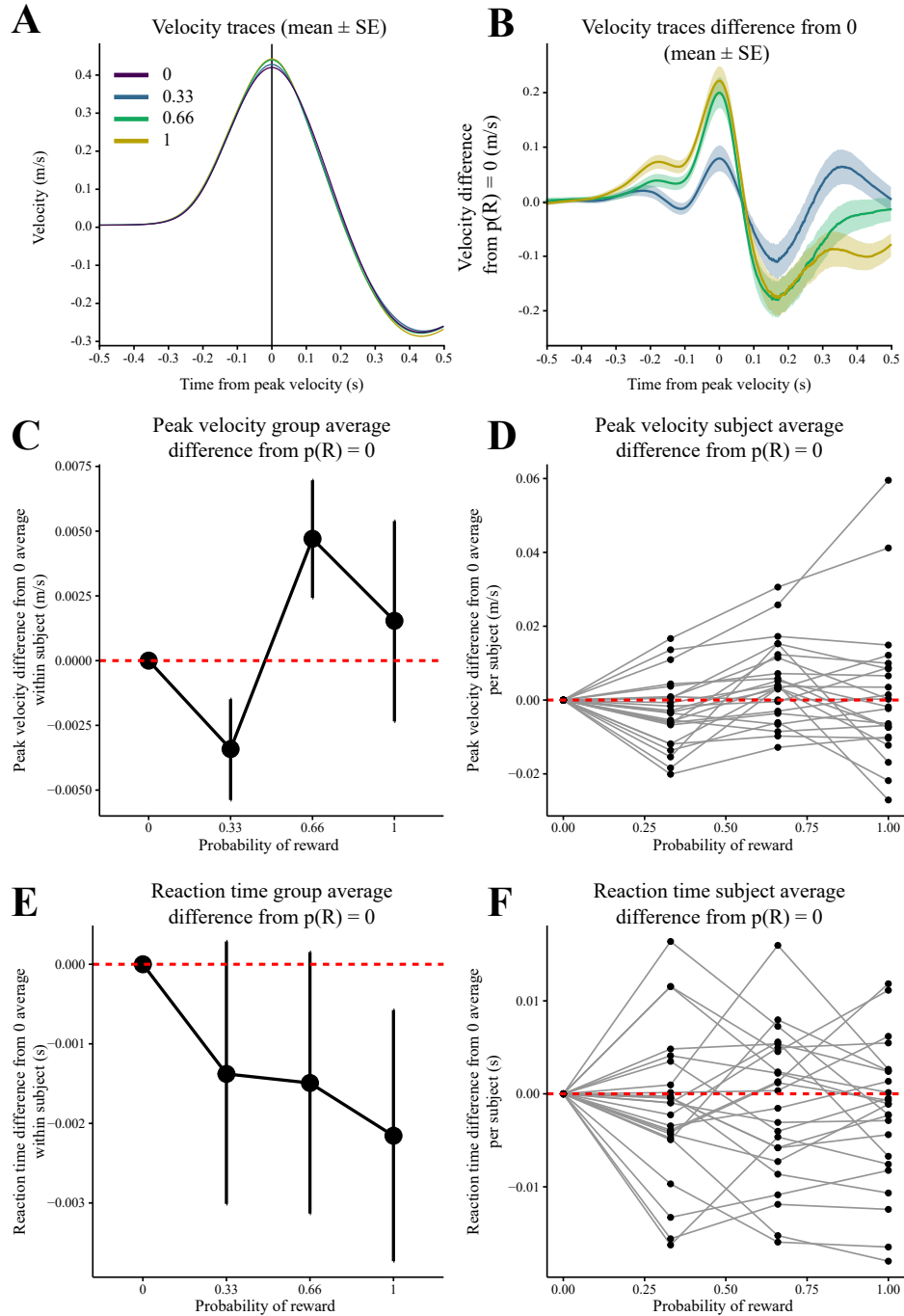


Figure 3.2: Effects of expected value on peak velocity and reaction time. (A) Average velocity traces split by reward probability and aligned to peak velocity. Data is averaged across all trials and not within subjects. Shown with mean plus standard error. (B) Average velocity traces difference from 0 $p(R)$ reward condition. 0 $p(R)$ traces are averaged for each subject, then subtracted from every trial for the other probabilities for that subject. We then calculate the average traces off this difference to have a subject specific difference. At the peak velocity we see the increase in velocity for $p(R)$ equal to 1 and 2/3, but a decrease in probability for 1/3. (C, E) Shows the difference of each subject average from the specific subject average of $p(R) = 0$. The effect of probability on the difference in vigor metric from 0 $p(R)$ rewarded condition for peak velocity (C) and reaction time (E). Red dashed line indicates no change from the 0 $p(R)$ condition. This change is calculated by subtracting the mean of the 0 $p(R)$ reward condition from every movement. (D, F) Subject specific difference averages from $p(R) = 0$ for peak velocity (D) and reaction time (F).

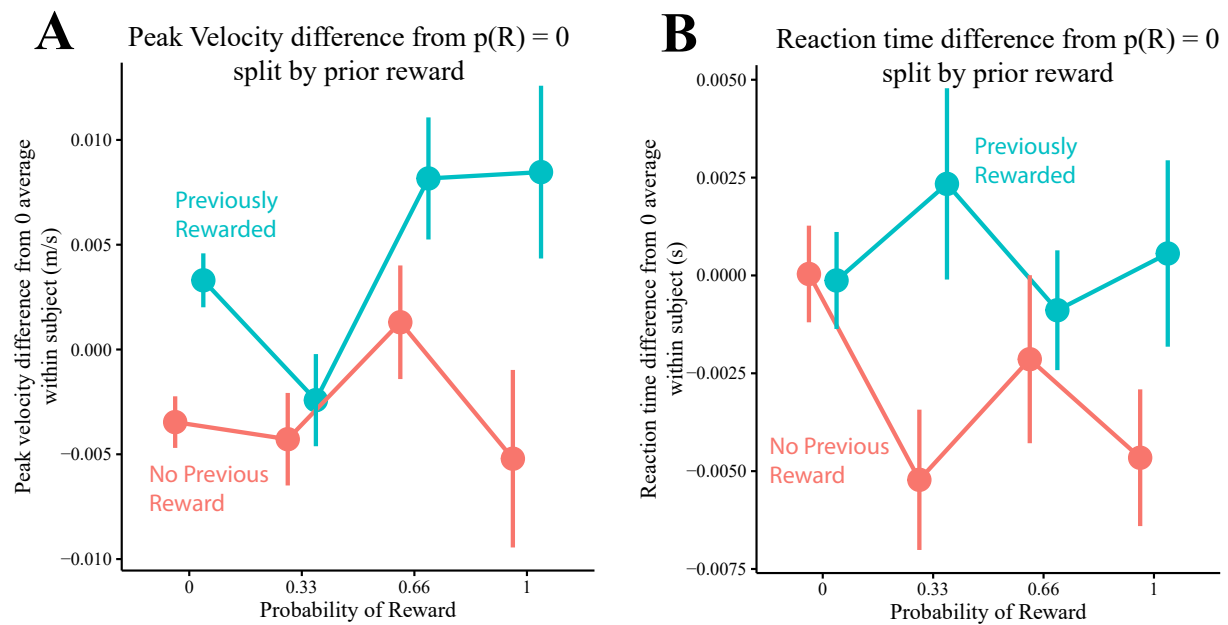


Figure 3.3: Effect of prior reward on peak velocity (A) and reaction time (B). Metrics are shown as subject average differences from the average of $p(R) = 0$. (A) Peak velocity increases with probability of reward only when rewarded on the previous trial. (B) Reaction time did not increase or decrease with probability of reward when split by reward on the previous trial.

Another way to examine the effect of prior reward on movement vigor is to directly measure the change in vigor from one trial to the following trial. We compute the difference in peak velocity and reaction time by subtracting the previous trial metric from the current trial. Our analysis shows that prior reward affects the trial-to-trial change in both peak velocity and reaction time. Using a paired t-test, peak velocity was higher in trials following reward when compared to trials not following reward ($p = 0.0234$). Moreover, subjects significantly increased their peak velocity following a rewarded trial ($p = 0.017$), and significantly reduced their peak velocity following an unrewarded trial ($p = 0.037$). Surprisingly, in contrast to the invigorating effects of prior reward on peak velocity, reaction time was higher (i.e., slower) in trials following reward compared to trials following an unrewarded trial ($p = 0.0016$). Subjects did increase their reaction time following reward compared to 0 change ($p = 0.0192$) and decreased their reaction time when not rewarded on the previous trial compared to no change ($p = 1.81e-4$).

3.4.3 Reward prediction error

To better understand the interacting effects of reward expectation and prior reward, we turned to a third potential modulator of movement vigor: reward prediction error (RPE). Results have shown that prior reward can invigorate movement by increasing the quality of the average reward rate of the environment. A recent reward leads to a small increase in the average reward rate and thus should lead to more vigorous movement. However, recent evidence has shown that reward prediction error can also modulate vigor, potentially independent of the effect of prior reward alone. Thus, in our study, it is possible that prior reward, independent of its likelihood, led to a general increase in vigor. An alternative hypothesis is that the invigorating or slowing effect of reward was modulated by its likelihood, reflected in the sign and magnitude of the RPE. Thus, we performed an analysis to determine whether vigor on the subsequent trial was modulated by RPE on the previous trial.

A linear mixed effects model with main effect of reward prediction error revealed that indeed, as RPE increases subjects tended to move faster on the following movement (Fig. 3.5A; $\beta = 9.356e-$

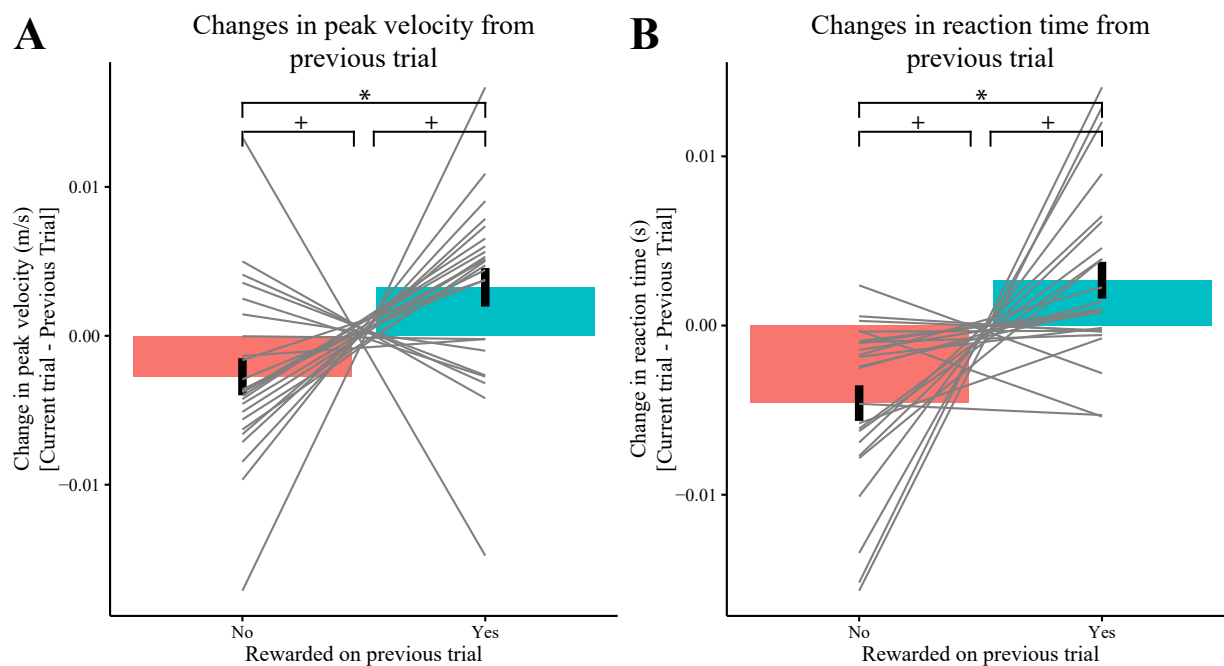


Figure 3.4: Reward modulates vigor on the following trial. We calculate the trial-to-trial differences for each metric and split this by previous reward. We then average each subject and prior reward condition and calculate a paired t-test. (A) Peak velocity was higher on trials following rewarded trials compared to those following unrewarded trials ($p = 0.0234$). (B) Reaction time was higher following rewarded trials compared to unrewarded trials ($p = 0.0016$). Grey lines indicate specific subject average changes. A * indicates a difference between prior reward and no prior reward. A + sign indicates a difference from 0.

$3, p = 1.457\text{e-}7$). We also see as before, that when reward prediction error is the same, 0, that there is a large difference in peak velocity due to prior reward. Taken together this suggests that both prior history of reward, as well as the likelihood of receiving it influenced the velocity of the following movement.

We also see an effect of RPE in reaction time; as RPE increases, reaction time increases (Fig. 3.5B; $\beta = 7.277\text{e-}3, p = 3.311\text{e-}5$). However, as prior reward and RPE are linked we also computed a linear mixed effect model with main effects of prior reward and prior RPE with an interaction. In this linear mixed model, the effect of RPE drops out ($p = 0.306$) while prior reward is significant ($\beta = 7.285\text{e-}3, p = 2.364\text{e-}4$) and no significant interaction ($p = 0.159$). This indicates that reaction time is more determined by reward on the previous trial, not reward prediction error on the previous trial.

Studies have shown that dopamine neurons increase their firing rate immediately following a reward prediction error. Based on this observation, we thought the effects of RPE on vigor may be more pronounced if we examine movements immediately following the RPE. Each movement consisted both of an outward portion and a return portion. Subjects were rewarded (or not rewarded) during the outward movement, when the cursor passed the perimeter of the 10cm circle. Thus, to examine the immediate effect of RPE, we looked to the velocity of the return movement immediately following the RPE. We calculated the difference between peak velocity on the outward movement and the movement back towards the home circle after reward is revealed. Overall, we found that the return movement was always slower than the outward movement (t-test, $p < 2\text{e-}16$), but the degree of slowing was remarkably modulated by RPE. The greater the RPE, subjects tended to slow down less on the return movement (Fig 3.5C). A linear mixed effects model revealed a very strong linear effect of RPE ($\beta = -1.74\text{e-}2, p < 2\text{e-}16$). This shows that when subjects experience a good surprising outcome, they slow down less on the return movement when compared to a surprising bad outcome.

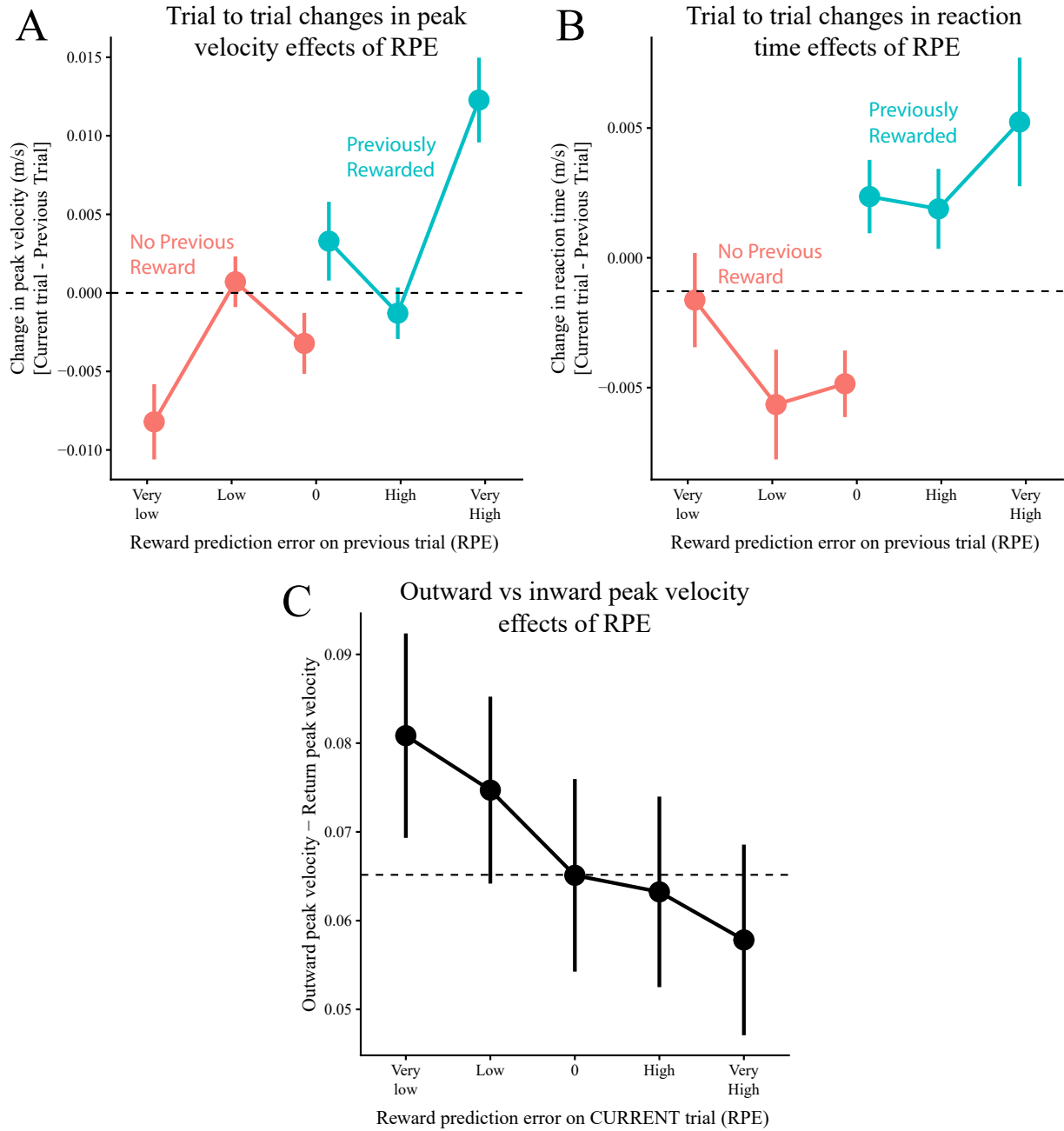


Figure 3.5: Reward prediction error results. Horizontal dashed line indicates the mean of 0 RPE. Reward prediction error is calculated as the reward obtained minus the expected value of the target. Positive RPE indicates a low expected value, with a reward. Low RPE indicates a high expected value with no reward. (A) Peak velocity affected by reward prediction error. As rewarded prediction error becomes more positive, the change in trial-to-trial peak velocity increases. (B) Reaction time trial-to-trial changes increase as reward prediction error becomes more positive, though this may be driven primarily by prior reward. (C) On the same movement, the outward minus inward reach difference in peak velocity becomes lower the more positive the RPE. This indicates that subjects slow down less when there is a good outcome vs a bad outcome.

3.4.4 Results Summary

Our results demonstrate that reach vigor is modulated by a combination of expectation of reward, prior reward and reward prediction error. Reach velocity generally increased with increasing probability of reward, was greater on trials following reward, and was greater following trials when reward was more unlikely. In contrast, reaction time did not seem to be affected by reward expectation or reward prediction error, while prior reward actually slowed down reaction time. Taken together our data indicate that expected value is not the only factor influencing movement vigor and that prior reward and RPE are large factors influencing vigor.

3.5 Discussion

This study investigated how expected value of a rewarding outcome as well as history of reward and reward prediction error can affect movement vigor within and across trials. Subjects completed a set of reaching trials towards targets that were probabilistically rewarded. We found that the peak velocity in outward reaches tended to increase with expectation of reward. Looking at the effect of prior reward we found that prior reward affected the trial by trial changes in peak velocity. Reward prediction error also influenced the change in peak velocity and reaction time between trials, however with reaction time prior reward may be driving this. Within a single trial, RPE predicted the change in velocity between the outward and inward reach.

Previous work has shown that when a single target is rewarded consistently (1 p(R)) that humans and monkeys will saccade and reach faster towards that target (101; 173; 175). We also compared the peak velocity and reaction times in the 0 p(R) and 1 p(R) rewarded conditions through a linear mixed effects model and paired t-test on subject averages. In both vigor metrics, and both statistical tests we found that there is no consistent increase or decrease. Peak velocity was not different between the 0 p(R) and 1 p(R) rewarding conditions (LMER: $\beta = 1.54\text{e-}3$, $p = 0.330$; t-test: $p = 0.692$). Reaction time as well was not different between the 0 p(R) and 1 p(R) rewarding conditions (LMER: $\beta = -2.16\text{e-}3$, $p = 0.063$; t-test: $p = 1$). This may be because

evidence points towards vigor being modulated more by the relative value of the target compared to the other targets rather than the expected value (101; 175). In these previous studies, the relative value of the rewarded condition is much higher than the relative value of all targets in this study. Compared to the other targets, the reward in this study was on average 0.66 higher, while in previous work it was 1 (a 50 p(R)) increase. This may explain why in our study we do not see a difference between the 0 p(R) and 1 p(R) rewarded conditions.

The history of reward may also explain our changes in movement vigor. Some work has shown that a reward rate can predict reaction times (70) while others show that reward does not affect subsequent trials (173). Summerside et al. shows that on trials following reward, peak velocity and reaction time were not different than trials not following reward. In our study we found that following reward, subjects tended to move faster and also react slower. Another way to view this is following no reward, subjects reacted faster. This may be subjects choosing to increase vigor on the subsequent trial to get reward while also reducing cost as increasing peak velocity may be much more costly. Guitart-Masip et al. found that immediate reward obtained on the previous trial does increase vigor in reaction times in a decision-making task. While we found that prior reward does impact reaction time, our results are in the opposite direction. Our data shows that following reward, subjects actually increase reaction time (decrease vigor). This may be driven by the fact that when rewarded, the chances of being reward on the next trial are now lower and subjects have internalized this and adjusted their vigor accordingly.

Another interesting prediction is that reward prediction error is what drives movement (161; 162). cleverly disassociate the current reward with a reward prediction error to find the effect of reward prediction error on saccade vigor. When reward prediction error was negative, a bad unexpected outcome, saccade vigor tended to decrease. Similarly, in our study, as reward prediction error was negative, peak velocity on the next trial was higher than the previous trial. The current trial as well was also affected, as subject tended to slow down less when they experienced a positive RPE (good outcome). This relationship was very strong in our study, indicating that reward prediction error and not necessarily expected value drives movement vigor when presented with

multiple possible rewarding targets.

Another possible explanation of the movement vigor when presented with many possible rewarding outcomes is to view the task as a foraging task (199). As subjects' complete reaches to rewarding targets, the average reward rate increases and as subjects complete movements that do not receive reward the reward rate decreases. We would expect as reward rate increases, vigor would as well (60; 70). We estimate the reward rate in our experiment with a decay function of recent reward shown in equation 3.1. In this equation, t is how many trials back the reward, R_{-t} , appeared. So as the target was rewarded further from the current reach, the reward on that trial influences the reward rate less.

$$\text{rate} = \sum_{t=1}^n 0.5^t R_{-t} \quad (3.1)$$

Using this reward rate and a linear mixed model with two main factors of reward rate and probability, we found that as reward rate increased peak velocity did as well ($\beta = 0.0130$, $p = 6.47e-11$) and that probability of reward also increased peak velocity ($\beta = 4.082e-3$, $p = 6.87e-3$). These results show again that expected value alone may not explain vigor, but a history of reward and RPE may be able to better explain movement vigor.

3.5.1 Limitations

Within this study, we did not randomize the order of blocks presented to subjects. During pilot testing we found an effect of trial or block on movement vigor. In this experimental data collection, we found that the presentation of blocks may affect our results. Specifically, the 0.66 p(R) target appeared in a low effort direction at the end of the experiment. We know that direction and trial may affect movement kinematics (63; 173). To account for this, we computed another linear mixed effects regression with main effects of probability and trial and a random crossed effect of subject and target. This showed that peak velocity still increased with probability of reward (LMER, $\beta = 3.82e-3$, $p = 4.4e-3$) and that reaction time was still not affected by probability of

reward (LMER, $p = 0.070$). These results held true for multiple variations of the linear mixed effects models. A much simpler linear mixed effects model with only a fixed effect of probability and random effect of subject indicated peak velocity increased (LMER, $\beta = 3.81\text{e-}3$, $p = 1.168\text{e-}2$) and reaction time did not change (LMER, $\beta = -1.97\text{e-}3$, $p = 0.11$). A future data collection will randomize the block presentation to better account for these trial effects.

Our data set may also suffer from return movements not being fully recorded during data collection. This may affect our return peak velocity metric, as sometimes data collection ended before a return peak velocity may have been found. This may have led to the return peak velocities presented being lower than in reality for some conditions. This tended to only occur negative RPE trials (no reward) and not on positive RPE trials (rewarded). Removing trials that only had either a positive RPE or 0 RPE, there was still a significant effect of RPE on the difference in peak velocity of the outward and inward reach (LMER, $\beta = -9.57\text{e-}3$, $p = 2.97\text{e-}4$). Similar, an LMER with only rewarded trials also indicated the same result (LMER, $\beta = -6.56\text{e-}3$, $p = 0.0253$). This indicates that when only investigating positive RPE, the magnitude of the RPE still modulated how fast subjects returned compared to the outward reach.

3.6 Conclusion

We sought to determine the effect of expected value, reward history, and reward prediction error on movement vigor. Our results indicate the effect of expected value increases peak velocity. Prior reward and reward prediction error seem to have much stronger effects on movement vigor. On a given trial, reward prediction error strongly predicted how much subjects slowed down on the return movement. Our findings indicate that reward plays multiple roles in modulating vigor through the expectation of reward, reward history, and reward prediction error.

Chapter 4

The role of effort in determining preferred movement speed

4.1 Abstract

More effortful movements tend to be slower, but a desire to minimize energetic cost alone is unlikely to account for this slowing. Recent findings suggest that the choice of movement speed reflects a neuroeconomic decision to maximize the movement's net reward rate, which consists of the reward to be acquired minus the metabolic energy to be expended, divided by the movement's duration. Indeed, maximization of net reward rate can explain why animals move faster when greater reward is at stake. However, the effects of effort and the underlying mechanisms remain unclear, largely because there has been no systematic measurement of both metabolic cost and preferred movement duration with increasingly effortful movements. Here, in two experiments, we examine how effort (modulated by adding mass) affects metabolic cost and preferred movement durations in a simple reaching task. We then asked whether preferred durations can be explained by maximization of a utility that considers net reward rate of the movement where effort is represented by the metabolic cost of the movement. We found that mass increased metabolic cost and led to slower movement durations. Movement durations were best explained by maximization of net rate of reward. Together these findings highlight the value of a neuroeconomic decision-making framework in understanding movement decisions as well as the critical role metabolic cost plays, as a representation of effort, in determining movement choice.

4.2 Introduction

The speed of our movements is influenced by both the expectation of the reward to be acquired and the effort to be expended. While there is a growing body of work demonstrating the effects of reward on invigorating movements (reaction time and movement time) and identifying their neural correlates, considerably less is understood regarding the effect of effort on movement vigor (61; 156; 156; 166).

More effortful movements tend to be slower. Animals choose to walk slower when carrying heavy loads and when walking up inclines (138; 191; 192). Even at the level of reaching, we reach slower in directions that involve moving more mass and prefer to reach in directions of lower effort (63; 64). While it may appear intuitive, it is actually not entirely clear why we and other animals do this. Slowing the movement down will not necessarily cost you less energy overall, and it certainly will not save you time. So why do we tend to move slower when the movement becomes more effortful?

Scientists have often looked to metabolic energy costs in order to explain the choice of movement speed. The total metabolic energy expenditure to walk or run a fixed distance, also called the cost of transport (COT), exhibit U-shaped curves with movement speed with distinct minima (11; 152; 164). The minima indicate the metabolically optimal gait speed, i.e., the speed that minimizes the total metabolic cost in joules to move a fixed distance. When allowed to freely select their gait speed, humans often choose walking and running speeds that approximately coincide with the metabolically optimal speeds (152; 154; 164). This has also been shown in a number of animals and gaits (91; 160; 164; 191). One study had horses walk on a treadmill inclined at various levels and measured cost of transport as well as the horses' preferred walking speed (45). Cost of transport increased with incline, and the metabolically optimal speed decreased. The horses' preferred walking speed slowed down at greater inclines and intriguingly, generally tracked the metabolically optimal speed. Thus, metabolic cost may help explain preferred speeds when altering effort.

These results would suggest that metabolic cost per unit distance uniquely determines pre-

ferred movement speed and that the slower movements indicate that the metabolically optimal speed has shifted. However, there are a few issues with this proposal. First, the metabolically optimal speed does not always shift with increasing mass (10). Despite this, humans walk slower with greater loads (93). Thus, it appears that minimizing metabolic cost of transport is not the sole factor determining movement speed. Second, there is a wealth of data demonstrating that animals move faster towards more rewarding targets (135; 173; 175; 198), as well as even faster to the same target but in more rewarding environments (199). Moving faster alters the movement's cost of transport, potentially shifting it away from the metabolically optimal speed. Third, faster movements are less accurate, referred to as the speed-accuracy trade off (54). Therefore, movement speed is often adjusted in the face of greater accuracy constraints despite the associated change in metabolic cost. Moreover, because of its role in movement accuracy, speed also affects the probability of acquiring reward. If one were to maximize only reward in the eyes of the speed-accuracy trade off, movement duration would be infinite to guarantee perfect accuracy which is clearly not what happens. Indeed, there are many possible factors that can influence movement choices and it is unclear what is being optimized.

By slowing down, perhaps animals are optimizing for a different currency of value, i.e., utility, that considers both the metabolic cost of the movement and the reward to be acquired as well. Support for this can be found in the behavioral ecology and neuroeconomics literature on optimal foraging theory (12; 29). A movement utility based on the maximization of net reward rate, where net reward rate is the net reward (metabolic rewards minus metabolic costs) divided by time, has been successful in explaining animal behavior (166). For example, net reward rate maximization can explain when starlings choose to walk or fly to obtain a food reward (12; 99), how long humans gaze at images of faces compared to objects and how fast they move their eyes to the next image (199). However, application of foraging theory to human decisions has thus far mainly relied on abstract estimates of effort, rather than the objective metabolic costs used in studies of other animals.

Here we approached the question of how effort determines movement speed from a combined

neuroeconomics and movement energetics perspective by. We quantified an objective measure of effort and then determined which representation of economic utility best explained measured reductions in preferred movement speed with increasing effort. Specifically, we measured the metabolic cost of reaching with added mass, obtaining an objective measure of reaching effort. Metabolic cost increased with mass, while the metabolically optimal movement speed decreased with mass. Next, we measured the effect of added mass on the choice of movement speed and observed that movement speed decreased with added mass. Lastly, we asked to what extent this reduction in vigor could be explained by a utility based on maximizing net reward rate, compared to alternative utility formulations. Ultimately, effort-based movement slowing was best explained with the maximization of a utility that maximized net reward rate, considering both the reward at stake and the effort to be expended, divided by time, where effort was represented objectively as metabolic cost.

4.3 Results

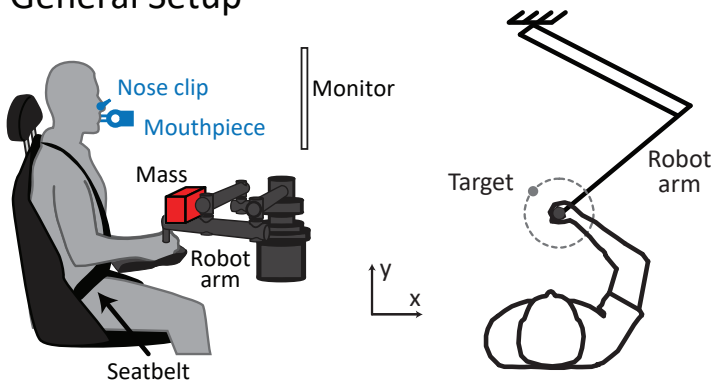
Our first step towards understanding the effect of effort on movement speed was to quantify an objective measure of increasing effort. To do so, we consider metabolic cost as an objective measure of effort and measured the metabolic cost of reaching with increasing effort where effort was modulated by increasing the mass at the hand.

4.3.1 Experiment 1 - The effect of mass on the metabolic cost of reaching

Healthy, young participants ($N = 8$) made 10cm reaching movements at six prescribed speeds with four different masses (0kg, 2.3kg, 4.5kg, and 9.1kg) added at the hand for a total of 24 sets of reaching conditions (Fig. 4.3). Conditions were blocked with each consisting of five minutes of reaching (200 trials). As they performed the task, we measured metabolic rate via expired gas analysis. Metabolic rate was calculated from the last three minutes of reaching within each block.

Measuring the Metabolics of Reaching

A. General Setup



B. Experiment 1 Protocol ($N = 8$)

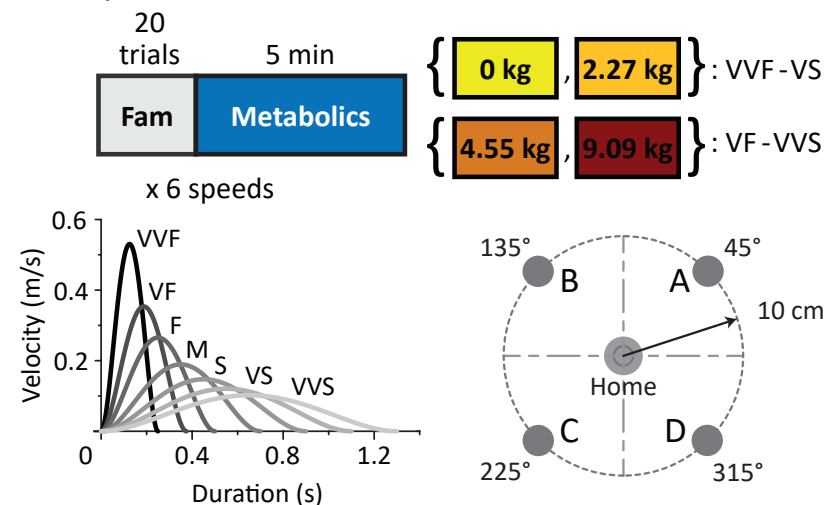


Figure 4.1: Experiment 1 setup. (A) Subjects made horizontal planar reaching movements while breathing into a mouthpiece. Mass was added at the hand. (B) Subjects made out-then-back reaching movements across a range of added masses and speeds to four targets 10 cm from the home circle. There were seven distinct speeds, and subjects completed six speeds with each mass. The two heaviest masses corresponded with the six slowest speeds; the two lighter masses corresponded with the six faster speeds. The number of trials within each speed was set to allow for approximately five minutes of reaching.

4.3.1.1 Metabolic expenditure increases with mass

Before participants performed the reaching task, we measured their resting metabolic rate, \dot{e}_r in three five-minute baseline periods, as they sat quietly in the experimental chair. On average, the resting metabolic rate was $\dot{e}_r = 73.33 \pm 3.6\text{W}$. As they performed the reaching task, gross metabolic rate increased with faster reaching speeds ($\beta = -7.67\text{e-}1$, $p < 2\text{e-}16$). With no added mass, gross metabolic rate ranged from $92.78 \pm 6.63\text{W}$ for the slowest reach to $171.98 \pm 18.51\text{W}$ for the fastest reach. Furthermore, across movement speeds, gross metabolic power increased significantly with added mass ($\beta = 1.73\text{e-}2$, $p = 2.52\text{e-}7$; Fig. 4.2A). For a movement at the second fastest speed condition, adding 9.1kg of mass at the hand led to an increase in gross metabolic rate from $131.65 \pm 14.32\text{W}$ to $222.06 \pm 24.39\text{W}$, a nearly 70% increase. Thus, faster reaches with greater mass led to increased metabolic expenditure.

We next sought to determine how mass influenced the metabolically optimal movement speed, i.e., the speed at which the metabolic cost of the movement was at a minimum. To do so, we parameterized metabolic rate as a function of mass and movement duration by fitting the gross metabolic rate data to the following equation based upon the observed effects of mass on the metabolic cost of walking:

$$\dot{e}_m = a + \frac{bm^i}{t_m^j} \quad (4.1)$$

where m represents the effective mass of the arm with the added mass (see Methods), and t_m is the movement duration. The best fit parameters were $a = 98.25 \pm 3.05$, $b = 0.86 \pm 0.43$, $i = 0.83 \pm 0.10$, and $j = 5.83 \pm 0.60$ (SSE = 120872.75, AIC = 1750.83). We tested an alternative formulation wherein the constant, a , was also scaled by the effective mass of the movement raised to a power:

$$\dot{e}_m = am^k + \frac{bm^i}{t_m^j} \quad (4.2)$$

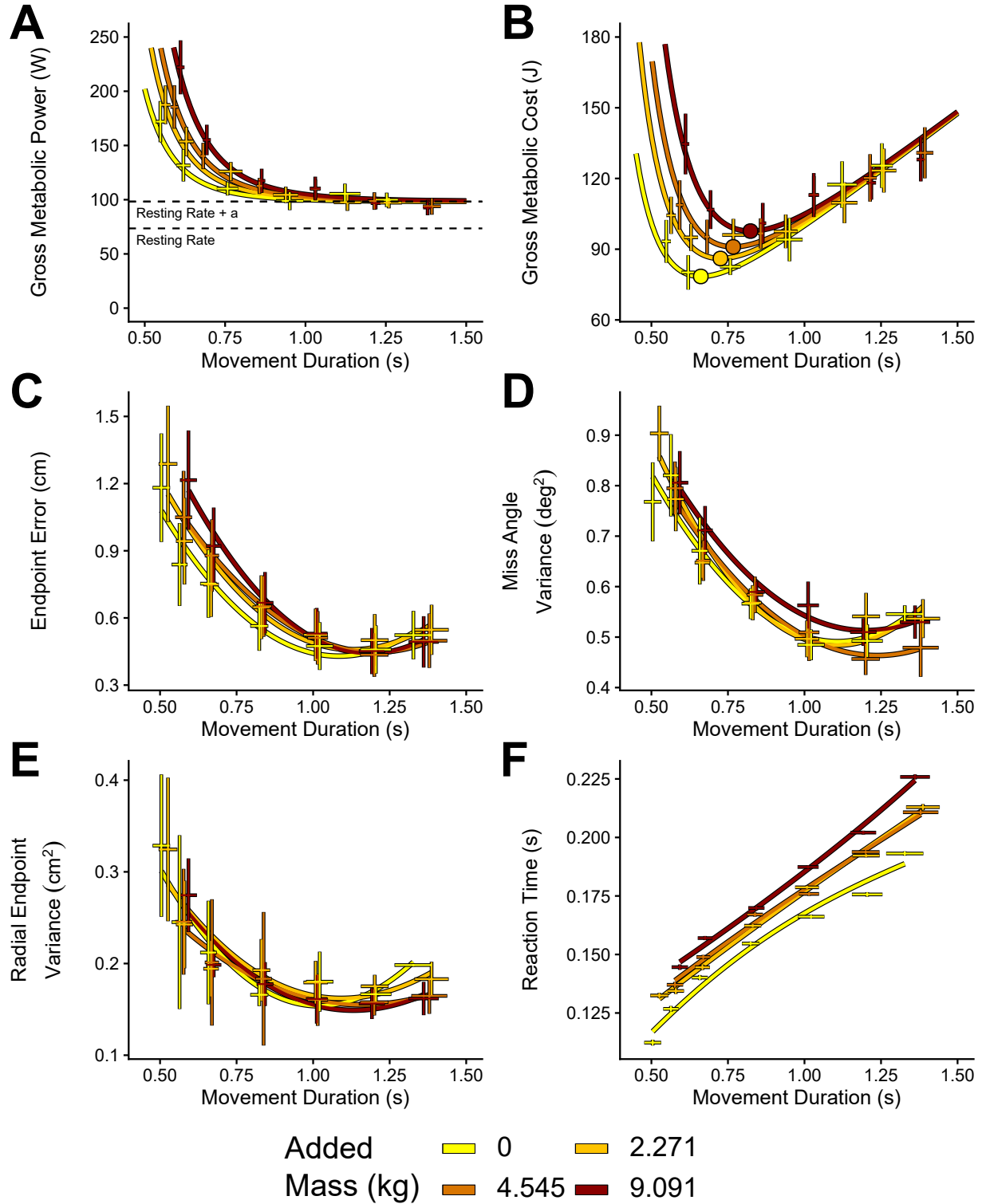


Figure 4.2: Experiment one results. (A) Gross metabolic power increases with added mass and movement speed (shorter durations). (B) Gross metabolic cost of a movement. Gross metabolic cost shows a distinct minimum, and this minimum duration increases with added mass. (C) Increased mass and speed (shorter duration) increased subjects' endpoint error. (D, E) Mass did not affect subjects' movement consistency. Faster movement speed did lead to less consistency (increased variance). (F) Reaction time increased with added mass and longer movement durations.

This fitted value for k was not different from zero and the model performed similarly compared to Eq. 4.1 ($k = -0.02 \pm 0.04$, $\neg\text{SSE} = 120743.07$, $\text{AIC} = 1752.63$), indicating that the time-invariant component of metabolic power did not change with added mass. Thus, we moved forward with Eq. 4.1.

Equation 4.1 represents the average rate of gross metabolic energy expenditure (joules/s), over the course of a reach for a given duration and mass. To obtain the total metabolic cost of that reach in joules, e_m , Eq. 4.1 is multiplied by the movement duration:

$$e_m = at_m + \frac{bm^i}{t_m^{j-1}} \quad (4.3)$$

The metabolic cost of a very fast reach is quite high, reducing as the movement slows down, but then increasing again at slower speeds (Fig. 4.2B). The minimum of this curve represents the movement duration that would minimize the metabolic cost of the reach, i.e., the duration that minimizes cost of transport. The minimum metabolic cost movement durations we find are 0.66, 0.70, 0.72, and 0.75s for the four mass conditions. The metabolic cost minimum at these movement durations are 78.31, 83.41, 85.98, and 89.24 J. We see that not only does the metabolic minimum shift to longer movements, but the metabolic minimum cost increases with added mass. We will return to this finding later.

4.3.1.2 The effect of mass on movement accuracy

Another aspect of movement that is affected by the speed of the movement is accuracy, i.e., the speed-accuracy trade off. We measured accuracy as the Euclidean endpoint error at movement offset (see Methods). As expected, endpoint error was reduced with longer movement durations ($\beta = -9.37\text{e-}1$, $p < 2\text{e-}16$). We also asked the analogous question of whether mass affects movement accuracy. Indeed, we found that mass slightly increased endpoint error ($\beta = 2.16\text{e-}2$, $p < 2\text{e-}16$), with the strongest effects seen at the fastest speeds (Fig. 4.2C).

Accuracy can also be reflected in the consistency of the movement, defined as the variability

in endpoint position, independent of the actual target error. We split consistency into two metrics, angular endpoint variability and radial endpoint variability. Radial endpoint is how far from the home circle participants ended their movement, and angular endpoint is the angle between the target vector and endpoint vector measured from the home circle. Both radial and angular variability decreased with movement duration ($\beta = -1.00$, $p < 2e-16$, $\beta = -1.14$, $p < 2e-16$), while mass did not affect either ($\beta = -6.92e-3$, $p = 0.287$, $\beta = 1.74e-2$, $p = 0.0114$, respectively; Fig. 4.2E).

4.3.1.3 Slower reaction times with added mass

An interesting question is how effort affects reaction time. While we enforced the duration with which subjects had to complete a reach, participants were free to select the combination of reaction time and movement duration. The choice of reaction time has been related to the process of planning the upcoming movement, suggesting that the predictable mass in this experiment should have little effect. Moreover, one might predict that reaction time should not be affected by mass because participants are not moving while preparing the action. Here we found that reaction time increased with mass ($\beta = 2.40e-3$, $p < 2e-16$) and movement duration ($\beta = 6.43e-2$, $p < 2e-16$; Fig. 4.2F). Thus, slower movements had longer reaction times, and for two movements of the same duration, the movement with the greater mass elicited a longer reaction time.

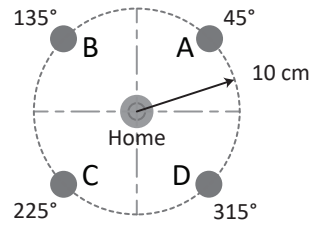
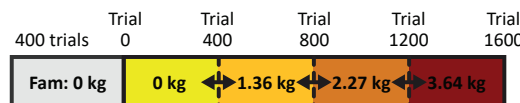
To summarize the results of Experiment 1, we found that it is more energetically costly to make reaching movements with greater mass and that the metabolically optimal movement duration increases with added mass. In other words, metabolic energy minimization predicts slower movements with added mass. Mass also led to an unexpected increase in reaction times, with participants reacting slower with added mass, even though the subsequent movements were of the same duration.

4.3.2 Experiment 2 - The effect of mass on preferred reach duration

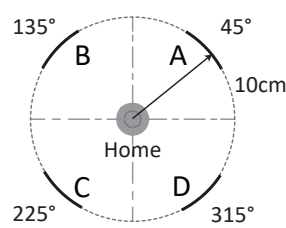
Given that mass leads to an increase in the metabolic cost of reaching, and that the metabolically optimal duration increases with added mass, how will this increased effort cost influence an individual's preferred movement speed? The second study was designed to answer this question. Similar to the previous experiment, participants made goal-directed reaching movements with added mass at the hand (Fig. 4.3). However, rather than reaching at a prescribed speed, participants were free to reach at a self-selected speed. At the beginning of each trial, one of four targets would appear centered on the circumference of a 10cm circle and participants were asked to reach to the target to complete the trial. To control for any confounding effects of accuracy on mass-related changes in preferred movement speed, three separate experiments were run each with a different target size or stopping requirement. In Experiment 2a, the target configuration was identical to Experiment 1, and participants were required to stop in the target. In Experiment 2b, accuracy requirements were increased. The target size was reduced to a thin (1 cm), narrow arc, where again participants were required to come to a stop in the target. In the third experiment, Experiment 2c, accuracy requirements were reduced to nearly nothing and target stopping requirements were removed altogether. Participants had to make an out and back movement in the direction of the target where the only requirement was to cross the outer 10cm circle, in the quadrant of the indicated target. All experiments consisted of 1600 total trials in the added mass conditions, divided into four sets of 400 trials each. In each set of 400 trials, a different mass would be added to the robot handle. The amount of added mass was hidden from the participant using an opaque container and could be 0 kg, 1.36 kg (3lbs), 2.27 kg (5lbs) or 3.64 kg (8lbs) (Fig. 4.3). All participants experienced each mass condition once, and the order was randomized across participants.

Measuring the Preferred Duration of Reaching

A. Experiment 2a ($N = 12$)



B. Experiment 2a ($N = 12$)



C. Experiment 2c ($N = 18$)

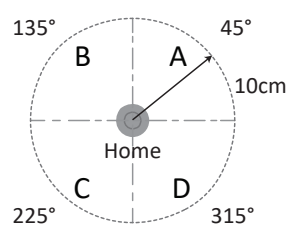
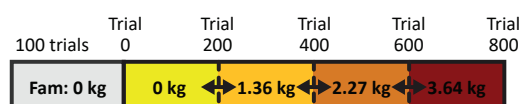


Figure 4.3: Experiment 2 Overview. Subjects underwent five blocks of reaching movements including a familiarization block and four added mass blocks. The order of mass conditions was randomized for each subject. The general setup is the same as experiment 1 (Fig. 4.3A). (A) Experiment 2a. Subjects completed 400 trials in familiarization and each mass condition. Similar to experiment 1, subjects made reaching movements from a home circle and stopped at one of four targets, 10 cm away from the home circle. (B) Experiment 2b. Subjects completed 400 trials of familiarization and 200 trials for each added mass condition. Subjects would make 10 cm reaching movements from a home circle to a thin arc-shaped target. After stopping at the target, subjects would move back towards the home circle. (C) Experiment 2c. Subjects completed 100 familiarization trials, and 200 out-a-back reaching movements for each mass. Subjects started in a home circle and reached in one of four directions with the only criteria that they move cross the perimeter of the outer circle.

4.3.2.1 Mass led to slower movements

In each of the three experiments, added mass led participants to make significantly slower movements. This is reflected in significantly longer movement durations and slower peak velocities across the three experiments (Movement Duration: $\beta = 3.63\text{e-}2$, $p < 2\text{e-}16$, Peak Velocity: $\beta = -1.56\text{e-}2$, $p < 2\text{e-}16$; Fig. 4.4D,E).

We also found that in each of these experiments, the changes in movement duration due to mass were relatively the same. We fit an individual linear mixed effects model predicting the effect of mass on movement duration for each experiment and compared the magnitude of the effect across experiments. Fitting a single linear model to all three experiments, we found mass increased movement duration ($\beta = 3.63\text{e-}2$, $p < 2\text{e-}16$). Fitting individual linear models, all experiments showed a significant effect of mass, with similar slope estimates, suggesting that the degree of mass-based slowing was conserved across experiments (2a $\beta = 3.29\text{e-}2$, $p < 2\text{e-}16$, 2b $\beta = 3.53\text{e-}2$, $p < 2\text{e-}16$; 2c $\beta = 3.92\text{e-}2$, $p < 2\text{e-}16$; supplemental table 1).

Similar to movement duration, but with the opposite effect, peak velocity was reduced with added mass (Fig. 4.4E). When fitting a single linear model to all three experiments mass decreased peak velocity ($\beta = -1.55\text{e-}2$, $p < 2\text{e-}16$). An individual linear mixed effects model fit to each experiment revealed linear estimates are similar between the experiments (2a $\beta = -1.31\text{e-}2$, $p < 2\text{e-}16$, 2b $\beta = -1.13\text{e-}2$, $p < 2\text{e-}16$; 2c $\beta = -1.99\text{e-}2$, $p < 2\text{e-}16$; supplemental table 2). Thus, across three experiments with different accuracy requirements and preferred speeds, we consistently observe mass-based slowing of preferred movement speed.

As expected, there was an effect of an experiment's accuracy requirements on the preferred movement duration (ANOVA, $p = 8.85\text{e-}5$) and peak velocity (ANOVA, $p < 1.17\text{e-}7$) (Fig. 4.4 D, E). Experiment 2b, the smallest target, exhibited the longest movement durations and lowest peak velocities. Experiment 2c, which had no stopping requirements, led to the shortest movement durations and highest peak velocities. Experiment 2a, which accuracy was an intermediate of 2b and 2c, had movement durations and peak velocity between 2b and 2c. Even when accuracy costs

are negligible, mass leads to a significant increase in movement duration and reduction in speed. This suggests that the changes in movement duration are driven by mass-related increases in effort, and not driven by mass-related changes in accuracy.

4.3.2.2 Mass increased reaction time

In these experiments, subjects were not only free to choose their movement duration but were also free to select their reaction time with no restrictions. Across all three experiments, reaction time increased with added mass ($\beta = 5.26\text{e-}3$, $p < 2\text{e-}16$; Fig. 4.4G; supplemental table 3). Fitting individual linear mixed effects models, we found that increasing mass led to increased reaction time in all three experiments and that the effect is similar across experiments (2a $\beta = 4.47\text{e-}3$, $p < 2\text{e-}16$; 2b $\beta = 6.16 \text{ e-}3$, $p < 2\text{e-}16$; 2c $\beta = 5.14\text{e-}3$, $p < 2\text{e-}16$; Fig. 4.4F). The effect of mass is conserved across experiments as seen in the linear estimates and in Fig. 4.4I. These results, together with our earlier observations from experiment 1, solidify the finding that mass increases reaction time.

Experimental accuracy requirements seem to influence reaction times (ANOVA $p = 2.72\text{e-}8$) (Fig. 4.4F). Experiment 2b, with the strictest requirements, tended to have the longest reaction times. Experiment 2a, with intermediate accuracy requirements, had the lowest reaction times. We find that experiment 2c, the most lenient accuracy requirements, had reaction times between 2a and 2b.

4.3.2.3 Experiment 2 Summary

In summary, added mass led to a slowing of preferred movement speeds. Increasing accuracy requirements also led to general movement slowing, however the effects of mass were conserved, and mass consistently led to reductions in movement speed independent of the task's accuracy requirement.

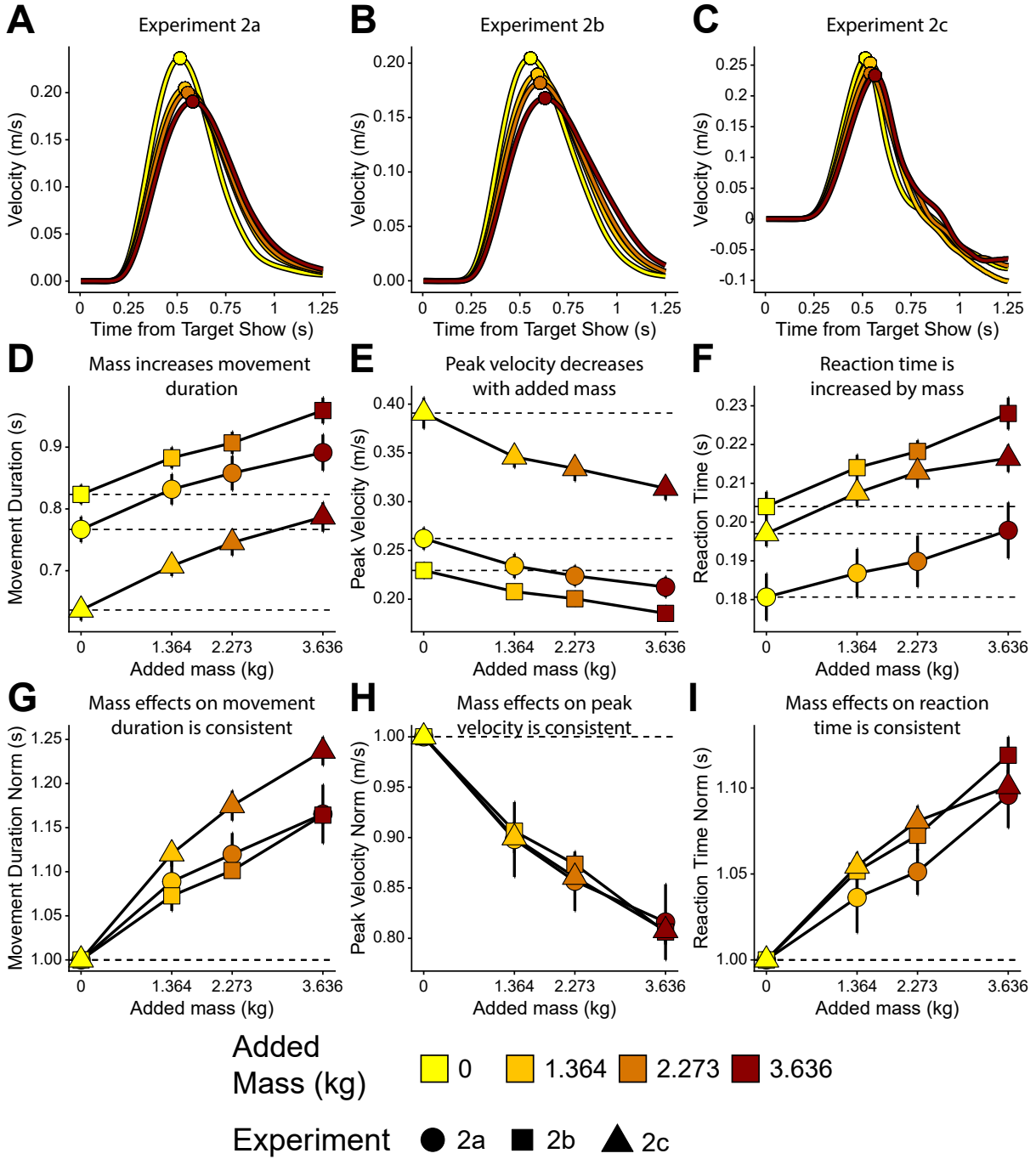


Figure 4.4: Experiment 2 Results: Added mass reduces preferred movement speed. Average velocity traces shown for experiment 2a (A), experiment 2b (B), and experiment 2c (C). Each line represents the subject average for one mass condition, with the peak velocity indicated by a dot. In panels D-I, each point represents the subject average for a specific mass condition. Error bars show standard error across subject averages. Horizontal dashed lines show the average value for 0 kg of added mass. (D) Mass increased movement duration (E) Mass reduced peak velocity. (F) Reaction time increased with increasing mass. Panels G-I: Movement metrics normalized as a fraction of each subjects 0kg condition. (G) Movement duration, (H) peak velocity, and (I) reaction time exhibited similar changes due to mass across all three versions of experiment 2.

4.3.3 Predicting preferred movement duration

In Experiment 1, we observed that mass increases the effort cost of movement. In Experiment 2 we saw that mass also increases preferred movement durations. Can we explain these effort-based changes in movement preference in the context of a movement utility that is conserved across individuals? As a first step, we looked to what metabolic minimization would predict. For the mass and movement distances used in experiment 2, we calculated the metabolically optimal durations using Eq. 4.3. We found that the minimum metabolic durations are 0.66, 0.70, 0.73, 0.75s for each mass condition, and are necessarily the same for both experiments 2a and 2b. Critically, the durations that minimize metabolic cost are much faster than the actual durations seen in both experiment 2a and 2b. While metabolic cost minimization correctly predicted a general slowing of movement, it could not fully explain preferred movement durations. Also, as expected, it could not explain the effect of different accuracy requirements.

4.3.4 A utility based on net reward rate to explain preferred movement duration

To further investigate the determinants of preferred movement duration, we turned to the literature on optimal foraging theory, wherein animal behavior is theorized to agree with the goal of maximizing net reward rate, maximizing the net reward (rewards minus costs) per unit time (29; 199). If we assume that the purpose of movement is to acquire reward as quickly as possible but with minimal effort, we can represent the utility of movement, J , similarly as its net reward rate:

$$J = \frac{\alpha - E}{T} \quad (4.4)$$

Here " α " is the reward to be obtained, " E " is the cost of obtaining the reward, and " T " is the total time spent acquiring the reward. In the context of movement, the primary cost is effort. In this study, we represent the movement effort cost as the measured metabolic cost of a reach with a given mass and duration, \dot{e}_m . However, there is also the time spent preparing the

movement, i.e., the reaction time. The effort cost associated with reaction time, \dot{e}_r , is equal to the metabolic expenditure when not reaching; this cost is represented as \dot{e}_r multiplied by the reaction time, t_r , shown in Eq 4.5. The total time to reward, "T", then is the sum of the reaction time and movement duration. This leads to the following expression for a utility reflecting the net reward rate where effort is represented as metabolic cost:

$$\begin{aligned} J &= \frac{\alpha P(\alpha|t_m, m) - e_r - e_m}{t_r + t_m} \\ e_r &= \dot{e}_r t_r \\ e_m &= at_m + \frac{bm^i}{t_m^{j-1}} \end{aligned} \quad (4.5)$$

We have included the term, $P(\alpha|t_m, m)$ to reflect the probability of reward and its dependence on the duration of the movement, i.e., the speed-accuracy trade off (54). As mass may affect accuracy from the previous experiments, we also included a term for mass in the probability function. We used a logistic function fit to endpoint accuracy data from experiment 1 to capture the relationship between movement duration, mass, and the probability of ending the movement within a target of a given size:

$$\begin{aligned} \ln\left(\frac{P}{1-P}\right) &= \beta_0 + \beta_1 t_m + \beta_2 m \\ P(\alpha|t_m, m) &= \frac{1}{1 + e^{-\beta_0 - \beta_1 t_m - \beta_2 m}} \end{aligned} \quad (4.6)$$

Since Experiments 2a and 2b had targets of different sizes, a separate logistic function was fit for each experiment using data from Experiment 1 but with different accuracy constraints. This yielded two sets of parameters and resulting curves reflecting the smaller target and greater accuracy requirements enforced in Experiment 2b (Experiment 2a: $\beta_0 = -1.45 \pm 0.13$, $\beta_1 = 5.88 \pm 0.19$, $\beta_2 = -0.10 \pm 0.01$; Experiment 2b: $\beta_0 = -2.93 \pm 0.09$, $\beta_1 = 6.09 \pm 0.13$, $\beta_2 = -0.08 \pm 0.01$). These speed-accuracy curves can be seen in figure 4.5. Figure 4.5 shows the fit to the

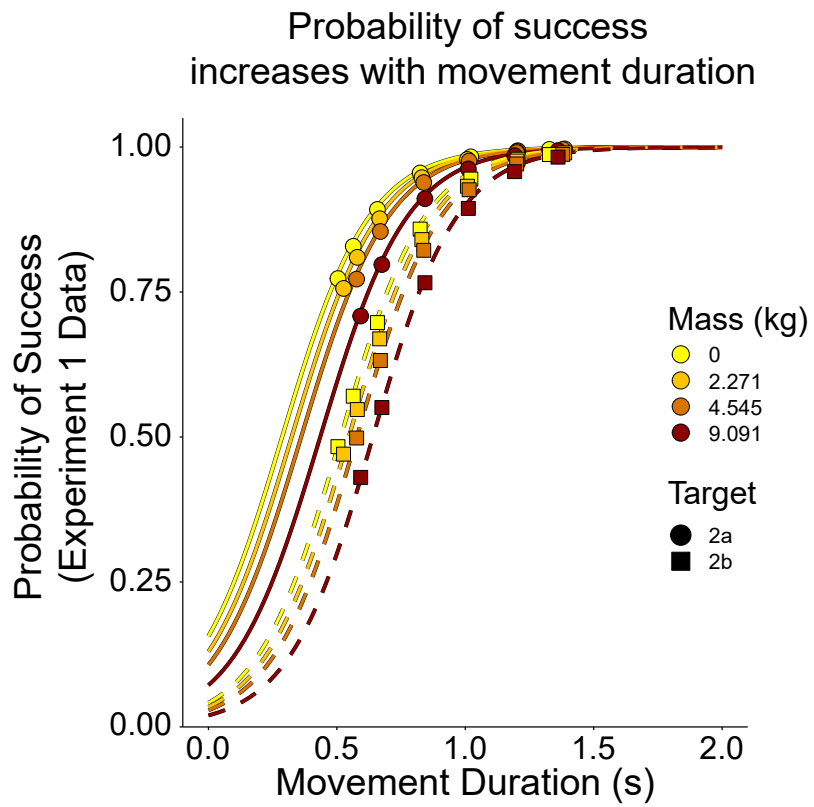


Figure 4.5: A function for the speed-accuracy trade off. Using the data from experiment 1, and the logistic regression shown in Eq. 4.6, we can compute the probability of success given the criteria for experiment 2a and 2b. Data points are the fraction of trials within that condition that were a success. The regression for experiment 2a criteria is shown with a solid line and circle data points. The regression for 2b criteria is shown with a dashed line and square data points. We see that the probability function can well represent the data seen in experiment 1. Each line is colored by mass added from experiment 1.

probabilities measured from the data in Experiment 1. The experimental probabilities of success measured in Experiment 2a for the added mass conditions were $0.977 \pm 8.32\text{e-}3$, $0.983 \pm 5.12\text{e-}3$, $0.975 \pm 9.48\text{e-}3$, $0.980 \pm 5.53\text{e-}3$. At the measured movement durations observed in Experiment 2a, the logistic regression predicts probabilities within a similar range, from 0.943 to 0.960. The measured probabilities of success in Experiment 2b ranged from 0.80 to 0.83. The logistic regression, at the movement durations seen in Experiment 2b, predicted probabilities that ranged from 0.867 to 0.961. Thus, overall, the fitted speed-accuracy functions capture the effect of duration on the probability of success in the two experiments.

At this point, for a given reward, α , we can calculate the optimal movement duration, t_m^* , that will maximize the net reward rate, J . To determine whether maximization of movement utility can explain the changes in preferred movement speeds seen in Experiment 2, we used numerical optimization to fit α that minimizes the sum of squared error between experimental data and predicted optimal durations. A single α was fit to the combined data from Experiments 2a and 2b across all mass conditions, based on the assumption that the experiment specific speed-accuracy curves account for the sole difference between the experiments. We did not attempt to fit durations from Experiment 2c, as the reaching movements were out-and-back, rather than out-and-stop, and thus their metabolic cost may not be accurately reflected by the function obtained from metabolic data measured in Experiment 1.

With only a single parameter to fit, across all mass conditions and two target sizes, we find that net reward rate can describe preferred movement durations rather well (Fig. 5c, $\alpha_{a,b} = 70.621$, 2a SSE = $1.16\text{e-}3$, 2b SSE = $4.11\text{e-}3$, 2a and 2b SSE = $5.28\text{e-}3$). The predicted movement durations for 2a are 0.758, 0.787, 0.808, and 0.835s for the added mass conditions; Experiment 2b had predicted movement durations of 0.869, 0.912, 0.936, and 0.967s for the added masses.

4.3.4.1 An alternative utility: maximization of net reward

An alternative to the net reward rate utility presented above is a slightly simpler model based solely on net reward, where the speed-accuracy trade off and metabolic cost are used to predict

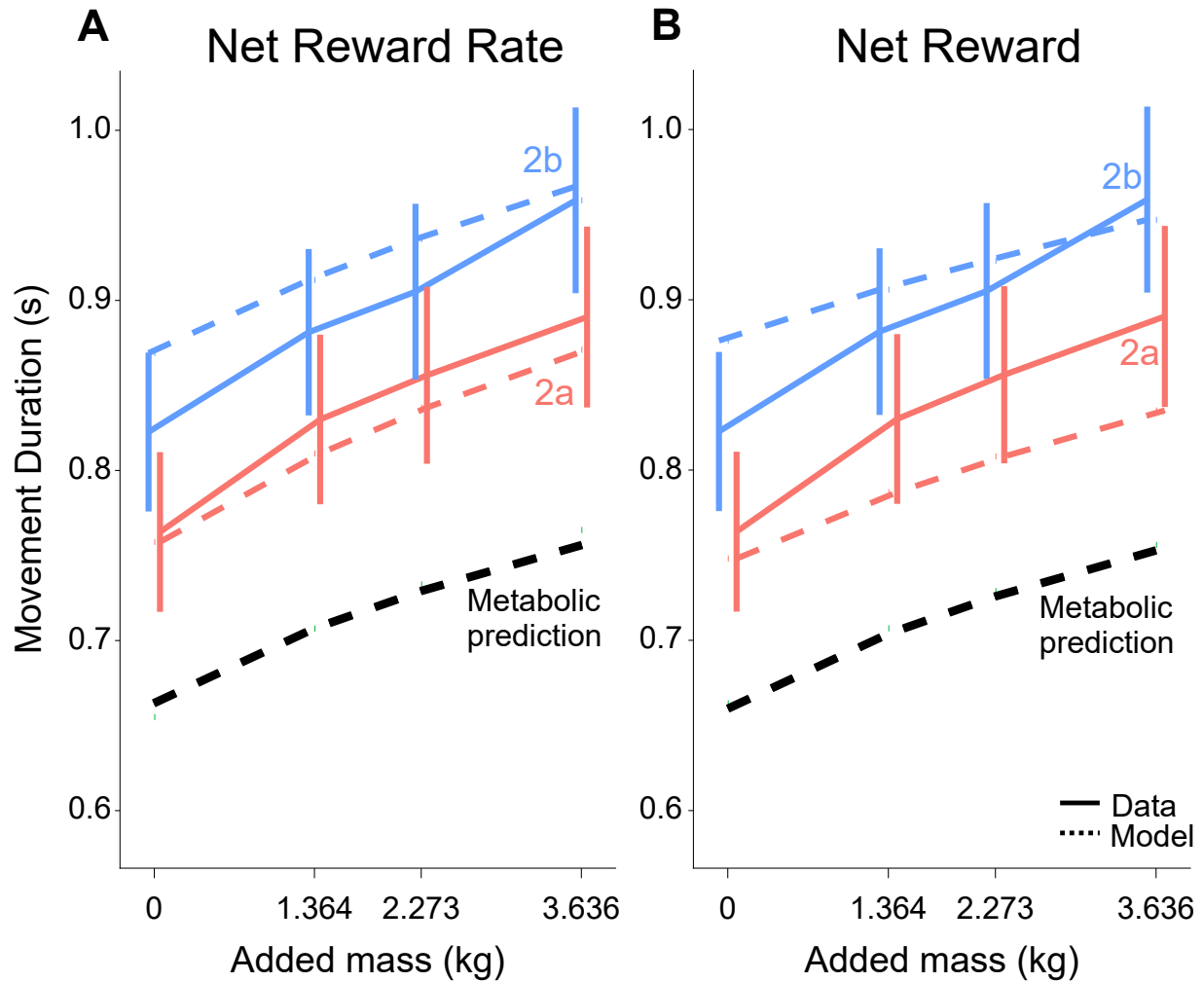


Figure 4.6: Optimal movement durations obtained by (A) maximization of net reward rate and (B) maximization of net reward across both experiments 2a and 2b. Solid lines represent the average movement duration for Experiment 2a (pink) and 2b (blue). Error bars represent standard error of subject averages. Dashed lines indicate optimal movement durations and are color-coded by experiment. Black dashed lines indicate durations predicted by minimizing metabolic cost alone.

movement duration. We define this as the net reward utility model. In essence, this model reflects the intuition that movement speed is determined by an interaction of the desires to acquire reward accurately, while also reducing metabolic cost. Therefore, this formulation can potentially account for the changing accuracy requirements in the two experiments and can be seen in equation 4.7. The speed accuracy trade off is represented by $\alpha P(\alpha|t_m, m)$, as subjects move faster the probability of success becomes lower. The effort term, $(at_m + \frac{bm^i}{t_m^{j-1}})$, represents how much metabolic energy the subject spent to complete the movement. The α parameter in this formulation determines whether speed accuracy or metabolic rate has more effect of overall utility.

$$J = \alpha P(\alpha|t_m, m) - (at_m + \frac{bm^i}{t_m^{j-1}}) \quad (4.7)$$

With this formulation, the primary factor influencing how fast movements occur is the speed accuracy trade off. As the target becomes harder to stop in, subjects should slow down. Fitting this net reward utility model to experimental data from 2a and 2b, we find $\alpha = 144.037$, and that the SSE for Experiment 2a and 2b were 7.45e-3 and 3.92e-2. The total SSE for 2a and 2b was 1.14e-2. The predicted movement durations for experiment 2a were 0.748, 0.787, 0.808, and 0.835s; the predicted durations were 0.867, 0.906, 0.923, and 0.967s for experiment 2b. As evidenced by the greater SSE, we find that the net reward utility model results in a slightly weaker fit (SSE=1.14e-2), compared with the capture rate utility presented above (SSE=5.28e-3). While the fit is only slightly weaker, it is important to note that this utility formulation would fail to explain the often observed increase in vigor towards reward when accuracy constraints are negligible.

In summary, we found the mass increased the metabolic cost of reaching and led to slower preferred movement speeds. These preferred movement durations could not be fully explained by metabolic cost minimization alone but were best explained as the outcome of decision aimed at maximizing the net reward rate of the movement, where net reward reflects the total reward to be acquired, the probability of acquiring that reward, and the metabolic cost of the movement.

4.4 Discussion

The goal of this study was to understand how mass and effort affect movement vigor in arm reaching. We found that adding mass at the hand increased the metabolic cost of reaching and led subjects to make slower movements. A recently proposed utility framework, that represents effort with metabolic cost discounted by time, can explain the movement duration across multiple experiments (166). When comparing the metabolic cost minimum to the preferred reach duration of subjects, we find that minimizing metabolic cost alone cannot predict the preferred movement duration.

4.4.1 Utility predictions

The main new finding in this study is the use of a utility model to predict multiple experiments. A common utility only maximized the utility as a function of reward, effort and movement time. In this study, we specifically added a probability of reward function and reaction time as determinants in movement vigor selection.

To complete a movement, subjects have some amount of planning involved in making that movement and this usually occurs before subjects react. To account for the total cost of a movement, we need to account for the cost of not reacting. The added term $a_0 t_r$ accounts for the energy used while subjects are in the chair, planning the movement, but have not yet moved. Adding this term aids the utility prediction by account for subjects planning their movement. A future experiment may be able to determine an optimal reaction time and movement time that maximizes this utility.

The second addition to utility we made is the introduction of the probability of reward based on movement vigor. This addition is similar to the speed accuracy trade-off, where as subjects move faster they tend to become less accurate leading to less successful movements. The opposite would also be true, where as the target requirements becomes more strict (harder to stop in target) subjects also tended to slow down. Previous work has shown that depending on reach distance, variability of the movement changes (146?). These studies did not investigate how movement variability affects

self selected speeds, only how far subjects would move. By including this probability of reward that is dependent on movement speed and mass into utility, we are able to reasonably predict the self-selected movement speed across two experiments with a single α parameter. To our knowledge, this is the first study that has been able to explain multiple self-selected speeds with a single model.

4.4.2 Cost of Transport

One common method used to explain movement speed is to minimize the total metabolic cost of the movement. Minimizing metabolic cost of transport has been used to explain preferred walking and running velocity across many different studies (2; 17; 26; 72; 86; 122; 137; 152; 154; 163; 164). In this study however, we found that subjects typically do not make their reaching movements at the metabolic minimum. A possible explanation is that when making reaching movements effort is discounted by time. Temporal discounting has been shown in relation to rewards as well as cost of time (142; 168; 172). The utility model presented here assumes that both reward (α) and effort (E) are both discounted by time (166). When discounting both by time, either gross metabolic cost or net metabolic cost can be used to explain the preferred reach duration. However, the type of metabolic cost that we use affects the parameter that is fit in the utility framework (Eq. 4.5). Interestingly, we do see that the change in the metabolic minima is also very similar to the change in self-selected movement speeds. According to our metabolic model, gross metabolic costs' movement duration increased by 6.4%, 9.7%, and 13.8% with the masses seen in experiment 2 (table 4.1). Experiment 2a increased by 8.6%, 12%, and 16% for the added masses. All the normalized movement durations are show in table 4.1 and shown in figure 4.7. We can see that across experiments and metabolic optimization the normalized durations remain consistent. This indicates that while metabolic cost may not alone predict movement vigor, it may still be an important factor in determining changes in movement vigor.

Exp	2a	2b	2c	Net Gross	Net Met
2.47 kg	1	1	1	1	1
3.80 kg	1.086	1.071	1.114	1.065	1.064
4.70	1.121	1.100	1.174	1.098	1.097
6.10	1.164	1.166	1.237	1.140	1.138

Table 4.1: Normalized movement durations for experiment 2a, 2b, 2c, gross metabolic cost and net metabolic cost.

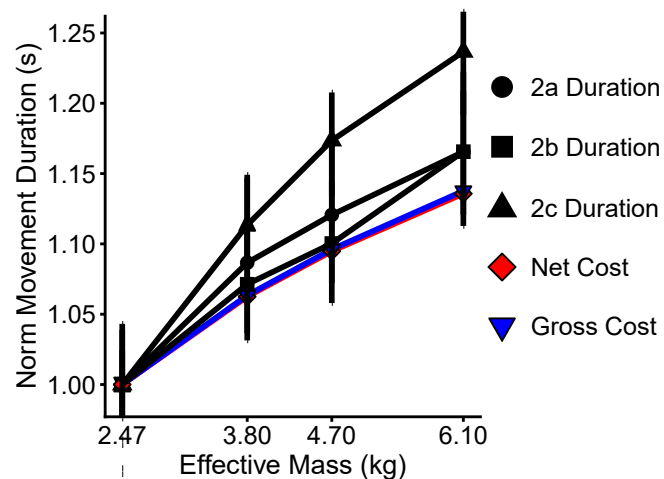


Figure 4.7: Normalized movement duration for experiment 2a, 2b, 2c, gross metabolic cost, and net metabolic cost. Generally, the changes in movement vigor due to increased mass is conserved across experiment and metabolic cost calculation.

4.4.3 Energetic Budget

One possible explanation as to why we slow down with increased effort is that for every movement there is only a set amount of energy planned to be used, and because of this we slow down for a given distance with increasing effort (93). When walking with loads, Goldman et al. show that the cost of walking (per kilogram meter) with added loads does not change. This may indicate that for a specific distance, humans have a specific energetic budget for the movement. When the difficulty of a movement increases, to keep the energetic budget the same we must slow down. This data indicates that humans do not have some budget, but that we slow down primarily due to increased effort. Using the metabolic model (Eq. 4.3) and applying the masses and movement durations in experiment 2a, we would find that the metabolic cost of the movements in 2a are 86.9, 89.5, 90.9, and 93.1 J for the added mass conditions. If we normalize these values to the added mass to get the same units as Goldman et al., we find 347, 226, 186, and 148 J/(kg m). This shows that as effort increases, not only do we slow down, but the total energy expended during the movement also changed.

4.4.4 Accuracy

Across both experiments, the effect of movement duration on endpoint error was much larger than the effect of mass. In experiment 1, subjects were forced to move in specific time windows which may have caused the effect of mass in this experiment. Experiment 2 did not show an effect of mass but experiment 1 did. In experiment 2, subjects were free to choose their movement duration. Increasing movement duration reduced error as the speed accuracy trade off would predict (40; 54). Mass did not change the consistency with which subjects made their movements in either experiment, but as expected, movement duration reduced the endpoint variability. Angular error variability may be affected by mass ($p = 0.0114$), but this could be driven by the subjects preferring to reach more towards the lower inertial directions of the arm as the lowest inertial directions are not oriented exactly at 45° and 225° , which caused subjects to reach slightly off center from the

target (63).

4.4.5 Reaction Time

We found that increasing the effort of a movement also increases the reaction time and this can be predicted by the utility model (166; 173). It has been shown that increasing reward leads to early reaction times by increasing the total utility of the following movement. The opposite is also true, where increasing effort reduces utility and leads to longer reaction times. The rate of evidence may be linked to the utility being assigned to the movement (166). This leads to lower utility movements having a lower evidence accumulation rate which leads to longer reaction times. Drift diffusion models have been shown to make accurate predictions of reaction time (140; 153). In this paradigm subjects react once evidence for a movement has accumulated to a certain threshold. In our study all the targets were the same shape within an experiment, so rate of evidence accumulation may be the same. Knowing this, our result that subjects reacted slower may indicate that more evidence was required before movement initiation for higher effort movements.

4.5 Conclusion

In this study we wanted to determine the effect of mass on the metabolic cost and the movement duration of reaching movements, and if we can use metabolic cost or a utility framework to explain these movement durations. Added effort (mass), lead to an increase in metabolic rate and cost. An effort model (eq. 4.1) predicts that this increase in cost is sublinear with mass. Adding mass (effort) to a movement also increased the movement duration. Minimizing the metabolic cost of the movement was not able to predict these movement durations. Using a utility framework (eq. 4.5), we can reasonably predict the experimental movement durations across multiple experiments.

4.6 Methods

This study is composed of two main experiments (1 and 2), and a model analysis. The first experiment measured the effect of mass and speed on the metabolic power of reaching. The second

experiment determined how mass affected preferred reaching speed. In the final model analysis, we used the measured metabolic data from Exp. 1 to determine which utility formulation can best explain the preferred movement observed in Experiment 2.

4.6.1 Experiment 1 - Effect of mass on metabolic power

In the first experiment, 5 male and 3 female, all right-handed, with an average age of 28.9 years (std = 5.5), average weight 66.7 kg (std = 11.7), and average height 173.4 cm (std = 10.4) completed the protocol. All subjects except one completed the experiment in two sessions. The remaining subject completed the protocol over 3 sessions. All participants reported no neurological, cardiovascular, or biomechanical problems that could interfere with the study. Subjects gave written informed consent, as approved by the University of Colorado Institutional Review Board.

4.6.1.1 Protocol

Subjects completed reaching movements with varying speed and mass requirements. Reach kinematic and metabolic data was collected as a function of mass and speed (Fig. 4.1A). Subjects sat in a chair that was height adjusted to place the screen 3 feet in front and 1 foot above of the subjects' line of vision, with their arm in a horizontal planar position. They were trained to move a cursor from a home circle and stop at a target circle within a specified time window. Subjects made reaching movements in seven distinct time windows across four different masses (Fig. 4.1B). A block refers to one speed combined with one mass condition. The number of trials per block was determined such that each block consisted of five minutes of reaching at the desired speed, where the first 20 trials of each block were used for training. To begin a trial subjects held a circular cursor ($r = 0.4$ cm, yellow colored) within the home circle ($r = 1.1$ cm, white circle) location for 200 ms. The home circle then disappeared and a target circle 10 cm away appeared randomly at 45, 135, 225, and 315 degrees from the right horizontal. In training, a blue dot would make a simulated movement from the home circle to the target circle using a minimum jerk trajectory. Feedback on movement duration was given when the center of the cursor was within the target the first time. If

subjects moved too slow the target circle would turn grey, whereas if the subject moved too quickly the target would turn green. Appropriately timed movements resulted in the target flashing yellow and a pleasant tone. Upon completing an outward reaching trial, the home and target circle would swap locations and the subject would make another reaching movement towards the center of the screen. Subjects completed four different mass conditions and six different speeds. The completed mass conditions were 0 kg (0 lbs), 2.3 kg (5 lbs), 4.5 kg (10 lbs), and 9.1 kg (20 lbs) of added mass at the robot handle which supported the vertical mass. The seven different time windows were: Very Slow (VS, 1.25 – 1.35 s, 160 trials), Slow (S, 1.05 – 1.15, 170 trials), Medium (M, 0.85-0.95 s, 200 trials), Fast (F, 0.65-0.75 s, 220 trials), Very Fast (VF, 0.45-0.55 s, 240 trials), Very, Very Fast (VVF, 0.325-0.425 s, 250 trials), and Very, Very, Very Fast (VVVF, 0.225-0.275 s, 260 trials). For 0 kg and 5 2.3 kg added, subjects would complete the speed conditions of S to VVVF. For 4.5 kg and 9.1 kg added, subjects would complete the speed conditions of VS to VVF.

4.6.1.2 Metabolic Data Collection

Metabolic data was collected for the duration of each five minute reaching block. Subjects wore a nose clip and breathed into a mouthpiece, connected to a metabolic cart (ParvoMedics, TrueOne 2400), which measured \dot{O}_2 consumption and \dot{CO}_2 production. Subjects were required to be well rested and have fasted for 8 hours before testing. Testing sessions began with the subject resting in a seated position in a chair for 10 minutes. Three baseline readings were then taken for 5 minutes each before the experimental protocol began. During these baseline readings, subjects sat quietly in the experiment chair, and held the robotic arm manipulandum. Subjects then began the arm reaching trials. Five-minute rest periods were provided between each block of reaching trials.

4.6.2 Experiment 2 - Effect of mass on preferred movement duration

In the second experiment, a separate cohort made seated horizontal arm reaching movements using a robotic arm manipulandum (Interactive Motion Technologies Shoulder-Elbow Robot 2) while secured to a chair by a 4-point seat belt. The seat was height-adjusted to place the screen

3 feet in front and 1 foot above the participant's plane of view, with their arm in a horizontal planar position in a similar manner to experiment 1 (Fig 4.1). All participants provided written informed consent and reported no neurological, cardiovascular, or biomechanical problems that could interfere with the study.

4.6.2.1 Kinematic Data Collection

Subjects made reaching movements within five blocks of mass conditions. The five blocks were a familiarization block, 0 kg, 1.36 kg (3 lbs), 2.27 kg (5 lbs) or 3.64 kg (8 lbs) added at the hand. The order of the weighted conditions was randomized for each subject. The downward weight of the added masses was supported by the robot, so these masses only added inertial effects to the arm. The position of the handle controlled a cursor on a computer screen that was placed just above head level and about 3 feet in front of the subject. Subjects arm positions started in approximately the same orientation. Visual feedback was provided to the subjects throughout the experiment on whether they completed the reach movement in the prescribed duration. To begin a trial subjects held a circular cursor ($r = 0.4$ cm, yellow colored) within the home circle ($r = 1.1$ cm, white circle) location for 200 ms. The home circle then disappeared and a target circle (shape dependent on experiment) 10 cm away appeared randomly at 45, 135, 225, and 315 degrees from the right horizontal. A subject would go through all four outward targets in a pseudorandom order then begin again (Fig. 4.3).

Experiment 2a In this experiment 8 male and 4 female subjects, all right-handed, with an average age of 26.2 years (std = 3.1), average weight 68.4 kg (std = 4.4), and an average height of 173.6 cm (std = 11.1) completed the experiment (Fig. 3B). Subjects underwent 5 different blocks of 400 reaching movements (200 out and back movements) to four different targets. The subjects would make horizontal arm reaching movements towards a circular target, similar to experiment 1 ($r = 1.4$ cm, red color). For each reaching movement, the target would explode indicating a correct movement duration as the movement duration criteria was set between 1ms and 10000 ms, so there were not time requirements imposed on the reaching movements. In this experiment we wanted

to ensure subjects came to a complete stop before the trial ended, so the dot would explode after the subject had remained in the target for 300 ms and the velocity during that time was under 0.5 mm/s.

Experiment 2b We wanted to ensure that the effects on movement duration from mass were not influenced by the size of the target or accuracy costs. We ran two more similar experiments in which we altered the shape of the target to change the accuracy costs of the movement.

In experiment 2b, there were 9 male and 3 female subjects who completed the protocol, with an average age of 25.0 years (std = 3.61), average height of 171.5 cm (std = 7.58), and an average weight of 67.5 kg (std = 2.99). Subjects completed 400 out and stop trials in familiarization, and 200 out and stop for each added mass condition. In this experiment, the target was a section of a 10 cm circular arc centered on the home circle oriented at the same positions as experiment 1 and 2a. Subjects would need to stop between 10 cm and 11 cm from the home circle and within 7 degrees (2.44 cm arc length) of the center of the arc target for the target arc to turn green. If subjects overshot the target (went past 11 cm) the target would turn red indicating an overshoot. Thus, this experiment had tighter accuracy constraints in the radial direction (1cm) compared to experiment 2a where the equivalent constraint in the radial direction was 2.8 cm.

Experiment 2c Experiment 2c was completed by 18 subjects, 9 male and 9 female, with an average age of 25.1 ± 3.7 years old. Subjects completed 100 out and back movements for familiarization, and 200 out and back movements for each mass condition. The target was a 90-degree section of a circle that subjects had to reach towards. However, subjects did not need to stop at any specific location, just hit the target arc, turn around and return to the home circle. In this experiment we used the point that they turned around as the end of their movement. This experiment was used to simulate a zero-accuracy cost with a very very large target.

4.6.3 Data Acquisition and Analysis

For all experiments, robot handle X and Y position data was recorded at 200 Hz and analyzed in MATLAB 2019a. Position data was filtered using a fourth order lowpass Butterworth filter (cutoff

frequency 10 Hz) and differentiated using a double five-point differentiation to obtain velocity and acceleration. To calculate radial velocity, we calculated the Euclidean distance from the home circle and differentiated using five-point differentiation.

4.6.3.1 Metabolic Processing

The gross metabolic rate was calculated in joules per second, \dot{e} , using the method described by Brockway (Eq. 4.8) (Brockway, 1987):

$$\dot{e} = 16.58V\dot{O}_2 + 4.51V\dot{CO}_2 \quad (4.8)$$

Average baseline metabolic rate from the three baseline sessions was subtracted from gross metabolic rate to determine the metabolic rate associated with the reaching movement only, or net metabolic rate. Subjects made reaching movements for 5 total minutes, but metabolic rate was calculated only using the last 3 minutes of each block to allow subjects to reach a steady metabolic rate while reaching. After data was collected, custom MATLAB scripts were used to parse the data by trial, mass, and speed. Movement duration was calculated using the last 3 minutes within a block. The overall metabolic rate is then normalized by the fraction of time spent moving.

4.6.3.2 Metabolic cost models

We used the measured metabolic power data, \dot{e} , to parameterize the metabolic cost of a movement, E , as a function of mass and movement duration. Parameter estimates were computed using the function nls from package nlstools. Using the data in experiment 1, we fit gross metabolic power to the following function 4.9 using average subject effective mass (described later in methods), metabolic power and movement durations. The fitted parameters are a , b , i , and j , where a represents is an offset representing the cost of not moving, b is a scaling parameter, i shows how effort scales with mass, and j shows how effort scales with time. Further, m represents the effective

mass of the movement and T represents the movement duration.

$$\dot{e} = a + \frac{bm^i}{T^j} \quad (4.9)$$

To obtain an expression for the total metabolic cost of the movement, E , we multiply 4.9 by movement duration, T:

$$E = aT + \frac{bm^i}{T^{j-1}} \quad (4.10)$$

Importantly, the above expression also tells us the metabolically optimal movement duration for a movement of a given mass.

To determine whether the cost of resting was influenced by added mass, we fit an additional metabolic cost model was fit to gross metabolic power data that included a term for effective mass that multiplies the a parameter. This represented a mass-dependent cost of resting, where k is the scaling on the resting mass cost:

$$\dot{e} = a * \text{Added Mass}^k + \frac{bm^i}{T^j} \quad (4.11)$$

AIC and BIC scores are calculated for each metabolic cost model.

4.6.3.3 Movement Onset and Offset

Many of our metrics are dependent on identifying the instant the movement began (movement onset) and the instant the movement ended (movement offset). To detect movement onset and offset we used a custom algorithm for all experiments. Movement onset algorithms are often influenced by movement speed and we wanted to minimize this effect (23; 156). We first computed the velocity towards the target by differentiating the distance from the center of the target. For movement onset we find the first time the velocity towards the target reached 20% of the maximum velocity towards the target. From there the algorithm searches backwards (in time) to a point where either there is either 4 frames of acceleration away from the target in the next 10 frames or where the

standard deviation in the velocity towards the target was less than 2e-3 in those 10 frames. Using this method, we detect the first time the subject begins consistently accelerating towards the target. This led to detecting movement onset much earlier than many velocity thresholding algorithms, where we find an average velocity at movement onset of -0.389 ± 8.019 for experiment one (mean \pm sd), 1.019 ± 2.220 mm/s in experiment 2a, -0.052 ± 5.552 m/s for experiment 2b, and -0.098 ± 5.077 mm/s in experiment 2c. To detect movement offset in experiment 2a and 2b, we found the first time the reaching movement was first 9 cm away from the home circle, then used the same method as reaction time to determine the offset. We find the first time the standard deviation of the velocity towards the target is less than 2e-3. In experiment 2c, movement offset is determined as the point subjects turn around and begin moving back towards the home circle.

Because reaction time algorithms can be dependent on movement duration (23; 156), we needed to compare these changes in reaction time to computed reaction times from simulated movements. These movements can be generated using the range of movement durations in experiment 1 or 2. This will inform us if the reaction time changes are due to changes in movement duration or added mass. We simulate reaching movements with similar movement times to the experiment using a minimum jerk trajectory and a simulation of the arm making reaching movements (Flash Hogan, 1985). Using the minimum jerk simulation, we found that over the span of movement durations for experiment 1 the reaction time would increase with increasing movement duration. Over the movement duration ranges (.45 s – 1.4 s) the reaction time would increase due to the algorithm by 40 ms. Simulating the minimum jerk for experiment two, over the movement durations (0.77s – 0.90s), the reaction time would increase by 0.3 ms. We also used a biomechanical model of the arm like other studies to test if the change in reaction time could be attributed to subjects using the same control signal for different masses (113). The reaction time change given the same control signal across masses was small, about 3 ms. In experiment one, the average reaction times across speeds ranged from 0.1377s to 0.245s. This is much larger than the effect of movement duration from the simulated movement durations simulation like experiment one (108 ms experimental vs 40 ms simulated). The algorithm used is affected by movement duration, but

the change in calculated reaction time is greater than the range from just the effect of speed on the calculated duration.

In experiment 2, the range of reaction times calculated from the simulated movements ranged 0.3ms. The reaction times calculated from this experiment ranged by 17 ms for experiment 2a, 24ms in experiment 2b, and 15 ms in 2c. The reaction time range in experiment one has a much larger range than the calculated reaction times of the simulated movements. This indicates that the changes in reaction time were due to mass, not the movement onset algorithm or changes in the movement durations.

4.6.3.4 Movement Duration

Movement duration is calculated as the time between movement onset and movement offset. The desired movement times in experiment 1 were generally longer than the prescribed movement times in the protocol. This is due to the feedback being given before the end of the movement as subjects would take some time to settle on the target and feedback was given as soon as they reached the target.

4.6.3.5 Error Calculations

We investigated three measures of error for all experiments. Endpoint error was the Euclidean distance between the cursor at movement offset and the center of the target. We then broke endpoint error into two components, angular error, and radial error. Angular error was calculated as the angle between the vector pointing from home circle to target circle, and the vector from home circle to the cursor at movement offset. A clockwise angular error was considered negative. The second metric, radial error, was calculated as the Euclidean distance from the target center (10 cm from the home circle, center of the arc) at movement offset. Maximum excursion was also calculated as the greatest Euclidean distance from the home circle during the movement. Experiment 2c had no stopping criteria, so endpoint error is defined as the maximum excursion.

4.6.3.6 Outlier Analysis

In experiment one, we removed outlier trials from the statistical analysis if they did not complete the movement correctly. Movement kinematic metrics were computed for every trial, then we removed trials based on specific criteria. We removed any trial where the endpoint error was greater than 10 cm (reached the wrong target), the movement duration was less than 0.2 seconds or greater than 2 seconds (did not make the movement), the reaction time was greater than 0.50 s (failed to initiate movement), or the absolute miss angle is greater than 50 degrees (reached to wrong target).

For the kinematic statistical analysis, the data is then split into outward and inward reaching movements and we only use the outward reaches in the statistics. Inward and outward trials are split because on inward movements subjects knew where the target would show before it was indicated, which affects movement kinematics. After removal of trials, 27 out of 15925 outward trials were removed.

In the second experiment, we removed trials that were outside 1.5x the interquartile range of movement duration, reaction time, reaction velocity, or miss distance (62). Reaches with a maximum excursion of more than 14cm were also filtered out in experiment 2a and 2b. The data from experiment 2a and 2b were also split into outward and inward trials for the same reason as experiment 1. Statistical and kinematic analysis were done on the outward trials. This removed 702 out of 9600 outward trials in 2a; 671 trials of 9600 are filtered out for experiment 2b; 2335 of 14400 trials are filtered out for experiment 2c.

4.6.4 Effective Mass Calculation

For all models, mass was represented by the subject-specific effective mass of the arm, averaged over the four reach directions. Effective mass is an estimate of the arm's resistance to motion when to a force applied in each direction (166). Segment lengths and masses are estimated from anthropometric tables. (34; 47; 193).

To determine the effective mass of the arm at a given time point we defined the Jacobian matrix for a two-link model of the arm, Λ , where l_1 is the length of the upper arm and l_2 is the length of the forearm. θ_s and θ_e are the shoulder and elbow joint angle respectively:

$$\Lambda = \frac{dx}{d\theta} = \begin{bmatrix} -l_1 \sin(\theta_s) - l_2 \sin(\theta_s + \theta_e) & -l_2 \sin(\theta_s + \theta_e) \\ l_1 \cos(\theta_s) + l_2 \cos(\theta_s + \theta_e) & l_2 \cos(\theta_s + \theta_e) \end{bmatrix} \quad (4.12)$$

The inertial matrix ($I(\theta)$) is defined in Eq. 4.13, where mass is mass added at the hand. The centroid lengths, r_1 and r_{22} , refer to the centroid length of the upper arm and forearm with mass added. $I_{COM,1}$ and $I_{COM,2}$ are the moment of inertia about the center of mass for the upper arm and forearm.

$$I = \begin{bmatrix} m_1 r_1^2 + I_{COM,1} + (mass + m_2)(l_1^2 + r_{22}^2 + 2l_1 r_{22} \cos(\theta_e)) + I_{COM,2} \\ (m_2 + mass)(r_{22}^2 + l_1 r_{22}^2 \cos(\theta_e)) + I_{COM,2} \\ (m_2 + mass)(r_{22}^2 + l_1 r_{22}^2 \cos(\theta_e)) + I_{COM,2} \\ m_2 r_2^2 + mass \cdot l_2^2 + I_{COM,2} \end{bmatrix} \quad (4.13)$$

The mass matrix (M) is defined as:

$$M = (\Lambda^{-1})^T I(\theta) \Lambda^{-1} \quad (4.14)$$

We obtain the effective mass, m , in a given reach direction by applying a unit vector acceleration in that direction and calculating the magnitude of the resultant force vector. Each subject's specific effective mass for experiment 1 and 2a was calculated using anthropomorphic measurements and estimates (34; 94; 193). In the first experiment the average effective masses of the four mass conditions were 2.44 ± 0.064 , 4.834 ± 0.068 , 7.127 ± 0.070 , and 11.691 ± 0.071 kg. In experiment 2a the effective masses of the subjects and robot arm in the four mass conditions were 2.506 ± 0.073 ,

3.959 ± 0.073 , 4.894 ± 0.075 , and 6.282 ± 0.076 kg. The average effective mass in experiment 2a is used for effective mass in 2b and 2c.

4.6.5 Models of optimal movement duration

Here we describe the modeling analysis employed to calculate predicted optimal movement durations with changing effort and accuracy requirements. We test the ability of three different formulations of utility to explain the preferred movement durations observed in experiments 2a and 2b. The three candidate utility formulations are: 1) maximization of net reward rate (reward minus metabolic cost, all divided by time), and 2) maximization of net reward (reward minus metabolic cost), and 3) minimization of metabolic cost. In all model fits, we use the group average data for effective mass, movement error, movement duration, and reaction time. Both the first and second utility formulations rely on fitting a single parameter, while the third utility involves no free parameters.

4.6.5.1 Optimal duration based on maximizing net reward rate

When the goal of the movement is maximizing net reward rate, the utility is determined by the sum of the reward of the movement (α) minus the sum of the effort (E), both discounted by time (T) and is shown in Eq. 4.15.

$$J = \frac{\alpha - E}{T} \quad (4.15)$$

Effort is the metabolic cost of the movement (Eq. 4.16) and is represented by the expression obtained from the measured metabolic data in experiment 1 (Eq. 4.9). Total time is split into reaction time, t_r , and movement time, t_m . We use the measured reaction times from experiments 2a and 2b and solve for the movement durations that maximize utility. Here the only parameter to be fit is α , which represents the subjective reward associated with completing the arm reaching movement. The reaction times used from experiment 2a are 0.178 ± 0.013 , 0.185 ± 0.014 , 0.190

± 0.013 , 0.196 ± 0.013 for 2.47kg, 3.80 kg, 4.70 kg, 6.10 kg respectively. Experiment 2b reaction times were 0.205 ± 0.013 , 0.215 ± 0.013 , 0.219 ± 0.013 , 0.229 ± 0.013 . Experiment 2c reaction times were 0.199 ± 0.012 , 0.208 ± 0.011 , 0.213 ± 0.012 , 0.216 ± 0.012 .

$$\begin{aligned} J &= \frac{\alpha P(\alpha|t_m, m) - e_r - e_m}{t_r + t_m} \\ e_r &= \dot{e}_r t_r \\ e_m &= at_m + \frac{bm^i}{t_m^{j-1}} \end{aligned} \quad (4.16)$$

A single parameter alpha is used to fit data from both experiments. The main difference between the experiment 2a and 2b is the size of the target, which can be represented as the probability of acquiring reward at a given movement duration. To incorporate this speed-accuracy trade-off into the utility equation, we scale by the probability of stopping within the target given the movement duration and mass:

$$\begin{aligned} \ln\left(\frac{P}{1-P}\right) &= \beta_0 + \beta_1 t_m + \beta_2 m \\ P(\alpha|t_m, m) &= \frac{1}{1 + e^{-\beta_0 - \beta_1 t_m - \beta_2 m}} \end{aligned} \quad (4.17)$$

The probability function scaling α was determined using target criteria from experiment 2a and 2b and movement kinematic data from experiment 1. Each arm reaching movement in experiment 1 was labeled as a success according to the success criteria (target size) from experiment 2a and 2b. Thus, each trial in experiment 1 will have two labels for success. The first label from success in experiment 2a and the second from success in experiment 2b. For experiment 2a labeling, we labeled a reach as a success if the endpoint error was less than 1.4 cm. For experiment 2b, we labeled each reach as a success if the maximum excursion was less than 11 cm (and greater than 10cm), and the angular error was less than 7 degrees. After determining if each reach was a success or not, we use an inverse logistic regression (R, glm model with binomial family and logit link

function) to fit function $P(\alpha|t_m, m)$ for each experiment, obtain two sets of beta coefficients.

For experiment 2a, we found the beta coefficients of the regression to be $\beta_1 = -0.0946 \pm 0.008$ for mass, $\beta_2 = 5.877 \pm 0.188$ for movement duration, and an intercept of $\beta_0 = -1.450 \pm 0.125$. Experiment 2b had coefficients of $\beta_1 = -0.0828 \pm 0.006$ for mass, $\beta_2 = 6.0912 \pm 0.129$ for movement duration, and $\beta_0 = -2.9312 \pm 0.091$ for an intercept. These logistic regressions represent $P(\alpha|t_m, m)$ in the utility model.

$$J = \frac{\alpha P(\alpha|t_m, m) - \left(a_0 t_r + a t_m + \frac{b m^i}{t_m^{j-1}} \right)}{t_r + t_m} \quad (4.18)$$

We optimize this utility model (Eq. 4.19) by finding the value that minimizes the sum of squared error between predicted movement duration and the average movement duration from experiments 2a and 2b. Data was analyzed with the function `optimize` in R and a custom written error function.

4.6.5.2 Optimal duration based on maximizing net reward

When the goal of the movement is maximizing net reward, the utility is determined by the sum of the reward to be acquired (α) minus the total effort of the movement (E):

$$J = \alpha P(\alpha|t_m, m) - \left(a t_m + \frac{b m^i}{t_m^{j-1}} \right) \quad (4.19)$$

Here again we fit a single parameter, `/alpha`, to find the optimal movement durations that best match the observed durations in experiments 2a and 2b.

4.6.5.3 Optimal duration based on maximizing gross efficiency

Another possibility is that subjects choose movement speed to be the most efficient in their gain. Efficiency we define as the reward gained divided by the total cost of the movement.

$$J = \frac{P(\alpha|t_m, m)}{a_o t_r + a t_m + \frac{bm^i}{t_m^{j-1}}} \quad (4.20)$$

In this model there is no fitted α value, as that does not change the optimal duration. Only the probability of successfully completing the movement does.

4.6.5.4 Optimal duration based on minimizing metabolic cost

The metabolically optimal duration is the movement duration that minimizes the metabolic cost of movement of a given mass. This is calculated, as described earlier, by minimizing Eq. 4.10.

4.6.6 Statistical Tests

Kinematic data was exported to R (v 1.2.5001) for statistical analysis. Linear mixed effects models were computed using the lme4 and multcomp package, and the functions used were lmer and cftest. To analyze the effect of mass on the kinematic variables we used linear mixed effects models. The effective mass used in the linear mixed effects models is the average effective mass from experiment 1 and experiment 2a. Experiment 2a effective mass values are applied to experiment 2b and 2c.

For experiment one, we tested a model with no between-subject variables and added mass and movement duration as within-subject variables. We tested gross metabolic power, endpoint error, endpoint angle variance, radial endpoint variance, and reaction time as dependent variables. Some variables were log-transformed to linearize the data for use in the linear mixed effects model. The outcome variables that were log transformed were metabolic power, the angle which subjects missed the target by (and variance), and subjects' radial endpoint (and variance).

Lme4 log formula: $\log(\text{Outcome}) \sim \log(\text{Movement Duration}) + \text{Effective Mass} + (\text{1Subject})$

Lme4 non-log formula: $\text{Outcome} \sim \text{Movement Duration} + \text{Effective Mass} + (\text{1Subject})$

For experiment two we tested main effects of movement direction and mass. We do not report p-values for movement direction as we are interested in the effects of mass, though it is known movement direction affects speed (63).

Lme4 formula: $\text{Outcome} \sim \text{Movement Direction} + \text{Effective Mass} + (\text{1Subject})$

An ANOVA (aov in r) with post hoc Tukey tests (TukeyHSD) were used to test differences between experiments (2a, 2b, and 2c). Experimental data was aggregated for each experiment and subject before use in the ANOVA and Tukey test.

ANOVA formula: $\text{Outcome} \sim \text{Experiment} + (\text{1Subject})$

We use a significance level of $\alpha = 0.001351$ or $1.351e-3$ as we made 37 comparisons. We compute 29 linear mixed effects models and 2 ANOVAs with 3 Tukey Post Hoc comparisons for each ANOVA. Exact p-values are reported unless it is less than $2e-16$. The linear model estimates are reported for the significant variables. For non-significant factors only the p-value is reported.

Chapter 5

An overview of musculoskeletal modeling of movement

In the previous chapter, we explain movement vigor using effort and utility. In that study, we attempt to represent effort with metabolic cost, but many times metabolic cost can be difficult to measure. In decision making studies, subjects complete hundreds of possible decisions where they weigh the effort and reward and then complete that movement. However, to get an accurate estimate of effort using metabolic cost subjects would need to make a decision, then repeat that movement multiple times. This has led researchers to using musculoskeletal modeling to estimate metabolic rate in movement. This chapter focuses on explaining the steps required for musculoskeletal modeling and showing some common metabolic rate representations. This is then used in the next chapter to evaluate the accuracy of these metabolic models.

5.1 Introduction

Muscle-driven biomechanical models of human motion are important tools in understanding the underlying mechanisms that drive movement and how alterations to the musculoskeletal system can lead to pathological movement (51; 130; 202). Musculoskeletal models allow biomechanists and researchers to simulate muscle forces and mechanical properties of the muscle using mathematical models for activation and contraction dynamics without needing to directly measure the internal workings of the muscles or joints. These studies have become popular in simulating a wide variety of movements including walking, running, cycling, reaching, and certain pathological gaits.

The advantage of these models is derived from the fact that specific properties (internal forces,

muscle forces, energetic rates or costs) during movement can be difficult to measure under some circumstances (83). One of the primary metrics that musculoskeletal modeling attempts to simplify is the measurement and calculation of metabolic cost in movement (section 2.3.2-2.3.3). Measuring metabolic cost experimentally requires repetition of similar movements at a steady metabolic rate, which cannot easily be achieved for novel movements (section 2.3.2). This can be constraining, given the importance of metabolic cost in determining movement choices. For example, if we wanted to determine the effort cost between two arm reaching decisions a subject would need to make a choice, make the chosen movement, then repeat this movement for 2-3 minutes. Making many of these decisions, and then measuring the effort for each decision would take an extreme amount of time and is unrealistic. The difficulty in measuring the metabolic cost forces researchers to use a representation of metabolic cost in their objective function (51; 106; 180). However, many of these metabolic cost models have not been validated for full body or multi-muscle systems. Recent studies have begun to quantify how well metabolic models, coupled with musculoskeletal models, represent the metabolic cost of common movements. (107; 131).

Muscle driven models are usually used to estimate muscle forces given a movement trajectory. By optimizing an objective function (neural drive, muscle active state, metabolic cost, etc.) these models can simulate the muscle forces to either replicate a movement or produce a new desired movement. When simulating these movements, there are three primary simulation methods used. The first two methods are used to replicate a specific movement trajectory (static optimization and electromyography (EMG) driven optimization), and the third is used to simulate new movements (dynamic optimization) (202).

The first and most common method is static optimization using inverse dynamics. Researchers record the movements of subjects with motion capture systems and then use inverse kinematics and dynamics to calculate joint trajectories, joint forces, and joint torques. An objective function is then optimized at each time step (static optimization) to determine the distribution of muscle forces.

The second method uses an objective function that includes matching the joint torques from

inverse dynamics and matching collected EMG signals to simulated EMG signals from the activation dynamics of the muscles (33). This method is difficult due to noisy EMG signals, but modeling methods can try to account for this by assuming both EMG and inverse dynamics data is noisy and using filtering techniques to reduce the noise (202).

The third method does not use empirical data but tries to generate de novo movement trajectories (and accompanying muscle activations) by minimizing an objective function; this is usually referred to as dynamic optimization. By minimizing the objective function, this method determines the input from the central nervous system to the muscles to control and produce a movement (39; 131). This method is sensitive to the objective function and very similar objective functions can produce very different movement (51). These muscle-driven models have simulated a large variety of movements and can give us insight into properties that are very difficult to measure.

In this chapter I will address the concepts required to simulate movements using musculoskeletal models, with a focus on the simulation of arm reaching movements with static optimization using inverse dynamics (first method described above). Many of the steps and properties can be extended to other paradigms such as walking. Lastly, I will outline common models used to predict metabolic cost or rate of movement, which are detailed in the appendix.

5.2 Estimating Muscle Forces

The primary goal of many musculoskeletal models is to determine the muscle forces that drive the kinematics of a specific motion. I will outline the how to match the joints' kinematic profiles by simulating muscles as the actuators to produce the joint torques for motion (41; 69). The eight steps in the muscle force estimation problem are shown in the flow chart below (fig. B.3) and described in more detail below. Arrows show the output from each step which is used as an input for the next step.

- (1) The first step is determining the trajectory by experimentally collecting kinematic data (55).

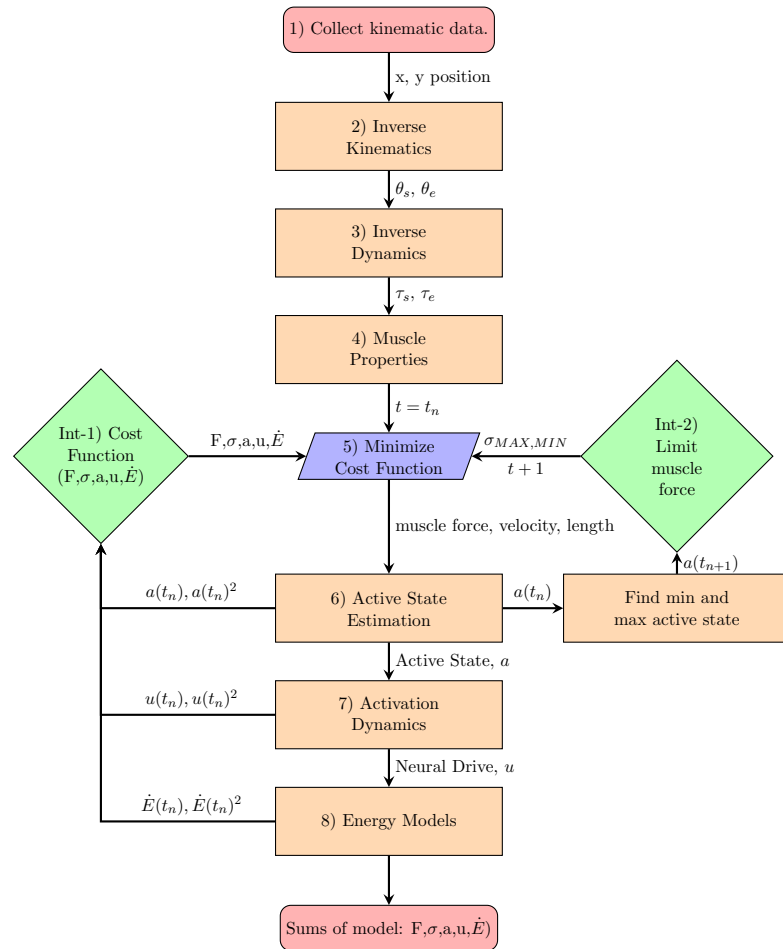


Figure 5.1: A model flow chart for simulating reaching movements.

- (2) Inverse kinematics is used to determine the joint positions and velocities.
- (3) Inverse dynamics is used to calculate the joint torque's across the joints (165).
- (4) Using the position of the joints, a muscle model computes the length and velocities of the muscles. These lengths and velocities are used to compute active state from muscle properties in step 6.
- (5) After joint positions, torques, and muscle parameters are determined, a muscle model is implemented at every time step to compute the muscle forces required to produce the motion through matching joint torques and minimizing an objective function (step Int-1) (202). The objective function has 3 inputs, including the objective function being used in the optimization and two constraints: matching the torque from the kinematic data and a limit on the change of activation state. The objective function can take many forms including minimizing active state, neural drive, and an energetic model. This is not discussed below as there are many optimization methods that can solve an under-determined system given an objective function.
- (6) The muscle model considers force length and force velocity properties to calculate the active state of the muscle (25; 130).
- (7) The control signal is approximated using activation dynamics which generally take the form of first order non-linear filters (25; 130; 177; 195).
- (8) Last, one of many models of metabolic cost can be implemented to simulate the cost of movement (18; 90; 114; 127; 136; 136; 179–181).

This document focuses on static optimization, though there are some issues that make it difficult. One issue with many static optimizations is the nonlinear interaction between the control signal and muscle force generation caused by time delay or force-length and force-velocity properties (69; 202). These interactions may not play an important role in determining muscle forces

though. Some physiological models of muscle properties had little effect on the outcome of static optimization when compared to optimization with models ignoring this non-linearity (8). In many static optimizations, this non-linearity is solved by just simulating the activation states of the muscles at every time point by minimizing some objective function and ignoring the time component. This however can lead to activation states greater than one which is not physiologically accurate. A solution to this is to limit the activation state at a time step by the previous point in time, this slows down computation time but allows for non-linear contraction and activation dynamics (69). This is shown in the right side of the flow chart (step Int-2) that we constrain the activation states based on their previous state. The left side of the flow chart (step Int-1) illustrates that many possible cost functions can exist to distribute muscle force (33; 50; 178). The next sections describe most of these specific steps outlined above in more detail.

5.3 Dynamics (Step 1-3)

The first step in the musculoskeletal modeling process is to determine the joint torques around each joint. Joint trajectories and body segment masses are used by inverse dynamics to calculate joint torques. The process for doing this in horizontally planar arm reaching movements is documented in the appendix (section B.2.3). After joint are determined, the next step is to use musculoskeletal modeling to calculate the muscle properties and determine the force production in each muscle to produce the movement.

5.4 Muscle Properties (Step 4, 6)

The structure and architecture of the muscle determine how the muscle functions (116). To be able to simulate how muscles generate force when activated we need some understanding of how muscles are organized. There are five main muscle properties that affect how a muscle can produce force: the pennation angle, sarcomere length, sarcomere shortening velocity, physiological cross-sectional area (PCSA), and percent muscle activation.

These five main properties can be determined through dissection studies of the whole muscle,

and using a smaller sample from the full muscle (116). The angle of the muscle fibers relative to the direction the produced muscle force or along the tendon defines pennation angle (ψ). The higher the pennation angle, the more force a sarcomere would need to produce to produce force along the tendon. Muscle fiber length (l_f) is determined by measuring the distance from the origin of the proximal fibers to the insertion of the distal fibers. Muscle fiber length in modeling is usually normalized to the optimal fiber length to determine force-length properties (25). Shortening velocity is the rate of change in length of the muscle fiber normalized to the optimal fiber length. PCSA can either be measured or estimated from other properties (141). Active state is an estimation of the percent of muscle currently active, which is mainly used in simulation. Using equation 5.1, and the total muscle volume (V_m), an estimate for PCSA can be calculated. PCSA has the greatest impact on total muscle force, but if all other properties are similar a muscle will function in the same manner.

$$PCSA = V_m \cos(\psi) / l_f \quad (5.1)$$

The major component of muscles that change during motion are the length and shortening velocity of the muscles. These two properties have a large impact on force production due to interactions between actin and myosin at different lengths and shortening velocities.

5.4.1 Force Length/Velocity

Where the muscles are in the shortening/lengthening cycle and how stretched the muscles are alter the force producing properties of the muscles by a large amount (47; 116). Fick first saw the relationship between the force in a stretching muscle vs static muscle (53), Blix showed these properties of muscles in frogs (20), and Hill defined the relationships between muscle force and velocity (84).

The primary driving force of the force length and velocity properties is the interaction between actin and myosin within the sarcomere. A diagram showing the basic structure of a sarcomere is

shown in figure 5.2. In 1954, Huxley proposed the sliding filament theory, which describes how these two proteins interact to produce force (95). In this process, calcium (Ca^{2+}) binds to troponin which causes conformational changes in the tropomyosin complex which exposes myosin binding cites on the actin protein. This allows the myosin heads to bind to the actin sites, and release the energy stored from being in the 'cocked' position. ATP is used to release the myosin head and 'recock' it to be ready to produce more force. The amount of myosin actin binding available leads to the force length properties of the muscle, and how fast these proteins can attach and detach leads to the force velocity properties of muscle.

The force length curve (fig. 5.3a) is determined by how many cross bridges are able to form at any given point, structural proteins being too close to each other, or viscous properties of the muscles. When the muscle is compressed to a very short length, the actin proteins begin to push against each other and hamper force production even though the muscle may have maximum ability to form cross bridges. At a very stretched muscle length, the myosin heads may no longer overlap with the actin binding cites, leading to a loss in force production. However, at this very stretched position another protein, titin, begins to affect the force. This protein acts as both an attachment for myosin to the z-disk and m-line and acts as a spring at these long muscle lengths providing force to stretched muscles. At the optimal muscle length, there is maximum ability for myosin actin cross-bridge interaction without any other proteins jamming into each other causing a reduction in force.

The force velocity dependence of muscles arises from issues with how fast the muscle can form cross bridges between actin and myosin (52). When a muscle is contracting at very high speed the actin-myosin binding cannot occur at a fast-enough pace to keep producing high amounts of force. For these types of contractions, the velocity can be very high but force very low which leads to a low power output (52). This leads to a high cost for very fast shortening contractions. When the muscle is lengthening however, the force of the muscles increases while keeping cost low (81). This has been proposed to occur because of cross bridge cycling changes during stretch (81) caused by rapid detachment of cross bridges (121) or rearrangement of myosin filaments (119). Though

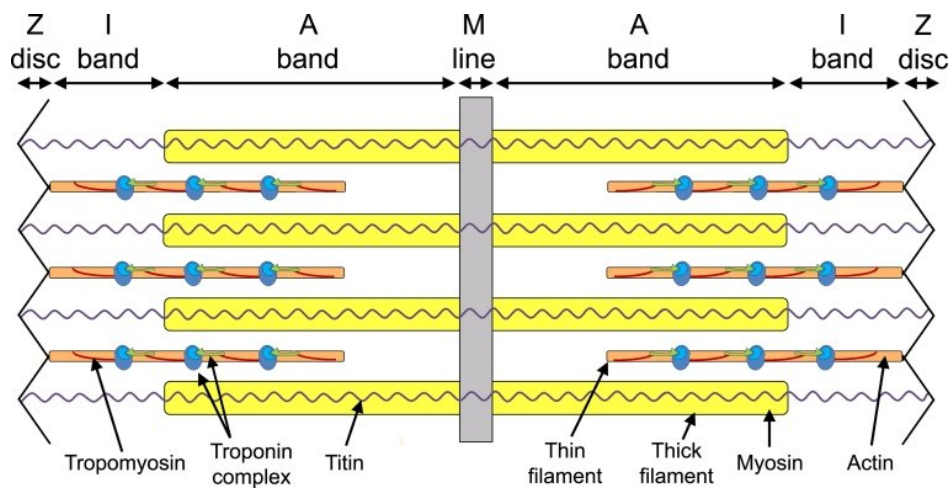


Figure 5.2: Diagram of a sarcomere in a muscle (from (46)).

recent evidence does show that cross bridge cycling cannot account for the full change in force production, and that titin may also play an affect (81). The amount of force produced for the energy required becomes very important when modeling metabolic cost and will be evident later on in the cost models section (section 5.6). An example of how the muscles can produce force with changing velocity is shown in figure 5.3b.

The primary muscle properties that have large effects on muscle force are pennation angle, sarcomere length, sarcomere shortening velocity, PCSA, and the active state of the muscle. Once the properties of the muscles are estimated, mathematical models of how the muscles act need to be developed.

5.4.2 Modeling Force Length/Velocity

The mathematical models of the muscles used in simulation need to be able to account for all previously discussed properties of muscles. The most common mathematical model used in biomechanics simulation is the Hill-type muscle model and is implemented in large packages like SIMM (41; 202). The Hill model represents the force of muscle by equation 5.2.

$$(F + a)(V + b) = (F_0 + a)b \quad (5.2)$$

In equation 5.2, F is the force the muscle can produce, V is the relative shortening velocity of the muscle, F_0 is the maximum isometric tension, a is a coefficient of shortening heat, b is a scaling coefficient where $b = a * V_0/F_0$ and V_0 is the maximum velocity of the muscle when the $F = 0$. The model simulates the force-length and force-velocity properties reasonably well. This is accomplished through a contractile element (CE) which is the muscle fiber, the parallel elastic element (PEE) which is the passive properties of the tissue around the muscle fibers, and the series elastic element (SEE) which represents the tendon and other elastic tissues. A diagram of this is shown in figure 5.4.

This model can be scaled to specific musculoskeletal actuators depending on the PCSA and

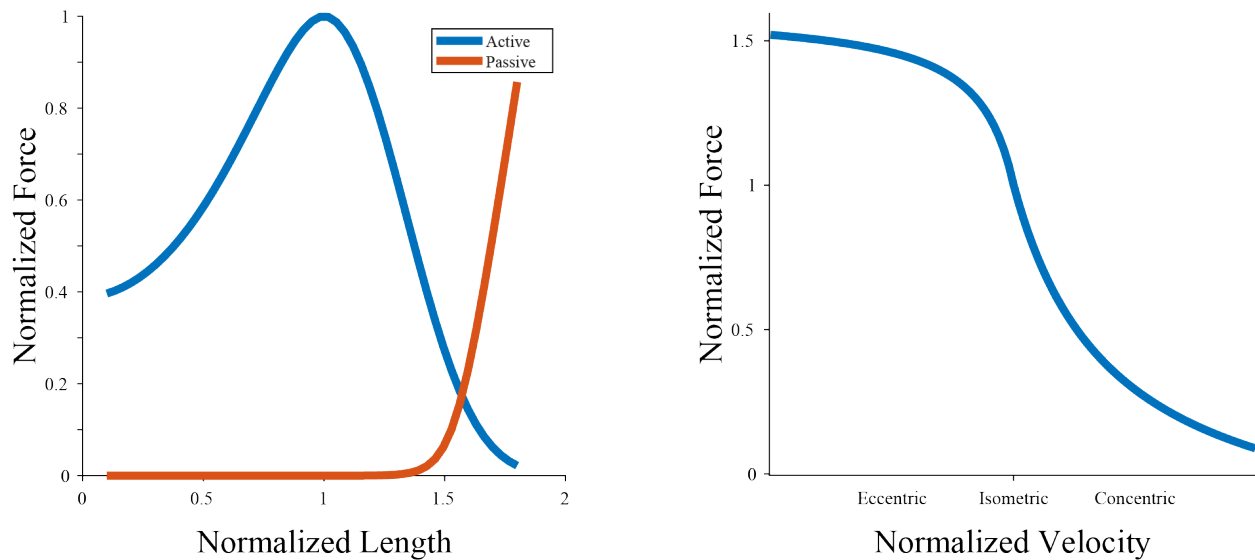


Figure 5.3: Example force length and velocity properties of a muscle (simulated from Brown (25))

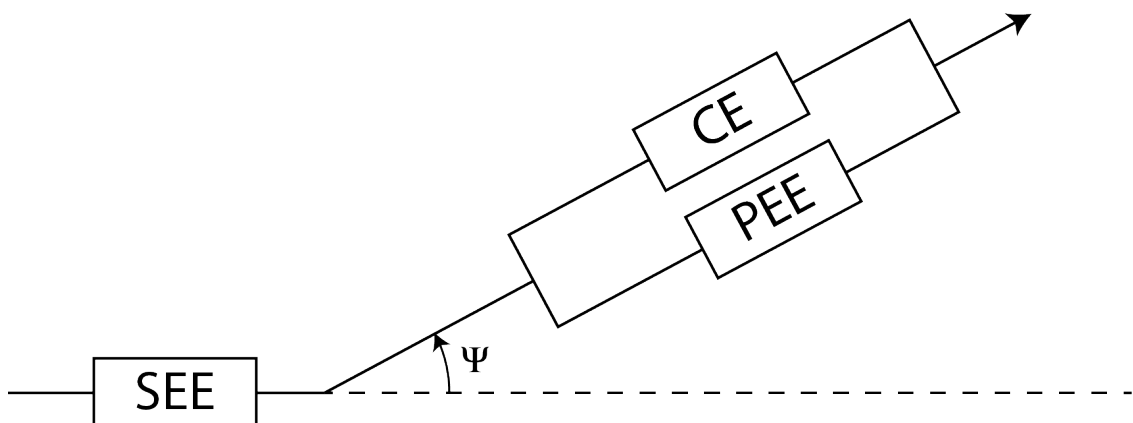


Figure 5.4: A typical Hill-type muscle model with three components (201).

activation levels (eq. 5.5). The Hill-type model has been expanded and further developed in many studies (74; 106), and many other models of muscle actuators have also been developed such as cross-bridge cycling models (200) or more complicated force length properties of muscles (25). In my research project, I use the Brown et al. model for simulation as it accounts for interactions between force length and force velocity (25).

The Brown model accounts for active and passive elements of the muscle tendon unit. l is defined as the normalized length l/l_{OPT} , v is in normalized units of L_{OPT}/s . Activate state (a) is computed using eq. B.15. The total force production is the sum of the passive elements and active elements in eq 5.3. $F_{p,1}$ is the passive force resisting tension. $F_{p,2}$ is the passive force resisting compression of the muscle. The passive force is subtracted from the total joint torque to solve for the active components of force that the muscles need to produce. The tendon (series elastic element) is sometimes set to be constant length in arm reaching because the forces are fairly low, thus providing no stretched force, and seems to be a reasonable approximation to make (130). Pennation angle (ψ) can be included to scale the active component and parallel elastic component in this model as well ($F_{p,2}$ and F_{CE}). Using these muscle properties and equations we can estimate the active state of the muscle.

The basic form of these equations are:

$$\begin{aligned}
 F_{PE} &= F_{p,1} + R * A_f * F_{p,2} \\
 F_{CE} &= R * A_F * F_L * F_V \\
 F_{total} &= F_{PE} + F_{CE} \\
 F_{total} &= F_{p,1} + R * A_f (F_L * F_V + F_{p,2})\psi
 \end{aligned} \tag{5.3}$$

$$F_{p,1} = 68.35 * 0.0495 * \log(\exp((l - 1.445)/(0.0495)) + 1)$$

$$F_{p,2} = -0.02\exp(13.8 - 18.7l)$$

$$F_v = \begin{cases} \frac{-5.72-v}{-5.72+v(1.38+2.09l)} & v \leq 0 \\ \frac{0.62-v(-3.12+4.21*l-2.67l^2)}{0.62v} & v > 0 \end{cases} \quad (5.4)$$

$$F_l = \exp\left(-\left|\frac{l^{1.93}}{1.03}\right|^{1.87}\right)$$

$$N_f = 2.11 + 4.16\left(\frac{1}{l} - 1\right)$$

$$A = \frac{T - Fp, 1}{F_l F_v + F_{p,2}}$$

$$a = 0.56 N_F 10^{\log_{10}(1-A)/N_f}$$

Once the active state is calculated, it is scaled by a normalized force to get muscle force.

This can be solved in the reverse order to calculate active state from force.

$$F = a \cdot \sigma \cdot A, \quad \text{where } A \text{ is area} \quad (5.5)$$

We now have a relationship between muscle force and the properties of the muscle (force length/velocity, PCSA, ψ) and the active state estimate of the muscle. The next step in the modeling process is to determine the relationship between the change in active state and an estimation of the control signal sent from the central nervous system.

5.5 Activation Dynamics (Step 7)

The active state of the muscles is changed through control signals sent from the central nervous system (CNS), and is referred to as the activation dynamics. This is modeled by passing an input signal representing the neural drive (u) through a first order non-linear filter to estimate

the changes in the active state (74; 113; 130; 181; 195). Models of activation dynamics are designed to simulate how motor units respond to stimulation from the CNS (59; 74). First, I will describe some properties of motor units that affect the force production and then describe some of the models used to simulate the changing active state of muscles due to stimulation from the CNS.

5.5.1 Motor Unit

The motor unit is the fundamental unit that controls muscle activation. It is defined as the motor neuron and all the muscle fibers that it innervates (78). Excitation of the motor unit is what leads to contraction of the muscles. The main components to characterizing motor units are the innervation number, twitch force, contraction speed, and recruitment threshold. How a signal from the spinal cord affects the muscle and motor unit is defined by the physiology of the motor neurons.

5.5.1.1 Characterization

A motor unit can be characterized by innervation number, twitch force, contraction speed, and recruitment threshold. These four properties are what the activation dynamics models account for when trying to replicate the activation state of the muscle.

The number of muscle fibers that a motor unit activates is the innervation number (47). The muscle fibers that a motor unit innervates is termed the muscle unit (48). Muscle fibers that a motor unit innervates can be distributed throughout the muscle and is termed the muscle unit territory. Fibers can be distribution across all the muscle but tend to be grouped near each other or in groups (47). The number of muscle fibers that a motor unit innervates varies greatly across motor units and varies exponentially within a motor nucleus. For example, innervation number ranges from 5 to 2000 in medial gastrocnemius (48).

A single twitch caused by a single action potential leads to some amount of force to be produced by the muscle, this force is termed the twitch force. A single twitch can be defined by its twitch force and contraction speed. Twitch force and contraction time have been approximated by

general exponential equations (59). These properties are distributed continuously with no breaks or groupings (59). How these properties are utilized is determined by the physiology of the motor neurons attached to the muscle fibers.

The last aspect to characterize motor units is the recruitment threshold. As the synaptic input increases in the muscle, smaller motor units are recruited first up to the larger motor units and is termed the size principle (80). The recruitment threshold of motor units is quantified by the force at which a motor unit begins firing. The peak twitch force of the motor unit tends to increase with this threshold (133; 134).

These properties are controlled mainly by the physiology of the motor unit itself. Action potentials sent from the alpha motor neurons from the spinal cord activate the motor units as described above. The next section describes how an action potential travels along the motor neuron to eventually activate a muscle fiber.

5.5.1.2 Physiology

The motor neurons are the primary integrator of signal from the spinal cord and other neurons. The neuron receives input from other neurons throughout the body on the neuron's dendrite, the input is conducted towards the cell body (soma), and then conveyed to another neuron through the axon. These signals are transduced through the flow of ions across the cell membrane. Each synaptic connection between axon and dendrite can be either excitatory or inhibitory, and when summated produce a net synaptic current. This current travels along the cell membrane to the cell body and trigger zone. If the current causes a change in voltage at the trigger zone that pushes the voltage over the voltage threshold, the neuron fires an action potential down the axon to either the next neuron or neuromuscular junction. At the neuromuscular junction, acetylcholine (ACh) is released to drive contraction of the muscle.

The propagation of the action potential through the neuron is caused by the opening and closing of specific ion channels (78). At rest, the neurons membrane potential is around -65 mV. This is kept at equilibrium by ion leakage channels and pumps in the membrane. Potassium (K^+),

sodium (Na^+), and chlorine (Cl^-) are the primary contributors to resting membrane potential. Potassium is kept at a high concentration within the cytoplasm, while sodium and chlorine are kept at high concentrations in the extracellular fluid (47). Leakage channels for these ions allow the ions to flow between the cytoplasm and the extracellular fluid, but the $\text{Na}^+ - \text{K}^+$ pump returns two K^+ ions to the cytoplasm and removes three Na^+ ions from the cytoplasm for every ATP spent. When a neuron is depolarized to about +15 mV, voltage gated potassium and sodium ion channels are opened to allow rapid depolarization of the cell resulting in an action potential. These action potentials are all or nothing, where past a certain threshold the membrane potential will be flipped within a few milliseconds. As a small (+15 mV) depolarization occurs, sodium ion channels open to allow a quick influx of sodium into the cytoplasm. At the same time, potassium ion channels are also opening to allow potassium to flow to the extracellular fluid. The membrane conductance for sodium (g_{in}) rises faster than potassium, allowing the cell membrane potential to quickly spike to about 30 mV. As potassium's conductance increases, the cell begins to repolarize towards resting. The repolarization overshoots resting membrane potential, called afterhyperpolarization, and is then returned to resting through the ion pumps. The action potential propagates down the axon, by utilizing the nodes of Ranvier, to the next neuron or the neuromuscular junction.

At the neuromuscular junction, acetylcholine is released to attach to the postsynaptic muscle fibers' membrane. This causes the same movement of K^+ and Na^+ ions across the membrane leading to a muscle fiber action potential. There are seven primary steps to muscle contraction once a muscle action potential has reached the muscle. First (1) the action potential needs to propagate along the muscle fiber and then (2) down the T-tubule. Third (3) the action potential causes a change in Ca^{2+} conductance in the sarcoplasmic reticulum, which then (4) releases Ca^{2+} from the sarcoplasmic reticulum which also causes (5) a reuptake of Ca^{2+} . Then (6) Ca^{2+} binds to troponin causing the conformation change in tropomyosin. Lastly (7) actin and myosin can interact to cause a contraction (sec B.2.4).

To summarize, I have described the neurophysiological pathway from a neural signal to a muscle contraction. The next step is to mathematically model the activation dynamics of this

system.

5.5.2 Modeling Activation Dynamics

Calcium concentration dynamics are the primary factor contributing to the activation dynamics of the muscle. To model the activation dynamics of human muscles we need to simulate the calcium concentration dynamics within the muscle (74–76; 200). This has been shown to replicate experimental data fairly well (105). Simulating calcium dynamics is fairly complex though, and these models have been simplified into just a few equations to model activation given excitation (25; 130; 177; 195).

A simplified version of the calcium dynamics is shown in equation 5.6 (74). This equation relates the active state (q) and calcium concentrations (γ) to the muscle stimulation (STIM).

$$\begin{aligned}\dot{\gamma} &= m(\text{STIM} - \gamma_{rel}), & q &= \frac{q_0 + (\rho * \gamma_{rel})^3}{1 + (\rho * \gamma_{rel}^3)} \\ \rho &= c * \eta \frac{(k - l)}{k - l_{CE,rel}} l_{CE,rel}\end{aligned}\tag{5.6}$$

The constants are listed in table 5.5.2.

Parameters for eq. 5.6

m	c	η	q_0	k
11.25	1.373×10^{-4}	52,700	0.005	2.90

The calcium dynamics are usually simplified more by creating a first-order linear activation dynamics model (113; 130; 177). The activation dynamics model computes the activation (a) from neural excitation (u) by creating a relation between the rate of change in activation and the neural drive. σ and ϵ represent noise in the neural drive signal. The activation constants can be altered

but are generally around $t_{ACT} = 50$ msec, and $t_{DEACT} = 66$ msec.

$$\dot{a} = \frac{(1 + \sigma_u \epsilon)u - a}{t(u, a)}$$

$$t(u, a) = \begin{cases} t_{deact} + u(t_{act} - t_{deact}) & u > a \\ t_{deact} & otherwise \end{cases} \quad (5.7)$$

Another method that alters the activation dynamics uses first order linear filters to estimate the change in activation due to neural drive (105; 181). This model has a parameter %FT (percent fast twitch) in equation 5.8, but this should be regarded as a fiber type distribution and not %FT (59). Delays between STIM (u) and ACT (a) were modeled as a first-order process. We use a relation for τ_{ACT} and τ_{DEACT} :

$$\tau_{ACT} = 80\text{ms} - 0.47\text{ms} \times \%FT \quad (5.8)$$

$$\tau_{DEACT} = 90\text{ms} - 0.56\text{ms} \times \%FT$$

Two rate constants are related to activation and deactivation by the time constants c_1 and c_2 :

$$c_1 = \frac{1}{\tau_{ACT}} - c_2 \text{ and } c_2 = \frac{1}{\tau_{DEACT}} \quad (5.9)$$

The time constants are scaled as well by the percent of fast twitch motor units. We assume that the ratio of $V_{CE(MAX)}$ for FT to ST fibers is 2.5:1. The activation dynamics are then modeled as a first order differential equation eq. 5.10.

$$\dot{a}(t) = (u(t) - a(t)) (c_1 u(t) + c_2)$$

$$\dot{a}(t) = (u(t) - a(t)) \left(u(t) \left[\frac{1}{\tau_{ACT}} - \frac{1}{\tau_{DEACT}} \right] + \frac{1}{\tau_{DEACT}} \right) \quad (5.10)$$

$$\dot{a}(t) = (u(t) - a(t)) \left(\frac{u(t)}{\tau_{ACT}} - \frac{u(t) - 1}{\tau_{DEACT}} \right)$$

The activation dynamics of the muscle are mainly dependent on the physiology of the motor neuron, the muscle, and the calcium dynamics in the muscle (76). The activation level of the muscle along with the muscle properties (FL, FV, PCSA) contributes to the total force production of the muscle (25). These properties are the primary determinants to simulated metabolic rate using musculoskeletal models. In the next section, these components are all integrated into an estimate of the metabolic rate for contracting muscles.

5.6 Energetics Models (Step 8)

Using proxies for effort and metabolic rate is a common practice as discussed earlier (sec 2.3.1, 2.3.2). Metabolic cost can be determined by multiplying the metabolic rate by movement time. Dividing metabolic cost by distance calculates the metabolic cost of transport. It is useful to build metabolic rate models as measuring the metabolic rate requires steady state mechanics. If we want to measure the metabolic rate of a single movement, that movement needs to be replicated for three minutes. Using a musculoskeletal model with muscles as actuators, we can simulate a metabolic rate using the muscle properties and the activation dynamics described earlier. There are many possible ways to estimate the metabolic rate of the movement using a musculoskeletal model (18; 90; 102; 114; 124; 136; 136; 179; 181). These models are described in detail in the appendix (chap. B, sec. B.2.9).

The basic idea underlying most models of metabolic rate is that the chemical reaction in the muscles consumes energy to produce force and work and can be represented by a combination of heat rates. Many of these models use a combination of the energy required to shorten and lengthen the muscle, activate and maintain the muscle state, maintain a basal heat rate, and a rate of doing work. Equation 5.11 shows the breakdown of the heat rate from the Umberger model, a commonly used metabolic model (180). These heat rates are dependent on many of the factors discussed earlier such as shortening and lengthening properties, activation properties, and size properties.

The basic form of the Umberger model takes the form shown in eq. 5.11, with \dot{E} representing the metabolic rate, \dot{h}_{SL} the shortening and lengthening heat rate, \dot{h}_{AM} the activation and

maintenance heat rate, and \dot{w} the amount of mechanical work. Many of the metabolic models are constructed in a similar fashion to this model.

$$\dot{E} = \dot{h}_A + \dot{h}_M + \dot{h}_{SL} + \dot{w}_{CE} \quad (5.11)$$

There are many possible ways to model metabolic rate, and while the Umberger model is the most common, many others have been developed. The details of each of these models can be found in the appendix (sec. B.2.9). The Ma and Zahalak model attempts to model the rate of calcium and ATP usage within the muscle and relates these to the work done by the muscle (124). Minetti et al. do not calculate heat rates but relate the angular power of the muscle to the metabolic power (136). The energy model from Umberger et al. relates the total heat rate to the activation and maintenance heat of the muscle, the shortening and lengthening heat rate of the muscle, and the total work done by the muscle (180; 181). The Bhargava, Lichtwark, Houdijk, and Kim models all use a similar heat rate estimation as the Umberger model but differ in their derivation (18; 90; 102; 114). The Uchida model uses Umberger's 2010 model with some modifications. Uchida changes the excitation model and how negative mechanical work is used and forces the total instantaneous power of the muscle to be greater than zero (179).

5.7 Evaluation Studies

All of these models were validated by comparison with muscle contraction studies, generally from dissected muscles of frogs (181). It is less clear however how these models translate into the metabolic rate of whole-body movements. A few studies have attempted to validate these models in walking by comparing many of the energetics models to collected metabolic rates (107; 131).

Miller et al. collected metabolic rate data on 14 healthy adults and calculated the metabolic cost of transport while walking (131). They then used a musculoskeletal model with 40 Hill-type muscles to simulate these movements by using both a tracking (static optimization and inverse dynamics) and optimal control approach. They computed the metabolic cost of transport per

kilogram for each model. The two simulations were different in that one, there was an error term for tracking the collected kinematic data, and two, the other only minimized the total energy cost. The objective function used was

$$\begin{aligned}
 J &= \epsilon_{track}^2 + w_1 R^2 + w_2 ||C||_1 \\
 \epsilon_{track} &= \frac{1}{7N_i} \sum_{i=1}^7 \sum_{j=1}^N \left| \frac{x_{ij}^{sim} - x_{ij}^{exp}}{SD_i} \right| \\
 R &= \frac{1}{40T} \sum_{k=1}^{40} \int_0^T u_i^{10}(t) dt \\
 C &= x(T) - x^*(0) - vT\dot{x}
 \end{aligned} \tag{5.12}$$

J is the total objective function to be optimized over, ϵ_{track} is the tracking error, and R is the cost function minimizing 'fatigue' or neural drive sent to the muscles.

Using the error tracking algorithm, Miller found that there was a large discrepancy in the calculated metabolic cost from each of the models shown in figure 5.5. Figure 5.6 shows the results of the metabolic cost predictions as a function of total and absolute cost for each of the metabolic models using an optimal simulation minimizing muscle 'fatigue' or neural drive. We see that these models produce widely varying distributions of cost for each joint as well as the proportion of the total cost.

A similar study was conducted in 2019 by Koelewijn et al. (107). Metabolic rate data was collected for subjects walking on different inclines. A biomechanical simulation was run using 8-muscles on each leg to simulate the walking movement by direct collocation minimizing muscle active state. Metabolic rate was converted into metabolic cost per distance, and then compared to simulated metabolic cost from 7 different models. The simulation found decent relation between collected metabolic cost and some of the metabolic cost models (fig. 5.7). However, there still is a wide range of metabolic cost predictions across the metabolic models.

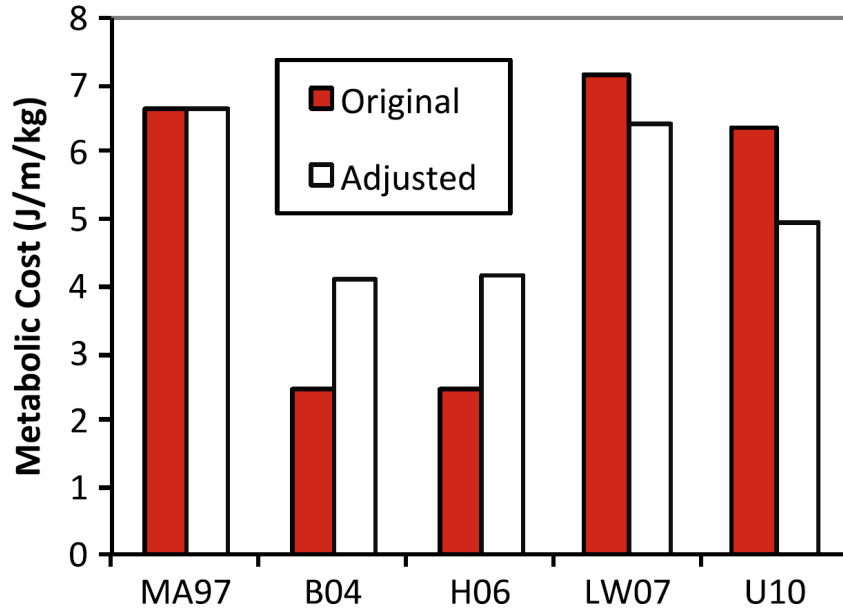


Figure 5.5: Results from tracking error simulation from Miller (131). The solid bars represent the energy model from the tracking simulation, and the white bars represent an adjustment to eccentric work. MA97 is the Minetti and Alexander model (136), B04 is the Bhargava model (18), H06 is the Houdijk model (90), LW07 is the Lichtwark model (114), U10 is the 2010 Umberger Model (180). The solid bars represent the original metabolic model, white bars represent adjusted estimates for eccentric contractions.

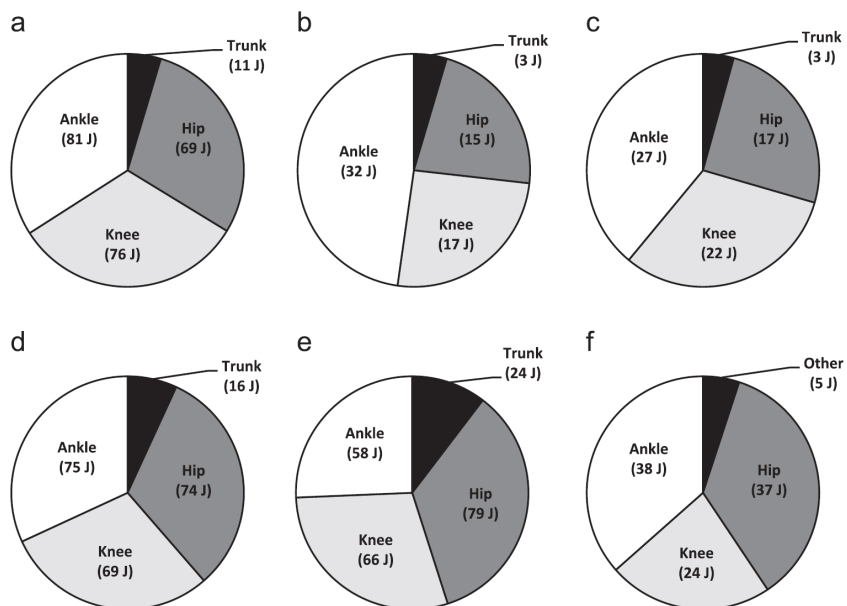


Figure 5.6: Results from optimal simulation from Miller (131). a is the Minetti and Alexander model, b is the Bhargava model, c is the Houdijk model, d is the Lichtwark model, e is the 2010 Umberger Model. f is an estimate from blood flow in walking guinea fowl.

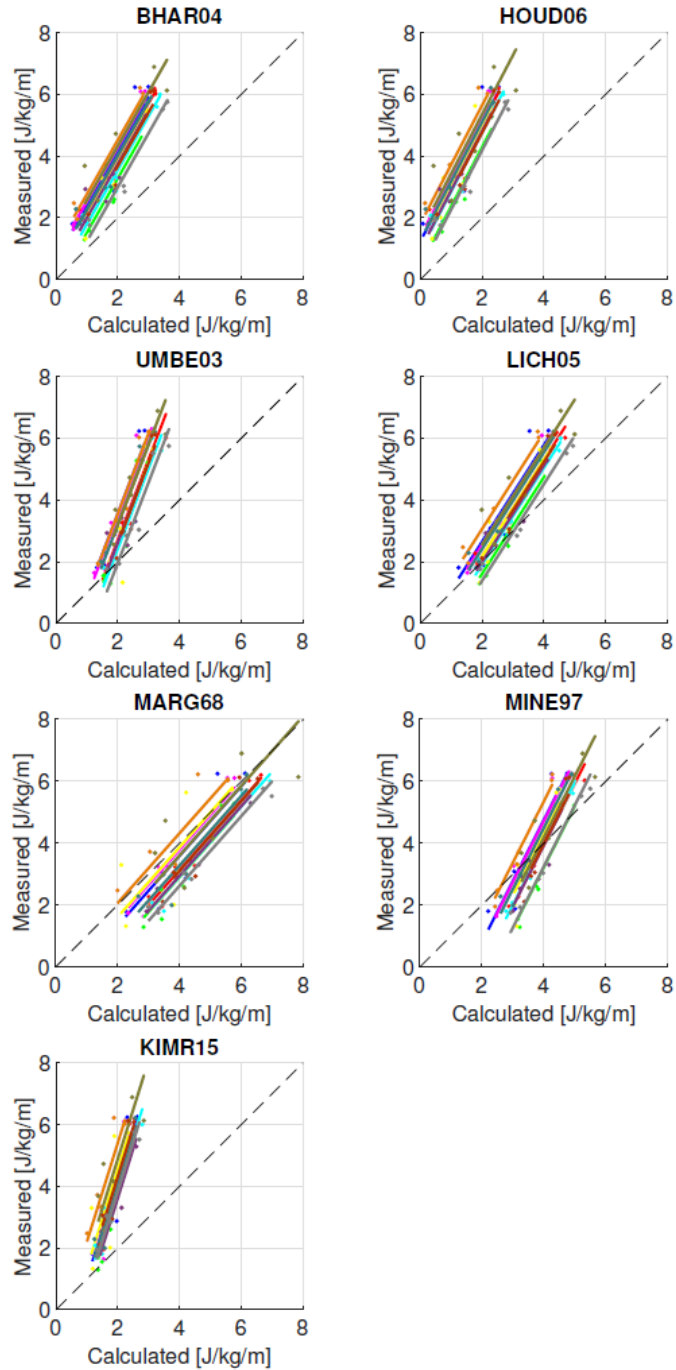


Figure 5.7: Relationship between collected metabolic cost and simulated metabolic cost from Koelewijn (107). The seven models were BHAR04 (18), HOUD06 (90), UMBE03 (181), LICH05 (114), MINE97 (136), MARG68 (127), and KIMR15 (102).

5.8 Summary

Modeling the metabolic rate and cost of a movement has become a common practice in biomechanical research studies. These musculoskeletal models can either model the metabolic rate of a movement through an inverse kinematics modeling approach or simulate new movements by minimizing energy costs. These models need to simulate muscles as actuators that produce the joint torques in movement. The muscle models implemented need to account for the force length properties of the muscles, force velocity properties of the muscles, and simulate the activity of motor units within the muscle. The last step is simulating the metabolic rate of the movement and calculating the metabolic cost, though it is unclear how accurately these metabolic models can predict metabolic cost in full body movements. The next chapter attempts to use these musculoskeletal modeling techniques to validate multiple metabolic rate models in arm reaching.

Chapter 6

A validation of metabolic energy models in arm reaching

6.1 Abstract

The consistency of movements across the human population has led to the proposal that there is a certain cost to making an arm reaching movement that humans attempt to minimize and that this cost is conserved across individuals. Metabolic costs likely play a role in determining the overall cost of movement and ultimately determining movement kinematics in arm reaching (166). However metabolic cost can be difficult to measure (15). Thus, some representation of metabolic cost is often used. Here we examine how five models of metabolic cost and six neuromechanical representations of effort can predict experimentally collected metabolic cost of reaching. Subjects made arm reaching movements across four masses and six speeds while collecting metabolic power data. A biomechanical model of the arm was developed to calculate measures of metabolic cost and neuromechanical variables. The predicted metabolic cost and effort representations were then compared to the experimentally measured metabolic cost. The best linear fit to the measured metabolic cost was Bhargava's metabolic model with an R^2 value of 0.640, with three other metabolic models providing similar predictive power. Four of the five neuromechanical effort representations performed poorly; only neural drive and neural drive squared provided a reasonable relation to metabolic rate ($R^2=0.581$, $R^2=0.589$). Notably, sum of squared joint torque, a common measure of effort in reaching, was a poor fit to the metabolic data. These neuromechanical variables can predict the general shape of the collected metabolic cost. However, they are poor at describing differences between conditions and fail at faster reaching speeds. Our analysis highlights the im-

portance of exercising caution when representing metabolic cost via model-derived biomechanical variables.

6.2 Introduction

When walking down the street, one may notice the surprising similarity in how everyone walks. When reaching for a cup of coffee, people will make very similar, straight, reaching movements. Every day we make hundreds of specific movements, such as walking and reaching, and somehow across the population these walking and reaching movements look very similar to each other (55). Because of the similarity in our movements, it has been proposed that there is a cost to making a movement that humans attempt to minimize and that this cost is conserved across individuals (4; 55; 164). In walking this cost is thought to be metabolic energy, while in other movements it has taken many forms from metabolic energy to various measures of effort derived from biomechanical measures (15; 44; 79; 152; 166).

In walking, this cost is generally thought to be the metabolic energy cost to contract and control muscles. The behavior to minimize the metabolic cost of a movement can be seen by humans choosing to walk at the metabolically optimal speed or choosing metabolically optimal gait patterns (152; 164; 174). This has led to researchers to investigate metabolic cost as an explanatory variable in many types of movements. However, metabolic cost may be difficult to impossible to measure in some circumstances, which has led to the use of estimations of metabolic cost. Metabolic cost has been represented with many possible estimates, such as work done on center of mass, total joint work, active muscle volume, and recently directly estimating metabolic cost from muscle-based energetics models. These models generally explain some, but not all, of the changes in metabolic cost in these studies (44; 65; 68; 131; 132).

In arm reaching studies, it is less clear what the optimized cost is. With the importance of metabolic cost in walking, researchers have begun to investigate metabolic cost in arm reaching (92; 166). Additionally, previous research has pointed toward the optimized cost being some form of effort. Effort in arm reaching has been represented by many neuromechanical measures including

joint torque, muscle force, muscle active state, and neural drive (6; 50; 55; 92; 113). Although the measurement of metabolic cost in arm reaching is relatively recent, it has been proposed that metabolic cost and effort may be the same (166). In the case of arm reaching and novel or difficult movements, it can be difficult to measure metabolic cost due to the nature of the task or requiring repetition of the task. Therefore, it would be useful to know how well metabolic models and various effort representations can predict the empirically measured metabolic cost of reaching.

Within movement studies, there have been many ways researchers have represented metabolic cost and effort with the goal of predicting movement trajectories (15; 107; 131). Metabolic cost models can range from sum of the torques about each joint to estimating the liberation of mechanical energy in muscles (18; 50; 102; 114; 126; 136; 179–181). Estimates of effort in arm reaching are similar, but do not rely on estimating a metabolic rate, rather focus on some intrinsic property of the muscle or joints such as torque squared (143; 183), muscle active state (50; 132; 193), and neural stimulation (113). Muscle energetic models have been used to simulate movements and to explain changes in metabolic cost for many locomotion studies (7; 8; 77; 131; 132; 179; 182). These simulations have shown that they can reasonably reproduce movement trajectories similar to human subjects (51; 151; 169; 176; 203). These models minimize some estimate of metabolic cost or effort (torque, jerk, muscle activation, etc.) to reproduce the human-like movements. While many of these estimates of metabolic cost can reproduce human-like movements, there are times where these functions fail. Humans, after being shown and trained on a curved path that minimizes a simulated metabolic cost, tend to reach in straight lines instead (106). While this study points that subjects may not be minimizing solely metabolic cost, it may also mean that the metabolic model is not complete. This shows that depending on the metabolic representation used, one may not be able recreate realistic movements or make accurate predictions about the simulated cost of the movements, leading to the question of how accurately these models estimate metabolic cost of a movement.

These effort and metabolic models have become commonplace in movement simulation and in biomechanics research, however the validation for full body motion is still lacking. Recently,

researchers have shown the relationship between simulated metabolic cost and actual metabolic cost in walking across many metabolic models (107; 131). These studies show varying degrees of success using metabolic energy models to estimate collected metabolic data. Miller et al. show that the energy models predict widely varying metabolic costs (131). Koelewijn et al. expanded on this by adding different speeds and slopes and found similar results; these estimations of metabolic cost have reasonable predictions but sometimes wide-ranging estimates for metabolic cost (107). This type of validation has yet to be done for arm reaching and with many representations of effort and metabolic cost in reaching, it is important to understand the relationship between these effort and metabolic representations and metabolic cost.

Here we develop a biomechanical model of the arm performing a reaching movement that allows us to calculate estimates of metabolic cost using five different models of metabolic rate and compare these to collected metabolic data (18; 114; 127; 179; 180). In addition, we compare four common effort representations to collected metabolic data. This analysis will inform us if these neuromechanical effort representation and metabolic representations are able to accurately predict the metabolic cost of arm reaching.

6.3 Methods

To investigate these questions, we collected metabolic and kinematic data as subjects made planar reaching movements across a range of speeds, distances, and while holding different amounts of mass at the hand. Next, we developed a neuromechanical model of the arm, and based on the measured movement kinematics used inverse dynamics to estimate the required shoulder and elbow torques for the movements, as well as additional neuromechanical variables of interest that have been used to represent effort: muscle force, muscle active state, and neural drive. To answer our first question of whether metabolic rate models (i.e.,metabolic representations) could capture the measured metabolic rate of reaching, we used five metabolic rate models to estimate the metabolic rate of the reaching movements and compared these estimates to the actual metabolic data collected experimentally. To answer our second question of how well alternative neuromechanical measures of

effort represent metabolic rate (i.e., effort representations), we compared the calculated joint torques, muscle force, muscle active state, and neural drive to the measured metabolic rate. Details of the data collection, and calculations of the metabolic rate and neuromechanical effort representations are described below.

6.3.1 Experimental Protocol

Seated subjects made a series of planar horizontal arm reaching movements while breathing into a metabolic cart (Parvo Medics TrueOne 2400) and holding the handle of a robotic arm that supported their arm against gravity (Interactive Motion Technologies, Shoulder-Elbow Robot 2). Five male and three female subjects completed the experiment (all right-handed, mean age 28.9 years (std = 5.7), mean weight 68.4 kg (std = 11.4), and mean height 174.1 cm (std = 10.2)). Subjects completed a set of arm reaching movements across eight targets, seven speeds, and four masses. All subjects gave written informed consent approved by the CU Boulder Institutional Review Board.

Subjects made reaches for a total of approximately 5 minutes while collecting metabolic data. Four different physical masses were added at the hand while subjects reached (0 kg, 2.27 kg, 4.55 kg, and 9.09 kg). The seven tested durations were: Very, Very Slow (VVS, 1.3 s, 160 trials), Very Slow (VS, 1.1 s, 170 trials), Slow (S, 0.9 s, 200 trials), Medium (M, 0.7 s, 220 trials), Fast (F, 0.5 s, 240 trials), Very Fast (VF, 0.375s, 250 trials), and Very, Very Fast (VVF, 0.25s, 260 trials). Conditions were blocked and randomized for each subject with each taking approximately five minutes. Every subject completed at least six speeds with each mass, where the two heavier masses were completed at the six slower speeds and the two lighter masses were completed at the six faster speeds. Four subjects did not complete the fastest speed with the lightest two mass conditions, and two of these completed the slowest with the lightest mass, and two other subjects completed the slowest condition with the second lightest mass.

Subjects controlled a cursor on a screen positioned slightly above eye level about two feet away by moving the handle of the robotic arm. Subjects began the experiment by holding the

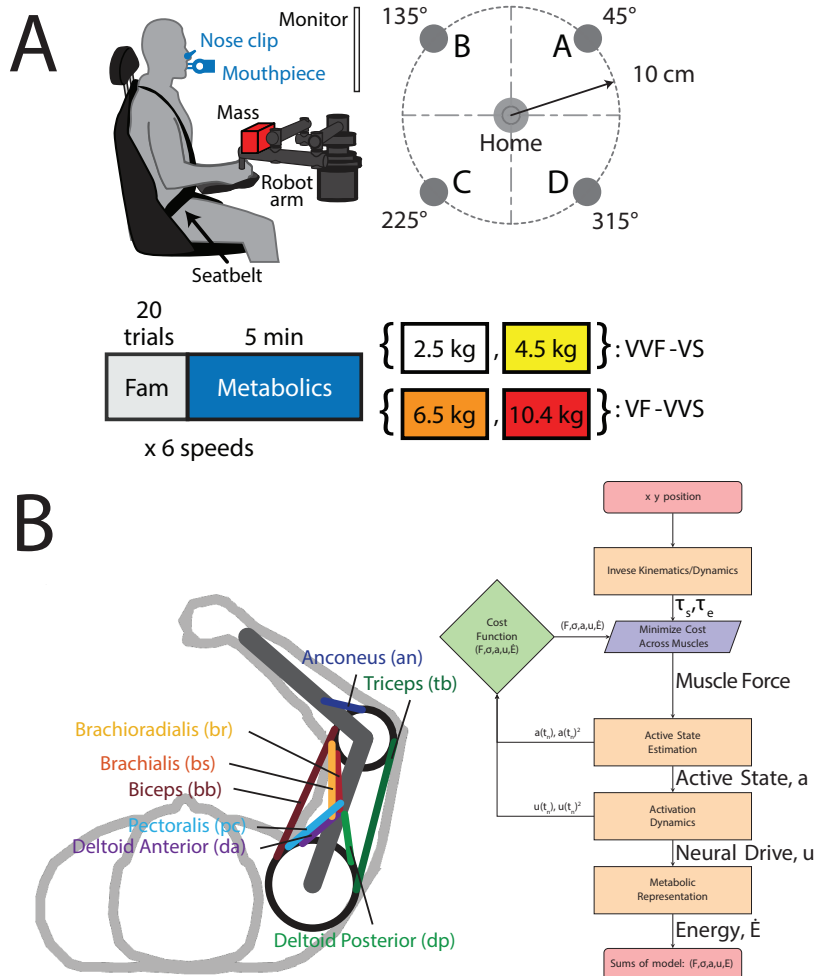


Figure 6.1: Description of experimental protocol and arm model. A. Subjects were in a seated position while collecting metabolic data. Mass was placed on a robotic manipulandum that subjects would hold onto. Subjects would make reaching movements to four different targets at six different speeds with four different masses added to their hands. B. Neuromechanical model of the arm with two joints and eight muscles. C. A flow chart describing calculation of metabolic and neuromechanical effort representation.

cursor in a home circle for 200 ms. The home circle would then disappear, and a target would randomly appear at 45°, 135°, 225°, and 315° from the right horizontal (fig. B.1A). Subjects were instructed to finish the movement within one of seven, 100 ms time windows. Visual and auditory feedback was provided depending on if the movement was too fast, too slow, or within the time window. After completing the first reach (an outward reach), the target would be replaced with a new home circle and a second target would then appear in the central location after holding the cursor in the new home circle for 200 ms. This led to four outward reaching directions, and 4 inward reaching directions, for a total of 8 reaching movements. The location of the target in the outward reach would appear in a pseudorandom order, requiring a reach to four different targets then repeating another pseudorandom set. The X-Y position of the hand was recorded at 200 Hz and then filtered with a lowpass Butterworth filter (cutoff frequency 10 Hz). Custom MATLAB scripts were used to parse the data by trial, mass, and speed. The positional data was differentiated using a double five-point differentiation to compute velocity and acceleration, which were used to calculate movement duration and reaction time.

Subjects were instructed to be well-rested and fasted before metabolic testing. When subjects entered the lab, they remained seated in the testing chair for 10 minutes. Three baseline recording of metabolic rate were then taken for 5 minutes each before reaching began. Subjects then began making reaching movements in one of the block conditions. Between each block subjects had a five-minute rest period to adjust back to baseline. Based on the measured rates of oxygen consumption and carbon dioxide production, the metabolic power, \dot{e} , was calculated in joules per second using the method described by Brockway (eq. B.1) (24).

$$\dot{e} = 16.58\dot{V}_{O_2} + 4.51\dot{V}_{CO_2} \quad (6.1)$$

Gross metabolic rate was calculated for each subject and each condition based on the last three minutes of reaching in each block. The average of the three baseline metabolic rates was subtracted from gross metabolic rate to determine the metabolic rate associated with the reaching

movement alone.

6.3.2 Neuromechanical Model

A neuromechanical model of the arm was developed that includes the forearm and upper arm along with 8 physiologically relevant muscles crossing the shoulder and elbow joints (fig. B.1B). The masses and lengths of the arm and muscles were scaled to the size of the subject and estimated using anthropomorphic measurements (34; 107; 193).

The X-Y position data was re-sampled to 100 data points for each experimental arm reach then averaged at each new re-sampled time point for each subject, mass, speed, and target. Position data was then used to calculate joint angles, which were differentiated using double five-point differentiation to compute joint velocities and accelerations. Joint position, velocity, and acceleration were in turn used to calculate joint torques and muscle forces using inverse dynamics on a per subject basis.

Once muscle force was determined, we calculated muscle active state and neural drive. To compute muscle active state, we estimated the force-length and force-velocity properties of each muscle and found the active state required to produce the given muscle force (25). After active state was estimated, a first order differential equation was used to calculate neural drive that estimates the active state rate as a function of neural drive (25; 113; 130; 177; 181; 195). Thus, this model allowed us to calculate the four neuromechanical representations of effort we sought to compare with metabolic rate: joint torque, muscle force, muscle active state and neural drive and their squared counterparts.

To calculate muscle force, we tested multiple minimization functions to distribute the individual muscle forces (106; 108; 113). The minimization functions included every neuromechanical effort representation as well as the metabolic rate calculated by the Umberger metabolic model (see Section 6.3.2.5). Minimizing muscle active state squared produced the highest overall R² value when comparing all calculated representations to measure metabolic rate. Therefore, all the main results presented are based on a muscle force distribution function that minimizes active state

squared.

6.3.2.1 Kinematics

The biomechanical model was set to make the same reaching movements as in the metabolics data collection. The model simulated reaching movements to and from four different targets located 10 cm from a central location, at 45, 135, 225, and 315 degrees from the right horizontal. X-Y position data was averaged from the metabolic data collection at 200 Hz. X-Y position was then spline interpolated to increase the sampling rate to 400 Hz to make the non-linear approximations better. The center location, also where the hand starts, was set at $x = -7.58$ cm and $y = 48.78$ cm from the shoulder joint. Kinematic trajectories were aligned to reaction time and then averaged and filtered with a lowpass Butterworth filter (cutoff frequency 10 Hz) for each subject, target, mass, and speed condition.

6.3.2.2 two-link Model

We simulated the arm as a two-link arm as the wrist was fixed during the experiment. The physical properties of the two-links are shown in table B.2. The masses and lengths of the arms were scaled to the size of the subject and estimated using anthropomorphic measurements (34; 193). The arm lengths and masses were relatively similar to other studies (1; 166). The centroid length of the arm segments is shown with 0 added mass, this distance was recalculated when mass was added. The center of mass length was estimated from Enoka (47).

In the biomechanical modeling equations (supplemental), l_1 and θ_s refer to the upper arm segment and shoulder joint. l_2 and θ_e refer to the forearm and elbow joint. We then converted the data (in x and y position data) to joint positions θ_e and θ_s . These angles are defined by their Euler Angles and not flexion/extension angles. From there, we differentiated angular position to calculate the angular velocities ($\dot{\theta}_e, \dot{\theta}_s$) and accelerations ($\ddot{\theta}_e, \ddot{\theta}_s$). The beginnings of movements sometimes accelerated too fast for the model to replicate, so a small buffer was added to reduce acceleration for the first few time steps in the model. Last, an estimate for how the arm resists motion, the

effective mass, was determined.

Object	Mass (kg)	Length (m)	$Cent_L$ (m)	I_{com}
Forearm	1.2500	0.4258	0.1674	0.0188
Upper arm	1.5909	0.3136	0.1367	0.0141

Table 6.1: Properties of the forearm and upper arm rigid segments for example subject of 56.81 kg and 1.62 m. The values for Forearm $Cent_L$ and I_{COM} are for 0 added mass at the hand.

Once joint torques were determined, we implemented an eight-muscle actuator model to match the computed joint torques. The muscle forces were calculated by distributing the force according to one of many (9) possible minimization functions representing some neuromechanical proxies (muscle force, muscle stress, active state, neural drive) for effort and one metabolic representation (180). Active state, an estimation of the percent of muscle activated, is calculated by simulating the properties of the muscles and estimating the portion of the muscle required to be active to match the torque. Neural drive, control signal from the central nervous system, is calculated from activation dynamics and the rate of change in active state. At each time step, the current active state and a neural drive of 1 and 0 are used to calculate the minimum and maximum possible active states at the next time point. This minimum and maximum active state are used as bounds for the muscle force allocation of the next time point. This process would repeat for each time step until the reach completed.

6.3.2.3 Muscle Properties

Muscles' properties of the eight simulated muscle actuators are shown in table B.3 (mass, physiological cross-sectional area, optimal length, and percent fast twitch fibers). The eight muscles simulated are the anconeus (an), brachioradialis (br), brachialis (bs), biceps brachii (bb), clavicle portion of the pectoralis (pc), deltoid anterior (da), deltoid posterior (dp), and the triceps brachii (tb).

Muscle	Mass (kg)	PCSA (m^2)	L_{OPT}	% FT
Anconeus (AN)	0.0291	4E-4	0.0687 (E)	40.0
Brachialis (BS)	0.0829	8.71E-4	0.090 (C)	40.0
Brachioradialis (BR)	0.0525	2.95E-4	0.1887 (L)	60.2
Deltoid Anterior (DA)	0.1005	5.46E-4	0.1296 (L)	42.9
Deltoid Posterior (DP)	0.1323	5.69E-4	0.1818 (L)	42.9
Pectoralis (PC)	0.0816	6.68E-4	0.1701 (E)	57.0
Biceps Brachii(BB)	0.1278	4.32E-4	0.225 (M)	53.6
Triceps Brachii (TB)	0.3920	11.94E-4	0.3235 (M)	52.9

Table 6.2: Muscle Properties. For L_{OPT} , the letter corresponds to which author the value was taken from or if it was estimated. C(28), L(110), M(141), E (estimated).

6.3.2.4 Active state and Neural drive

The calculations of muscle properties such as the force length and force velocity properties are shown in the supplemental (sec. B.2.7). Once muscle force and muscle properties were calculated, we then estimated the active state of the muscles by simulating a modified Hill-type muscle (25). This model estimates how much force a muscle can produce depending on the portion of muscle active and the muscle properties. The tendon (series elastic element) is set to be constant length and seems to be a reasonable approximation to make for low forces (7; 97; 111; 118; 130; 169). After active state is estimated, a first order differential equation is used to calculate neural drive that estimates the active state rate as a function of neural drive (113; 181).

6.3.2.5 Metabolic Representations

We calculated five metabolic rate estimates from the neuromechanical model (18; 114; 126; 179; 180). The Umberger (180), Bhargava (18), Uchida (179), and Lichtwark (114) models all calculate energy rate (\dot{E}) as a summation of heat rates of the activation (\dot{h}_a), maintenance (\dot{h}_m), and shortening (\dot{h}_s) and lengthening (\dot{h}_l) of the contractile element and the total work rate (\dot{w}), with subtle differences in how each of the heat rates are calculated.

$$\dot{E} = \dot{h}_a + \dot{h}_m + \dot{h}_{sl} + \dot{w} \quad (6.2)$$

The activation heat rate is calculated as the energy required to initiate contraction of the muscle and is related to the neural drive and active state. The maintenance heat rate reflects the cost of keeping the muscle activated and depends on the active state and neural drive. The shortening and lengthening heat rates depend on the force-length and force-velocity properties of the muscle as well as the active state of the muscle. The work rate of the muscle is approximately the mechanical work done by or on the muscle.

The Margaria model (127) estimates the metabolic rate assuming that muscles are 25% efficient when shortening and 120% efficient while lengthening:

$$\dot{E} = \begin{cases} \frac{\dot{w}}{0.25} & \text{if } v_{CE} \leq 0 \\ -\frac{\dot{w}}{1.20} & \text{if } v_{CE} \geq 0 \end{cases} \quad (6.3)$$

6.3.2.6 Quantifying relationship to metabolic rate

The time series data for each of these metabolic and neuromechanical effort representations was integrated and averaged over all reaches (eight different reach types) to get an estimate of cost for each subject, mass, and speed condition. The metabolic and effort representations were then divided by the movement duration to get an estimate of the average metabolic rate over the movement. This rate was then fit to collected metabolic rate data using simple linear regression (150). A fit was performed for each predictor variable and each minimization function. For each variable we determined the significance of the slope and fits were ranked by the variance accounted for (R^2). A similar analysis comparing metabolic calculations and collected metabolic data in walking used a repeated measures correlation (RMCORR) to account for inter-subject variability (107). In our analysis, we scale the size of the biomechanical model to the size of each subject to account for this. When computing our results using an RMCORR, while the variance accounted for increases, our primary findings do not change with regards to the relative performance of the representations.

We also sought to parameterize the metabolic and effort representations in order to better describe how these representations varied as a function of mass and duration. We fit a parametric effort model with four free parameters to the measured metabolic rate, the five metabolic representations, and each neuromechanical effort representation (eq. B.51)(166). The general form of this equation has been shown to characterize the metabolic rate of both reaching and walking (166). The metabolic or effort representation is indicated by \dot{e} , a is an offset term, b a scaling factor, c determines the scaling due to mass, and d determines the scaling due to time. The effective mass of the arm is m , and T is the movement duration (166).

$$\dot{e} = a + \frac{bm^c}{T^d} \quad (6.4)$$

After computing the best parameter fits, we compared the parameters to the metabolic data using equation B.52 (197) where SE represents the standard error of the mean. If this inequality is true, there would be a significant difference between parameter estimates. In our study, we are interested in parameters that are not significantly different than the parameters fit to the measured metabolic data.

$$|mean_A - mean_B| > 2\sqrt{(SE_A^2 + SE_B^2)} \quad (6.5)$$

6.4 Results

We developed a neuromechanical model of the human arm and simulated reaches with four different masses, at six different speeds, and towards four targets. We then calculated four different neuromechanical effort representations (sum of joint torque, muscle force, active state, neural drive and their squared counterparts) and five different metabolic estimates for the metabolic rate of each movement. These candidate representations were then compared to collected metabolic rate data for each movement and we determined how metabolic rate and each of these candidate representations are affected by added mass and movement duration.

6.4.1 Metabolic rate representations generally capture metabolic rate of reaching

The primary goal of this study is to determine the relationship between the measured metabolic power and each of the model-derived metabolic calculations. We performed linear regression between the metabolic representation and metabolic power, and computed the variance accounted for (R^2 , Fig 6.2A). Across all metabolic representations, the Bhargava energy model performed the best with an R^2 value of 0.64 when minimizing active state squared (Fig. 6.2B). The relative performance of the metabolic representations and neuromechanical representations remained the same regardless of the minimization function used for muscle force distribution (Fig. 6.2B). Since minimizing active state squared produced the highest overall R^2 value, all results presented are based on a muscle force distribution function that minimizes active state squared.

The best linear fit to measured metabolic rate was obtained using the Bhargava energy expenditure model (Fig. 6.3, $R^2 = 0.64$, $y = 2.19x - 28.6$). The Umberger ($R^2 = 0.618$), Uchida ($R^2 = 0.629$), and Margaria ($R^2 = 0.614$) model had relatively high R^2 values. The Lichtwark model performed poorly compared to the other metabolic representations ($R^2 = 0.481$).

These models provide a general linear relationship to metabolic rate, but many show a trend of not being able to predict the metabolic rate of fast movements with low mass (Fig. 6.3). This can be seen in the data points far above the regression line, and generally near the top left of the graph. Specifically, the measured metabolic rate for a fast 0 kg and 2.27 kg movement is much greater than that predicted by any of the metabolic models. The Lichtwark and Margaria models exemplify this, as the 0 kg metabolic data is greater at the higher speeds than either metabolic representation predicts (Fig. 6.3).

We can also compare the ability of each representation to capture the absolute value of metabolic rate (Table 6.3). An ideal model will increase the same as metabolic rate or have a linear estimate as close to one as possible. While all the models reveal a slope that is significantly different than one, the Umberger model predicted a slope closest to one (1.37 ± 0.079 [1.29-1.45]; mean \pm SEM [95%CI]) indicating that it may have the best absolute prediction of the changes

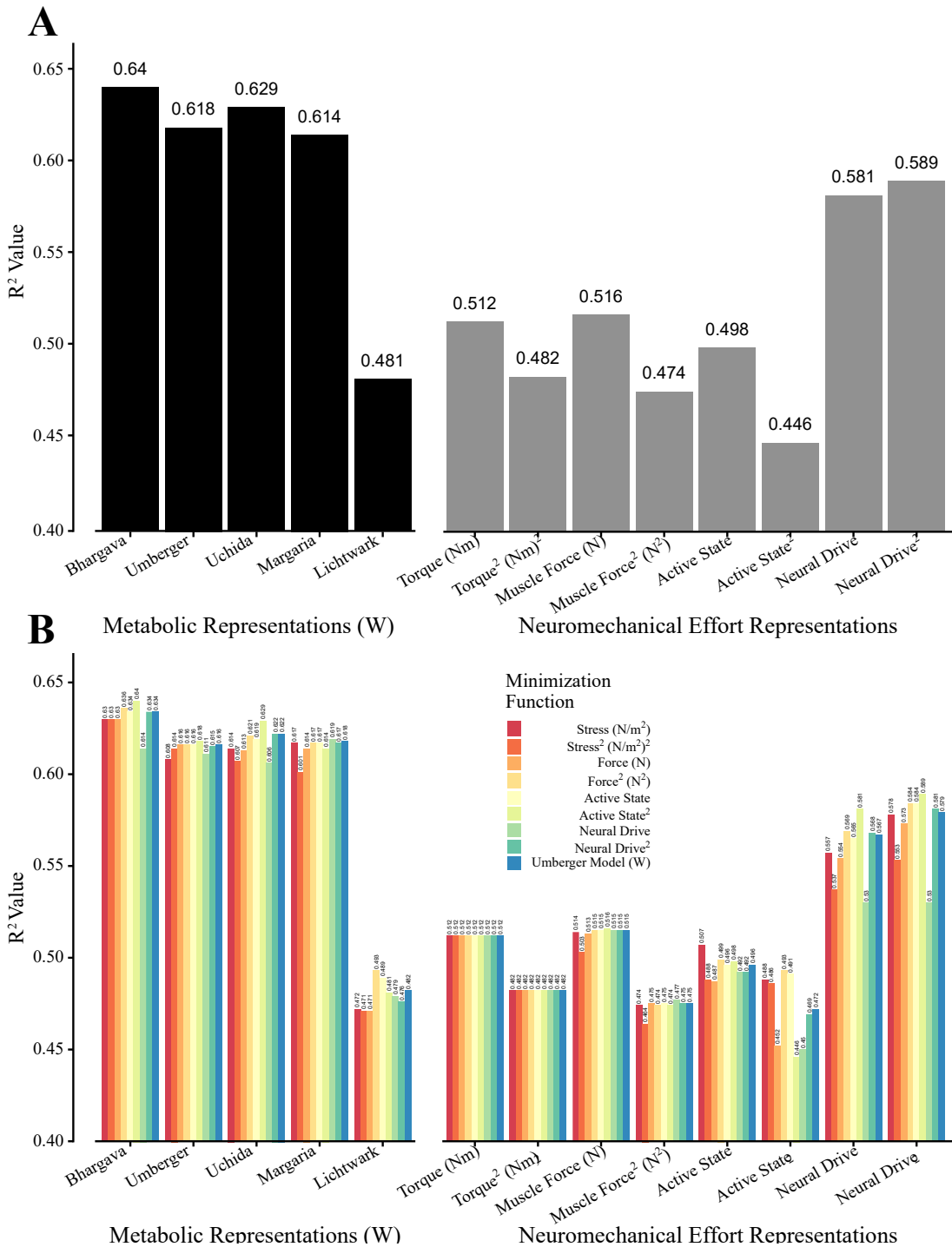


Figure 6.2: Correlation coefficients of representation predicting metabolic rate. In both plots the x axis is representation, with metabolic representations on the left and neuromechanical effort representations on the right. A. Computed R^2 values for the best fit minimizing Active State squared. B. R^2 value as a function of the minimization parameter and the predictor variable for a linear fit. Each bar is a different minimization function, and each grouping is a different neuromechanical effort representation.

Representation	Slope \pm SE (95% CI)
Umberger	1.37 \pm 0.079 (1.29 - 1.45)
Bhargava	2.194 \pm 0.121 (2.07 - 2.31)
Uchida	2.430 \pm 0.137 (2.29 - 2.57)
Lichtwark	0.313 \pm 0.024 (0.289 - 0.337)
Margaria	2.387 \pm 0.139 (2.25 - 2.53)

Table 6.3: Linear estimates for each metabolic representation. The linear estimate is shown as mean \pm standard error.

in metabolic rate. The Bhargava, Uchida, and Margaria models all had slopes slightly above 2, under-predicting the absolute change of the metabolic rate. The Lichtwark model over-predicted the metabolic rate by about three times (0.313 ± 0.024 [0.289 - 0.337]).

6.4.2 Do neuromechanical effort representations explain metabolic rate of reaching?

Unlike the metabolic representations, the neuromechanical effort representations generally did not represent metabolic rate well (Fig. 4). A common estimate used in computational motor control, sum of joint torques squared, performed poorly compared to the metabolic representations ($R^2 = 0.482$). Many of the neuromechanical representations had relatively low R^2 values. While neural drive and neural drive squared performed well, they remain weaker estimates compared to the metabolic representations ($R^2 = 0.581$, $R^2 = 0.589$, respectively).

6.4.3 Effect of mass and speed on metabolic and effort representations

In addition to investigating the variance accounted for by the metabolic and neuromechanical effort representations, we can compare how the measured metabolic rate and each candidate representation vary with mass and movement duration. For example, a measure may have weak explanatory power as evidenced by the R^2 value, but it may nonetheless accurately capture how metabolic rate varies with mass or duration. For a representation to be a good fit, we would expect it to scale in the same manner as metabolic power. To determine this, we parameterized metabolic power and each metabolic and effort representation, as a function of mass and movement duration

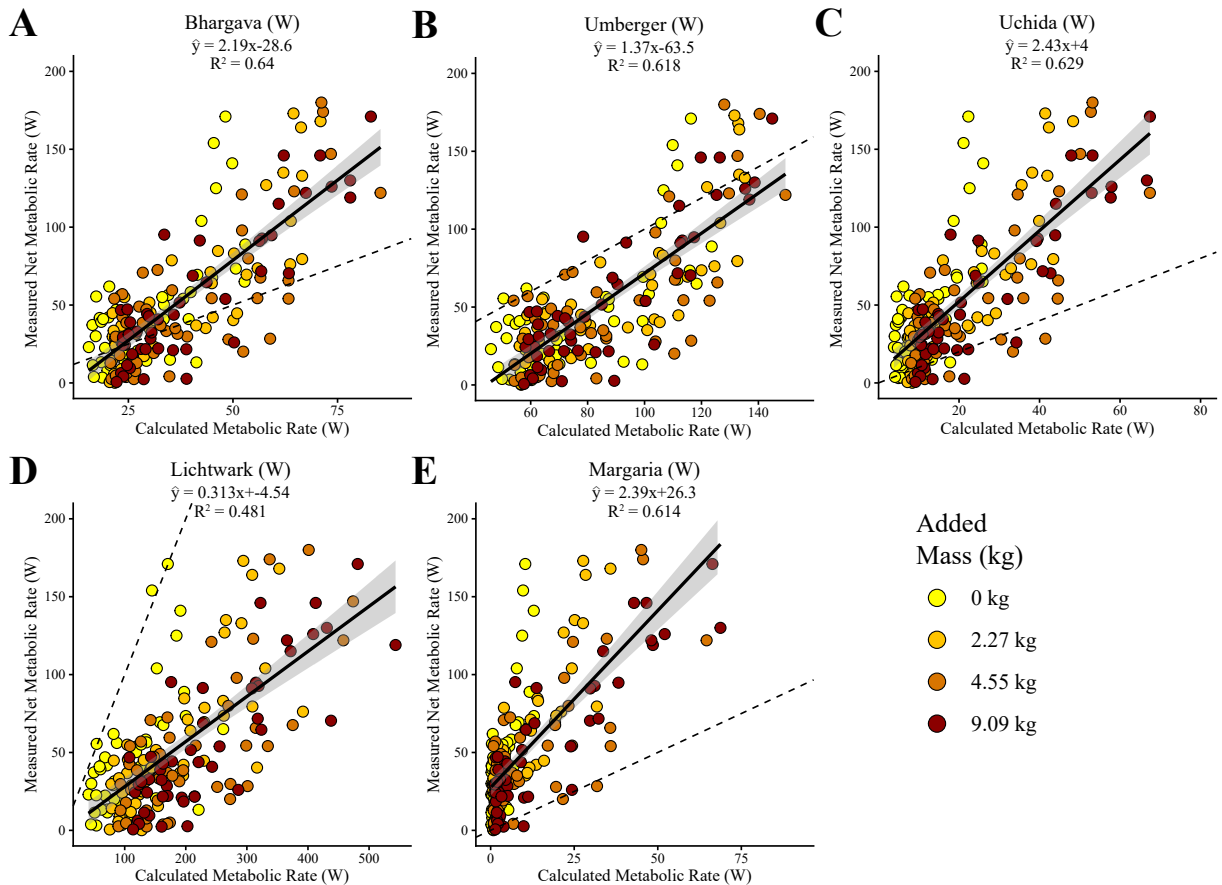


Figure 6.3: Linear model fits between the metabolic representations and the collected metabolic rate data. In each panel the solid line represents the linear model, and the shaded region shows the standard error bounds of the linear model, and the dashed line represents the line of unity. Each data point is colored by mass added at the hand. One data point (movement duration = .54, net metabolic rate = 295) is removed from this figure to improve visualization, but it is not removed for any linear models or analyses. A. The Bhargava 2004 model (18). B. The Umberger 2010 model (180). C. The Uchida 2016 model (179). D. The Lichtwark 2005 model (114). E. The Margaria 1968 model (127).

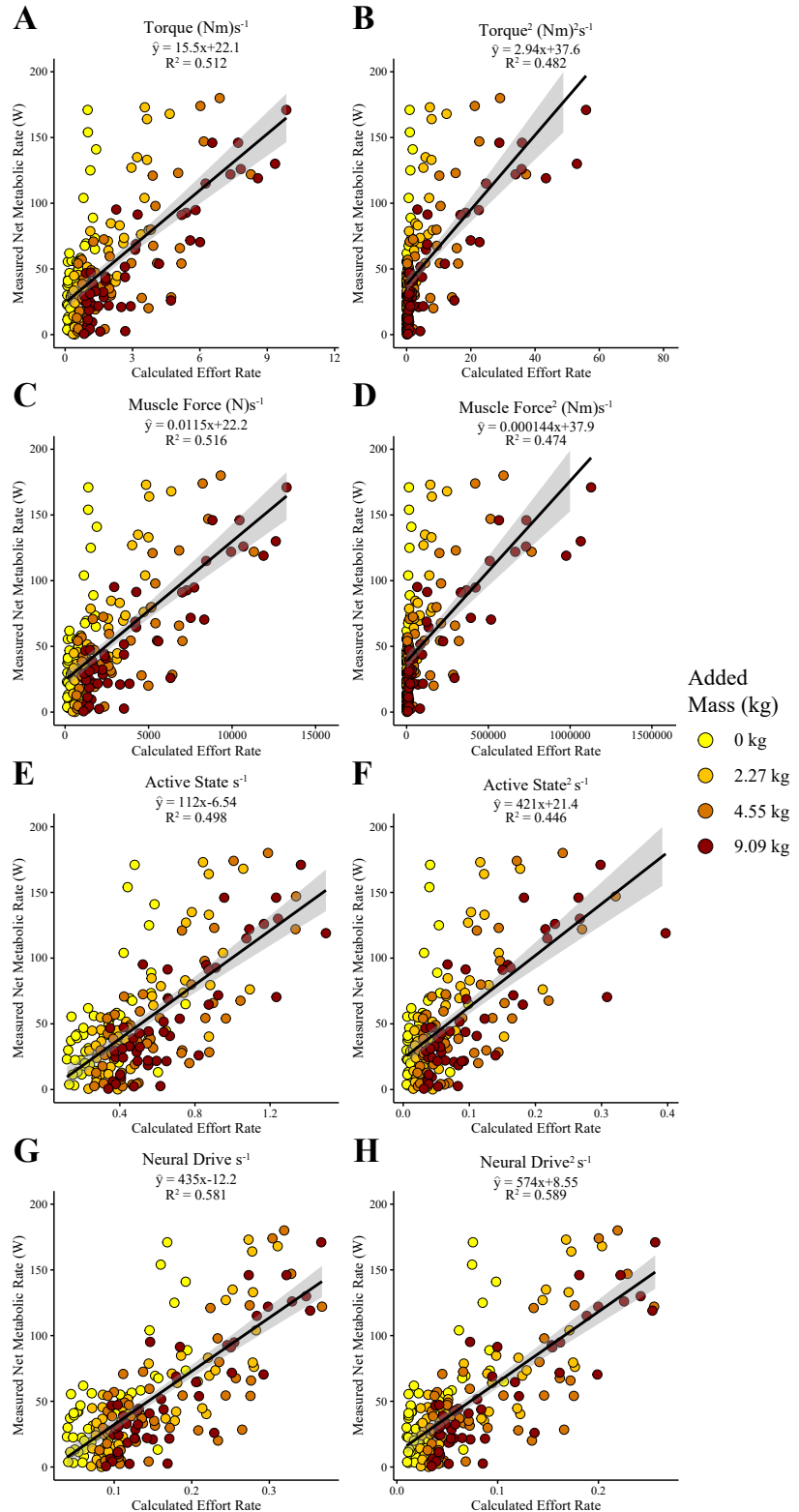


Figure 6.4: The linear model fits for the four neuromechanical variables and their squared counterparts when minimizing active state squared. In each panel the solid line represents the linear model and the shaded region shows the standard error bounds of the linear model. The data points are colored by mass added at the hand. Panel A, B shows torque and torque squared, C, D muscle force and muscle force squared, E, F muscle active state and muscle active state squared, G, H neural drive and neural drive squared.

(Eq. B.51, Table 6.4).

When fit to the measured metabolic data, eq. B.51, we obtained the following parameters (all of which are significantly different than 0): $a = 23.7 \pm 2.91$ [18.01-29.43], $b = 1.05 \pm 0.476$ [0.0012-0.0198], $c = 0.793 \pm 9.007e-2$ [0.616-0.969], $d = 5.634 \pm 0.5451$ [4.566-6.702] (mean \pm standard error [95% confidence interval]). For the ensuing analysis, we will focus specifically on parameters a , c and d . The parameter b represents a scaling factor applied to each representation and is not important for this analysis.

The parameter a in this equation represents the metabolic offset. In theory its existence suggests that a zero-velocity movement still incurs a metabolic rate which has been shown previously for both reaching and walking metabolics (166; 171). For the Umberger, Bhargava, and Uchida metabolic calculations the fitted a parameter is similarly statistically greater than 0 (Umberger: $a = 34.5 \pm 2.54$ [29.5-39.5], Bhargava: $a = 13.4 \pm 1.09$ [11.2-15.5], Uchida = 3.75 ± 0.674 [2.43-5.07]). None of the neuromechanical effort representations produce an offset that is significantly greater than zero.

The parameter c captures how metabolic rate is affected by the mass being moved. Like the metabolic rate data, the scaling of mass, c , is significantly less than one for all metabolic representations except Margaria. However, only the Uchida and Lichtwark model scale with mass in a manner not significantly different than that observed in the measured metabolic rate data. Most of the neuromechanical representations scaled with mass to a power greater than one except for active state, neural drive and neural drive squared. Notably, sum of torque squared and muscle force squared significantly overestimate the cost of added mass.

How the representations and metabolic rate are affected by movement duration is represented by the parameter d . Similar to the measured metabolic rate data, all the representations had exponents on duration that were greater than 1. However, none of the metabolic representations were statistically similar to metabolic power. Interestingly, sum of torque squared and sum of muscle force squared were the only neuromechanical effort representation that scaled with movement duration similarly to metabolic power.

Representation	<i>a</i>	<i>b</i>
Metabolics	23.7 ± 2.91 (18.01-29.43)	1.05 ± 0.476 (0.0012-0.0198)
Bhargava	13.4±1.09 (11.2-15.5)*	5.43±0.649 (4.16-6.71)
Umberger	34.5±2.54 (29.5-39.5)*	21.3±2.14 (17.1-25.5)
Uchida	3.75±0.674 (2.43-5.07)*	1.68±0.227 (1.23-2.12)
Lichtwark	15.4±16.9 (-17.7-48.5)	36.7±9.33 (18.4-55)
Margaria	-0.0386±0.455 (-0.93-0.853)	0.261±0.0464 (0.17-0.352)
Torque	-0.0367±0.0849 (-0.203-0.13)	0.0928±0.0147 (0.0639-0.122)
Torque ²	0.107±0.27 (-0.422-0.636)	0.00531±0.00155 (0.00228-0.00834)
Muscle Force	-40.4± 114 (-263- 182)	122±19.5 (84.3-161)
Muscle Force ²	117±5.67e+03 (-1.1e+04-1.12e+04)	116±34.8 (48.2-185)
Active State	0.0364±0.0476 (-0.0568-0.13)	0.111±0.0267 (0.0584-0.163)
Active State ²	0.00144±0.00642 (-0.0111-0.014)	0.00485±0.00152 (0.00187-0.00783)
Neural Drive	0.0132±0.00948 (-0.00541-0.0317)	0.0347±0.00583 (0.0233-0.0461)
Neural Drive ²	0.000871±0.00444 (-0.00784-0.00958)	0.0106±0.00184 (0.00701-0.0142)
Representation	<i>c</i>	<i>d</i>
Metabolics	0.793 ± 9.007e-2 (0.616-0.969)	5.634 ± 0.5451 (4.566-6.702)
Bhargava	0.524±0.0247 (0.475-0.572)	2.33±0.111 (2.11-2.54)
Umberger	0.279±0.0159 (0.248-0.31)	1.75±0.0918 (1.57-1.93)
Uchida	0.844±0.0325 (0.781-0.908)†	2.92±0.123 (2.68-3.17)
Lichtwark	0.656±0.0631 (0.532-0.78)†	1.65±0.165 (1.32-1.97)
Margaria	1.3±0.0444 (1.22-1.39)	4.43±0.175 (4.08-4.77)
Torque	1.27±0.0459 (1.18-1.36)	2.85±0.115 (2.63-3.08)
Torque ²	2.4±0.085 (2.24-2.57)	.29±0.254 (5.79-6.78)†
Muscle Force	1.27±0.0456 (1.18-1.36)	2.91±0.117 (2.68-3.14)
Muscle Force ²	2.39±0.0877 (2.22-2.56)	6.18±0.259 (5.67-6.69)†
Active State	0.653±0.0602 (0.535-0.771)	1.58±0.151 (1.29-1.88)
Active State ²	1.13±0.0893 (0.95- 1.3)	2.54±0.221 (2.1-2.97)
Neural Drive	0.551±0.0373 (0.478-0.624)	1.79±0.127 (1.55-2.04)
Neural Drive ²	0.766±0.042 (0.684-0.849)	2.46±0.146 (2.17-2.75)

Table 6.4: Parameterization values for each representation. Each value shown mean ± standard error with the 95% confidence interval in parenthesis. The *a* parameter represents some offset at infinite movement duration, for this analysis a value greater than 0 is indicated with a *. A scaling parameter, *b*, is not important to this analysis. How each representation scales with mass, *c*, and how they are affected by time, *d*, are tested to determine if they are different than the parameters found in the metabolic rate with equation B.52. This non-difference from metabolic rate effect of time is indicated with a †.

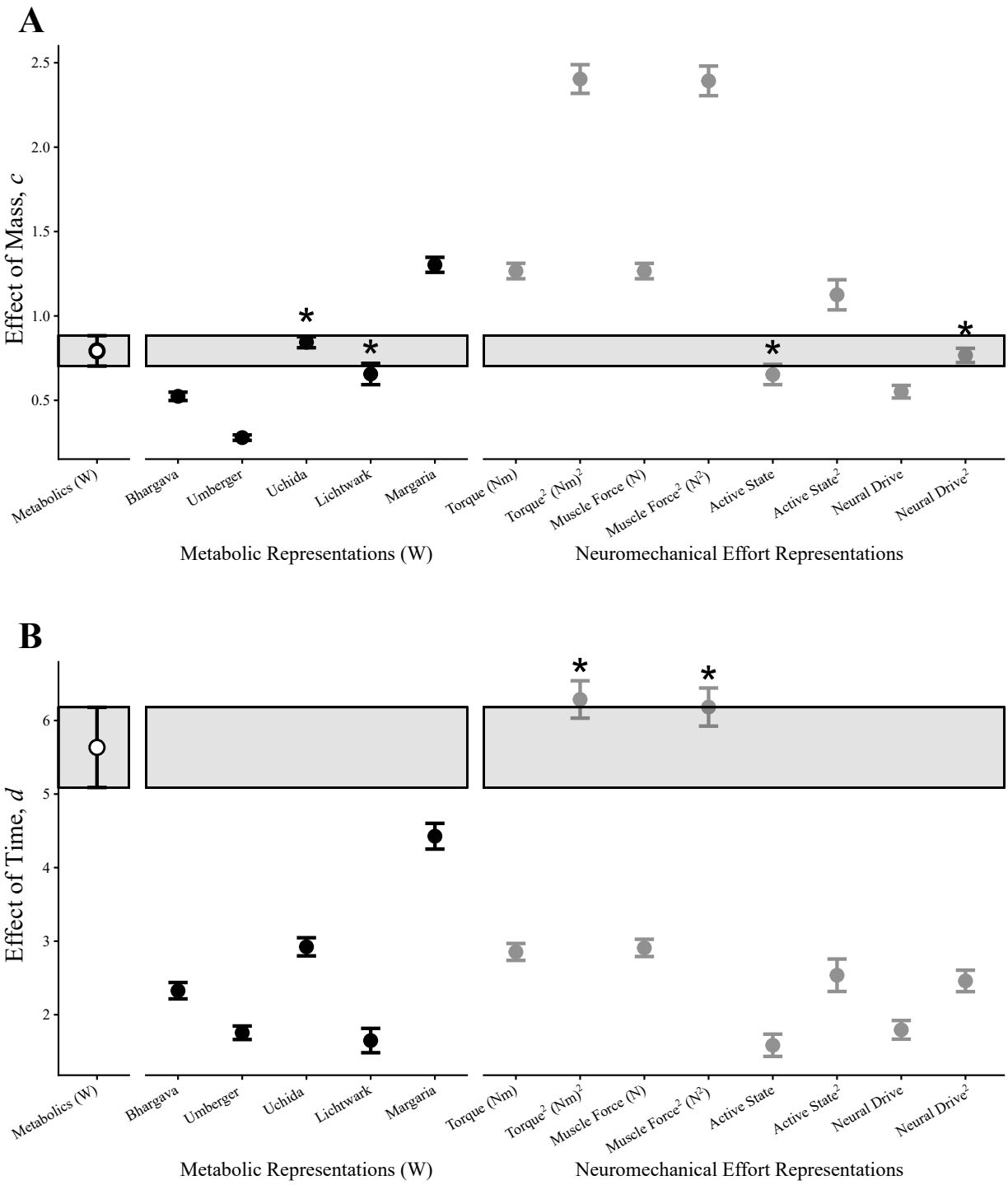


Figure 6.5: Parameterization values for each representation. Each Value shown mean \pm standard error. In this plot we show the scaling of mass, c , and time, d for each representation. If the parameterized value is not different than the parameter from metabolic rate as determined by equation B.52, it is indicated with a *.

6.5 Discussion

The goal of this study was to determine how well different metabolic and neuromechanical effort representations are able to capture the metabolic rate of arm reaching movements. We collected metabolic data from subjects making reaching movements at a range of speeds and masses added at the hand. We developed a neuromechanical model of the arm and computed model-based representations for metabolic rate and effort and compared these to measured metabolic rate of arm reaching. We found that nearly all the metabolic representations performed well in predicting metabolic rate, with the Bhargava energy expenditure model able to provide the best predictive performance. In contrast, most of the neuromechanical effort measures performed poorly in comparison.

We found that the Bhargava metabolic model provided the best estimate of the metabolic power of reaching, with most of the other metabolic representations performing similarly, albeit somewhat worse. In theory, these metabolic representations which have been validated in walking should perform similarly in reaching as they are based on general muscle properties. A recent study validated multiple metabolic models in a walking simulation and found relatively similar results (107). They also found that the Bhargava model predicted the highest R^2 value (18). However, in our analysis, out of the metabolic representations the Lichtwark model performed poorly compared to the others (114). In this study all metabolic representations but the Lichtwark model underpredicted the metabolic rate similar to Koelewijn et al. The Umberger model showed the closest linear relationship to metabolic rate, unlike previous research which showed the Margaria model having the closest linear relationship. While the Koelewijn study reports correlation coefficients above 0.9, (seemingly much greater than the R^2 values we report), they used a repeated measures correlation. As a secondary analysis we performed a repeated measures correlation and obtained similar findings regarding the relative performance of each model, but with the correlation coefficients obtained being higher. Specifically, we obtained a correlation coefficient of 0.870 (0.823 - 0.901) for the Bhargava model, similar to the 0.96 (0.93 - 0.97) obtained for the Bhargava model

for walking data. Our results agree with previous work that the Bhargava model has the highest correlation but disagree in that in our study the Umberger model has the closest linear slope to one and in previous work the Margaria model did.

When simulating arm reaching movements many different neuromechanical effort costs have been proposed to represent the effort cost of reaching (15; 106; 113; 181). While these effort representations can capture the general shape of the metabolic rate of reaching, we show that in certain situations these representations may not be good to use to estimate metabolic rate. A common representation of cost in arm reaching, sum of squared joint torques, performs poorly when predicting metabolic rate with an R^2 of 0.51 (0.41 – 0.61). Many of the other neuromechanical representations show similarly low R^2 values. Many of these representations fail at specific aspects of the changing cost landscape, either scaling far too much with mass or scaling far too little with time. We show that using these neuromechanical representations of metabolic rate may lead to inaccurate results as these representations do not well represent metabolic rate.

We can also compare how each of these representations exhibit an offset to the cost of movement as well as how they change with mass and speed. Ideally, the representation will exhibit an offset to the cost of movement and change to the same degree as metabolic rate with either mass or speed. The offset parameter (a) represents the metabolic power of a reach of infinite duration. The metabolic power data revealed an offset value significantly greater than zero, indicative of a cost that is independent of mass and time. The Umberger, Bhargava, and Uchida model have an offset greater than 0. The offset value fitted via the Bhargava model was also the most similar to the metabolic rate data fit. This could help explain why the Bhargava model had the highest R^2 value, while many representations have poor prediction at longer movement durations, as the cost should collapse to this offset. All of the neuromechanical representations lack an offset that is greater than 0, implying that as the movement duration increases to infinity, joint torque, muscle force, active state, and neural drive will all, not surprisingly, asymptote to 0. Thus, a major limitation of these neuromechanical representations is that they cannot account for this offset which may lead to more inaccurate predictions.

We can see how these parametric fits align with the metabolic data in figure 6.6 and compare these to the metabolic parametric fits. In this plot the points indicate the metabolic rate data or simulated rate data, and lines represent the parametric fits. We focus on how these representations change with mass and time. Metabolic power was increased by mass (c) to the power of 0.793, a slightly sub-linear scaling. The sub-linear increase in metabolic power due to mass was captured by all metabolic representations but the Margaria model. The Uchida (0.844 ± 0.0325 [0.781-0.908]) and Lichtwark (0.656 ± 0.0631 [0.532-0.780]) model were also not significantly different than the scaling of mass of the metabolic rate data. Almost all the neuromechanical effort representations (except active state, neural drive, and neural drive squared) scaled supra-linearly with mass, likely leading to a large source of error in these estimates. The spread of the lines in figure 6.6 show how each scale with mass, the closer together the lines the lower the c parameter, and the more spread out the lines are the higher the c parameter will be. The Uchida and Lichtwark model had the closest scaling of mass to metabolic rate, but it is unclear by these graphs that the spread of the lines is most similar to metabolic rate. This is primarily due to the scaling with time shaping these curves more than mass. Generally, we find that the metabolic representations can capture the effect of mass in arm reaching while only a few of the neuromechanical representations can.

The very sharp rise in metabolic power due to an increase in speed is shown in figure 6.6, but none of the metabolic representations reflect a similar sharp rise, as evidenced by how they scale with movement duration and quantified by the fitted d parameter. The scaling with time, d , can be viewed as how sharply the lines rise as low movement durations or how flat the lines become at high movement durations. Metabolic power scales with time by an exponent of 5.6, whereas many of the other candidate representations are around the range of 2. The Margaria model, with the highest scaling ($d = 4.43 \pm 0.175$ [4.08-4.77]) shows a steep rise in metabolic rate but not as high as experimental data shows. This means that generally, at the very fast speeds (low movement durations), the representations are all under-predicting the cost of the movement. Many of the metabolic representations do not show this flattening at higher movement durations. The Margaria model, does flatten, but again, not quite as much as metabolic rate. Torque², which

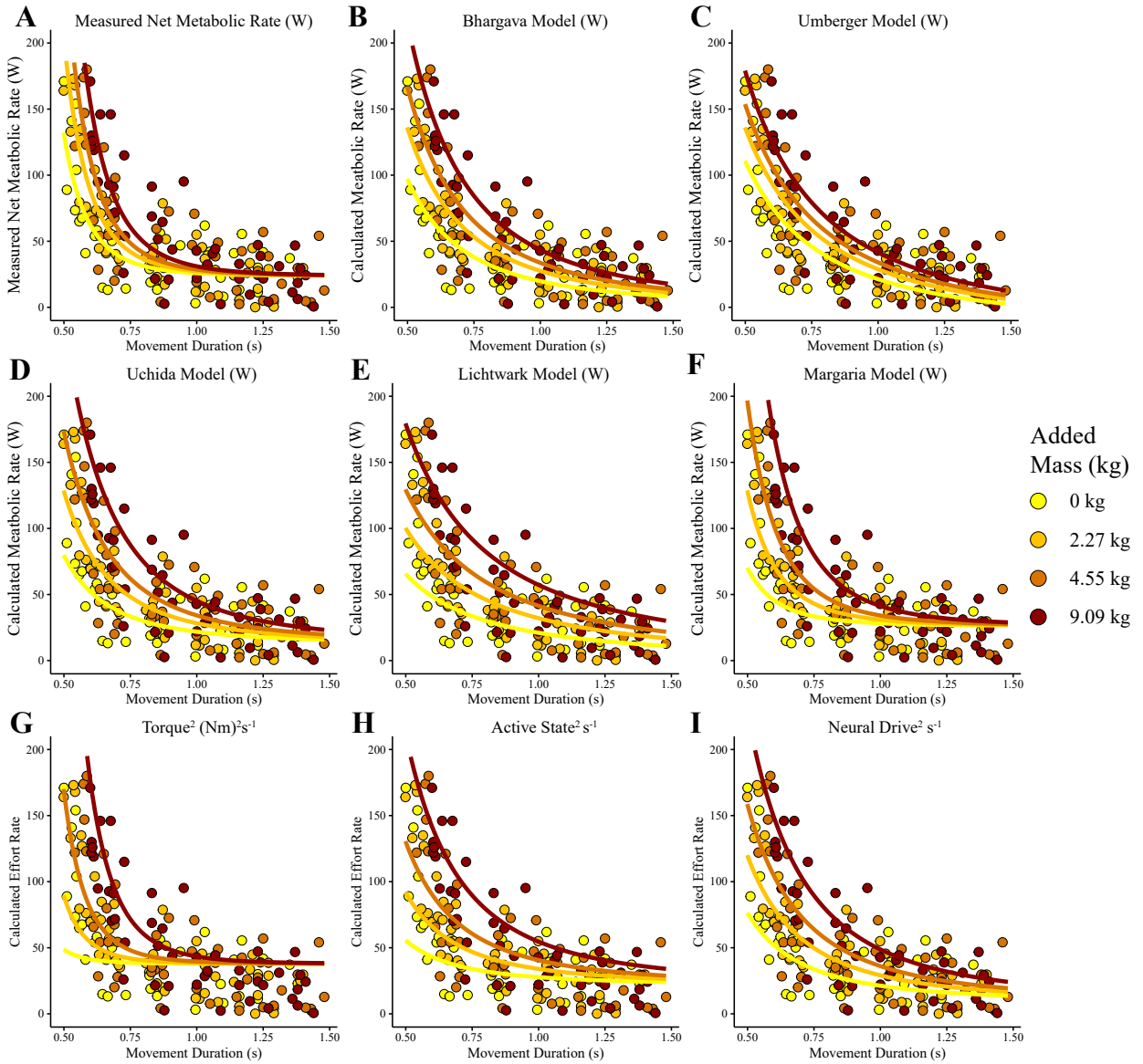


Figure 6.6: Parametric curves for metabolic rate, metabolic representation, and select neuromechanical representations. Data points indicate the metabolic rate or calculated representation, and lines indicate parametric fits. As the scale for the representations may not be very good, the linear model is applied to each parametric fit to get each representation on the same relative magnitude to metabolic rate. This allows us to see how each representation scales with mass and time when compared to the metabolic data and metabolic rate parametric fit. A. Metabolic Rate. B. Bhargava Model. C. Umberger model. D. Uchida Model. E. Lichtwark Model. F. Margaria model. G. Torque 2 . H. Active State 2 . I. Neural Drive 2 .

has a high time exponent ($d = 6.286$), does show this very sharp rise and flattening but suffers from scaling very poorly with mass as can be seen in the 0 kg condition. The low mass conditions show a much higher metabolic power than the representation would predict. The scaling with time exemplifies one of the primary faults of the metabolic representations; they generally cannot account for the sharp rise in metabolic power in the low mass high speed conditions.

It is unclear which minimization function humans use to determine which muscles get activated versus others. Some evidence points towards minimizing the activation state of the muscle activation and effort (21; 32; 33; 36; 50?). Because of this, we computed the metabolic and effort estimates while utilizing many possible minimization functions. We found that minimizing active state squared lead to the highest predicted values, which is presented in the main body results. Interestingly, previous work has shown that when compared to EMG muscle activation, minimizing active state squared provides a good representation of how the muscles are activated (50). We also show that across minimization functions, generally specific models still have the highest predictive power (Fig. 6.2B). However, for some of these metabolic and effort representations, the minimization function had a large effect on the predictive power. Neural drive for example, had a maximum R^2 value of 0.589 minimizing active state squared. When minimizing neural drive, neural drive dropped in predictive power to 0.53. Interestingly, minimizing neural drive had relatively low predictive power across all representations. Our data generally aligns with the theory that minimizing active state squared yields the best prediction of muscle force, as it led to the higher predictive power of the representations.

6.5.1 Limitations

The exact time delays between changes in movement kinematics, expired gas, and changes in metabolic power are unknown for arm reaching (92). For this reason, we only use the last three minutes of expired gas data in each block as we assume that by that point subjects had reached a steady state. The metabolic power data is also noisy, leading to some inconsistencies with the metabolic power data. The metabolic data suffers from not being normally distributed

and highly skewed. A Shapiro-Wilk test on the metabolic power data show that it is non-normal and skewed heavily right ($\text{skew} = 1.632523$, $p\text{-value} = 1.495\text{e-}12$). After removing the very high metabolic data point (movement duration = 0.56s, mass = 4.55 kg, metabolic power = 295 W), the data is still highly skewed and non-normal ($\text{skew} = 1.205073$, $p\text{-value} = 3.049\text{e-}11$). This leads our analysis to be mainly affected by lower cost movements and lacking higher cost movements. The residuals of the linear fits are also non-normal and skewed right (fig B.10), indicating that the metabolic representations have higher errors when the metabolic power was high. Having a better distribution of metabolic data points could lead to a more accurate analysis. For example, in the collected metabolic data, the fastest speed with 2.27 kg added mass resulted in a very similar metabolic rate than the fastest speed for 4.55 kg added. However, in all the model predictions, the fastest speed for 4.55 kg had a much higher metabolic rate prediction than 2.27 kg. This can also be seen at longer movement durations as the differences in metabolic power become very similar. At the fifth movement duration, 2.27 kg added has a higher average metabolic power than with 4.55 kg added while the average movement durations were very similar (0.7509 and 0.7539).

6.5.2 Conclusion

This analysis shows that current models of metabolic expenditure used for explaining walking metabolics are also able to generally predict reaching metabolics as well, with the Bhargava model providing the best predictive power. Of the neuromechanical effort representations, only neural drive and its squared counterpart showed a good relation to metabolic power, although still not as accurate as the better metabolic representations. Critically, sum of squared joint torque, an oft-used measure of effort in computational models was found to be a substantially less accurate predictor of the metabolic cost of reaching.

Chapter 7

Conclusions

In this thesis I described the effect of reward and effort on movement and how musculoskeletal models can be developed to estimate energetic rates of movement. In decision-making approach, where the goal of a movement is to maximize its utility, reward and effort can both alter movement choices and characteristics by weighting them against each other. Using this approach, we can gain better insights into the underlying determinants of movement choices. A major component of movement choices is measuring effort. Musculoskeletal models have become commonplace for estimating movement energetics, though many models exist and there may be issues with how well the metabolic models perform. Below I summarize the main conclusions from the three studies I completed to add to our body of knowledge on the roles of reward and effort in determining movement vigor, and estimation of metabolic cost.

- (1) Study 1: I evaluated the effects of expected value of reward, reward history, and reward prediction error in human subjects making planar arm reaching movements.
 - (a) Increasing probability of reward leads to faster movements.
 - (b) Reward invigorates the movement that follows, whereas absence of reward leads to slowing of the movement that follows.
 - (c) Vigor of the following movement is also modulated by how surprising the reward or absence of reward is. A very surprising reward (high +RPE) leads to faster reaches on subsequent trials, compared to a less surprising reward (low +RPE). Conversely,

a very surprising negative outcome leads to slower movements compared to a less surprising, but still negative outcome.

- (2) Study 2: I evaluated whether humans optimize the metabolic cost of a movement in arm reaching by determining how increasing mass affects the metabolic cost and self-selected movement vigor.
 - (a) Metabolic cost of reaching increases with added mass.
 - (b) The metabolically optimal movement duration increases with mass.
 - (c) Independent of accuracy requirements, added mass at the hand leads to slower movement speeds.
 - (d) Independent of accuracy requirements, added mass at the hand leads to slower reaction times.
 - (e) Preferred movement durations are not fully explained by minimization of metabolic cost alone.
 - (f) A utility framework that combines reward and effort (discounted by time), where effort is critically represented as metabolic cost, can reasonably explain the effect of increased effort on movement vigor.
- (3) Study 3: I developed a neuromechanical model of the arm, simulated the metabolic rate of arm reaching movements across a range of masses and speeds and compared estimates to measurement of metabolic cost.
 - (a) By simulating the metabolic rate of arm reaches with five metabolic rate models, four of the five models performed similarly in terms of predictive power.
 - (b) Of many possible neuromechanical representations, only neural drive and neural drive² had comparable predictive power to the metabolic models.
 - (c) Many of the metabolic representations can capture the changes due to increased mass but cannot capture the changes in metabolic rate due to increased speed.

This dissertation contributes to the body of work on how reward and effort can affect movement choices and how we can better estimate effort in arm reaching. These findings provide novel insights on how and potentially why humans respond to changing reward and effort landscapes and have the potential to inform future work aimed at understanding the neural, psychological and biomechanical determinants of why we move the way we do.

Bibliography

- [1] S. Adewusi, S. Rakheja, and P. Marcotte. Biomechanical models of the human hand-arm to simulate distributed biodynamic responses for different postures. *International Journal of Industrial Ergonomics*, 42(2):249–260, March 2012.
- [2] Stamatis Agiovlasitis, Robert W. Motl, Sushant M. Ranadive, Christopher A. Fahs, Huimin Yan, George H. Echols, Lindy Rossow, and Bo Fernhall. Energetic optimization during over-ground walking in people with and without Down syndrome. *Gait & Posture*, 33(4):630–634, April 2011.
- [3] George Ainslie. *Picoeconomics : the strategic interaction of successive motivational states within the person*. Cambridge University Press, Cambridge, 2010.
- [4] R. McN Alexander. A minimum energy cost hypothesis for human arm trajectories. *Biological Cybernetics*, 76(2):97–105, February 1997.
- [5] M. Allais. Le Comportement de l'Homme Rationnel devant le Risque: Critique des Postulats et Axiomes de l'Ecole Americaine. *Econometrica*, 21(4):503–546, 1953.
- [6] K. N. An, B. M. Kwak, E. Y. Chao, and B. F. Morrey. Determination of Muscle and Joint Forces: A New Technique to Solve the Indeterminate Problem. *Journal of Biomechanical Engineering*, 106(4):364–367, November 1984.
- [7] Frank C. Anderson and Marcus G. Pandy. Dynamic Optimization of Human Walking. *Journal of Biomechanical Engineering*, 123(5):381–390, May 2001.
- [8] Frank C. Anderson and Marcus G. Pandy. Static and dynamic optimization solutions for gait are practically equivalent. *Journal of Biomechanics*, 34(2):153–161, February 2001.
- [9] A. Terry Bahill, Michael R. Clark, and Lawrence Stark. The main sequence, a tool for studying human eye movements. *Mathematical Biosciences*, 24(3):191–204, January 1975.
- [10] G. J. Bastien, P. A. Willems, B. Schepens, and N. C. Heglund. Effect of load and speed on the energetic cost of human walking. *European Journal of Applied Physiology*, 94(1-2):76–83, May 2005.
- [11] Matthew E. Batliner, Shalaya Kipp, Alena M. Grabowski, Rodger Kram, and William C. Byrnes. Does Metabolic Rate Increase Linearly with Running Speed in all Distance Runners? *Sports Medicine International Open*, 2(1):E1–E8, November 2017.
- [12] Luis M. Bautista, Joost Tinbergen, and Alejandro Kacelnik. To walk or to fly? How birds choose among foraging modes. *Proceedings of the National Academy of Sciences*, 98(3):1089–1094, January 2001.
- [13] Hannah M. Bayer and Paul W. Glimcher. Midbrain Dopamine Neurons Encode a Quantitative Reward Prediction Error Signal. *Neuron*, 47(1):129–141, July 2005.
- [14] Daniel Bernoulli. Exposition of a New Theory on the Measurement of Risk. *Econometrica*, 22(1):23, January 1954.

- [15] Bastien Berret, Enrico Chiovetto, Francesco Nori, and Thierry Pozzo. Evidence for Composite Cost Functions in Arm Movement Planning: An Inverse Optimal Control Approach. *PLOS Computational Biology*, 7(10):e1002183, October 2011.
- [16] Bastien Berret, Christian Darlot, Frédéric Jean, Thierry Pozzo, Charalambos Papaxanthis, and Jean Paul Gauthier. The Inactivation Principle: Mathematical Solutions Minimizing the Absolute Work and Biological Implications for the Planning of Arm Movements. *PLOS Computational Biology*, 4(10):e1000194, October 2008.
- [17] JOHN E. A. Bertram and ANDY Ruina. Multiple Walking Speed–frequency Relations are Predicted by Constrained Optimization. *Journal of Theoretical Biology*, 209(4):445–453, April 2001.
- [18] Lindsay J. Bhargava, Marcus G. Pandy, and Frank C. Anderson. A phenomenological model for estimating metabolic energy consumption in muscle contraction. *Journal of Biomechanics*, 37(1):81–88, January 2004.
- [19] W. K. Bickel, A. L. Odum, and G. J. Madden. Impulsivity and cigarette smoking: delay discounting in current, never, and ex-smokers. *Psychopharmacology*, 146(4):447–454, October 1999.
- [20] Magnus Blix. The length and tension of the muscle. *Skandinavisches Archiv Für Physiologie*, 5(1):150–173, January 1894.
- [21] Daniele Borzelli, Denise J. Berger, Dinesh K. Pai, and Andrea d’Avella. Effort minimization and synergistic muscle recruitment for three-dimensional force generation. *Frontiers in Computational Neuroscience*, 7, 2013.
- [22] B. Brenner, L. C. Yu, L. E. Greene, E. Eisenberg, and M. Schoenberg. Ca²⁺-sensitive cross-bridge dissociation in the presence of magnesium pyrophosphate in skinned rabbit psoas fibers. *Biophysical Journal*, 50(6):1101–1108, December 1986.
- [23] Eli Brenner and Jeroen B. J. Smeets. How Can You Best Measure Reaction Times? *Journal of Motor Behavior*, August 2018.
- [24] J. M. Brockway. Derivation of formulae used to calculate energy expenditure in man. *Human nutrition : clinical nutrition*, 1987.
- [25] I. E. Brown, E. J. Cheng, and G. E. Loeb. Measured and modeled properties of mammalian skeletal muscle. II. The effects of stimulus frequency on force-length and force-velocity relationships. *Journal of Muscle Research and Cell Motility*, 20(7):627–643, October 1999.
- [26] Raymond C. Browning and Rodger Kram. Energetic Cost and Preferred Speed of Walking in Obese vs. Normal Weight Women. *Obesity Research*, 13(5):891–899, 2005.
- [27] Raymond C. Browning, Jesse R. Modica, Rodger Kram, and Ambarish Goswami. The Effects of Adding Mass to the Legs on the Energetics and Biomechanics of Walking:. *Medicine & Science in Sports & Exercise*, 39(3):515–525, March 2007.
- [28] Yi-Wen Chang, Fong-Chin Su, Hong-Wen Wu, and Kai-Nan An. Optimum length of muscle contraction. *Clinical Biomechanics*, 14(8):537–542, October 1999.

- [29] Eric L. Charnov. Optimal foraging, the marginal value theorem. *Theoretical Population Biology*, 9(2):129–136, April 1976.
- [30] Lewis L. Chen, Y. Mark Chen, Wu Zhou, and William D. Mustain. Monetary reward speeds up voluntary saccades. *Frontiers in Integrative Neuroscience*, 8, June 2014.
- [31] Jennie E. S. Choi, Pavan A. Vaswani, and Reza Shadmehr. Vigor of Movements and the Cost of Time in Decision Making. *Journal of Neuroscience*, 34(4):1212–1223, January 2014.
- [32] Jacek Cholewicki and Stuart M. McGill. EMG assisted optimization: A hybrid approach for estimating muscle forces in an indeterminate biomechanical model. *Journal of Biomechanics*, 27(10):1287–1289, October 1994.
- [33] J. J. Collins. The redundant nature of locomotor optimization laws. *Journal of Biomechanics*, 28(3):251–267, March 1995.
- [34] Renato Contini. Body Segment Parameters, Part II. *Artificial Limbs*, 16(1):20, 1972.
- [35] Ignasi Cos, Nicolas Bélanger, and Paul Cisek. The influence of predicted arm biomechanics on decision making. *Journal of Neurophysiology*, 105(6):3022–3033, March 2011.
- [36] Roy D. Crowninshield and Richard A. Brand. A physiologically based criterion of muscle force prediction in locomotion. *Journal of Biomechanics*, 14(11):793–801, January 1981.
- [37] Paula L. Croxson, Mark E. Walton, Jill X. O'Reilly, Timothy E. J. Behrens, and Matthew F. S. Rushworth. Effort-Based Cost–Benefit Valuation and the Human Brain. *The Journal of Neuroscience*, 29(14):4531–4541, April 2009.
- [38] Raja Dahmane, Srdjan Djordjević, Bostjan Šimunič, and Vojko Valenčič. Spatial fiber type distribution in normal human muscle: Histochemical and tensiomyographical evaluation. *Journal of Biomechanics*, 38(12):2451–2459, December 2005.
- [39] Friedl De Groote, Allison L. Kinney, Anil V. Rao, and Benjamin J. Fregly. Evaluation of Direct Collocation Optimal Control Problem Formulations for Solving the Muscle Redundancy Problem. *Annals of Biomedical Engineering*, 44(10):2922–2936, 2016.
- [40] Mark Dean, Shih-Wei Wu, and Laurence T. Maloney. Trading off speed and accuracy in rapid, goal-directed movements. *Journal of Vision*, 7(5):10–10, March 2007.
- [41] S. L. Delp, F. C. Anderson, A. S. Arnold, P. Loan, A. Habib, C. T. John, E. Guendelman, and D. G. Thelen. OpenSim: Open-Source Software to Create and Analyze Dynamic Simulations of Movement. *IEEE Transactions on Biomedical Engineering*, 54(11):1940–1950, November 2007.
- [42] S. L. Delp, J. P. Loan, M. G. Hoy, F. E. Zajac, E. L. Topp, and J. M. Rosen. An interactive graphics-based model of the lower extremity to study orthopaedic surgical procedures. *IEEE Transactions on Biomedical Engineering*, 37(8):757–767, August 1990.
- [43] F. J. Diedrich and W. H. Warren. Why change gaits? Dynamics of the walk-run transition. *Journal of Experimental Psychology. Human Perception and Performance*, 21(1):183–202, February 1995.

- [44] J. Maxwell Donelan, Rodger Kram, and Arthur D. Kuo. Mechanical work for step-to-step transitions is a major determinant of the metabolic cost of human walking. *Journal of Experimental Biology*, 205(23):3717–3727, December 2002.
- [45] M. D. Eaton, D. L. Evans, D. R. Hodgson, and R. J. Rose. Effect of treadmill incline and speed on metabolic rate during exercise in thoroughbred horses. *Journal of Applied Physiology*, 79(3):951–957, September 1995.
- [46] Jennifer England and Siobhan Loughna. Heavy and light roles: myosin in the morphogenesis of the heart. *Cellular and Molecular Life Sciences*, 70(7):1221–1239, April 2013.
- [47] Roger Enoka. *Neuromechanics of Human Movement*. Human Kinetics, 5th edition, 2002.
- [48] Roger M. Enoka and Andrew J. Fuglevand. Motor unit physiology: Some unresolved issues. *Muscle & Nerve*, 24(1):4–17, 2001.
- [49] Marcelo Epstein and Walter Herzog. *Theoretical Models of Skeletal Muscle: Biological and Mathematical Considerations*. Wiley, 1998.
- [50] Andrew H. Fagg, Ashvin Shah, and Andrew G. Barto. A Computational Model of Muscle Recruitment for Wrist Movements. *Journal of Neurophysiology*, 88(6):3348–3358, December 2002.
- [51] Falisse Antoine, Serrancolí Gil, Dembia Christopher L., Gillis Joris, Jonkers Ilse, and De Groote Friedl. Rapid predictive simulations with complex musculoskeletal models suggest that diverse healthy and pathological human gaits can emerge from similar control strategies. *Journal of The Royal Society Interface*, 16(157):20190402, August 2019.
- [52] Axel J. Fenwick, Alexander M. Wood, and Bertrand C. W. Tanner. Effects of cross-bridge compliance on the force-velocity relationship and muscle power output. *PLOS ONE*, 12(12):e0190335, December 2017.
- [53] Adolf Fick. *Mechanical Work and Heat Development in Muscular Activity*. AbeBooks, 1882.
- [54] Paul M Fitts. The Information Capacity of the Human Motor System in Controlling the Amplitude of Movement. *Journal of Experimental Psycholog*, 121(3):8, 1992.
- [55] T. Flash and N. Hogan. The coordination of arm movements: an experimentally confirmed mathematical model. *Journal of Neuroscience*, 5(7):1688–1703, July 1985.
- [56] Martino V. Franchi, Neil D. Reeves, and Marco V. Narici. Skeletal Muscle Remodeling in Response to Eccentric vs. Concentric Loading: Morphological, Molecular, and Metabolic Adaptations. *Frontiers in Physiology*, 8, July 2017.
- [57] Shane Frederick, George Loewenstein, and Ted O'Donoghue. Time Discounting and Time Preference: A Critical Review. *Journal of Economic Literature*, 40(2):351–401, June 2002.
- [58] J. Fridén, D. Albrecht, and R. L. Lieber. Biomechanical analysis of the brachioradialis as a donor in tendon transfer. *Clinical Orthopaedics and Related Research*, 383:152–161, February 2001.

- [59] A. J. Fuglevand, D. A. Winter, and A. E. Patla. Models of recruitment and rate coding organization in motor-unit pools. *Journal of Neurophysiology*, 70(6):2470–2488, December 1993.
- [60] Joseph M Galea, Elizabeth Mallia, John Rothwell, and Jörn Diedrichsen. The dissociable effects of punishment and reward on motor learning. *Nature Neuroscience*, 18(4):597–602, April 2015.
- [61] Koren Gast, Rodger Kram, and Raziel Riemer. Preferred walking speed on rough terrain: is it all about energetics? *Journal of Experimental Biology*, 222(9), May 2019.
- [62] Asghar Ghasemi and Saleh Zahediasl. Normality Tests for Statistical Analysis: A Guide for Non-Statisticians. *International Journal of Endocrinology and Metabolism*, 10(2):486–489, 2012.
- [63] Jacob A. Goble, Yanxin Zhang, Yury Shimansky, Siddharth Sharma, and Natalia V. Dounskaya. Directional Biases Reveal Utilization of Arm’s Biomechanical Properties for Optimization of Motor Behavior. *Journal of Neurophysiology*, 98(3):1240–1252, September 2007.
- [64] J. Gordon, M. F. Ghilardi, S. E. Cooper, and C. Ghez. Accuracy of planar reaching movements. II. Systematic extent errors resulting from inertial anisotropy. *Experimental brain research*, 99(1):112–130, 1994.
- [65] Keith E. Gordon, Daniel P. Ferris, and Arthur D. Kuo. Metabolic and Mechanical Energy Costs of Reducing Vertical Center of Mass Movement During Gait. *Archives of Physical Medicine and Rehabilitation*, 90(1):136–144, January 2009.
- [66] Alena Grabowski, Claire T. Farley, and Rodger Kram. Independent metabolic costs of supporting body weight and accelerating body mass during walking. *Journal of Applied Physiology*, 98(2):579–583, February 2005.
- [67] Leonard Green and Howard Rachlin. Economic Substitutability of Electrical Brain Stimulation, Food, and Water. *Journal of the Experimental Analysis of Behavior*, 55(2):133–143, 1991.
- [68] Timothy M. Griffin, Thomas J. Roberts, and Rodger Kram. Metabolic cost of generating muscular force in human walking: insights from load-carrying and speed experiments. *Journal of Applied Physiology*, 95(1):172–183, July 2003.
- [69] F. De Groote, G. Pipeleers, I. Jonkers, B. Demeulenaere, C. Patten, J. Swevers, and J. De Schutter. A physiology based inverse dynamic analysis of human gait: potential and perspectives. *Computer Methods in Biomechanics and Biomedical Engineering*, 12(5):563–574, October 2009.
- [70] Marc Guitart-Masip, Ulrik Beierholm, Raymond Dolan, Emrah Duzel, and Peter Dayan. Vigor in the Face of Fluctuating Rates of Reward: An Experimental Examination. *Journal of cognitive neuroscience*, 23:3933–8, July 2011.
- [71] Adrian M. Haith, Thomas R. Reppert, and Reza Shadmehr. Evidence for Hyperbolic Temporal Discounting of Reward in Control of Movements. *Journal of Neuroscience*, 32(34):11727–11736, August 2012.

- [72] Matthew L. Handford and Manoj Srinivasan. Sideways walking: preferred is slow, slow is optimal, and optimal is expensive. *Biology Letters*, 10(1), January 2014.
- [73] Matthias N. Hartmann, Oliver M. Hager, Philippe N. Tobler, and Stefan Kaiser. Parabolic discounting of monetary rewards by physical effort. *Behavioural Processes*, 100:192–196, November 2013.
- [74] H. Hatze. A myocybernetic control model of skeletal muscle. *Biological Cybernetics*, 25(2):103–119, June 1977.
- [75] H. Hatze. A general myocybernetic control model of skeletal muscle. *Biological Cybernetics*, 28(3):143–157, 1978.
- [76] H. Hatze. Myocybernetic control models of skeletal muscle : characteristics and applications. 1981.
- [77] Herbert Hatze. The fundamental problem of myoskeletal inverse dynamics and its implications. *Journal of Biomechanics*, 35(1):109–115, January 2002.
- [78] C. J. Heckman and Roger M. Enoka. Motor Unit. *Comprehensive Physiology*, pages 2629–2682, 2012.
- [79] Richard P. Heitz. The speed-accuracy tradeoff: history, physiology, methodology, and behavior. *Frontiers in Neuroscience*, 8, 2014.
- [80] Elwood Henneman, George Somjen, and David O. Carpenter. Excitability and inhibitibility of motoneurons of different sizes. *Journal of Neurophysiology*, 28(3):599–620, May 1965.
- [81] Anthony L. Hessel, Stan L. Lindstedt, and Kiisa C. Nishikawa. Physiological Mechanisms of Eccentric Contraction and Its Applications: A Role for the Giant Titin Protein. *Frontiers in Physiology*, 8, February 2017.
- [82] Rainer Hessmer. *Kinematics for Lynxmotion Robot Arm*. October 2009.
- [83] Jennifer L. Hicks, Thomas K. Uchida, Ajay Seth, Apoorva Rajagopal, and Scott L. Delp. Is My Model Good Enough? Best Practices for Verification and Validation of Musculoskeletal Models and Simulations of Movement. *Journal of Biomechanical Engineering*, 137(2):020905, February 2015.
- [84] A. V. Hill. The heat of shortening and the dynamic constants of muscle. *Proceedings of the Royal Society of London. Series B - Biological Sciences*, 126(843):136–195, October 1938.
- [85] Hoa X. Hoang, Claudio Pizzolato, Laura E. Diamond, and David G. Lloyd. Subject-specific calibration of neuromuscular parameters enables neuromusculoskeletal models to estimate physiologically plausible hip joint contact forces in healthy adults. *Journal of Biomechanics*, 80:111–120, 2018.
- [86] Paul Hogberg. How do stride length and stride frequency influence the energy-output during running? *Arbeitsphysiologie*, 14(6):437–441, 1952.
- [87] Katherine R. S. Holzbaur, Scott L. Delp, Garry E. Gold, and Wendy M. Murray. Moment-generating capacity of upper limb muscles in healthy adults. *Journal of Biomechanics*, 40(11):2442–2449, January 2007.

- [88] Katherine R. S. Holzbaur, Wendy M. Murray, and Scott L. Delp. A Model of the Upper Extremity for Simulating Musculoskeletal Surgery and Analyzing Neuromuscular Control. *Annals of Biomedical Engineering*, 33(6):829–840, June 2005.
- [89] R. Horowitz. Passive force generation and titin isoforms in mammalian skeletal muscle. *Biophysical Journal*, 61(2):392–398, February 1992.
- [90] H. Houdijk, M. F. Bobbert, and A. de Haan. Evaluation of a Hill based muscle model for the energy cost and efficiency of muscular contraction. *Journal of Biomechanics*, 39(3):536–543, January 2006.
- [91] Donald F. Hoyt and C. Richard Taylor. Gait and the energetics of locomotion in horses. *Nature*, 292(5820):239, July 1981.
- [92] Helen J. Huang, Rodger Kram, and Alaa A. Ahmed. Reduction of Metabolic Cost during Motor Learning of Arm Reaching Dynamics. *Journal of Neuroscience*, 32(6):2182–2190, February 2012.
- [93] A. L. Hughes and R. F. Goldman. Energy cost of "hard work". *Journal of Applied Physiology*, 29(5):570–572, November 1970.
- [94] Ronald Huston. *Principles of Biomechanics*. December 2008.
- [95] A. F. Huxley and R. Niedergerke. Structural Changes in Muscle During Contraction: Interference Microscopy of Living Muscle Fibres. *Nature*, 173(4412):971–973, May 1954.
- [96] Kun Hwang, Jin Yi Han, and In Hyuk Chung. Topographical Anatomy of the Anconeus Muscle for Use as a Free Flap. *Journal of Reconstructive Microsurgery*, 20(08):631–636, November 2004.
- [97] Yifeng Jiang, Tom Van Wouwe, Friedl De Groote, and C. Karen Liu. Synthesis of Biologically Realistic Human Motion Using Joint Torque Actuation. [arXiv:1904.13041 \[cs\]](https://arxiv.org/abs/1904.13041), April 2019.
- [98] M. A. Johnson, J. Polgar, D. Weightman, and D. Appleton. Data on the distribution of fibre types in thirty-six human muscles: An autopsy study. *Journal of the Neurological Sciences*, 18(1):111–129, January 1973.
- [99] Alejandro Kacelnik. Central Place Foraging in Starlings (*Sturnus vulgaris*). I. Patch Residence Time. *Journal of Animal Ecology*, 53(1):283–299, 1984. Publisher: [Wiley, British Ecological Society].
- [100] Daniel Kahneman and Amos Tversky. Prospect Theory: An Analysis of Decision under Risk. *Econometrica*, 47(2):263, March 1979.
- [101] Reiko Kawagoe, Yoriko Takikawa, and Okihide Hikosaka. Reward-Predicting Activity of Dopamine and Caudate Neurons—A Possible Mechanism of Motivational Control of Saccadic Eye Movement. *Journal of Neurophysiology*, 91(2):1013–1024, February 2004. Publisher: American Physiological Society.
- [102] Joo H. Kim and Dustyn Roberts. A joint-space numerical model of metabolic energy expenditure for human multibody dynamic system. *International Journal for Numerical Methods in Biomedical Engineering*, 31(9):e02721, 2015.

- [103] Shalaya Kipp, William C. Byrnes, and Rodger Kram. Calculating metabolic energy expenditure across a wide range of exercise intensities: the equation matters. *Applied Physiology, Nutrition, and Metabolism*, 43(6):639–642, February 2018.
- [104] Dinant A. Kistemaker, Arthur J. (Knoek) Van Soest, and Maarten F. Bobbert. A model of open-loop control of equilibrium position and stiffness of the human elbow joint. *Biological Cybernetics*, 96(3):341–350, March 2007.
- [105] Dinant A. Kistemaker, Arthur (Knoek) J. Van Soest, and Maarten F. Bobbert. Length-dependent [Ca²⁺] sensitivity adds stiffness to muscle. *Journal of Biomechanics*, 38(9):1816–1821, September 2005.
- [106] Dinant A. Kistemaker, Jeremy D. Wong, and Paul L. Gribble. The Central Nervous System Does Not Minimize Energy Cost in Arm Movements. *Journal of Neurophysiology*, 104(6):2985–2994, September 2010.
- [107] Anne D. Koelewijn, Dieter Heinrich, and Antonie J. van den Bogert. Metabolic cost calculations of gait using musculoskeletal energy models, a comparison study. *bioRxiv*, page 588590, July 2019.
- [108] Ryan Koeppen, Meghan E. Huber, Dagmar Sternad, and Neville Hogan. Controlling Physical Interactions: Humans Do Not Minimize Muscle Effort. *Proceedings of the ASME Dynamic Systems and Control Conference*. ASME Dynamic Systems and Control Conference., page V001T36A003, October 2017.
- [109] David Laibson. Golden Eggs and Hyperbolic Discounting. *The Quarterly Journal of Economics*, 112(2):443–478, May 1997.
- [110] Joseph Langenderfer, Seth A Jerabek, Vijay B Thangamani, John E Kuhn, and Richard E Hughes. Musculoskeletal parameters of muscles crossing the shoulder and elbow and the effect of sarcomere length sample size on estimation of optimal muscle length. *Clinical Biomechanics*, 19(7):664–670, August 2004.
- [111] Sung-Hee Lee, Eftychios Sifakis, and Demetri Terzopoulos. Comprehensive Biomechanical Modeling and Simulation of the Upper Body. *ACM Trans. Graph.*, 28(4):99:1–99:17, September 2009.
- [112] Dino J. Levy and Paul W. Glimcher. Comparing Apples and Oranges: Using Reward-Specific and Reward-General Subjective Value Representation in the Brain. *Journal of Neuroscience*, 31(41):14693–14707, October 2011.
- [113] W. Li and E. Todorov. Iterative linearization methods for approximately optimal control and estimation of non-linear stochastic system. *International Journal of Control*, 80(9):1439–1453, September 2007.
- [114] G. A. Lichtwark and A. M. Wilson. A modified Hill muscle model that predicts muscle power output and efficiency during sinusoidal length changes. *Journal of Experimental Biology*, 208(15):2831–2843, August 2005.
- [115] R. L. Lieber and S. C. Bodine-Fowler. Skeletal muscle mechanics: implications for rehabilitation. *Physical Therapy*, 73(12):844–856, December 1993.

- [116] Richard L. Lieber and Jan Fridén. Clinical significance of skeletal muscle architecture. *Clinical orthopaedics and related research*, 383:140–151, 2001.
- [117] John R. B. Lighton. *Measuring Metabolic Rates: A Manual for Scientists*. Oxford University Press, June 2008.
- [118] Yi-Chung Lin, Tim W Dorn, Anthony G Schache, and Marcus G Pandy. Comparison of different methods for estimating muscle forces in human movement. *Proceedings of the Institution of Mechanical Engineers, Part H: Journal of Engineering in Medicine*, 226(2):103–112, February 2012.
- [119] Marco Linari, Elisabetta Brunello, Massimo Reconditi, Luca Fusi, Marco Caremani, Theyencheri Narayanan, Gabriella Piazzesi, Vincenzo Lombardi, and Malcolm Irving. Force generation by skeletal muscle is controlled by mechanosensing in myosin filaments. *Nature*, 528:276, November 2015.
- [120] Marco Linari, R C Woledge, and N A Curtin. Energy storage during stretch of active single fibres from frog skeletal muscle. *The Journal of Physiology*, 548(Pt 2):461–474, April 2003.
- [121] V Lombardi and G Piazzesi. *The contractile response during steady lengthening of stimulated frog muscle fibres*. 1990.
- [122] Leroy L. Long and Manoj Srinivasan. Walking, running, and resting under time, distance, and average speed constraints: optimality of walk-run-rest mixtures. *Journal of the Royal Society, Interface*, 10(81):20120980, April 2013.
- [123] Fang Lou, N. A. Curtin, and R. C. Woledge. Contraction with shortening during stimulation or during relaxation: how do the energetic costs compare? *Journal of Muscle Research & Cell Motility*, 19(7):797–802, October 1998.
- [124] Shiping Ma and George I. Zahalak. A distribution-moment model of energetics in skeletal muscle. *Journal of Biomechanics*, 24(1):21–35, January 1991.
- [125] Sanjay G. Manohar, Trevor T.-J. Chong, Matthew A.J. Apps, Amit Batla, Maria Stamelou, Paul R. Jarman, Kailash P. Bhatia, and Masud Husain. Reward Pays the Cost of Noise Reduction in Motor and Cognitive Control. *Current Biology*, 25(13):1707–1716, June 2015.
- [126] R. Margaria. *On the physiology and especially on the energy consumption of the march and the race at various speeds and inclinations of the ground*. Mem. d. R. accad. naz. dei Lincei, classe di sci. fis., mat. e nat. Bardi, 1938.
- [127] Rodolfo Margaria. Positive and negative work performances and their efficiencies in human locomotion. *Internationale Zeitschrift für angewandte Physiologie einschließlich Arbeitsphysiologie*, 25(4):339–351, December 1968.
- [128] J E Mazur. Estimation of indifference points with an adjusting-delay procedure. *Journal of the Experimental Analysis of Behavior*, 49(1):37–47, January 1988.
- [129] Carl Menger, Peter G Klein, Friedrich A. von Hayek, James Dingwall, and Bert F Hoselitz. *Principles of economics*. Ludwig von Mises Institute, Auburn, Ala., 1871.

- [130] Matthew Millard, Thomas Uchida, Ajay Seth, and Scott L. Delp. Flexing Computational Muscle: Modeling and Simulation of Musculotendon Dynamics. *Journal of Biomechanical Engineering*, 135(2):021005–021005–11, February 2013.
- [131] Ross H. Miller. A comparison of muscle energy models for simulating human walking in three dimensions. *Journal of Biomechanics*, 47(6):1373–1381, April 2014.
- [132] Ross H. Miller, Brian R. Umberger, Joseph Hamill, and Graham E. Caldwell. Evaluation of the minimum energy hypothesis and other potential optimality criteria for human running. *Proceedings of the Royal Society of London B: Biological Sciences*, page rspb20112015, November 2011.
- [133] H. S. Milner-Brown, R. B. Stein, and R. Yemm. The contractile properties of human motor units during voluntary isometric contractions. *The Journal of Physiology*, 228(2):285–306, January 1973.
- [134] H. S. Milner-Brown, R. B. Stein, and R. Yemm. The orderly recruitment of human motor units during voluntary isometric contractions. *The Journal of Physiology*, 230(2):359–370, 1973.
- [135] David M. Milstein and Michael C. Dorris. The Influence of Expected Value on Saccadic Preparation. *Journal of Neuroscience*, 27(18):4810–4818, May 2007.
- [136] A. E. Minetti and R. McN. Alexander. A Theory of Metabolic Costs for Bipedal Gaits. *Journal of Theoretical Biology*, 186(4):467–476, June 1997.
- [137] Alberto E. Minetti, Lorenzo Boldrini, Laura Brusamolin, Paola Zamparo, and Tom McKee. A feedback-controlled treadmill (treadmill-on-demand) and the spontaneous speed of walking and running in humans. *Journal of Applied Physiology*, 95(2):838–843, August 2003.
- [138] Alberto E. Minetti, Christian Moia, Giulio S. Roi, Davide Susta, and Guido Ferretti. Energy cost of walking and running at extreme uphill and downhill slopes. *Journal of Applied Physiology*, 93(3):1039–1046, September 2002.
- [139] Pierre Morel, Philipp Ulbrich, and Alexander Gail. What makes a reach movement effortful? Physical effort discounting supports common minimization principles in decision making and motor control. *PLOS Biology*, 15(6):e2001323, June 2017.
- [140] Milica Milosavljevic Mormann, Jonathan Malmaud, Alexander Huth, Christof Koch, and Antonio Rangel. The Drift Diffusion Model Can Account for the Accuracy and Reaction Time of Value-Based Choices Under High and Low Time Pressure. October 2010.
- [141] Wendy M. Murray, Thomas S. Buchanan, and Scott L. Delp. The isometric functional capacity of muscles that cross the elbow. *Journal of Biomechanics*, 33(8):943–952, August 2000.
- [142] Joel Myerson and Leonard Green. Discounting of delayed rewards: Models of individual choice. *Journal of the Experimental Analysis of Behavior*, 64(3):263–276, November 1995.
- [143] Eri Nakano, Hiroshi Imamizu, Rieko Osu, Yoji Uno, Hiroaki Gomi, Toshinori Yoshioka, and Mitsuo Kawato. Quantitative Examinations of Internal Representations for Arm Trajectory Planning: Minimum Commanded Torque Change Model. *Journal of Neurophysiology*, 81(5):2140–2155, May 1999.

- [144] Ali A. Nikooyan and Alaa A. Ahmed. Reward feedback accelerates motor learning. *Journal of Neurophysiology*, 113(2):633–646, October 2014.
- [145] Yael Niv, Nathaniel D. Daw, Daphna Joel, and Peter Dayan. Tonic dopamine: opportunity costs and the control of response vigor. *Psychopharmacology*, 191(3):507–520, April 2007.
- [146] Megan K. O’Brien and Alaa A. Ahmed. Does risk-sensitivity transfer across movements? *Journal of Neurophysiology*, 109(7):1866–1875, January 2013.
- [147] Benjamin Pasquereau and Robert S. Turner. Limited Encoding of Effort by Dopamine Neurons in a Cost–Benefit Trade-off Task. *Journal of Neuroscience*, 33(19):8288–8300, May 2013.
- [148] Sarah E. Pekny, Jun Izawa, and Reza Shadmehr. Reward-Dependent Modulation of Movement Variability. *The Journal of Neuroscience*, 35(9):4015–4024, March 2015.
- [149] Pascale Pigeon, L’Hocine Yahia, and Anatol G. Feldman. Moment arms and lengths of human upper limb muscles as functions of joint angles. *Journal of Biomechanics*, 29(10):1365–1370, October 1996.
- [150] Gervasio Piñeiro, Susana Perelman, Juan Guerschman, and José Paruelo. How to Evaluate Models: Observed vs. Predicted or Predicted vs. Observed? *Ecological Modelling*, 216:316–322, September 2008.
- [151] Boris I. Prilutsky and Vladimir M. Zatsiorsky. Optimization-Based Models of Muscle Coordination. *Exercise and sport sciences reviews*, 30(1):32, January 2002.
- [152] H. J. Ralston. Energy-speed relation and optimal speed during level walking. *Internationale Zeitschrift für angewandte Physiologie einschließlich Arbeitsphysiologie*, 17(4):277–283, October 1958.
- [153] Roger Ratcliff and Hans P. A. Van Dongen. Diffusion model for one-choice reaction-time tasks and the cognitive effects of sleep deprivation. *Proceedings of the National Academy of Sciences of the United States of America*, 108(27):11285–11290, July 2011.
- [154] Joseph K. Rathkey and Cara M. Wall-Scheffler. People choose to run at their optimal speed. *American Journal of Physical Anthropology*, 163(1):85–93, 2017.
- [155] Thomas R. Reppert, Karolina M. Lempert, Paul W. Glimcher, and Reza Shadmehr. Modulation of Saccade Vigor during Value-Based Decision Making. *The Journal of Neuroscience*, 35(46):15369–15378, November 2015.
- [156] Thomas R. Reppert, Ioannis Rigas, David J. Herzfeld, Ehsan Sedaghat-Nejad, Oleg Komogortsev, and Reza Shadmehr. Movement vigor as a traitlike attribute of individuality. *Journal of Neurophysiology*, 120(2):741–757, August 2018.
- [157] Lionel Rigoux and Emmanuel Guigon. A Model of Reward- and Effort-Based Optimal Decision Making and Motor Control. *PLOS Computational Biology*, 8(10):e1002716, October 2012.
- [158] Gordon Robertson, Graham Caldwell, Joseph Hamill, Gary Kamen, and Saunders Whittlesey. *Research Methods in Biomechanics*, 2E. Human Kinetics, September 2013.

- [159] Paul A. Samuelson. A Note on Measurement of Utility. *The Review of Economic Studies*, 4(2):155–161, 1937.
- [160] Natalia Sanchez, Surabhi Simha, J. Maxwell Donelan, and James Micah Finley. Taking advantage of external mechanical work to reduce metabolic cost: the mechanics and energetics of split-belt treadmill walking. *bioRxiv*, page 500835, December 2018.
- [161] Wolfram Schultz. Dopamine reward prediction error coding. *Dialogues in Clinical Neuroscience*, 18(1):23–32, March 2016.
- [162] Ehsan Sedaghat-Nejad, David J. Herzfeld, and Reza Shadmehr. Reward Prediction Error Modulates Saccade Vigor. *Journal of Neuroscience*, 39(25):5010–5017, June 2019.
- [163] Nidhi Seethapathi and Manoj Srinivasan. The metabolic cost of changing walking speeds is significant, implies lower optimal speeds for shorter distances, and increases daily energy estimates. *Biology Letters*, 11(9), September 2015.
- [164] Jessica C. Selinger, Shawn M. O'Connor, Jeremy D. Wong, and J. Maxwell Donelan. Humans Can Continuously Optimize Energetic Cost during Walking. *Current Biology*, 25(18):2452–2456, September 2015.
- [165] Reza Shadmehr. *Computational Neurobiology of Reaching and Pointing A Foundation for Motor Learning*. MIT Press, 2005.
- [166] Reza Shadmehr, Helen J. Huang, and Alaa A. Ahmed. A Representation of Effort in Decision-Making and Motor Control. *Current Biology*, 26(14):1929–1934, July 2016.
- [167] Reza Shadmehr, Thomas R. Reppert, Erik M. Summerside, Tehrim Yoon, and Alaa A. Ahmed. Movement Vigor as a Reflection of Subjective Economic Utility. *Trends in Neurosciences*, 0(0), March 2019.
- [168] Reza Shadmehr, Jean Jacques Orban de Xivry, Minnan Xu-Wilson, and Ting-Yu Shih. Temporal Discounting of Reward and the Cost of Time in Motor Control. *Journal of Neuroscience*, 30(31):10507–10516, August 2010.
- [169] Weiguang Si, Sung-Hee Lee, Eftychios Sifakis, and Demetri Terzopoulos. Realistic Biomechanical Simulation and Control of Human Swimming. *ACM Trans. Graph.*, 34(1):10:1–10:15, December 2014.
- [170] Moncrieff Smith and Glenn C. Kinney. Sugar as a reward for hungry and nonhungry rats. *Journal of Experimental Psychology*, 51(5):348–352, 1956.
- [171] Manoj Srinivasan. Optimal speeds for walking and running, and walking on a moving walkway. *Chaos: An Interdisciplinary Journal of Nonlinear Science*, 19(2):026112, June 2009.
- [172] Erik M. Summerside, Kram Rodger, and Ahmed Alaa A. Contributions of metabolic and temporal costs to human gait selection. *Journal of The Royal Society Interface*, 15(143):20180197, June 2018.
- [173] Erik M. Summerside, Reza Shadmehr, and Alaa A. Ahmed. Vigor of reaching movements: reward discounts the cost of effort. *Journal of Neurophysiology*, 119(6):2347–2357, March 2018.

- [174] Natalia Sánchez, Sungwoo Park, and James M. Finley. Evidence of Energetic Optimization during Adaptation Differs for Metabolic, Mechanical, and Perceptual Estimates of Energetic Cost. *Scientific Reports*, 7(1):7682, August 2017.
- [175] Yoriko Takikawa, Reiko Kawagoe, Hideaki Itoh, Hiroyuki Nakahara, and Okihide Hikosaka. Modulation of saccadic eye movements by predicted reward outcome. *Experimental Brain Research*, 142(2):284–291, January 2002.
- [176] Yoshiaki Taniai and Jun Nishii. Optimality of Upper-Arm Reaching Trajectories Based on the Expected Value of the Metabolic Energy Cost. *Neural Computation*, 27(8):1721–1737, June 2015.
- [177] Darryl G. Thelen. Adjustment of Muscle Mechanics Model Parameters to Simulate Dynamic Contractions in Older Adults. *Journal of Biomechanical Engineering*, 125(1):70, 2003.
- [178] Emanuel Todorov and Michael I. Jordan. Optimal feedback control as a theory of motor coordination. *Nature Neuroscience*, 5(11):1226–1235, November 2002.
- [179] Thomas K. Uchida, Jennifer L. Hicks, Christopher L. Dembia, and Scott L. Delp. Stretching Your Energetic Budget: How Tendon Compliance Affects the Metabolic Cost of Running. *PLOS ONE*, 11(3):e0150378, March 2016.
- [180] Brian R. Umberger. Stance and swing phase costs in human walking. *Journal of The Royal Society Interface*, 7(50):1329–1340, September 2010.
- [181] Brian R. Umberger, Karin G. M. Gerristen, and Philpe E. Martin. A Model of Human Muscle Energy Expenditure. *Computer Methods in Biomechanics and Biomedical Engineering*, 6(2):99–111, May 2003.
- [182] Brian R. Umberger and Jonas Rubenson. Understanding Muscle Energetics in Locomotion: New Modeling and Experimental Approaches. *Exercise and Sport Sciences Reviews*, 39(2):59, April 2011.
- [183] Y. Uno, M. Kawato, and R. Suzuki. Formation and control of optimal trajectory in human multijoint arm movement. Minimum torque-change model. *Biological Cybernetics*, 61(2):89–101, 1989.
- [184] E. J. van Zuylen, A. van Velzen, and J. J. Denier van der Gon. A biomechanical model for flexion torques of human arm muscles as a function of elbow angle. *Journal of Biomechanics*, 21(3):183–190, January 1988.
- [185] Mark E. Walton, David M. Bannerman, and Matthew F. S. Rushworth. The Role of Rat Medial Frontal Cortex in Effort-Based Decision Making. *Journal of Neuroscience*, 22(24):10996–11003, December 2002.
- [186] Wanyue Wang and Natalia Dounskoia. Load emphasizes muscle effort minimization during selection of arm movement direction. *Journal of NeuroEngineering and Rehabilitation*, 9(1):70, 2012.
- [187] Tyler W. Watts, Greg J. Duncan, and Haonan Quan. Revisiting the Marshmallow Test: A Conceptual Replication Investigating Links Between Early Delay of Gratification and Later Outcomes. *Psychological Science*, 29(7):1159–1177, July 2018.

- [188] Geoffrey B. West, James H. Brown, and Brian J. Enquist. A General Model for the Origin of Allometric Scaling Laws in Biology. *Science*, 276(5309):122–126, April 1997.
- [189] Andrew Westbrook and Todd S. Braver. Cognitive effort: A neuroeconomic approach. *Cognitive, affective & behavioral neuroscience*, 15(2):395–415, June 2015.
- [190] T. L. Wickiewicz, R. R. Roy, P. L. Powell, and V. R. Edgerton. Muscle architecture of the human lower limb. *Clinical Orthopaedics and Related Research*, 179:275–283, October 1983.
- [191] S. J. Wickler, D. F. Hoyt, E. A. Cogger, and K. M. Hall. Effect of load on preferred speed and cost of transport. *Journal of Applied Physiology*, 90(4):1548–1551, April 2001.
- [192] S. J. Wickler, D. F. Hoyt, E. A. Cogger, and M. H. Hirschbein. Preferred speed and cost of transport: the effect of incline. *Journal of Experimental Biology*, 203(14):2195–2200, July 2000.
- [193] David Winter. *Biomechanics and Motor Control of Human Movement*, 4th Edition. John Wiley & Sons, Ltd, October 2009.
- [194] J. M. Winters and L. Stark. Muscle models: What is gained and what is lost by varying model complexity. *Biological Cybernetics*, 55(6):403–420, March 1987.
- [195] Jack M. Winters. An improved muscle-reflex actuator for use in large-scale neuromusculoskeletal models. *Annals of biomedical engineering*, 23(4):359–374, 1995.
- [196] Jack M. Winters and Lawrence Stark. Estimated mechanical properties of synergistic muscles involved in movements of a variety of human joints. *Journal of Biomechanics*, 21(12):1027–1041, January 1988.
- [197] Rory Wolfe and James Hanley. If we’re so different, why do we keep overlapping? When 1 plus 1 doesn’t make 2. *CMAJ: Canadian Medical Association Journal*, 166(1):65–66, January 2002.
- [198] Minnan Xu-Wilson, David Zee, and Reza Shadmehr. The intrinsic value of visual information affects saccade velocities. *Experimental brain research. Experimentelle Hirnforschung. Experimentation cerebrale*, 196(4):475–481, July 2009.
- [199] Tehrim Yoon, Robert B. Geary, Alaa A. Ahmed, and Reza Shadmehr. Control of movement vigor and decision making during foraging. *Proceedings of the National Academy of Sciences*, page 201812979, October 2018.
- [200] George I. Zahalak and Shi-Ping Ma. Muscle Activation and Contraction: Constitutive Relations Based Directly on Cross-Bridge Kinetics. *Journal of Biomechanical Engineering*, 112(1):52, 1990.
- [201] F. E. Zajac. Muscle and tendon: properties, models, scaling, and application to biomechanics and motor control. *Critical Reviews in Biomedical Engineering*, 17(4):359–411, 1989.
- [202] Felix E. Zajac and Jack M. Winters. Modeling Musculoskeletal Movement Systems: Joint and Body Segmental Dynamics, Musculoskeletal Actuation, and Neuromuscular Control. In Jack M. Winters and Savio L-Y. Woo, editors, *Multiple Muscle Systems: Biomechanics and Movement Organization*, pages 121–148. Springer New York, New York, NY, 1990.

- [203] Lelai Zhou, Shaoping Bai, Michael R. Hansen, and John Rasmussen. Modeling of Human Arm Energy Expenditure for Predicting Energy Optimal Trajectories. Modeling, Identification and Control; Kristiansand, 32(3):91, 2011.

Appendix A

Mass Results Supplemental

This chapter is the supplemental results for chapter 4. I show average movement metrics for specific movement vigor traits and also show how alternative models of utility can predict movement vigor.

A.1 Movement Metrics

Effective Mass (kg)	2a	2b	2c
2.5	0.764±0.038	0.823±0.031	0.632±0.036
3.8	0.83±0.041	0.881±0.033	0.703±0.034
4.7	0.856±0.042	0.905±0.034	0.741±0.043
6.1	0.89±0.043	0.959±0.036	0.781±0.048

Table A.1: Movement duration (s) from experiment 2a, 2b, and 2c. Data is shown as mean ± standard deviation.

Effective Mass (kg)	2a	2b	2c
2.5	0.264±0.076	0.23±0.066	0.393±0.093
3.8	0.235±0.068	0.208±0.06	0.347±0.082
4.7	0.225±0.065	0.201±0.058	0.334±0.079
6.1	0.213±0.061	0.185±0.054	0.315±0.074

Table A.2: Peak velocity (m/s) from experiment 2a, 2b, and 2c. Data is shown as mean ± standard deviation.

Effective Mass (kg)	2a	2b	2c
2.5	0.18±0.012	0.204±0.013	0.198±0.012
3.8	0.186±0.013	0.215±0.013	0.207±0.011
4.7	0.189±0.013	0.219±0.013	0.212±0.012
6.1	0.197±0.013	0.228±0.013	0.216±0.011

Table A.3: Reaction time (s) from experiment 2a, 2b, and 2c. Data is shown as mean ± standard deviation.

A.2 Alternative models predicting movement duration

We sought to quantify how alternative representations of effort or utility can predict preferred reaching duration. We tested 4 alternative models for utility and 2 alternative models of effort. The models predicted movement durations and sum of squared errors when compared to experimental movement is shown in table A.4, A.5, A.6. The sum of squared errors for each model can be seen in figure A.1.

First is the same utility formulation as before (Eq. 4.15), but instead of using gross metabolic power as effort we use net metabolic power as effort. We also test using sum of torque squared as effort in the same utility. We test an alternative utility formulation, shown in equation 4.7, that does not include the temporal discounting factor as before. We also investigate if minimizing only the cost of the movement can predict the preferred movement duration. Gross metabolic cost and net metabolic cost find the movement duration that minimizes the cost of the movement. The sum of squared error for each of these models compared to experiment 2 is shown in figure A.1 A, B. We also compare the normalized movement durations sum of squared errors between each utility model in figure A.1 C, D.

Mass	Exp	Ut Gross	Ut Net	Ut Torque	Net RWD	Efficiency	Gross Cost	Net Cost
0	0.7638	0.7580	0.7470	0.6430	0.7480	0.7230	0.6627	0.8561
1.364	0.8300	0.8100	0.7970	0.7230	0.7870	0.7670	0.7074	0.9130
2.273	0.8560	0.8370	0.8230	0.7750	0.8080	0.7900	0.7291	0.9407
3.636	0.8902	0.8710	0.8570	0.8560	0.8350	0.8190	0.7556	0.9743
SSE		0.0012	0.0036	0.0338	0.0074	0.0151	0.0595	0.0296

Table A.4: Movement duration and predictions for experiment 2a. Ut represents Utility, RWD represents reward. These values are found fitting one α value to experiment 2a/2b, then applying it to 2c.

Mass	Exp	Ut Gross	Ut Net	Ut Torque	Net RWD	Efficiency	Gross Cost	Net Cost
0	0.8226	0.8690	0.8850	0.9090	0.8760	0.8440	0.6627	0.8561
1.364	0.8813	0.9120	0.9260	0.9630	0.9060	0.8810	0.7074	0.9130
2.273	0.9051	0.9360	0.9490	0.9980	0.9230	0.9010	0.7291	0.9407
3.636	0.9588	0.9670	0.9800	1.0580	0.9470	0.9290	0.7556	0.9743
SSE		0.0041	0.0083	0.0326	0.0039	0.0014	0.1281	0.0036

Table A.5: Movement duration and predictions for experiment 2b. Ut represents Utility, RWD represents reward. These values are found fitting one α value to experiment 2a/2b, then applying it to 2c.

Mass	Exp	Ut Gross	Ut Net	Ut Torque	Net RWD	Efficiency	Gross Cost	Net Cost
0	0.6316	0.699	0.6730	0.3130	0.6630	0.6630	0.6627	0.8561
1.364	0.7033	0.754	0.7270	0.4530	0.7070	0.7070	0.7074	0.9130
2.273	0.7412	0.782	0.7540	0.5390	0.7290	0.7290	0.7291	0.9407
3.636	0.7811	0.816	0.7880	0.6680	0.7560	0.7560	0.7556	0.9743
SSE		0.010	0.0025	0.2178	0.0018	0.0018	0.0018	0.1715

Table A.6: Movement duration and predictions for experiment 2c. Ut represents Utility, RWD represents reward. These values are found fitting one α value to experiment 2a/2b, then applying it to 2c.

A.2.1 Net Metabolic Utility

The lack of a resting cost in the sum of squared torques effort representation may have contributed to the poor fit to the data. To provide a more direct comparison of effort representations, we considered the net metabolic cost of the action, rather than the gross metabolic cost of the action. Gross metabolic cost is the sum of metabolic expenditure required for an action and includes the cost of the movement as well as the cost of resting. Net metabolic cost is only cost associated with the movement and is calculated as shown in Eq. A.7. Substituting net metabolic cost (Eq. 4.3) for e_m in Eq. 4.5 and setting e_r to 0:

$$J_{net} = \frac{\alpha P(\alpha|t_m, m) - \dot{e}_r t_r - (a - \dot{e}_r)t_m - \frac{bm^i}{t_m^{i-1}}}{t_r + t_m} \quad (\text{A.1})$$

, we find that the model performs similarly to a utility based on gross metabolic cost for both absolute ($\text{SSE} = 3.56\text{e}3, 8.26\text{e}-3, 2.42\text{e}-3$, for Experiments 2a,b, and c, respectively), and normalized movement durations ($\text{SSE} = 8.64\text{e}-4, 3.58\text{e}-4, 1.53\text{e}-2$, for Experiments 2a,b, and c, respectively). It also appreciably outperforms the sum of squared torques model.

A.2.2 Sum of squared torques as effort in utility

In the field of movement neuroscience, computational models of reaching movements often use forms of effort other than metabolic cost to represent movement costs. One such approach is to quantify movement effort cost as the sum of squared joint torques required to generate the movement. In the ensuing analysis, we sought to determine whether a utility in which effort was represented as the sum of squared joint torques, rather than metabolic cost, could also explain the observed changes in preferred movement speed. To obtain an expression for sum of squared torque effort, \dot{e}_{torque} , like that obtained for metabolic cost, we simulated participant-specific reaching movements with the mass and durations prescribed in Experiment 1. The required joint torques were backed out using inverse dynamics based on a planar two-link model of the arm and the effort rate of each movement was calculated as the sum of squared shoulder and elbow torques divided

by the movement duration. Next, we fit an equation of similar form as Eq. 4.1, to parameterize the relationship between effort rate, represented as the sum of squared torques, and movement duration and mass:

$$\dot{e}_{torque} = \frac{b_{torque} m^{i_{torque}}}{t_m^{j_{torque}-1}} \quad (\text{A.2})$$

where ($b_{torque} = 0.040 \pm 0.0076$, $i_{torque} = 2.14 \pm 0.07$, $j_{torque} = 3.50 \pm 0.12$, SSE = 99742.63, AIC = 9610.64). Notably, there are distinct differences between the two effort representations. The sum of squared torques increases quadratically with mass, in stark contrast to the near-linear growth observed in metabolic cost. We also are limited in that there is no accounting for a resting metabolic rate, as we only represent torques associated with the reaching movement, thus e_r is zero. Another consequence of only representing movement torques (as most computational models do) is that there is no cost associated with a zero-velocity movement (or movement of infinite duration), thus the term equivalent to the time-invariant reach cost, a , in Eq. 4.1 is also zero and not included in Eq. 4.5. Replacing e in Eq. 2.6 with e_{torque} , provides the following utility:

$$J_{torque} = \frac{\alpha P(\alpha|t_m, m) - \dot{e}_r t_r - \frac{b_{torque} m^{i_{torque}}}{t_m^{j_{torque}-1}}}{t_r + t_m} \quad (\text{A.3})$$

Employing the same fitting procedure as described above and fitting a single parameter, α , we find that the sum of squared torques does a significantly worse job in predicting the experimental data in all three experiments ($\alpha = 43.96$; 2a SSE = 3.38e-2; 2b SSE = 3.26e-2; 2c SSE = 2.18e-1; total SSE = 2.84e-1) compared to when effort is represented as metabolic cost. This is true for both predictions of the absolute movement durations as well as the changes in movement duration with added mass (SSE = 3.61e-2, 1.51e-4, 1.22, for Experiments 2a,b, and c, respectively; total SSE = 1.255).

A.2.3 Net Reward

The goal of the movement may be to maximize the net gain. We represent this as the sum of the reward minus the total cost of the movement.

$$J = \alpha P(\alpha|t_m, m) - \left(a_o t_r + at_m + \frac{bm^i}{t_m^{j-1}} \right) \quad (\text{A.4})$$

We found that the net gain provides a comparable approximation of self-selected movement speed as utility depending on the experiment. Net gain predicted movement durations with an SSE of 0.0074, 0.0039, and 0.0018 for experiment 2a, 2b, and 2c respectively. The total SSE was 0.0131. The net gain model can well predict experiment 2c, is comparable in 2b, but not as good as utility in experiment 2a.

A.2.4 Efficiency

Another possible explanation of movement vigor is maximizing total movement efficiency. We quantify efficiency as the total reward gained (not discounted by time) divided by the movement cost.

$$J = \frac{P(\alpha|t_m, m)}{a_o t_r + at_m + \frac{bm^i}{t_m^{j-1}}} \quad (\text{A.5})$$

This model well predicts experiment 2a (SSE = 0.0151), very well predicts experiment 2b (SSE = 0.0014), and very well predicts experiment 2c (SSE = 0.0018). This model is not affected by probability of reward and becomes 1/cost in experiment 2c, and only relies on the metabolic minima speed. To maximize this model, we minimize the cost leading to the same prediction as the net reward model and minimizing gross metabolic cost..

A.2.5 Gross Metabolic Cost

A popular hypothesis in locomotion research is that humans and other animals choose the speed that minimizes the gross metabolic cost to move a fixed distance. We can test that hypothesis

using the present data set. In this case, utility is solely comprised of a cost which accordingly needs to be minimized. We can represent this utility as the negative of e_m , the cost to reach 10 cm with a given mass at a given duration:

$$J_{grossOnly} = -at_m - \frac{bm^i}{t_m^{j-1}} \quad (\text{A.6})$$

As shown earlier in Figure 2B, the cost of reaching exhibits a U-shaped curve, initially decreasing with slower movements, but then increasing (Figure 4.2B). The minimum of the curve indicates the optimal speed predicted by a utility that is solely dependent on the gross metabolic cost of reach; in this utility formulation there are no free parameters to fit to the preferred duration data.

We find that minimizing gross metabolic cost alone (i.e., maximizing, $J_{grossOnly}$) underestimates preferred movement durations, predicting significantly slower movements than observed (2a SSE = 6.27e-2, 2b SSE = 1.33e -1, 2c SSE = 1.91e-3), and is also unable to explain differences in movement duration with target size across experiments. However, when looking at the changes in movement duration with added mass normalized to reaching with no added mass, minimizing gross metabolic cost alone does an excellent job (2a SSE = 1.63e-3, 2b SSE = 7.14e-4, 2c SSE = 1.74e-2). Indeed, it performs like a utility-based capture rate where effort is represented as metabolic cost (2a SSE = 9.13e-3, 2b SSE = 6.10e-3, 2c SSE = 1.60e-2). Thus, while minimizing gross metabolic cost alone does not predict absolute movement durations, it can explain changes in preferred movement speed with added mass.

A.2.6 Net Metabolic Cost

One can also consider the cost of reaching alone (no base metabolic rate), referred to as the net metabolic cost, as opposed to the gross metabolic cost reported above. Net metabolic rate is calculated as the gross metabolic rate, \dot{e}_m , minus the resting metabolic rate: $\dot{e}_{net} = \dot{e}_m - \dot{e}_r$. From Eq. 2, we can then derive an expression for the net metabolic cost of a reach of a given mass and

duration:

$$e_{net} = (a - \dot{e}_r)t_m + \frac{bm^i}{t_m^{j-1}} \quad (\text{A.7})$$

The relation between net metabolic cost and movement duration also exhibits a minimum, representing the reach duration that would minimize net metabolic cost, and this duration also increases with added mass. However, the predicted durations are much higher than the durations that minimize gross metabolic cost. The coefficient ($a - \dot{e}_r$ in equation (26) tells us that net metabolic cost has a much lower cost of time, and thus longer duration movements are penalized less. The best fit parameters for net metabolic cost were $a = 24.72 \pm 2.91$, $b = 1.03 \pm 0.47$, $i = 0.80 \pm 0.09$, and $j = 5.66 \pm 0.55$ (SSE = 105365.4, AIC = 1725.16).

As with gross metabolic cost, it does a fairly poor job at predicting absolute movement durations (2a SSE = 2.67e-2, 2b SSE = 2.66e-3, 2c SSE = 1.63e-1, fig S1 A. Total SSE = 1.94e-1, fig S1 B). Net metabolic cost however does a good job at predicting the normalized movement durations (2a SSE = 1.847e-3, 2b SSE = 8.425e-4, 2c SSE = 1.812e-2, fig S1 C. Total SSE = 2.08e-2, fig S1 D).

A.2.7 Accuracy

It is possible that participants are adjusting their movement durations to maintain a fixed accuracy level. To examine this, we solved for the single probability that best predicted preferred movement durations across masses in experiments 2a and 2b. Experiment 2c was omitted from the analysis since it had negligible accuracy requirements and no stopping requirements. The best-fit probability was 0.9804 for Experiment 2a and 0.8283 for Experiment 2b. These numbers are similar to the average success probabilities measured for each experiment (0.9543 and 0.8937, respectively), and captures the reduction in probability of success with the smaller target in Exp. 2b. However, in the experiments, actual success probability was not the same across added mass, but varied, especially in Exp 2b. Thus, compared with a utility based on capture rate, this accuracy-based

model performed worse in predicting participants' preferred durations in both experiments, as evidenced by higher SSEs and AIC scores (SSEs: 3.59e-3 (Exp. 2a), 1.46e-2 (Exp. 2b), AICs: -26.1 (Exp. 2a), -20.5 (Exp. 2b)).

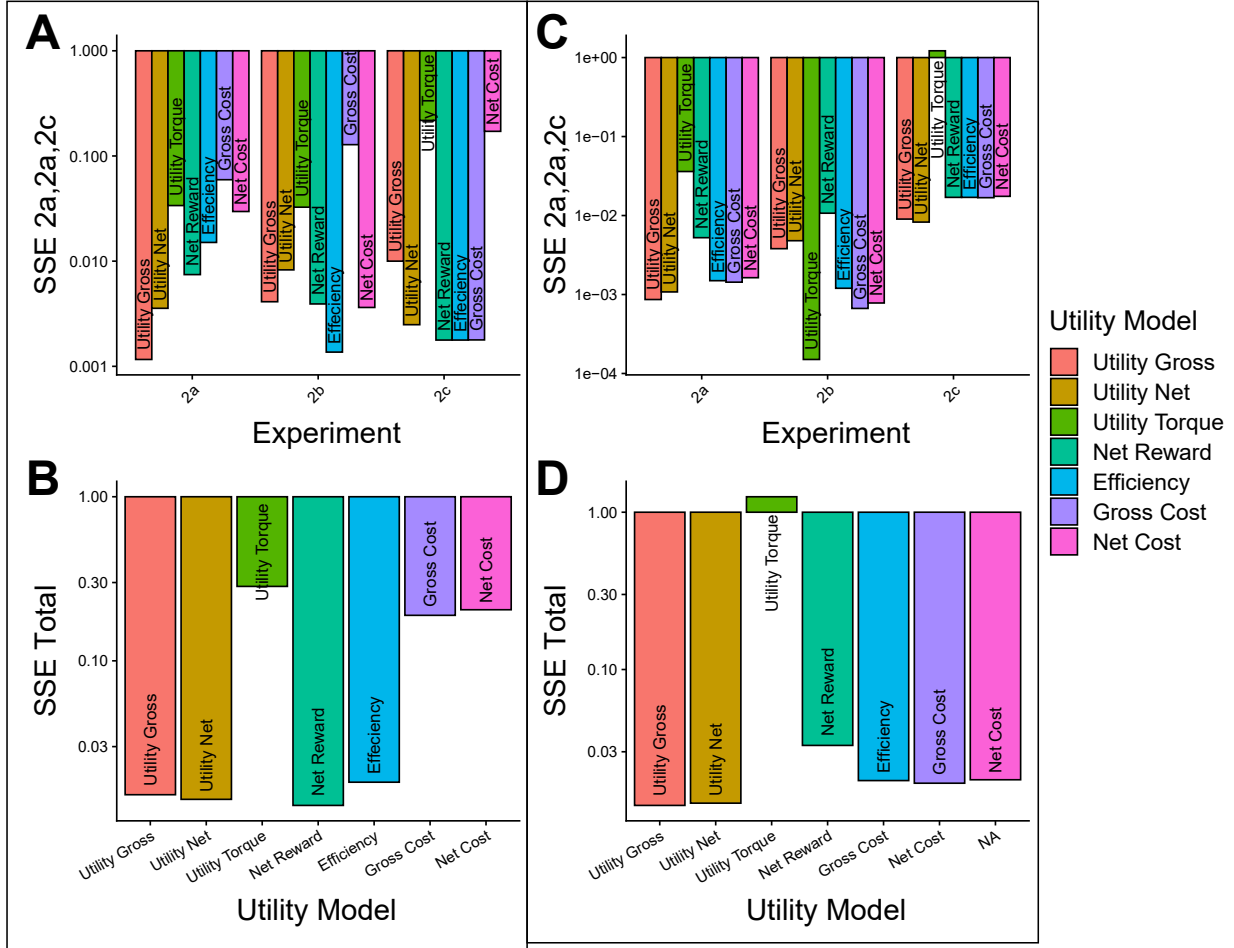


Figure A.1: Alternative model SSE comparisons to preferred reaching speed. Exact SSE's can be found in the text. Each color represents a single model. Here we compare six models to preferred duration. Four are utility maximizing models, and two are effort minimization models. We test the utility from earlier shown in equation 4.5. Utility net is the same formulation as the previous utility, except the effort term is net metabolic cost instead of gross and is shown in equation A.1. We also fit a model with sum of squared torque as the effort term in the utility model (Eq. A.3). The speed accuracy with cost model is similar to our utility model, just lacking the temporal discounting of reward and effort. This formulation is shown in equation 4.7. The efficiency model is the reward gained divided by total effort (Eq. A.5). Reward here is represented by the probability of success function. Each utility model is fit with a single α value to experiment 2a and 2b, then used to predict experiment 2c. Gross cost and net cost are models that minimize the effort associated with a movement, with gross metabolic cost (Eq. A.6) and net metabolic cost (Eq. A.7). These two models have no α value fitted, as these models are derived from the metabolic data.

Figure A.1: (A) Sum of squared errors for each individual experiment and model. We find that our utility model (Eq. 4.5) does a good job across all three experiments, but maybe not the best. Utility net also provides a comparable SSE across all three. Utility with torque² has a poor representation of the movement durations. The speed-accuracy with cost model does a comparable job to the utility model with gross and net cost, however this model may be poor because for experiment 2c this model is only affected by cost and not by the speed-accuracy trade-off. Gross cost and net cost only provide good predictions for one experiment. Gross cost predicts experiment 2c well, and net cost predicts 2b fairly well, but not the others. (B) By summing the error across three experiments, we can see that the utility models (baring torque²) provide the highest explanatory power of preferred duration. Utility with gross metabolic cost and net metabolic cost both provide low SSEs. The model for speed-accuracy with cost provides the lowest SSE, but it is driven by experiment 2a and 2b and may not be a valid model for experiment 2c. Minimizing gross cost and net cost provide poor explanation of all three experiments. (C) The same plot as panel A, except with normalized to 0 kg added durations. We see this is where gross and net metabolic cost have good predictions and have comparable predictions with utility. (D) The sum of squared error for normalized movement durations total for experiment 2a, 2b, and 2c. This exemplifies how gross and net metabolic cost predicts the changes in movement duration well.

Appendix B

Metabolic Rate Modeling Supplemental

B.1 Supplemental Methods

The primary goal of this musculoskeletal model is to determine the muscle forces that drive the kinematics of arm reaching kinematic data. This supplemental describes the method we used to match the joints' kinematic profiles by simulating muscles as the actuators to produce the joint torques for motion (41; 69). The eight steps in the muscle force estimation problem are shown in the flow chart below (fig. B.3) and described in more detail below. Arrows show the output from each step which is used as an input for the next step.

B.1.1 Metabolic Data Collection

Seated subjects made a series of planar horizontal arm reaching movements while breathing into a metabolic cart (Parvo Medics TrueOne 2400) and holding the handle of a robotic arm that supported their arm against gravity (Interactive Motion Technologies, Shoulder-Elbow Robot 2). Five male and three female subjects completed the experiment (all right-handed, mean age 28.9 years (std = 5.7), mean weight 68.4 kg (std = 11.4), and mean height 174.1 cm (std = 10.2). Subjects provided written and informed consent approved by the University of Colorado Institutional Review Board. Subjects completed a set of arm reaching movements across eight targets, seven speeds, and four masses. All subjects gave written informed consent approved by the CU Boulder Institutional Review Board.

Subjects made reaches for a total of approximately 5 minutes while collecting metabolic data.

Four different physical masses were added at the hand while subjects reached (0 kg, 2.27 kg, 4.55 kg, and 9.09 kg). The seven tested durations were: Very, Very Slow (VVS, 1.3 s, 160 trials), Very Slow (VS, 1.1 s, 170 trials), Slow (S, 0.9 s, 200 trials), Medium (M, 0.7 s, 220 trials), Fast (F, 0.5 s, 240 trials), Very Fast (VF, 0.375s, 250 trials), and Very, Very Fast (VVF, 0.25s, 260 trials). Conditions were blocked and randomized for each subject with each taking approximately five minutes. Every subject completed at least six speeds with each mass, where the two heavier masses were completed at the six slower speeds and the two lighter masses were completed at the six faster speeds. Four subjects did not complete the fastest speed with the lightest two mass conditions, 2 of these completed the slowest with the light mass, and two completed the slowest condition with the second lightest mass.

Subjects controlled a cursor on a screen positioned slightly above eye level about two feet away by moving the handle of the robotic arm. Subjects began the experiment by holding the cursor in a home circle for 200 ms. The home circle would then disappear, and a target would randomly appear at 45°, 135°, 225°, and 315° from the right horizontal (fig. B.1A). Subjects were instructed to finish the movement within one of seven, 100 ms time windows. Visual and auditory feedback was given depending on if the movement was too fast, too slow, or within the time window. After completing the first reach (an outward reach), the target would be replaced with a new home circle and a second target would then appear in the central location after holding the cursor in the new home circle for 200 ms. This led to four outward reaching directions, and 4 inward reaching directions, for a total of 8 reaching movements. The location of the target in the outward reach would appear in a pseudorandom order, requiring a reach to four different targets then repeating another pseudorandom set.

Subjects were instructed to be well-rested and fasted before metabolic testing. When subjects entered the lab, they remained seated in the testing chair for 10 minutes. Three baseline recording of metabolic rate were then taken for 5 minutes each before reaching began. Subjects then began making reaching movements in one of the block conditions. Between each block subjects had a five minute rest period to adjust back to baseline. The metabolic power, \dot{e} , was calculated in joules per

second using the method described by Brockway (eq. B.1)

(24).

$$\dot{e} = 16.58\dot{V}_{O_2} + 4.51\dot{V}_{CO_2} \quad (\text{B.1})$$

Gross metabolic rate was calculated for each subject and each condition based on the last three minutes of reaching in each block. Seated metabolic rate, also the average of the three baseline metabolic rates, was subtracted from gross metabolic rate to determine the metabolic rate associated with the reaching movement only. Custom MATLAB scripts to parse the data by trial, mass, and speed. Using these scripts, movement related variables were calculated such as velocity, movement duration, reaction time, and metabolic rate of the movement.

Kinematic Data X-Y positional data was filtered with a lowpass Butterworth filter (sampling frequency 200 Hz, cutoff frequency 10 Hz).

B.2 Biomechanical Model

A biomechanically relevant model of the arm was developed that includes the forearm and upper arm, the shoulder and elbow joint, and 8 physiologically relevant muscles crossing both the shoulder and elbow joint to act as actuators (fig. B.1B). Movement trajectories were computed from the average trajectories for each subjects' target, mass, and speed condition from the metabolic data collection. Joint torques were calculated using inverse dynamics. We tested multiple minimization functions to distribute the individual muscle forces as it is unclear how humans coordinate muscle contractions (106; 108; 113). Next, muscle active state, neural drive, and five models for energy expenditure were calculated.

Four neuromechanical proxies (torque, muscle force, active state, and neural drive), their squared counterparts, and the five metabolic representations were fit in a linear model to the collected metabolic power data to determine the correlation between them. We also compared how the neuromechanical proxies and metabolic representations changed with added mass and changing movement duration to test if they were affected by mass and movement duration in a similar manner

to metabolic power.

The final calculation estimates the metabolic rate of each muscle through five different metabolic representations (18; 114; 127; 179; 180). In all representations but Margaria, these costs are split into a few rate components, the activation and maintenance heat rate (h_{AM}), shortening lengthening heat rate (h_{SL}), and the mechanical work rate (w) (18; 114; 179; 180). The Margaria model estimates the energetic rate as a function of concentric power and eccentric power (127). The specific equations used here are presented in the supplemental materials. Example traces for the muscle force, active state, neural drive, and the Umberger energy expenditure model is shown in figure B.2.

- (1) The first step is determining the trajectory from experimentally collecting kinematic data (55).
- (2) Inverse kinematics is used to determine the joint positions and velocities.
- (3) Inverse dynamics is used to calculate the joint torque's across the joints (165).
- (4) Using the position of the joints, a muscle model computes the length and velocities of the muscles. These lengths and velocities are used to compute active state from muscle properties in step 6.
- (5) After joint positions, torques, and muscle parameters are determined, a muscle model is implemented at every time step to compute the muscle forces required to produce the motion through matching joint torques and minimizing an objective function (step Int-1) (202). The objective function has 3 inputs, including the objective function being used in the optimization and two constraints: matching the torque from the kinematic data and a limit on the change of activation state. The objective function can take many forms including minimizing active state, neural drive, and an energetic model. This is not discussed below as there are many optimization methods that can solve an under-determined system given an objective function.

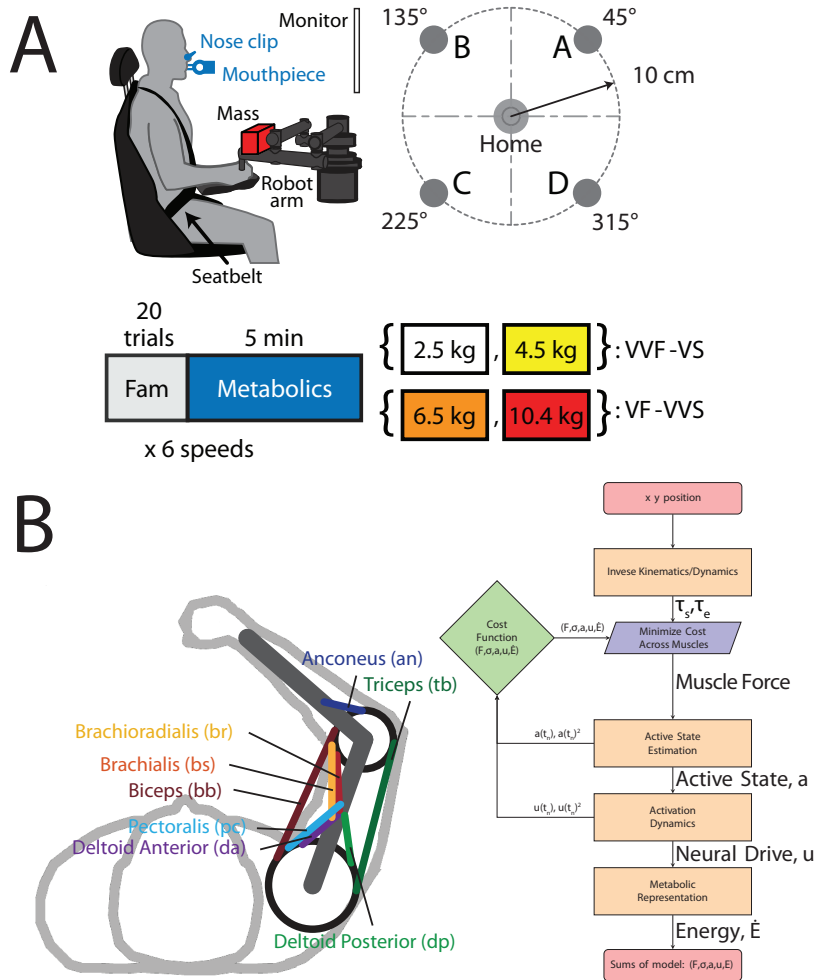


Figure B.1: A. Subjects were in a seated position while collecting metabolic data. Mass was placed on a robotic manipulandum that subjects would hold onto. Subjects would make reaching movements to four different targets at six different speeds with four different masses added to their hands. Metabolics was collected over the whole trial, but we used only the last three minutes in data analysis. B. Diagram of the simulated arm and the eight different muscles. C. A flow chart showing where the neuromechanical proxies are calculated.

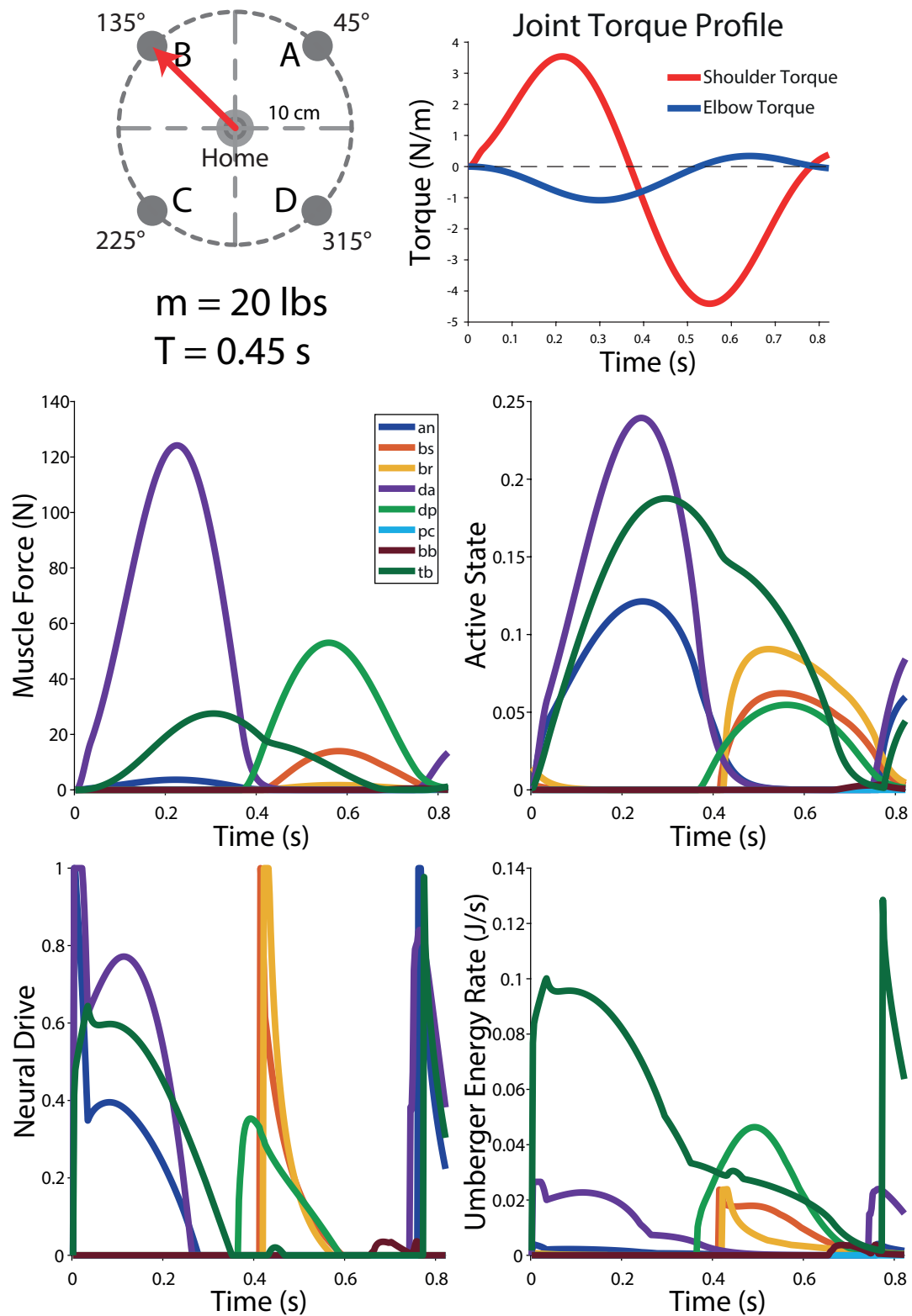


Figure B.2: Example traces for muscle force (A), Active state (B), Neural Drive (C), and the Energy model (D). All example plots are for a reach towards target 2 at the fastest speed when minimizing Active State Squared. Muscles are colored to match the arm diagram in Figure B.1.

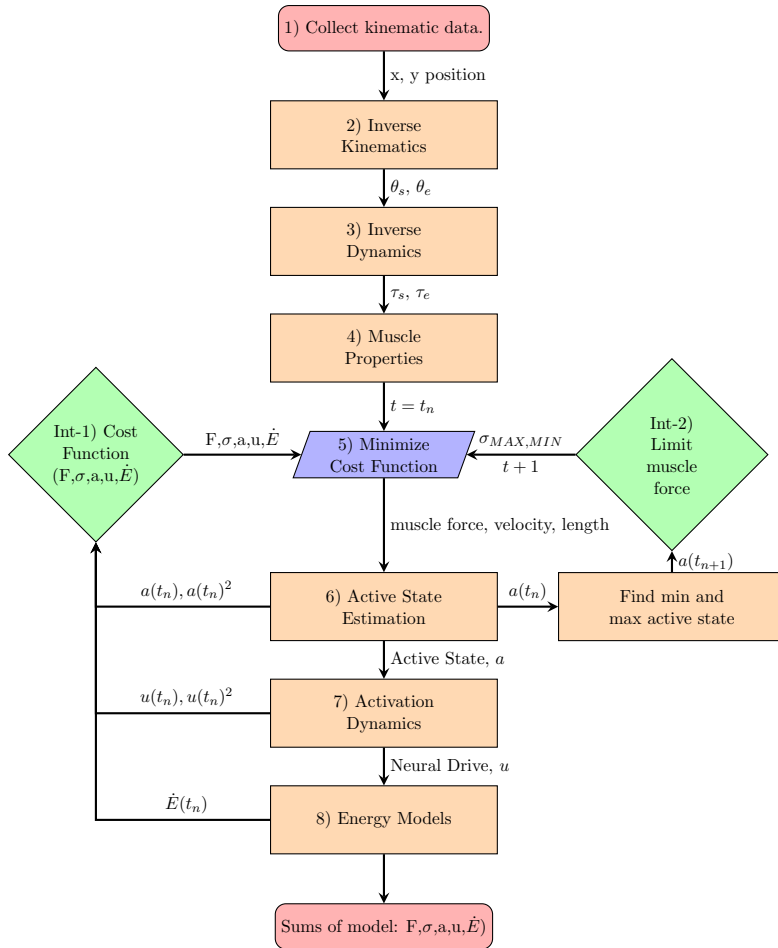


Figure B.3: Modeling flow chart for simulating reaching movements.

- (6) The muscle model takes into account force length and force velocity properties to calculate the active state of the muscle (25; 130).
- (7) The control signal is approximated using activation dynamics which generally take the form of first order non-linear filters (25; 130; 177; 195).
- (8) Last, one of many models of metabolic cost can be implemented to simulate the cost of movement (18; 90; 114; 127; 136; 136; 179–181).

B.2.1 Step 1 - Kinematic Data

The biomechanical model was set to make the same reaching movements as in the metabolics data collection. The model simulated reaching movements to and from four different targets located at 45°, 135°, 225°, and 315° from the right horizontal (Figure B.4). This simulated eight targets, with four masses, seven speeds, and eight subjects for a total of 1874 Figure B.4 shows the setup for the targets. X-Y positional data was filtered with a lowpass Butterworth filter (sampling frequency 200 Hz, cutoff frequency 10 Hz). Many of the movements in the metabolic data collection were cut-off at the end before the movement was completed. To account for this, we use the last x-y position point and extend this for 0.5 seconds after the movement. X-Y position was then spline interpolated for two reasons. First to ensure smoothness to the kinematic data, and second, to increase the sampling rate to 400 Hz to make the non-linear approximations better. The center location, also where the hand starts, was set at $x = -7.58$ cm and $y = 48.78$ cm from the shoulder joint. Movement kinematics were taken from movement averages during the metabolic experiment and then used in the model. Average trajectories from each condition were filtered to create smooth trajectories.

B.2.1.1 Kinematic Validation

We wanted to determine if the model well replicated the desired movements. We took the simulated neural drive signals from the minimization procedure (minimizing active state squared),

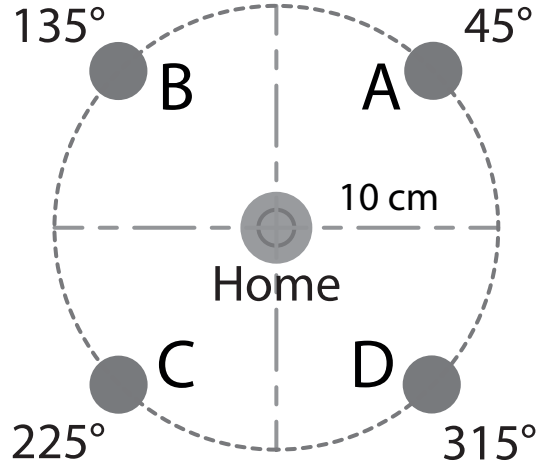


Figure B.4: Target Orientation from start position (home).

and then used a forward model to simulate the movement. We compare this simulated movement with the collected kinematic data. Figure B.5 shows a comparison between the metabolic movement trajectories and simulated movement trajectories. The dashed lines represent the simulated movement, solid lines the average metabolic trajectory, and the shaded regions represent one standard deviation from the mean of the metabolic trajectories. We see that the model does a good job of recreating the movements. The different speeds are color coded with the faster speeds being darker (purple) with the slower speeds lighter (yellow). On average, subjects reached slightly further than 10 cm at the fastest speeds because subjects were not able to slow themselves to a stop for the fastest movements to rest at the target. Subjects tended to reach through the target and turn around at a distance past the target. This led to slightly longer movement durations than expected for the metabolic data for higher velocity reaches.

B.2.2 Step 2 - Inverse Kinematics

The second step converts the data (in x and y position data) to joint positions θ_e and θ_s and torques (τ_e , τ_s). These angles are defined by their Euler Angles and not flexion extension angles. After determining the joint angles, we differentiate to get the angular velocities ($\dot{\theta}_e$ and $\dot{\theta}_s$) and accelerations ($\ddot{\theta}_e$ and $\ddot{\theta}_s$). In these equations l_1 and θ_s refer to the upper arm segment and shoulder

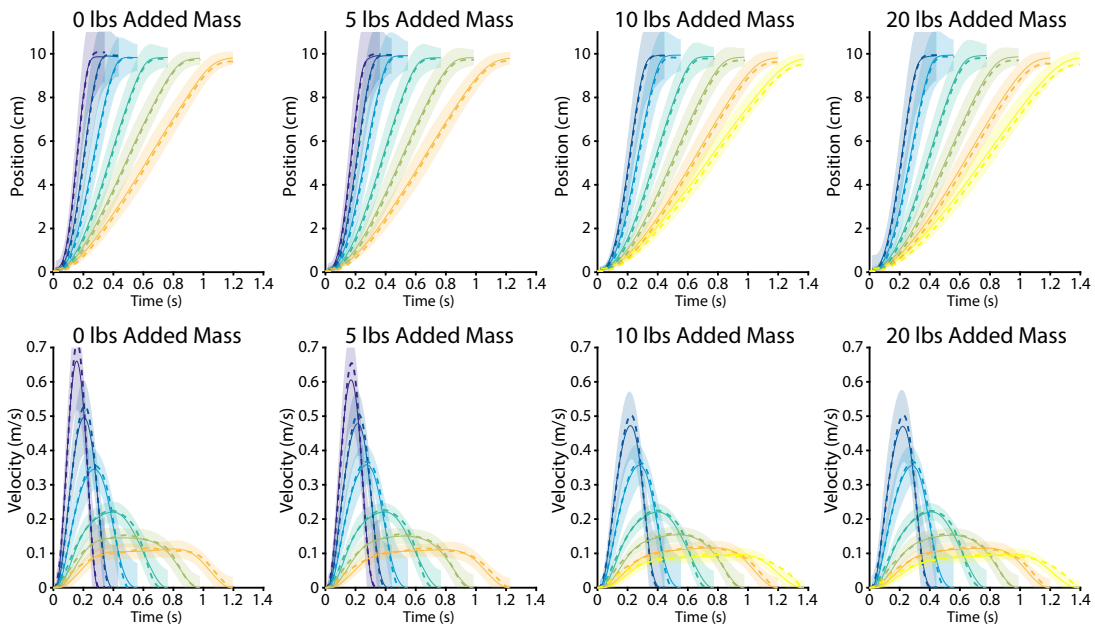


Figure B.5: Movement trajectories compared to model simulation using minimum jerk trajectories. Dashed lines represent the simulated movement, solid lines represent the average of the metabolic data, and shaded bars are one standard deviation from the mean. Each column from left to right is increasing in added mass to the hand (0 kg, 2.27 kg, 4.55 kg, 9.90 kg). The top row shows the distance from initial positions as a function of time. Bottom row is velocity as a function of time. The lines are color coded by the intended movement duration with darker (purple) representing shorter durations and lighter (yellow) lines longer movement durations.

joint. l_2 and θ_e refer to the forearm and elbow joint. A diagram of this system is shown in fig B.6, $\theta_1 = q_1$ and $\theta_2 = q_2$.

We first define how endpoint position relates to joint positions in equation B.2. Details can be found in multiple sources (82; 158).

$$\begin{aligned}\theta_e &= \arccos\left(\frac{x^2 - y^2 - l_1^2 - l_2^2}{2l_1l_2}\right) \\ \theta_s &= \text{atan}2(y, x) - \arcsin\left(\frac{l_2\sin(\theta_e)}{\sqrt{x^2 + y^2}}\right)\end{aligned}\quad (\text{B.2})$$

B.2.3 Step 3 - Inverse Dynamics

B.2.3.1 Arm Properties

We simulated the arm as a two-link arm, the wrist was fixed during the experiment. The properties of the two-links are shown in table B.2. The masses and lengths of the arms were scaled to the size of the subject and estimated using anthropomorphic measurements (34; 193). The arm lengths and masses were relatively similar to other studies (1; 166). The centroid length of the arms is shown with 0 added mass, this distance was recalculated when mass was added. The center of mass length was estimated from Enoka (47).

In the biomechanical modeling equations (supplemental), l_1 and θ_s refer to the upper arm segment and shoulder joint. l_2 and θ_e refer to the forearm and elbow joint. We then converted the data (in x and y position data) to joint positions θ_e and θ_s . These angles are defined by their Euler Angles and not flexion/extension angles. From there, we differentiated angular position to get the angular velocities ($\dot{\theta}_e, \dot{\theta}_s$) and accelerations ($\ddot{\theta}_e, \ddot{\theta}_s$). The beginnings of movements sometimes accelerated too fast for the model to replicate, so a small buffer was added to reduce acceleration for the first few time steps in the model. Last, an estimate for how the arm resists motion, the effective mass, was determined.

Object	Mass (kg)	Length (m)	$Cent_L$ (m)	I_{com}
Forearm	1.2500	0.4258	0.1674	0.0188
upper arm	1.5909	0.3136	0.1367	0.0141

Table B.1: Properties of the forearm and upper arm rigid segments for example subject of 56.81 kg and 1.62 m. The values for Forearm $Cent_L$ and I_{COM} are for 0 added mass at the hand.

B.2.3.2 Forearm Moment of Inertia

To find the new moment of inertia about the center of mass of the forearm plus added mass we need to use the parallel axis theorem.

$$Cent_{L,new} = \frac{Cent_{L,old} \cdot m_2 + l_2 \cdot (\text{mass added})}{m_2 + \text{mass added}} \quad (B.3)$$

$$I_{com,new} = 0.01882 + m_2(Cent_{L,old} - Cent_{L,new})^2 + \text{added mass}(l_2 - Cent_{L,new})^2$$

Object	Mass (kg)	Length (m)	$Cent_L$ (m)	I_{com}
Forearm	1.2500	0.4258	0.1674	0.0188
upper arm	1.5909	0.3136	0.1367	0.0141

Table B.2: Properties of the forearm and upper arm rigid segments for example subject of 56.81 kg and 1.62 m. The values for Forearm $Cent_L$ and I_{COM} are for 0 added mass at the hand.

To convert the joint angles into joint torques we need to apply the Lagrange-Euler equations of motion. We define the trajectory of θ 's that minimize the cost function (eq B.4).

$$H(\theta(t)) = \int_{t_1}^{t_2} (KE - PE)dt = \int_{t_1}^{t_2} L(\theta, \dot{\theta}, t)dt \quad (B.4)$$

By minimizing this function, if no external forces are applied, we can say that the derivative of this function is equal to 0 ($H(\theta(t)) = 0$). However, we know that external conservative forces (joint torques) are being applied so we know the derivative of $H(\theta(t))$ is equal to τ . We get the following relationship (eq. B.5).

$$\frac{\partial}{\partial t} \left(\frac{\partial L}{\partial \dot{\theta}} \right) - \frac{\partial L}{\partial \theta} = \tau \quad (B.5)$$

Because $L(\theta, \dot{\theta}, t) = KE - PE$, we now solve for the kinetic energy and potential energy of the system. Here we detail the equations for a two-link arm in the horizontal plane, but eq. B.5 can be applied to many high dimensional systems such as walking or 3-dimensional reaching. A diagram of variables used in the following equation is shown in figure B.6. ${}^s x_{1c}$ is the distance to the centroid of segment one, q_1 is the shoulder angle from horizontal, l_1 is the length of the first. The same variables apply to the second arm segment. ${}^e y$ and ${}^e x$ represent the coordinate frame around the elbow defined along the shoulder segment.

The following equations compute the torque from kinetic energy of the system (eq. B.8). We define the inertial matrix of the arm as I (eq B.6).

$$\begin{aligned} {}^s I_1 &= {}^c I_1 + m_1 \begin{bmatrix} |{}^s x_{1c}|^2 \sin^2(\theta_1) & -|{}^s x_{1c}|^2 \cos(\theta_1) \sin(\theta_1) & 0 \\ -|{}^s x_{1c}|^2 \cos(\theta_1) \sin(\theta_1) & |{}^s x_{1c}|^2 \cos^2(\theta_1) & 0 \\ 0 & 0 & |{}^s x_{1c}|^2 \end{bmatrix} \\ {}^s I_2 &= {}^c I_2 + m_2 \begin{bmatrix} |{}^s x_{2c}|^2 \sin^2(\theta_2) & -|{}^s x_{2c}|^2 \cos(\theta_2) \sin(\theta_2) & 0 \\ -|{}^s x_{2c}|^2 \cos(\theta_2) \sin(\theta_2) & |{}^s x_{2c}|^2 \cos^2(\theta_2) & 0 \\ 0 & 0 & |{}^s x_{2c}|^2 \end{bmatrix} \end{aligned} \quad (\text{B.6})$$

Then we compute the kinetic and potential energy (eq. B.7) of the segments to use in the

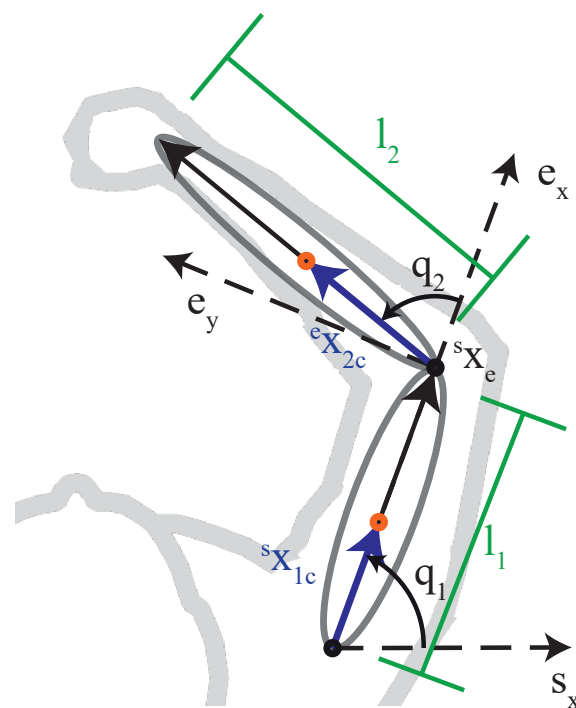


Figure B.6: Diagram for variables in the inverse dynamics of a two-link arm using Euler angles and the Lagrangian Method (165).

Lagrangian formula (eq. B.5).

$$\begin{aligned}
 \theta_1 &= q_1, \theta_2 = q_1 + q_2, \dot{\theta}_1 = \dot{q}_1, \dot{\theta}_2 = \dot{q}_1 + \dot{q}_2 \\
 KE_2 &= \frac{1}{2} \underbrace{m_2 l_1^2}_{a_4} \dot{q}_1^2 + \underbrace{m_2 l_1 |^e x_{2c}|}_{a_3} \dot{q}_1 (\dot{q}_1 + \dot{q}_2) \cos(q_2) + \frac{1}{2} \left(\underbrace{m_2 |^e x_{2c}|^2}_{a_2} + {}^c I_{2zz} \right) (\dot{q}_1 + \dot{q}_2)^2 \\
 &= \frac{1}{2} a_4 \dot{q}_1^2 + a_3 \dot{q}_1 (\dot{q}_1 + \dot{q}_2) \cos(q_2 - 2) + \frac{1}{2} a_2 (\dot{q}_1 + \dot{q}_2)^2 \\
 KE_1 &= \frac{1}{2} \left(\underbrace{m_1 |^s x_{1c}|^2}_{a_1} + {}^c I_{1zz} \right) \dot{q}_1^2 = \frac{1}{2} a_1 \dot{q}_1^2 \\
 KE &= KE_1 + KE_2 \\
 &= \frac{1}{2} \begin{bmatrix} \dot{q}_1 & \dot{q}_2 \end{bmatrix} \begin{bmatrix} a_1 + a_4 + 2a_3 \cos(q_2) + a_2 & a - 2 + a_3 \cos(q_2) \\ a_2 + a_3 \cos(q_2) & a_2 \end{bmatrix} \begin{bmatrix} \dot{q}_1 \\ \dot{q}_2 \end{bmatrix}
 \end{aligned} \tag{B.7}$$

Substitute into the Lagrange equation (eq. B.5) and solve for torque (eq. B.8).

$$\begin{aligned}
 \tau &= \begin{bmatrix} \tau_s \\ \tau_e \end{bmatrix} = \frac{\partial}{\partial t} \left(\frac{\partial L}{\partial \dot{q}} \right) - \frac{\partial L}{\partial q} \\
 \begin{bmatrix} \tau_s \\ \tau_e \end{bmatrix} &= \begin{bmatrix} a_1 + a_4 + 2a_3 \cos(q_2) + a_2 & a_2 + a_3 \cos(q_2) \\ a_2 + a_3 \cos(q_2) & a_2 \end{bmatrix} \begin{bmatrix} \ddot{q}_1 \\ \ddot{q}_2 \end{bmatrix} + \\
 &\quad \begin{bmatrix} -a_3 \dot{q}_2 \sin(q_2) & -a_3 (\dot{q}_1 + \dot{q}_2 \sin(q_2)) \\ a_3 \sin(q_2) \dot{q}_1 & 0 \end{bmatrix} \begin{bmatrix} \dot{q}_1 \\ \dot{q}_2 \end{bmatrix}
 \end{aligned} \tag{B.8}$$

After joint torques have been determined, the next step is to use musculoskeletal modeling to calculate the muscle properties and determine the force each muscle is required to output to produce the movement.

B.2.3.3 Effective Mass Calculation

The effective mass is used to estimate the arms resistance to a force in a given direction and is used as m when parameterizing each effort representation as a function of time and mass (166). Effective mass is estimated by inducing a force of 1 in the reach direction to compute the effective mass of the reaching movement. In equation B.9, θ is the angle of reaching direction, and +1 is added at the end to account for the inertia of the robotic arm manipulandum.

$$\text{Effective mass} = \text{norm}(M * \begin{bmatrix} \cos(\theta) & \sin(\theta) \end{bmatrix}) + 1 \quad (\text{B.9})$$

The mass (M) matrix is defined as:

$$M = (\Lambda^{-1})^T I(\theta) \Lambda^{-1} \quad (\text{B.10})$$

The mass matrix is computed from Jacobian matrix Λ (eq. B.11) and the inertial matrix of the arm (eq. B.12). In equations we define the variables as follows: m_1 = upper arm mass, r_1 = upper arm centroid length, l_1 = upper arm length, $I_{COM,1}$ = moment of inertia about its center of mass. m_2 = forearm mass, r_2 = the length to the center of mass of the forearm, r_{22} = the length to the centroid (arm + mass), l_1 = forearm length, $I_{COM,1}$ = moment of inertia about its centroid with the added mass.

$$\Lambda = \frac{dx}{d\theta} = \begin{bmatrix} -l_1 \sin(\theta_s) - l_2 \sin(\theta_s + \theta_e) & -l_2 \sin(\theta_s + \theta_e) \\ l_1 \cos(\theta_s) + l_2 \cos(\theta_s + \theta_e) & l_2 \cos(\theta_s + \theta_e) \end{bmatrix} \quad (\text{B.11})$$

$$I = \begin{bmatrix} m_1 r_1^2 + I_{COM,1} + (mass + m_2)(l_1^2 + r_{22}^2 + 2l_1 r_{22} \cos(\theta_e)) + I_{COM,2} \\ (m_2 + mass)(r_{22}^2 + l_1 r_{22}^2 \cos(\theta_e)) + I_{COM,2} \\ (m_2 + mass)(r_{22}^2 + l_1 r_{22}^2 \cos(\theta_e)) + I_{COM,2} \\ m_2 r_2^2 + mass \cdot l_2^2 + I_{COM,2} \end{bmatrix} \quad (B.12)$$

B.2.4 Step 4 - Muscle Properties

Once joint torques were determined, we implemented an eight-muscle actuator model to match the computed joint torques. The muscle forces were calculated by distributing the force according to one of many (9) possible minimization functions representing some neuromechanical proxies (muscle force, muscle stress, active state, neural drive) for effort and one metabolic representation (Umberger 2010). Active state, an estimation of the percent of muscle activated, is calculated by simulating the properties of the muscles and estimating the portion of the muscle required to be active to match the torque. Neural drive, control signal from the central nervous system, is calculated from activation dynamics and the rate of change in active state. At each time step, the current active state and a neural drive of 1 and 0 are used to calculate the minimum and maximum possible active states at the next time point. This minimum and maximum active state are used as bounds for the muscle force allocation of the next time point. This process would repeat for each time step until the reach completed.

Muscles' properties of the eight simulated muscle actuators are shown in table B.3 (mass, physiological cross-sectional area, optimal length, and percent fast twitch fibers). The eight muscles simulated are the anconeus (an), brachioradialis (br), brachialis (bs), biceps brachii (bb), clavicle portion of the pectoralis (pc), deltoid anterior (da), deltoid posterior (dp), and the triceps brachii (tb). Estimated muscle masses were computed by multiplying the optimal length by cross section area then multiplying by muscle density ($\rho = 10.6 \text{ kg/m}^3$). The physiological cross-sectional area (PCSA) for each muscle was estimated from cadaver studies (96; 110). The cross-sectional area for

the brachioradialis was taken from Friden et al. (58). The PCSA for each muscle can be estimated similar to the Todorov model (113) or estimated from cadaver studies by dividing the muscle volume by the optimal fiber length (88; 141). Optimal lengths were taken from multiple cadaver studies (28; 110; 141). The optimal length of the anconeus and pectoralis muscles were set to occur at a shoulder flexion angle of 45° as the anconeus muscle did not have values listed and we only used the clavicle portion of the pectoralis. Kistemaker et al. shows that the optimal elbow flexor angle to maximize the elbow moment is also 90° (104). The lengths of the muscles are determined by Pigeon et al, which models the muscle lengths and moment arms using cadaver studies and a polynomial equation (149). The percent fast twitch of the eight muscles was estimated from Dahmane et al. and Johnson et al. (38; 98). For data that is listed as deep and superficial portions, percent fast twitch is averaged between the deep and superficial muscle and used in the model.

Muscle	Mass (kg)	PCSA (m^2)	L_{OPT}	% FT
Anconeus (AN)	0.0291	4E-4	0.0687 (E)	40.0
Brachialis (BS)	0.0829	8.71E-4	0.090 (C)	40.0
Brachioradialis (BR)	0.0525	2.95E-4	0.1887 (L)	60.2
Deltoid Anterior (DA)	0.1005	5.46E-4	0.1296 (L)	42.9
Deltoid Posterior (DP)	0.1323	5.69E-4	0.1818 (L)	42.9
Pectoralis (PC)	0.0816	6.68E-4	0.1701 (E)	57.0
Biceps Brachii(BB)	0.1278	4.32E-4	0.225 (M)	53.6
Triceps Brachii (TB)	0.3920	11.94E-4	0.3235 (M)	52.9

Table B.3: Muscle Properties. For L_{OPT} , the letter corresponds to which author the value was taken from or if it was estimated. C(28), L(110), M(141), E (estimated).

B.2.4.1 PCSA, Optimal Length, and %FT

The muscle masses can be computed using $mass = L_{OPT} \cdot PCSA \cdot \rho$ where ρ is $10.6 \text{ kg}/m^3$ (ρ taken from (115; 190). The PCSA for each muscle is estimated from cadaver studies (96; 110). The cross-sectional area for the brachioradialis is taken from (58). The cross-sectional areas are all increased by 1 as it was needed for the muscles to be strong enough for the faster movements. The *PCSA* for each muscle can be estimated similar to the Todorov model (113), or from cadaver studies done by Holzbaur and Murray by dividing the muscle volume by the optimal fiber length

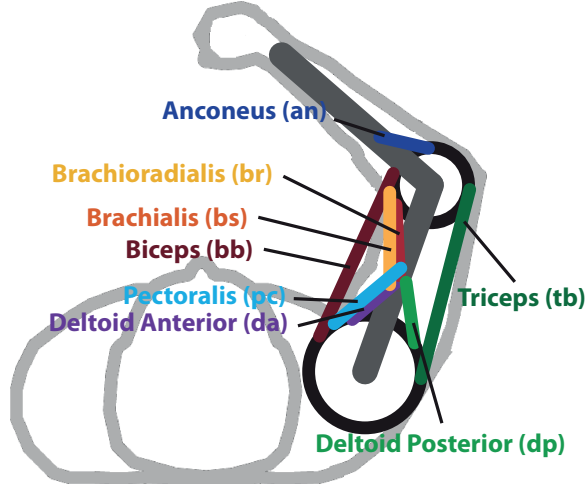


Figure B.7: Diagram of the 8 simulated muscles and which muscles they represent.

(88; 141).

Currently the model uses the optimal muscle lengths from Murray (141) and combining the heads of muscles. Some of these values are taken from Langenderfer (110) as Murray does not test them. However, Chang et al.(28) shows that the optimal lengths of the muscles are quite a bit shorter than reported by Langenderfer and Murray. I think the optimal muscle lengths for the brachialis should agree more with the shorter values in Chang (28) as these values match up closer to Pigeon(149) and Van Zuylen(184).

If not listed, the model assumes the optimal fiber lengths occur at 45° shoulder flexion and 90° elbow flexion, and that the length of the muscle at that position is given in equation B.13. This method may not be accurate for some muscles as they would vary greatly if the equation were used when compared to the Langenderfer model (110). Kistemaker shows 5 references that show that the optimal elbow flexor angle to maximize the elbow moment is also 45° (104).

Percent fast twitch of each of the muscles can be estimated from (38; 98). For data that has deep and superficial values an average is taken for percent fast twitch.

B.2.4.2 Muscle Moment arms

The moment arms were set to vary with shoulder and elbow position as defined below (149). A negative moment arm is used to provide a negative torque around the joint as muscle force can never be less than 0.

The Pigeon model fits polynomials to the moment arm and muscle lengths as a function of shoulder and elbow angle. A graph showing how the moment arms are changing is shown in figure B.8a.

$$\begin{aligned} MA &= x_n q_j^n + x_{n-1} q_j^{n-1} + \cdots + x_1 q_j + x_0 \\ ML &= cst + \sum_{j=1}^3 (Y_n q_j^n + y_{n-1} q_j^{n-1} + \cdots + y_1 q_j) \end{aligned} \quad (\text{B.13})$$

The coefficients for this equation are shown in the tables below. Most of the coefficients are scaled to a power of 10.

Moment Arm Coefficients							
	Elbow flexion/extension					Shoulder F/E	
DF	$c_5 \times 10^9$	$c_4 \times 10^7$	$c_3 \times 10^5$	$c_2 \times 10^3$	$c_1 \times 10^1$	c_0	d_0
Muscle							
AN	-2.7306	10.448	-14.329	8.4297	-2.2841	-5.3450	
BS			-2.0530	2.3425	2.3080	5.5492	
BR			-6.5171	10.084	1.6681	19.490	
DA							33.02
DP							-78.74
PC							50.80
BB			-2.9883	1.8047	4.5322	14.660	29.21
TB	-3.5171	13.277	-19.092	12.886	-3.0284	-23.287	-25.40

Table B.4: Coefficients for polynomial fits to moment arm lengths.

B.2.4.3 Muscle Lengths

The following equations describe how I calculate the lengths of the muscles. They are solved for in a similar way to moment arms (149). A graphical representation of the muscle lengths is

shown in figure B.8b.

Muscle Length Coefficients								
DF		Elbow flexion/extension					Shoulder F/E	
Muscle	cst(mm)	$t_6 \times 10^{11}$	$t_5 \times 10^8$	$t_4 \times 10^7$	$t_3 \times 10^5$	$t_2 \times 10^3$	$t_1 \times 10^2$	$u_1 \times 10^1$
AN	53.57	4.7658	-1.8235	25.008	-14.713	3.9865	9.3288	
BS	137.48			3.5832	-4.0884	-4.0282	-9.6852	
BR	276.13			11.374	-17.600	-2.9114	-34.017	
DA	172.84							-5.7631
DP	157.64							13.743
PC	155.19							-8.8663
BB	378.06			5.2156	-3.1498	-7.9101	-25.587	-5.0981
TB	260.05	6.1385	-2.3174	33.321	-22.491	5.2856	40.644	4.4331

Table B.5: Coefficients for polynomial fits to moment arm lengths.

The optimal lengths of the muscles as shown in table B.3 and are estimated with the arm in a neutral position where $\theta_s = 45^\circ$ and $\theta_e = 90^\circ$ if data from literature could not be found.

B.2.5 Int1 - Cost Function Minimization

There are many possible minimization functions to distribute muscle forces due to the mechanical redundancy of the musculoskeletal system. Here we test 9 possible minimization functions, many shown on the left side of the flow chart (step Int-1). We also minimize muscle force (squared) and muscle stress (squared).

B.2.6 Int2 - Muscle force bounds

Our model bound the active start of the muscle to a minimum of 0 and a maximum of 1. This is achieved by computing the minimum and maximum at every time point through the activation dynamics from the previous time point. The active state of the previous time point is fed a neural drive of either 0 or 1 to estimate the minimum and maximum active state at the current time point. This is done for every muscle at every time point to keep the active state between 0 and 1.

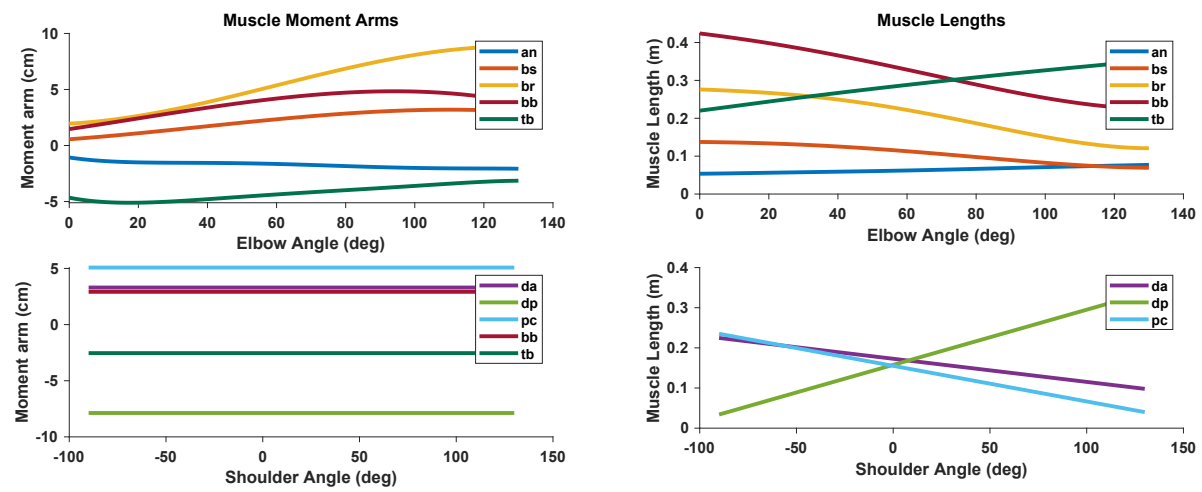


Figure B.8: Muscle moment arms and lengths.

B.2.7 Step 6 - Active State Estimation

Once muscle force and muscle properties were calculated, we then estimated the active state of the muscles by simulating a modified Hill-type muscle (25). This model estimates how much force a muscle can produce depending on the portion of muscle active and the muscle properties. The tendon (series elastic element) is set to be constant length and seems to be a reasonable approximation to make for low forces (7; 97; 111; 118; 130; 169).

B.2.7.1 Force-length/velocity properties

The model used is the Brown, Cheng and Loeb model to estimate the force length/velocity properties (25). Other models can also be used such as cross-bridge cycling models (22; 200) or hill type models (42; 49; 74; 104; 194). The Brown model accounts for active and passive elements of the muscle tendon unit. l is defined as the normalized length l/l_{OPT} , v is in normalized units of L_{OPT}/s . Activate state (a) is computed using Eq. B.15. $F_{p,1}$ is the passive force resisting tension. $F_{p,2}$ is the passive force resisting compression of the muscle. The tendon (series elastic element) is assumed to be constant length, thus providing no stretched force, and seems to be a reasonable approximation to make (7; 97; 111; 118; 130; 169).

The basic form of these equations are

$$\begin{aligned} F_{PE} &= F_{p,1} + R * A_f * F_{p,2} \\ F_{CE} &= R * A_F * F_L * F_V \\ F_{total} &= F_{PE} + F_{CE} \end{aligned} \tag{B.14}$$

Which simplifies to

$$F_{total} = F_{p,1} + R * A_f (F_L * F_V + F_{p,2})$$

$$F_{p,1} = 68.35 * 0.0495 * \log(\exp((l - 1.445)/(0.0495)) + 1)$$

$$F_{p,2} = -0.02\exp(13.8 - 18.7l)$$

$$F_v = \begin{cases} \frac{-5.72-v}{-5.72+v(1.38+2.09l)} & v \leq 0 \\ \frac{0.62-v(-3.12+4.21*l-2.67l^2)}{0.62v} & v > 0 \end{cases} \quad (\text{B.15})$$

$$F_l = \exp\left(-\left|\frac{l^{1.93}}{1.03}\right|^{1.87}\right)$$

$$N_f = 2.11 + 4.16\left(\frac{1}{l} - 1\right)$$

$$A = \frac{T - Fp, 1}{F_l F_v + F_{p,2}}$$

$$a = 0.56 N_F 10^{\log_{10}(1-A)/N_f}$$

The passive force is subtracted from the total joint torque to solve for the active components of force that the muscles need to produce.

Once the active state is calculated, it is scaled by a normalizing factor ($\sigma = 200 \text{Nm N/m}^2$) to calculate muscle force. This value was chosen to reasonably match maximum shoulder and elbow flexion torques (87). This model produces, at elbow angle of 90° and shoulder angle of 45° , a maximum elbow flexion of 59 Nm, elbow extension of 47 Nm, shoulder flexion of 65 Nm, and shoulder extension 73 Nm.

$$F = a \cdot \sigma \cdot A, \quad \text{where } A \text{ is area} \quad (\text{B.16})$$

The passive force properties of the muscles seem to line up relatively well with Horowitz (89). He reports at long sarcomere lengths the human muscles produce about $0.2\text{-}0.3 \text{ kg/cm}^2$. The biceps brachii at its longest length was producing 0.35 kg/cm^2 passively.

B.2.8 Step 7- Activation Dynamics

After active state is estimated, a first order differential equation is used to calculate neural drive that estimates the active state rate as a function of neural drive (113; 181). The active state is estimated from neural drive by passing u (neural drive) through a filter that describes calcium dynamics (113). It is approximated using a first order non-linear filter. This is similar to other methods (25; 130; 177; 195).

$$\dot{a} = \frac{(1 + \sigma_u \epsilon)u - a}{t(u, a)}$$

$$t(u, a) = \begin{cases} t_{deact} + u(t_{act} - t_{deact}) & u > a \\ t_{deact} & otherwise \end{cases} \quad (B.17)$$

σ and ϵ represent noise in the neural drive signal. Currently I have 0 zero noise added to the signal. $t_{ACT} = 50$ msec, and $t_{DEACT} = 66$ msec. Using our muscle parameters of %FT we would get activation and deactivation times shown in table B.6.

Muscle	%FT	t_{ACT} (ms)	t_{DEACT} (ms)
1	50.3	56.36	61.83
2	42.9	59.84	65.98
3	53.6	54.81	59.98
4	64.7	49.59	53.77
5	54.5	54.39	59.48
6	64.7	49.59	53.77

Table B.6: Activation and deactivation times using the Umberger Model

B.2.9 Step 8 - Metabolics Models

B.2.9.1 Umberger Model 2003

One of the most prevalent models is the Umberger energy model (180? ; 181). This model assumes that there is some heat rate (\dot{E}) associated with the activation (h_A), maintenance (h_M),

shortening/lengthening (\dot{h}_{SL}), and work (\dot{w}) done by the muscle that when added together is equal to the total energy rate (\dot{E}) shown in eq. B.18.

$$\dot{E} = \dot{h}_A + \dot{h}_M + \dot{h}_{SL} + \dot{w}_{CE} \quad (\text{B.18})$$

Activation and maintenance heat rate, \dot{h}_{AM} The activation and maintenance are often grouped together into one term, \dot{h}_{AM} . Scaling factors are added to account for the length and activation dependence of \dot{h}_{AM} and \dot{h}_{SL} . \dot{h}_{AM} and \dot{h}_{SL} are scaled by the normalized, isometric force-length relation (F_{iso}) when $L_{CE} > L_{CE(OPT)}$.

We define \dot{h}_{AM} below; this value will be scaled by the factors above depending on the length and velocity of the muscle (eq. B.19).

$$\dot{h}_{AM} = 1.28 \times \%FT + 25 \quad (\text{B.19})$$

To get appropriate activation dependence a scaling factor (A) that depends on STIM and ACT is defined:

$$A = \begin{cases} STIM & \text{when } STIM > ACT \\ (STIM + ACT)/2 & \text{when } STIM \leq ACT \end{cases} \quad (\text{B.20})$$

Then for scaling \dot{h}_{AM} and \dot{h}_{SL} we define:

$$\begin{aligned} A_{AM} &= A^{0.6} \\ A_{SL} &= A^{2.0} \end{aligned} \quad (\text{B.21})$$

\dot{h}_{SL} is scaled by A_{SL} when $\tilde{V}_{CE} \leq 0$ and by A when $\tilde{V}_{CE} > 0$.

Shortening and lengthening heat rate, \dot{h}_{SL} This model uses a modified Hill-Type model. It was modified to better account for force production at submaximal activation and the effects of between-muscle fiber type differences. These are based on a hill type model of the muscle that consists of a contractile element(CE) and a series elastic element (SEE).

The normalized hill constants $A_{REL}(= a/F_{MAX})$ and $B_{REL}(= b/L_{CE(OPT)})$ determine the shape of force-velocity curve and maximal shortening velocity (and power that can be generated given maximal isometric force (F_{MAX})). When multiple muscles are modeled simultaneously, a common approach is to assign all muscles same normalized Hill-constants. Here, they scale A_{REL} and B_{REL} by the percent of type II fibers.

$$\begin{aligned} A_{REL} &= 0.1 + 0.4(\%FT/100) \\ B_{REL} &= A_{REL}\tilde{V}_{CE(MAX)} \end{aligned} \quad (\text{B.22})$$

$\tilde{V}_{CE(MAX)}$ is the maximum shortening velocity of the muscle relative to its length. In these constants, $\tilde{V}_{CE} = V_{CE}/L_{CE(OPT)}$ and is expressed in $L_{CE(OPT)}s^{-1}$. A value of 12 $L_{CE(OPT)}s^{-1}$ is used for $\tilde{V}_{CE(MAX)}$.

Shortening heat coefficients for slow twitch and fast twitch fibers:

$$\begin{aligned} \alpha_{S(ST)} &= \frac{4 \times 25}{\tilde{V}_{CE(MAX-ST)}} \\ \alpha_{S(FT)} &= \frac{1 \times 153}{\tilde{V}_{CE(MAX-FT)}} \end{aligned} \quad (\text{B.23})$$

For these coefficients, $\tilde{V}_{CE(MAX-FT)}$ is defined by the Hill coefficients A_{REL} and B_{REL} . $\tilde{V}_{CE(MAX-FT)}$ is assumed to be 2.5 times greater than $\tilde{V}_{CE(MAX-ST)}$

Combining these equations, we get the shortening heat rate:

$$\dot{h}_{SL} = -\alpha_{S(ST)}\tilde{V}_{CE}(1 - \%FT/100) - \alpha_{S(FT)}\tilde{V}_{CE}(\%FT/100) \quad \text{for } \tilde{V}_{CE} \leq 0 \quad (\text{B.24})$$

The rate of extra heat production in lengthening can be represented as a product of a coefficient α_L and CE velocity, with a slope slightly greater than shortening.

$$\alpha_L = 4\alpha_{S(ST)} \quad (\text{B.25})$$

Where $\alpha_{S(ST)}$ is defined in equation B.23. We then get the heat rate for a lengthening muscle.

$$\dot{h}_{SL} = \alpha_L \tilde{V}_{CE} \quad \text{for } \tilde{V}_{CE} \geq 0 \quad (\text{B.26})$$

Mechanical Work Rate, \dot{w} Mass specific mechanical work rate is given by:

$$\dot{w}_{CE} = -\frac{F_{CE} V_{CE}}{m} \quad (\text{B.27})$$

Where m is the mass of the muscle.

Total work rate The parameters \dot{h}_{AM} , \dot{h}_{SL} , \dot{w} are all scaled by the parameters above depending on the length and velocity of the muscle while contracting to get an estimate for the total energy rate. The total energy liberation for a muscle in W/kg (total muscle mass) is:

if $L_{CE} \leq L_{CE(OPT)}$

$$\dot{E} = \dot{h}_{AM} A_{AM} S$$

$$+ \begin{cases} [-\alpha_{S(ST)} \tilde{V}_{CE} (1 - \%FT/100) - \alpha_{S(FT)} \tilde{V}_{CE} (\%FT/100)] \cdot A_S S & \text{if } \tilde{V}_{CE} \leq 0 \\ \alpha_L \tilde{V}_{CE} A_S S & \text{if } \tilde{V}_{CE} > 0 \\ -(F_{CE} V_{CE})/m & \end{cases} \quad (\text{B.28})$$

$$\begin{aligned}
& \text{if } L_{CE} > L_{CE(OPT)} \\
\dot{E} = & (0.4 \times \dot{h}_{AM} + 0.6 \times \dot{h}_{AM} F_{ISO} A_{AM} S) \\
+ & \begin{cases} [-\alpha_{S(ST)} \tilde{V}_{CE} (1 - \%FT/100) - \alpha_{S(FT)} \tilde{V}_{CE} (\%FT/100)] F_{ISO} A_S S & \text{if } \tilde{V}_{CE} \leq 0 \\ \alpha_L \tilde{V}_{CE} F_{ISO} A_S & \text{if } \tilde{V}_{CE} > 0 \end{cases} \\
& - (F_{CE} V_{CE}) / m
\end{aligned} \tag{B.29}$$

2010 Model In 2010, a slight alteration to the model was made to better account for the actual ATP cost during lengthening by excluding negative CE work from the summation by redefining the lengthening heat rate coefficient (α_L) (180). Equation B.30 shows the new relation, which is then used in the full metabolic model above (eq. B.28).

$$\alpha_L = 0.3\alpha_{S(ST)} \tag{B.30}$$

B.2.9.2 Bhargava Model 2004

Following suit of Umberger, this model estimates the metabolic rate of the muscle from the activation, maintenance, shortening, and basal heat rate (18). Bhargava collected heat data on frog sartorius muscles, then used a walking model to estimate energetics to evaluate the model. The total energy is divided into five energy terms

$$\dot{E} = \dot{A} + \dot{M} + \dot{S} + \dot{B} + \dot{W} \tag{B.31}$$

where \dot{A} is the activation heat rate, \dot{M} is the maintenance heat rate, \dot{S} is the shortening heat rate, \dot{B} is the basal metabolic rate, and \dot{W} is the work rate.

The activation heat as with the others represents the heat produced by stimulation of the

muscle and is primarily due to Ca^{2+} ion movement. The activation heat is broken into two terms, one for fast twitch fibers and another for slow twitch fibers.

$$\dot{A} = \phi m f_{fast} \dot{A}_{fast} u_{fast}(t) + \phi m f_{slow} \dot{A}_{slow} u_{slow}(t) \quad (\text{B.32})$$

m is the total mass of the muscle, f_{fast} and f_{slow} are the fractions of the muscle that are labeled as fast or slow twitch, \dot{A}_{fast} and \dot{A}_{slow} are the activation heat rate constants for fast and slow twitch fibers. In equation B.32, ϕ is a decay function that models observed heat production where most of the heat is produced at the beginning of activation and decays over time to 6% of the initial level with a time constant of 45 ms.

$$\phi = 0.06 + e^{-t_{stim} u(t)/\tau_\phi} \quad (\text{B.33})$$

where τ_ϕ is the time constant (45 ms), t_{stim} is the amount of time the muscle is excited about 10%. $u_{fast}(t)$ and $u_{slow}(t)$ are the excitation levels of the fast and slow twitch fibers. A single input $u(t)$ is used for the entire muscle, so a conversion is used to separate into $u_{fast}(t)$ and $u_{slow}(t)$.

$$\begin{aligned} u_{fast}(t) &= 1 - \cos(\pi/2 * u(t)) \\ u_{slow}(t) &= \sin(\pi/2 * u(t)) \end{aligned} \quad (\text{B.34})$$

Bhargava argues that these generally represent the size principle within muscles, that at low levels of excitation only the small fibers will be recruited and at high levels of excitation both fibers will be recruited.

The maintenance hate rate is split into two terms as well, one for fast twitch and one for slow twitch.

$$\dot{M} = L(\tilde{l}^M) m f_{fast} \dot{M}_{fast} u_{fast}(t) + L(\tilde{l}^M) m f_{slow} \dot{M}_{slow} u_{slow}(t) \quad (\text{B.35})$$

\dot{M}_{fast} and \dot{M}_{slow} represent the hate rate constants for fast and slow fibers, $L(\tilde{l}^M)$ is a function

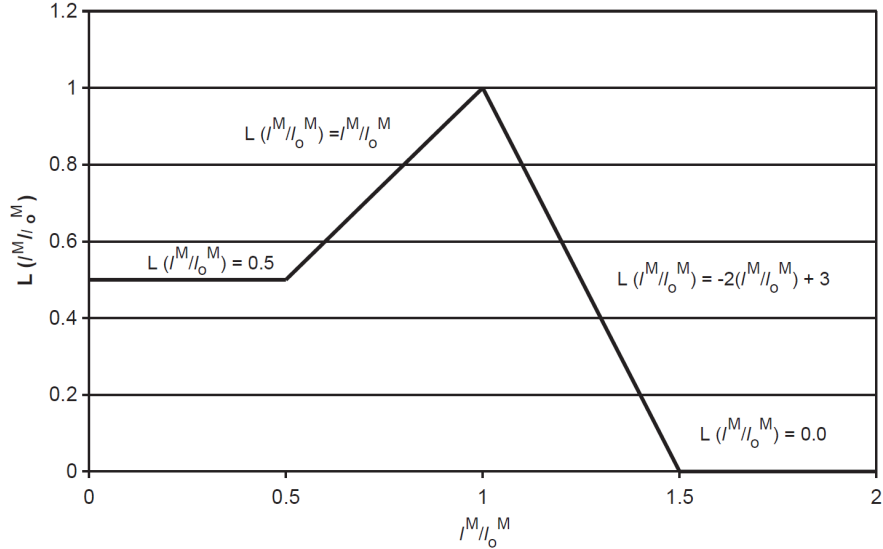


Figure B.9: Length dependence of maintenance heat rate used in equation B.35. This graph is from Bhargava (18).

describing the dependence on muscle length. $L(\tilde{l}^M)$ is modeled by a piece-wise function of normalized muscle fiber length (fig B.9). At very long lengths, the muscle uses no heat for maintenance because there is no overlap of action-myosin, and at very low lengths the overlap does not change so a constant maintenance heat rate is applied.

The shortening heat rate is related to the velocity of shortening by

$$\dot{S} = -\alpha v_{CE} \quad (\text{B.36})$$

where α is a proportionality constant, and v_{CE} is the velocity of the contractile element in the hill type model. The parameter α is dependent on the velocity of the contractile element.

$$\alpha =$$

$$\begin{cases} 0.16F_{iso}^M(a(t), l^M) + 0.18F^M, & \text{if } v_{CE} \leq 0 \\ 0.157F^M, & \text{if } v_{CE} > 0 \end{cases} \quad (\text{B.37})$$

The basal rate of the muscle is just a scalar of the mass of the muscle

$$\dot{B} = 0.0225m \quad (\text{B.38})$$

where m is the mass of the muscle.

The last component, \dot{W} is the force of the contractile element (F_{CE}) multiplied by the shortening velocity (V_{CE}). F_{CE} is determined from the activation, force length, and force velocity properties of the muscle (B.2.4).

$$\dot{W} = F_{CE}(l_{CE}, v_{CE}, a(t))v_{CE} \quad (\text{B.39})$$

Parameter values for $\dot{A}_{fast}, \dot{A}_{slow}, \dot{M}_{fast}, \dot{M}_{slow}, l_0^M, F_0^M$ can be found in Bhargava (18).

B.2.9.3 Lichtwark Model 2005

In a similar fashion to the previous models, Lichtwark modeled the heat rate of the muscles based off the mechanical efficiency of the muscles (114). This model breaks the rate of heat production into four functions that when added together produce the total heat rate.

$$\frac{dH}{dt} = \frac{dH_M}{dt} + \frac{dH_L}{dt} + \frac{dH_S}{dt} + \frac{dH_T}{dt} = f(Act) + f(Act, t) + f(Act, V_{CE}) + f(P) \quad (\text{B.40})$$

where H_M is the stable (maintenance) heat rate, H_L is the labile heat rate, H_S is the shortening heat rate, H_T is the thermoelastic heat rate, P is the relative force produced, Act is the activation level, V_{CE} is the velocity of the contractile element.

H_M is the heat rate to produce isometric force for a given activation state. This has been shown to be well approximated by multiplying the Hill type force-velocity constants $a \times b$. The relationship for H_M is then defined as

$$\frac{dH_M}{dt} = Act \left(\frac{a}{P_0} \times \frac{b}{V_{max}} \times \frac{V_{max}}{L_0} \right) = Act \left(\frac{V_{max}}{G^2} \right) \quad (\text{B.41})$$

where $G = P_0/a = V_{max}/b$ and V_{max} are the maximum shortening velocity. a and b are determined from the normalization constants of the hill-type model. These can be determined in a similar manner to the Umberger model (sec B.2.9.1) and are further described by Winters and Stark (181; 196). P_0, L_0 are used for normalizing the units.

When a muscle contracts over time, the maintenance heat rate can decay in an exponential fashion to about 2-3x, and this is termed labile heat. Knowing this the liable heat rate can be defined as

$$\frac{dH_L}{dt} = 0.8 \frac{dH_M}{dt} e^{-0.72t} + 0.175 \frac{dH_M}{dt} e^{-0.022t} \quad (\text{B.42})$$

The shortening heat rate relates the cost to shortening a muscle for a given activation level. The following equation relates the shortening velocity to the heat rate only when the muscle is shortening.

$$\frac{dH_s}{dt} = Act \left(\frac{a}{P_0} \times \frac{V_{CE}}{L_0} \right) = Act \left(\frac{V_{CE}}{G} \right) \quad (\text{B.43})$$

In eccentric contractions energy cost is generally lower than concentric or isometric contractions. This model assumes that during active lengthening that the minimum heat rate must be 30% of the stable heat rate (123). There is also an exponential decay of energy production as lengthening velocity increases (120). The rate of heat during a lengthening contraction is approximated by

$$\frac{dH_S}{dt} = 0.3 \frac{dH_M}{dt} + 0.7 \left(\frac{dH_m}{dt} e^{-8[\frac{P}{Act} - 1]} \right) \quad (\text{B.44})$$

The last component accounts for the heat absorbed by the muscle, which is proportional to the rate of force production.

$$\frac{dH_T}{dt} = -0.014 \frac{dP}{dt} \quad (\text{B.45})$$

These components are combined with the input parameters ($F, L_{CE}, Act, V_{max}, G$) to create

the full model for energy expenditure

$$\begin{aligned} \frac{dH}{dt} = & Act\left(\frac{V_{max}}{G^2}\right) \\ & + 0.8 \frac{dH_M}{dt} e^{-0.72t} + 0.175 \frac{dH_M}{dt} e^{-0.022t} \\ & + \begin{cases} Act\left(\frac{V_{CE}}{G}\right) & \text{if } V_{CE} > 0 \\ 0.3 \frac{dH_M}{dt} + 0.7 \left(\frac{dH_m}{dt} e^{-8[\frac{P}{Act}-1]} \right) & \text{if } V_{CE} < 0 \end{cases} \\ & - 0.014 \frac{dP}{dt} \end{aligned} \quad (\text{B.46})$$

B.2.9.4 Uchida Model 2016

The Uchida model takes components from the Umberger model and Bhargava model to create a new model (179). The primary aspects of this model are the same as the Umberger model, where the only changes are how this model handles muscle excitation and negative power.

Uchida uses the excitation model of Bhargava to create orderly recruitment of muscle fibers (18).

$$\begin{aligned} u_{slow}(t) &= \sin\left(\frac{\pi}{2}u(t)\right) \\ u_{fast}(t) &= 1 - \cos\left(\frac{\pi}{2}u(t)\right) \\ f_{slow}^{rec}(t) &= \begin{cases} 1, & \text{if } u(t) = 0 \\ \frac{f_{slow}u_{slow}(t)}{f_{slow}u_{slow} + (1-f_{slow})u_{fast}(t)}, & \text{otherwise} \end{cases} \end{aligned} \quad (\text{B.47})$$

$u(t)$ is the muscle excitation level, $u_{slow}(t)$ and $u_{fast}(t)$ are the broken-down components of $u(t)$ into slow and fast twitch fibers, f_{slow} is the fraction of slow twitch fibers within the muscle, and $f_{slow}^{rec}(t)$ is the fraction of the fibers recruited that are slow twitch. This allows for different energetics models based on the fiber type and properties within the model.

The second change Uchida made to the Umberger model is how negative mechanical work

is dealt with. The 2003 Umberger model included negative mechanical work, but was revised in the 2010 model (180; 181). Negative work accounts for much of the differences in some energetics models (131). During eccentric contractions, the muscles were allowed to absorb energy in the Uchida model if the negative mechanical work rate exceeded the total positive heat rate in a similar fashion to the 2003 Umberger model. Instead of returning this energy to the muscle however as the chemical reactions cannot be easily reversed in the muscle, the absorbed energy was immediately dissipated as heat. This prevents the total instantaneous power being less than zero.

The average power for each muscle was calculated by integrating the energy and normalizing to muscle mass.

$$P_{avg} = \frac{m}{t_1 - t_0} \int_{t_0}^{t_1} \dot{E}(t) dt \quad (\text{B.48})$$

B.2.9.5 Margaria 1968

The Margaria model (127) estimates the metabolic rate assuming that muscles are 25% efficient when shortening and 120% efficient while lengthening:

$$\dot{E} = \begin{cases} \frac{\dot{w}}{0.25} & \text{if } v_{CE} \leq 0 \\ -\frac{\dot{w}}{1.20} & \text{if } v_{CE} \geq 0 \end{cases} \quad (\text{B.49})$$

B.3 Data Processing and Statistics

Metabolic and kinematic data were processed using MATLAB 2020a. The biomechanical model was also simulated using MATLAB 2020a. Statistics were computed using R (4.0.3) and the lme4 and multcomp packages. Linear models were computed using the lm function from the lme4 package. Repeated measure correlation was calculated using the rmcrr function in the psychometric package in R. Parametric effort models were fit using the nls function from the multcomp package.

Raw metabolic was saved in a csv file from the metabolic data cart, and raw kinematic data

was saved in .dat files on the computer controlling the robot. These files were used in conjunction to determine the movement kinematics and metabolic power/cost of the movements using MATLAB 2020a and custom scripts and exported to a .csv. The musculoskeletal model was simulated in MATLAB and variables were extracted from the model and exported to a csv. The two csv files were imported into RStudio where the linear and parametric models were fit.

B.3.1 Linear Models

Explanatory variable (effort and metabolic representation) was regressed onto the metabolic power using the lm function from the lme4 package in R (150). R squared values were calculated from the linear model.

$$\text{Metabolic Power} = a * \text{Model} + b \quad (\text{B.50})$$

B.3.2 Parametric Model

The parametric model was fit for each effort and metabolic representation as well as the metabolic power data. Four free parameters were fit (a, b, c, d). This fit was computed using the nls function within the multcomp package in R. The variable a represents some offset to the model, b is a scaling factor, c represents how the model scales with added mass, and d how the model scales with time.

$$\dot{e} = a + \frac{bm^c}{T^d} \quad (\text{B.51})$$

After computing the best parameter fits, we then compare the parameters to the metabolic data using equation B.52 (144; 197). SE represents the standard error of the mean. If this inequality is true, there would be a significant difference. In our study, we are interested in parameters that

are not significantly different than the metabolic data parameters.

$$|mean_A - mean_B| > 2\sqrt{(SE_A^2 + SE_B^2)} \quad (B.52)$$

B.4 Limitations

For data collection we intended for subjects to make arm reaching movements at fairly low movement durations. For 0 and 2.27 kg mass added, the fastest enforced duration was 0.25s, and for 4.55 kg and 9.90 kg it was 0.375s with a 100 ms time window. Subjects seemed to struggle to make these reaching movements and would generally overshoot the target by reaching through the target and not stopping. The average movement durations for the fastest enforced durations were 0.3285s, 0.3567s, 0.4244s, and 0.4372s for 0 kg, 2.27 kg, 4.55 kg, and 9.90 kg respectively. This led to the end of the movements not being captured for the faster movements in the metabolic data. This could mean the metabolic power calculated is higher than reality because it is normalized by trial time divided by movement time. Increasing movement time would lower the metabolic power at the faster speeds. Lowering the metabolic power at the faster speeds may also improve accuracy of the metabolic representations, as this is where they specifically began to fail. The metabolic representations struggled to predict the very fast, low added mass conditions. If these metabolic data points are in fact lower than shown here, our predictions by the metabolic representations could become much better with the scaling of speed.

We were not able to validate our neuromechanical model apart from judging the muscle force traces and confirming they make reasonable sense. The example traces shown in figure B.2 show that for a shoulder flexion and elbow extension movement that the deltoid anterior, triceps brachii, and then deltoid posterior would be activated. This makes logical sense as the triceps extends the elbow, the deltoid anterior first horizontally adducts the shoulder then the deltoid posterior horizontally abducts the shoulder at the end of the movement. One possible way of validating our model would be to simulate EMG signals and compare these to EMG collected during the movement (50; 85). Previous research has shown that doing this, a minimization function of activation state

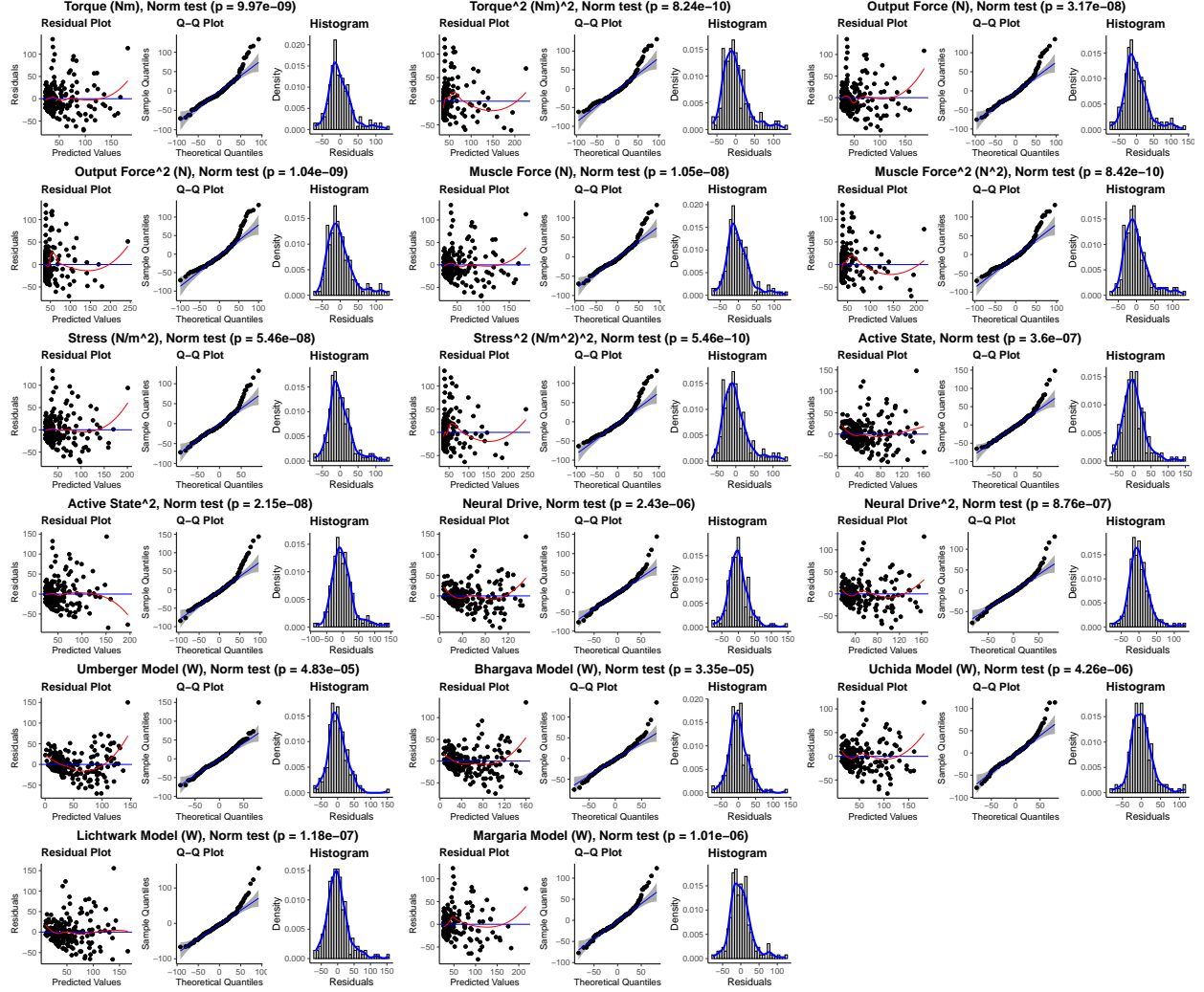


Figure B.10: Linear model diagnostic plots for all proxies minimizing active state squared. Residual by proxy value, QQ plot, and residual histogram for each of the metabolic proxies, while minimizing active states squared.

squared leads to good results which is the same minimization function in our model that led to the best result. Using an optimization that produces similar EMG signals to that of collected EMG could lead to better predictive results of our model.